

JOHANNES JERMAKKA

Electrochemical Methods for Source-separated Urine Treatment and Nutrient Recovery

JOHANNES JERMAKKA

Electrochemical Methods for
Source-separated Urine Treatment
and Nutrient Recovery

ACADEMIC DISSERTATION

To be presented, with the permission of
the Faculty of Engineering and Natural Sciences
of Tampere University,
for public discussion in the Small Auditorium 1 (FA032)
of the Festia building, Korkeakoulunkatu 8, 33720 Tampere,
on 10th September 2021, at 12 o'clock.

ACADEMIC DISSERTATION

Tampere University, Faculty of Engineering and Natural Sciences
Finland

<i>Responsible supervisor and Custos</i>	Associate Professor Marika Kokko Tampere University Finland	
<i>Supervisors</i>	Dr. Pablo Ledezma The University of Queensland Australia	Dr. Stefano Freguia The University of Melbourne Australia
<i>Pre-examiners</i>	Prof. Dr. Kai Udert EAWAG Switzerland	Dr. Ir. Annemiek ter Heijne Wageningen UR Netherlands
<i>Opponent</i>	Prof. Dr. Falk Harnisch UFZ Leipzig Germany	

The originality of this thesis has been checked using the Turnitin OriginalityCheck service.

Copyright ©2021 author

Cover design: Roihu Inc.

ISBN 978-952-03-2084-3 (print)
ISBN 987-952-03-2085-0 (pdf)
ISSN 2489-9860 (print)
ISSN 2490-0028 (pdf)
<http://um.fi/URN:ISBN:978-952-03-2085-0>

PunaMusta Oy – Yliopistopaino
Joensuu 2021

ACKNOWLEDGEMENTS

This thesis is based on joint research effort implemented at Tampere University, Faculty of Engineering and Natural Sciences (Laboratory of Chemistry and Bioengineering at Tampere University of Technology) and University of Queensland Advanced Water Management Centre. My work was funded by Maj and Tor Nessling foundation, Walter Ahlström foundation, Finnish Cultural Foundation and Emil Aaltonen foundation.

I'm grateful for my responsible supervisors Dr. Pablo Ledezma from University of Queensland for his overarching electrochemical knowledge, constant support and presence, and Associate Professor Dr. Marika Kokko from Tampere University for her patient endorsement, dependable aid, and long-term work for a healthy working environment. Further I'd like to extend my gratitude to Dr. Stefano Freguia, who acted as my primary supervisor for the first part of my work and gave me an invaluable example in work-life balance management on top of excellent command of bioelectrochemistry.

I would like to thank Professor Dr. Damien Batstone and Professor Dr. Jukka Rintala for enabling my joint PhD studies. I'd like to thank my co-author Dr. Emma Thompson Brewster whose work on electrodialysis is a great inspiration to me and with whom I experienced the largest moments of insight during this work.

I'm grateful to all my friends at University of Queensland who made our stay a life changing experience and to the golden heart of AWMC Vivienne Clayton as well as all friends and colleagues at Tampere University. Special thank you to Tarja Ylijoki-Kaiste and Antti Nuottajärvi for constant assistance in the laboratory.

I'd like to thank all the hands and hearts who have cared for our children while mine have been in the laboratory and at the computer.

The largest gratitude however I owe to my partner Anna-Mari, who has supported me and our family through these years in ways unrequitable. *Thank you.*

Tampere, March 2021
Johannes Jermakka

ABSTRACT

Achieving sustainability of nutrient use is identified as one of mankind's large challenges as current fertilizer use practices cause widespread eutrophication and rely on mined phosphorus and potassium, that are non-renewable, and fossil fuel-based nitrogen production. This doctoral thesis focuses on a novel method of nitrogen recovery from source-separated human urine. Source-separated urine contains approximately 85 % of human consumed nitrogen in a concentrated form, and methods for separate, undiluted collection of urine are readily available. Urine is simple to store and an enzymatic degradation process called ureolysis spontaneously forms an alkaline liquid, from which water hardness (Ca and Mg) is precipitated away and nitrogen, present in fresh urine as urea, is hydrolysed into ammonium.

In this doctoral thesis, electrochemical methods of electro-concentration and electro-oxidation were investigated for urine treatment and ammonium capture as a nutrient product from source-separated human urine. Electro-concentration of synthetic urine was investigated in a three-chamber reactor configuration using graphite electrodes. In parallel, the configuration was modelled, revealing the theoretical limits, and limiting factors of urine electro-concentration. The electro-concentration was able to form concentrates strong enough to produce a directly usable nutrient product, solid ammonium bicarbonate crystal, the yield of which was revealed to be limited by competing salt ions (Na, Cl).

Electro-oxidation for urine treatment was studied using boron-doped-diamond anodes and the complex relationship between chloride and ammonium ratio and anodic pH towards ammonium oxidation rate was uncovered. The results enable a new method of selective organics electro-oxidation over ammonium by rapidly lowering chloride concentration in electrochemically lowered anodic pH. Finally, a proof-of-concept study combining electro-concentration and electro-oxidation enabled tailored nutrient product formation, including ammonium and sodium separation, lowering the sodicity of the nutrient product.

This work expands the perimeter of electrochemical source-separated urine treatment and nutrient capture and forms a scaffolding for a platform, from which electrochemical technologies can be further developed into mature treatment and resource recovery technologies for urine in a circular nutrient economy.

TIIVISTELMÄ

Ravinteiden tuotannon kestävyys on yksi ihmiskunnan suurista haasteista. Nykyinen kertakäyttölannoitus aiheuttaa rehevöitymistä ja perustuu fossiilisten fosfori- ja kaliummineraalien tuotantoon, sekä maakaasun poltolla sidotun typen tuotantoon. Tämä väitöskirja keskittyy uudelleen menetelmään, jolla typpi voidaan ottaa talteen erilliskerätystä virtsasta ja muodostaa ravinnetuotetta. Virtsa sisältää n. 85% ihmisen syömästä typestä tiiviissä muodossa, ja menetelmät virtsan erilliskeräykseen ovat pitkälle kehittyneitä ja saatavilla. Virtsa on helppo säilöä ja se hajoaa spontaanisti entsyymaattisesti muodostaen emäksisen liuoksen, josta veden kovuus (kalsium ja magnesium) saostuu suoloina pois ja typpi hydrolysoituu ureasta ammoniumiksi.

Tässä väitöskirjassa sähkökemiallista konsentroidintia ja sähkökemiallista hapetusta tutkittiin erilliskerätyn virtsan käsittelemiseksi ja typen talteenottamiseksi ravinnetuotteeksi. Erilliskerätyn virtsan sähkökemiallista konsentroidintia tutkittiin grafiittielektrodein varustetussa kolmikammioisessa reaktorissa. Reaktori myös mallinnettiin matemaattisesti, tuoden esiin sähkökemiallisen konsentroidinnin teoreettiset rajat ja rajoittajat tekijät. Konsentroidinnilla pystyttiin tuottamaan virtsasta kiinteää ammoniumbikarbonaattisuolaa, joka on suoraan käytettävissä ravinnetuotteena. Ravinnetuotteen kiteytystä rajoittavaksi tekijäksi paljastui virtsan kilpailevat suolaionit (Na, Cl).

Sähkökemiallista hapetusta tutkittiin käyttäen booritimanttianodia. Kloorin ja ammoniakkin suhteen sekä anodin pH:n välinen monimutkainen vuorovaikutus ammoniumin hapetusketjuun selvitettiin hapetuskokeilla, mikä mahdollistaa orgaanisen aineen hapettamisen virtsasta ammoniumia hapettamatta käyttäen sähkökemiallisesti laskettua anodin pH:ta. Aikaisemmat hapetus ja konsentroidintitulokset yhdistettiin tutkimuksessa, joka mahdollisti natriumin ja ammonium erottamisen sähkökemiallisen konsentroidinnin ja hapetuksen yhdistävällä tekniikalla, alentaen ravinnetuotteen suolapitoisuutta.

Tämä väitöskirja laajentaa sähkökemiallisten tekniikoiden käyttömahdollisuuksia erilliskerätyn virtsan käsittelyyn ja tuotteistukseen. Se antaa suuntaviivoja erilliskerätyn virtsan ja sähkökemiallisten tekniikoiden soveltamiseksi ravinteiden kiertotaloudessa.

CONTENTS

1	Introduction	1
2	Background	4
2.1	Source-separation and nutrients in urine	4
2.2	Nitrogen chemistry.....	6
2.3	Ammonium bicarbonate crystallization in urine	6
2.4	Electrodialysis and electro-concentration of source-separated urine.....	9
2.5	Modelling electro-concentration.....	12
2.6	Electro-oxidation	12
2.6.1	Electro-oxidation of chloride	14
2.6.2	Electro-oxidation of ammonium	16
2.6.3	Electro-oxidation of organic material.....	17
2.7	Electrochemical concentration and oxidation of source-separated urine	17
3	Aims and hypotheses of the study.....	21
4	Summary of materials and methods	23
4.1	Feed composition.....	23
4.2	Reactor design and equipment.....	25
4.3	Sample analysis.....	28
4.4	Modelling	28
5	Summary of results and discussion.....	29
5.1	Electro-concentration and ammonium precipitation	29
5.1.1	Nitrogen recovery via electro-concentration reaches a plateau (I, II).....	30
5.1.2	Parameters dictating ammonium bicarbonate precipitation in the concentrate (I).....	31
5.1.3	Electro-concentration is limited by back migration and current leak (II).....	33
5.2	Electro-oxidation of source-separated urine on BDD anode.....	34
5.2.1	TAN electro-oxidation depends on the Cl/TAN ratio (III)	34
5.2.2	TOC electro-oxidation proceeds with constant rate (III, IV).....	36

5.2.3	Anodic pH control allows selective TOC electro-oxidation in source-separated urine (III).....	37
5.3	Combined electro-concentration and electro-oxidation for formation of nutrient product with reduced sodicity (IV).....	38
5.3.1	Reagent-free pH control allows Na/TAN separation and adjustment of product sodicity (IV).....	38
5.3.2	TAN and Cl losses depend on sequential oxidation and reduction within the reactor chambers (IV).....	40
5.4	TAN recovery from source-separated urine in electrochemical systems.....	42
6	Conclusions and future outlook	45

List of Figures

- Figure 1 Operating principle of electro dialysis stack: Cations pass through Cation Exchange Membrane (CEM) but are inhibited by the Anion Exchange Membrane (AEM) and remain in the concentrate and vice versa for anions. + = anode, - = cathode.
- Figure 2 Concentration profiles for cations and anions through a cell pair in a single ion pair system. + = anode, - = cathode.
- Figure 3 a) Flow diagram of the two-chamber reactor utilized in Publication III, and b) Flow diagram of the double three-chamber reactor utilized in Publication IV. CEM = Cation Exchange Membrane, AEM = Anion Exchange Membrane, BDD = Boron Doped Diamond, WE = Working Electrode, SS = Stainless Steel, CE = Counter Electrode. U = Urine Feed Pump, F = Loop Feed Pump.
- Figure 4 a) Assembled three chamber reactor used in Publications I, II and IV (the same reactor was used without the middle chamber in Publication III), b) close-up of a double-reactor configuration showing collected product and waste concentrates in Publication IV, and c) overview of laboratory setup used in experiments done for Publication IV showing two parallel double reactor configurations.
- Figure 5 Ion concentrations before (upconcentration) and during steady state. (a) Concentrate conductivity reaching steady state, (b) Concentrate conductivity in steady state, (c) Concentrate ion concentrations reaching steady state, (d) Concentrate ion concentrations in steady state. Upconcentration = phase from start to steady state. Steady state = operational phase with steady concentrations. ACE, NO ACE, ABC = feed characteristics (see Chapter 4.1). (modified from Publication I, Fig. 2)
- Figure 6 Ratio of ammonium bicarbonate ionic strength and ionic strength (IS_{ABC}/IS) presented in relation to (a) current density (J) and (b) ammonium bicarbonate ionic product (IP_{ABC}). ABC and ACE are synthetic urine feed compositions (see Chapter 4.1.). Supernatant refers to concentrate after cooling and removal of solid crystals. (Publication I, Fig 5)
- Figure 7 Measured TAN and chloride amount relative to their initial amounts (mol/mol_0) in synthetic urine in a) neutral pH, b) pH 5, and c) pH 3 and below. (Modified from Publication III, Fig 2)
- Figure 8 Hypothesised pathways (simplified) dominating TOC and TAN oxidation under a) neutral and b) low anodic pH-conditions. Boxes indicate feed substances, bubbles end products and arrow widths relative scale of reaction rates. In neutral conditions, active chlorine diffuses to bulk and is responsible for most of TOC and TAN decay measured. At low pH, formed chloride radicals (RCS) have reaction pathways with competitive reaction rates including further oxidation and removal as gaseous chlorine, and diffusion of active chlorine to bulk is low and cannot induce breakpoint chlorination -type TAN decay. (Publication III, Fig 7)

- Figure 9 Total Organic Carbon (TOC) amount relative to the initial amount in the feed (mol/mol_0) during electro-oxidation of synthetic urine at different pH values. (Publication III, Fig 3)
- Figure 10 a) Product sodicity indicated by Na/TAN concentration ratio, and b) specific energy consumption in product reactor (P) and waste reactor (W) against TAN captured in the product (modified from Publication IV, Fig 2)
- Figure 11 Chloride and b) total ammonium nitrogen (TAN) losses (mol/mol_0) plotted against the difference of product and waste reactor anode potentials, an indicator of the oxidation and reduction potential for chloride compounds in the reactor. (Publication IV, Fig 4)

List of Tables

- Table 1 Source-separated urine measured before and after ureolysis in the literature.
- Table 2 Solubilities of selected salts, adapted from Haynes (2012).
- Table 3 Active and passive anode materials based on their oxygen evolution potential in acidic media. The arrow in the rightmost column represents a gradual change from physisorption to chemisorption. (Comninellis and Chen, 2010; Martínez-Huitile et al., 2015)
- Table 4 Synthetic urine recipes used in different Publications. Units in g L^{-1} , if not otherwise mentioned. See Chapter 4.1. for explanation on different feed compositions.
- Table 5 The real concentrations in synthetic and real urine feed used in different Publications, units in mmol L^{-1} .
- Table 6 Differences in experimental design between Publications.
- Table 7 Compilation of current densities used in electrochemical TAN capture from source-separated urine and percentual TAN recovery, specific energy consumption and current efficiency (CE) obtained in these experiments. Adapted from reviews (Kuntke et al., 2018; Liu et al., 2020) and other sources in the reference-column. EC=electro-concentration, MFC = Microbial Fuel Cell, MEC = Microbial Eletrolysis Cell, TMCS = Transmembrane Chemisorption, C = Concentration, CE = Current Efficiency.

ABBREVIATIONS

ABC	Ammonium Bicarbonate Feed
ACE	Acetate containing Feed
AEM	Anion Exchange Membrane
AEOP	Advanced Electrochemical Oxidation Processes
BDD	Boron-Doped-Diamond
CEM	Cation Exchange Membrane
Cl	Chloride
CO ₂	Carbon Dioxide
DSA	Dimensionally Stable Anode
EAWAG	Swiss Federal Institute of Aquatic Science and Technology
ED	Electrodialysis
EO	Electrochemical Oxidation
HRT	Hydraulic Retention Time
IC	Ionic Chromatogram
IP	Ionic Product
IS	Ionic Strength
MET	Microbial Electrochemical Technology
MFC	Microbial Fuel Cell
Na	Sodium
NO ACE	No-Acetate containing Feed
NO ₂ ⁻	Nitrite
NO ₃ ⁻	Nitrate
ODE	Ordinary Differential Equation
RCS	Reactive Chloride Species
ROS	Reactive Oxygen Species
SHE	Standard Hydrogen Electrode
TAN	Total Ammonium Nitrogen
TIC	Total Inorganic Carbon
TOC	Total Organic Carbon

ORIGINAL PUBLICATIONS

- Publication I Jermakka, J., Thompson Brewster, E., Ledezma, P., Freguia, S. Electro-concentration for chemical-free nitrogen capture as solid ammonium bicarbonate. *Separation and Purification Technology* 203 (2018) 48-55.
- Publication II Thompson Brewster, E., Jermakka, J., Freguia, S., Batstone, D. J. Modelling recovery of ammonium from urine by electro-concentration in a 3-chamber cell. *Water Research* 124 (2017) 210-218.
- Publication III Jermakka, J., Freguia, S., Kokko, M., Ledezma, P. Electrochemical system for selective oxidation of organics over ammonia in urine. *Environmental Science: Water Research & Technology* 7 (2021) 942-955.
- Publication IV Jermakka, J., Thompson Brewster, E., Freguia, S., Ledezma, P., Kokko, M. Electro-concentration of urine designed for separation of sodium from nitrogen. *Separation and Purification Technology* 276 (2021) 119275.

AUTHOR CONTRIBUTIONS

- Publication I JJ is the corresponding author of the paper. JJ designed and conducted most of the experimental work, interpreted the data, and wrote the original draft manuscript. The work was revised by, and conducted under the supervision and of PL and SF.
- Publication II JJ is responsible for the experimental design and procedure. JJ is credited for all experimental work, 85% experimental design, 10% conceptualized modelling and 10% manuscript writing. EB is the corresponding author, responsible for the main part of conceptualized modelling and conducting the modelling. The work was revised by, and conducted under the supervision of SF and DB.
- Publication III JJ is the corresponding author of the paper. JJ designed and conducted all the experimental work, interpreted the data, and wrote the original draft manuscript. The work was revised by, and conducted under the supervision of SF, MK, and PL.
- Publication IV JJ is the corresponding author of the paper. JJ designed and conducted all the experimental work and interpreted the data. The original manuscript was written by JJ and EB. The work was revised by EB, SF, PL, and MK, and conducted under the supervision of SF, PL, and MK.

1 INTRODUCTION

Global food production was revolutionized during the 20th century through the large-scale adoption of industrial production of three key macro-nutrients: nitrogen, phosphorus, and potassium. The mining of potassium and phosphorus and artificial fixation of atmospheric nitrogen through Haber-Bosch process has revolutionized agriculture, enabling rapid population growth. Currently the world produces around 6000 Mt/a of food for which 41 Mt/a of potash (K_2O), 53 Mt/a of phosphate (as P_2O_5) and 113 Mt/a of nitrogen (as reactive nitrogen) as added fertilizers are used (FAO, 2017), when manure and organic streams are not considered. Without nutrients produced outside the natural nutrient cycling, the world could feed approximately 3-4 billion people (Erisman et al., 2008), while current world population exceeds 7.8 billion. While enabling surplus of food production, the large scale nutrient production and use brings a multitude of problems and threats, including finite minable K and P rock resources, high energy footprint of N fixation (1.4 % of global fossil energy is used for nitrogen fixation) and environmental impact of nutrient leaching (Capdevila-Cortada, 2019; Sutton et al., 2013). Nutrient recycling is identified as a key component of future food security and part of circular economy (FAO, 2012).

Source-separation of urine can enable water and nutrient recovery and reuse. Urine contains the majority of human consumed nutrients (79:47:71% of N:P:K) in a compact form, rendering it promising for nutrient recovery (Jönsson and Vinnerås, 2013; Randall and Naidoo, 2018). While direct reuse is often deemed impractical due to liquid transportation costs, salinity, handling, and health and safety issues (Larsen et al., 2013; Patel et al., 2020), nutrients can be recovered from urine using a wide variety of chemical, biological and physical methods (Chipako and Randall, 2020; Patel et al., 2020; Perera et al., 2019). Electrochemical technologies are versatile alternatives for urine treatment and nutrient recovery as they can be made reagent-free and require only electricity to function, can be operated intermittently on renewable electricity availability basis, and require only small units for operation (Ma et al., 2018). Urine is extremely well suited for electrochemistry, being (i) highly

conductive, (ii) well buffered after hydrolysis, and (iii) highly concentrated in nutrients (Ledezma et al., 2015).

Electrochemical technologies utilize external electron acceptors and electron supply to catalyze chemical oxidation and reduction reactions creating a flow of charged ions through the liquid. Electrochemical concentration, electro-concentration or electro-dialysis is a technology that utilizes electric current to move ions through charged membranes to concentrate ionic species from the feed to a concentrate. While most prominently applied in sea water desalination, it is well suited for removing nutrient and salt content from urine to form a product concentrate, and is considered a technically and economically feasible technology for this application (Pronk et al., 2006a; Pronk et al., 2006b; Pronk et al., 2007; Thompson Brewster et al., 2017b; Ward et al., 2018). Electrochemical oxidation, or electro-oxidation, refers to the oxidation of organic matter, ammonium, or other inorganic substances through electrochemical reactions. Electro-oxidation can occur via direct electron transfer on the anode, or indirectly via radical formation at the anode. Most common radicals are oxygen radicals (hydroxyl radical and other Reactive Oxygen Species, ROS) and chloride species (hypochlorite and other Reactive Chloride Species, RCS), that first pass electrons to the electrode as they are formed, and subsequently can receive electrons from e.g. organic matter or ammonium. Electro-oxidation has been researched and applied as a means for water treatment, especially for applications with difficult to treat compounds such as dyes or pharmaceuticals (Brillas and Martínez-Huitle, 2015; Martínez-Huitle et al., 2015), but also for wastewater and source-separated urine (Cho and Hoffmann, 2014; Zöllig et al., 2015c; Zöllig et al., 2015a; Zöllig et al., 2017).

The application of electrochemical technologies for source-separated human urine holds promise for rapid and flexible treatment and nutrient recovery but involves challenges. Optimization of electro-concentration for nutrient recovery or urine treatment is not straightforward and is limited by phenomena resulting from high concentration differences if high concentrate product and low concentrate effluent are simultaneously targeted. Electro-oxidation, on the other hand, is naturally insensitive to the target of oxidation and can destroy nitrogen, one of the main nutrients of interest. Electro-oxidation can also produce toxic and unwanted by-products (Radjenovic and Sedlak, 2015). The energy demand of both electro-concentration and electro-oxidation can also vary due to the selected operation parameters, and significantly different nitrogen capture energy efficiencies can be achieved by different operation strategies. Further, the high salinity of source-separated urine is a problem for nutrient use (Johansson et al., 2001).

In this thesis, electro-concentration and electro-oxidation of source-separated urine are further developed and combined to create a novel method for simultaneous treatment and recovery of a nutrient-rich product with decreased salinity.

2 BACKGROUND

2.1 Source-separation and nutrients in urine

An adult human expels all nutrition consumed after extracting energy. Nutrients eaten in food are concentrated mainly into urine which contains 79:47:71% of N:P:K consumed, respectively (Friedler et al., 2013). As urine comprises less than 1 % of produced municipal wastewater (Larsen et al., 2013; Randall and Naidoo, 2018), source-separated urine can be considered the most promising municipal stream for nutrient recovery (Ledezma et al., 2015).

The human metabolism system in kidneys binds ammonium and carbonate into urea, $(\text{NH}_2)_2\text{-CO}$, as a means of nitrogen excretion. Fresh urine contains only urea, which breaks down through ureolysis by indigenous bacterial enzymes within days or weeks. To prevent ureolysis in source-separated urine, collected urine needs to be sterilized immediately or stored in alkaline or acidic environment (Udert and Sarina, 2013), but ammonium typically is a favorable form for nitrogen recovery. Ureolysis releases two parts of ammonium (Total Ammonium Nitrogen, TAN) and one part of inorganic carbon, forcing the pH to rise – while fresh urine is neutral in pH, the pH of ureolysed urine is 8.5-9.5. The rise in alkalinity and pH causes precipitation of calcium and magnesium with phosphates, and very low levels of magnesium and calcium remain after extended storage (Udert et al., 2006).

Urine is high in total salinity and conductivity, it has high sodium, potassium and chloride concentrations and a moderately high organics content. While urine may contain thousands of individual organic molecules, the organic substances comprising the largest concentrations are creatinine, hippuric acid, citric acid and glycine – averaging 85% of oxygen demand (Bouatra et al., 2013). Urine composition and strength changes considerably depending on e.g. diet and levels of hydration, and creatinine is typically used as a calibration component for strength of organic content (Blaszkewicz and Liesenhoff-Henze, 2012). Measured urine compositions before and after ureolysis from literature are presented in Table 1.

Table 1. Source-separated urine measured before and after ureolysis in the literature.

Parameter	Unit	Ureolysed urine													Reference	
		Fresh Urine					Ureolysed urine									
pH	-	6.2	6.3	9	9.1	9	9.1	9	9.1	8.85	8.8	9.6	8.9	9.3	8.69	8.9
EC	mS cm ⁻¹		9.1	-	-	-	-	-	-	35	35.2	25.9	18-23	27.3	-	15.9
Total COD	mg O ₂ L ⁻¹	-	-	-	-	6346	10000	3900	4500	4300	4500	-	4300	4500	4500	2110
Urea	mg N L ⁻¹	-	890	-	89	281	0	-	-	-	50	-	-	-	-	-
NH ₄ -N	mg N L ⁻¹	463	260	5439	4768	6615	8100	4050	4918	4300	1040	4300	3700	2390	1790	
PO ₄ -P	mg P L ⁻¹	800-2000	930	636	417	292	540	210	237	408	350	408	227	208	108	
K	mg L ⁻¹	2737	-	2652	1333	2962	2200	1490	1731	1360	-	1360	1900	1410	897	
IC	mg C L ⁻¹	-	-	-	-	3715	3200	-	-	-	-	-	-	1210	970	
Ca	mg L ⁻¹	233	-	48	24	108	0	7.1	-	5.7-8.6	-	5.7-8.6	17	16	10	
Mg	mg L ⁻¹	119	-	5	14.8	4	0	<5.0	-	0.1-2.3	-	0.1-2.3	0.9	<5	<5	
Na	mg L ⁻¹	3450	-	2976	1613	3219	2600	1850	1969	2085	-	2085	2400	1740	966	
SO ₄ -S	mg SO ₄ L ⁻¹	1315	1610	682	441	1123	1500	210	681	830	910	830	800	778	316	
Cl	mg L ⁻¹	4970	-	7576	2357	5385	3800	3290	3818	3430	-	3430	3400	3210	1830	
Reference		(Ciba-Geigy, 1977)	(Jaatinen et al., 2016)	(Kirchmann and Pettersson, 1994)	(Jönsson et al., 1997)	(Udert et al., 2003)	(Udert et al., 2006)	(Kumke et al., 2012)	(Pronk et al., 2006b)	(Jaatinen et al., 2016)	(Tiettenbom et al., 2007)	(Zamora et al., 2017b)	(Udert et al., 2012)	(Eiter et al., 2013)		

2.2 Nitrogen chemistry

Nitrogen chemistry is complex, with 9 oxidation states (-3 to $+5$), the most stable forms being nitrogen gas (N_2 , 0), nitrate (NO_3^- , $+5$), nitrite (NO_2^- , $+3$) and ammonium ($\text{NH}_3/\text{NH}_4^+$, -3). Nitrogen chemistry is characterized by wide bonding ability (nitrogen can form compounds with all elements except noble gases) resulting from the second electron shell that can be filled or emptied, and the ease of double and triple bonding by the small covalent radius. As a result, nitrogen is a vital component in all organic chemistry and many biological nitrogen reaction pathways exist (Atkins and de Paula, 2006; Zumdahl and DeCoste, 2012). While the atmosphere contains 80% N_2 , forming an essentially limitless supply of nitrogen, living organisms use bound forms of nitrogen, termed fixed nitrogen, which is found mainly as total ammonium nitrogen ($\text{NH}_3/\text{NH}_4^+$, TAN), nitrite (NO_2^-) and nitrate (NO_3^-) (Keeney and Hatfield, 2008). Before human intervention, fixed nitrogen was produced mainly by biological nitrogen fixation, commonly found symbiotically with leguminous plants (Heinonen-Tanski and van Wijk-Sijbesma, 2005). Currently, anthropogenic nitrogen fixation is almost twice as large as biological nitrogen fixation on a global scale (Galloway et al., 2004).

Ammonium-ammonia nitrogen, referred to as TAN, is the oxidation state that is utilized by living cells, being the most important macronutrient by weight on Earth. TAN has a pK_a of 9.25 at 25°C (Stumm and Morgan, 1996) and has significantly different physical properties in ammonium and ammonia form – while ammonium is relatively non-volatile, non-toxic, and has a single charge, ammonia is chargeless, highly volatile and acutely toxic to aquatic life forms, inhibiting oxygen transfer by hemoglobin (Rosca et al., 2009).

2.3 Ammonium bicarbonate crystallization in urine

The ammonium carbonate system is a ternary mixture of ammonia (NH_3), carbon dioxide and water and can precipitate into a multitude of salt mixtures, which mainly compose of three pure substances: ammonium bicarbonate (NH_4HCO_3), ammonium carbonate ($(\text{NH}_4)_2\text{CO}_3$), and ammonium carbamate ($\text{NH}_4\text{CO}_2\text{NH}_2$). All of these compounds dissolve into carbonate/bicarbonate/carbon dioxide and TAN species when dissolved in water, with distinction between ionic forms depending on

the pH and temperature (Kroschwitz and Seidel, 2004). In liquid samples the concentrations are expressed as TAN and total inorganic carbon (TIC) referring to all three ionic forms of carbonate.

Ammonium carbonate salts volatilize before melting when heated, and volatilize readily also from water solution when heated at below 100°C (Darde et al., 2010). High concentrations of ammonium carbonate in solution are challenging as both ions are readily volatilized in non-neutral pH: carbonate volatilises as carbon dioxide in low pH ($\text{pH} \leq 5$) and ammonium volatilizes as ammonia in high pH ($\text{pH} \geq 10$). At pH 7, the solubility of ammonium bicarbonate is reported to range between 11.9g/100g water at 0°C and 59.2g/100g water at 60°C (Kroschwitz and Seidel, 2004), with values of 21g/100g water at 20°C (Perry et al., 2008) and 24.8g/100g water at 25°C (Haynes, 2012). Due to the soluble and volatile nature of ammonium carbonate system, precipitation from a liquid phase is not common, and no references are found in the literature of practical applications. Solubilities of other carbonates are markedly lower with e.g. sodium bicarbonate solubility at 10.3g/100g water at 25°C (Haynes, 2012).

Precipitation is the transfer of solutes into solid form from a dissolved form. There is a driving force for precipitation when a concentration above the solubility of the compound, i.e. supersaturation, is reached. Supersaturation can be achieved by changing the temperature of the solution (most compounds have direct solubility, i.e. solubility increases with temperature), changing the concentration (e.g. through evaporation or membrane processes), adding an antisolvent chemical or changing the pH (solubilities are to varying extents pH-dependent) (Coquerel, 2014). Precipitation of a salt is a complex kinetic process affected by all ionic species in the liquid, temperature, precipitation rates of other precipitates and presence of seeding surfaces or particles (Myerson, 2001). In supersaturated conditions, solubilized species tend to precipitate as this is energetically favoured. However, a critical supersaturation level is required to enable primary nucleation, i.e. formation of new solid surfaces from a liquid phase. As a rule, less supersaturation is required to precipitate on an existing foreign surface and least on a crystal of the solute. In an ideal case, where infinite crystal surface area and contact time are provided, crystallization happens at zero supersaturation, which is the theoretical solubility of the solute. (Beckmann, 2013a; Beckmann, 2013b; Takiyama, 2012)

The rate of concentration change, mixing and seeding parameters can affect solids formation significantly and great care is used in commercial crystallization processes to ensure desired product composition, crystal lattice form and particle size distribution (Beckmann, 2013b). Already crystallized forms are in equilibrium

with the saturated solution around them. During nucleation phase, usually significant amounts of microcrystals are formed, but a process referred to as Ostwald ripening shifts the crystal size distribution towards larger crystals to minimize interface area and free energy of the system. (Coquerel, 2014)

Ureolysed urine composition is naturally favourable for ammonium capture as ammonium bicarbonate: assuming ideal total organics oxidation to inorganic carbon, >90% of ammonia can be coupled with bicarbonate as ammonium bicarbonate in modelled typical synthetic source-separated urine (from Table 1). When concentrating ureolysed source-separated urine, calcium and magnesium species are least soluble and first to precipitate, but their concentration is expected to be very low in ureolysed urine due to precipitation with phosphates triggered by the pH increase during ureolysis. After calcium and magnesium, most species are extremely soluble and only precipitate in very high concentrations or low temperatures. Solubilities of selected pure species are listed in Table 2. It is not directly evident which salt species will precipitate from highly concentrated urine first, as speciation and solubilities have not been modelled at high concentrations or low temperatures.

Table 2. Solubilities of selected salts, adapted from Haynes (2012).

Species	Solubility at 25°C (g/100g H₂O)	Molar solubility at 25°C (mol/L)
NH ₄ HCO ₃	24.8	3.14
NaHCO ₃	10.3	1.23
KHCO ₃	36.5	3.65
NH ₄ CH ₃ COO	150	19.46
NaCH ₃ COO	50.4	6.14
Na ₂ HPO ₄	11.8	0.83
KH ₂ PO ₄	25	1.84
Na ₂ SO ₄	28.1	1.98

Ionic product (IP) and ionic strength (IS) are measures used in evaluating saturation and strength in chemistry. Ionic product is the product of concentrations in a solution, raised to the power of each species' molar ratio in a solid's crystal structure. For a supersaturated compound in a single salt solution, this represents the solubility product of the salt. The ionic product is thus a measure of saturation. Ionic strength is a sum of concentrations of all ions to the power of their charges and is a measure of total salinity of the solution. IP and IS can be used to estimate supersaturation conditions for concentrated urine. (Zumdahl and DeCoste, 2012)

2.4 Electrodialysis and electro-concentration of source-separated urine

An electrochemical cell consists of two solid electrode surfaces immersed in a conductive electrolyte solution and connected through a resistor or a power supply. Depending on the electrolyte and electrode materials, oxidation and reduction reactions can spontaneously occur on the electrode surfaces discharging electrons into the anode and collecting electrons from the cathode surface, respectively, resulting in a current flowing in the electrical wiring as electrons and in the electrolyte as ions. Alternatively, an external power supply can be used to create a potential gradient through the cell, potentially triggering reduction reactions at the cathode and oxidation reactions at the anode. Ions in the electrolyte of an electrochemical cell are subjected to an electric field resulting in migration of anions towards the anode and cations towards the cathode. Migration of ions can be used for separation processes through the use of ion exchange membranes in the cell. Placing anion- and cation exchange membranes in an alternating arrangement between cathode and anode allows for depletion of ions from the source feed into a concentrate feed (see Figure 1). This is called electrodialysis (ED). (Strathmann, 2004; Strathmann, 2010)

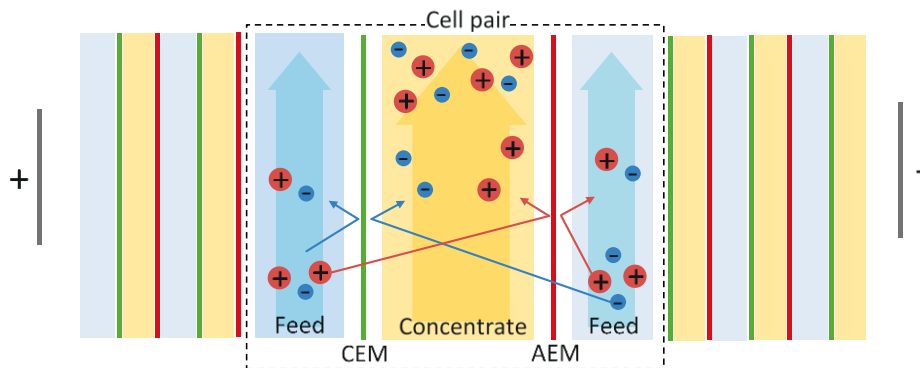


Figure 1. Operating principle of electrodialysis stack: Cations pass through Cation Exchange Membrane (CEM) but are inhibited by the Anion Exchange Membrane (AEM) and remain in the concentrate and vice versa for anions. + = anode, - = cathode.

In an ED electrolyte, the ions experience forces due to convection, electromigration driven by electric potential gradients, and diffusion driven by concentration gradients. The liquid adjacent to a membrane surface forms a boundary layer, in which convection is negligible and only diffusion and migration are typically

considered. The flux of ions is directly linked to the current over the electrodes as each unit of charge moving through the external circuit must be matched by an equal charge moving through the membrane as flux of ions. (Galama et al., 2014; Nikonenko et al., 2002; Strathmann, 2004; Strathmann, 2010)

An ion exchange membrane consists of a porous media embedded with a fixed charge, enabling the integration and movement of opposite charges in the media but excluding same-charged particles from the media (Strathmann, 2004; Strathmann, 2010). Ideally, the co-ion concentration within an ion exchange membrane is zero and counter-ion concentration equals the fixed charge density. As electrical potential gradient is applied, ions move faster in the membrane than in the adjacent boundary layers, forming a concentration depletion in the dilute boundary layer and concentration increase in the concentrate boundary layer (Strathmann, 2004; Strathmann, 2010). Electroneutrality is required in all compartments, including membrane and boundary layers (Galama et al., 2014; Strathmann, 2004). This requirement effectively forms equal co-ion and counter-ion concentration profiles in boundary layers. This effect of concentration difference over the membrane is referred to as concentration polarization and is visualized in Figure 2 (Strathmann, 2004).

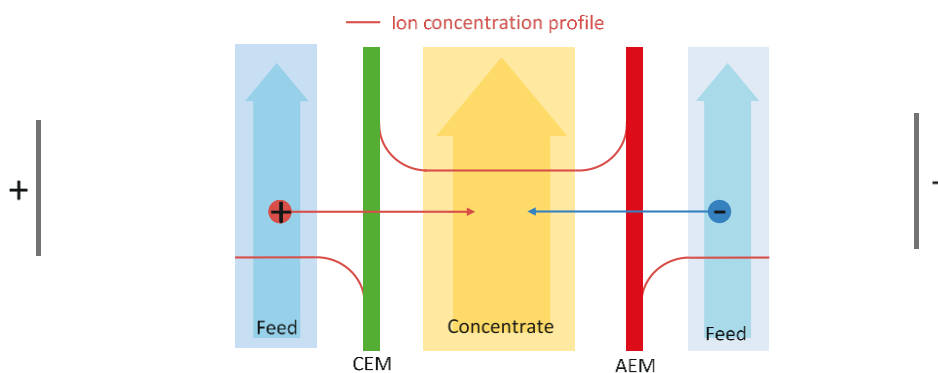


Figure 2. Concentration profiles for cations and anions through a cell pair in a single ion pair system. + = anode, - = cathode.

As current density over the membrane is increased, concentration polarization intensifies until the feed boundary layer transport rate is exceeded, the concentration of ions at the surface drops below a critical value and at that point increased cell voltage no longer provides increased current. This current density is called the limiting current density. If cell voltage is further increased, at some point so called

over-limiting current is reached, in which ion flux through the membrane increases again, consisting partly of hydroxyl-ions and protons from water splitting at the membrane surface. The phenomenon of over-limiting current is not currently fully understood. For practical solutions, current density should always be below limiting current density to retain energy efficiency and to avoid damage to membranes from water splitting. (Strathmann, 2004) Due to the concentration polarization phenomenon, potentially occurring saturation conditions are always first achieved on or in a membrane instead of bulk solution. As the membrane surface is a surface area, potentially facilitating precipitation, the membrane surface is the most likely place where precipitation can occur if electrodialysis is operated close to saturation conditions. This can result in physical damage to membranes due to crystal formation in or on the membrane (Strathmann, 2004).

Concentration to high levels by ED is limited through several phenomena. Firstly, there is an osmotic pressure difference between different concentration compartments, resulting in water flow across membranes (Ippersiel et al., 2012; Mondor et al., 2008; Strathmann, 2004). Secondly, water moves across with ions as bound water, specific to the ion type moving through the membrane (Strathmann, 2004). Thirdly, capillaries with surface charges exhibit water flow in an electric field due to the formation of a charged layer next to the capillary surface. This layer then experiences a force from the electric field and moves through the capillary, a phenomenon called electro-osmosis. (Strathmann, 2004) Fourthly, as concentrations of ions grow large, activities of their chargeless speciation forms (e.g. NH_3 for NH_4^+) and ion pairs (such as NH_4HCO_3) can form a significant concentration. The movement of chargeless species is not affected by the electric field or blocked by charge in the ion exchange membranes, and they can therefore diffuse through membranes forming potentially significant streams if their concentrations are high (Thompson Brewster et al., 2017a). These phenomena together result in plateauing of concentrate concentrations with ED, limiting the electro-concentration achievable with a single unit. Multiple units in series can be used to overcome this effect. (Strathmann, 2004) Concentration to levels close to saturation through electrodialysis is not common in the literature for the reasons listed above.

2.5 Modelling electro-concentration

To model an electro-concentration cell, it is necessary to calculate the ionic speciation in the bulk, boundary layer and inside the membrane for each chamber and account for (i) the relationship between mass transfer based on charge transport of ions with ionic activity correction; (ii) pH effects to speciation including current transport by H^+ and OH^- ; (iii) speciation effects including ion-pairing and acid-base dissociation, and (iv) total cell voltage, including the effect of solution resistance, membrane resistance and electrode resistance. This is achieved by Ordinary Differential Equation (ODE) relaxation operated in Matlab2014b in combination with speciation model built with C and operated by MEX -executable (Flores-Alsina et al., 2015). A Nernst-Planck equation governs the ionic flux perpendicular to the membrane and the model takes into account 71 possible ionic species based on 10 components: sodium, potassium, ammonium, chloride, acetate, calcium, magnesium, carbonate, sulphate and phosphate.

The majority of previous electrochemical models have been single salt models (Lee et al., 2006; Mohammadi et al., 2005; Moon et al., 2004; Ortiz et al., 2005; Tanaka, 2013), or incorporated up to three ions (Kim et al., 2012; Kraaijeveld et al., 1995; Nikonenko et al., 2003). Some models have considered pH (Kraaijeveld et al., 1995; Nikonenko et al., 2003; Nikonenko et al., 2010; Zabolotskii et al., 2013), but no work incorporated a full physico-chemical model incorporating ion speciation with pH and complex solution that are used in physical modelling (Flores-Alsina et al., 2015; Solon et al., 2015). By meticulously calculating all species available for mass transport on membranes, phenomena including current leakage (H^+ and OH^- transport), competitive ion transport, and ionic activity and ion-pairing can be measured, quantified and predicted. Urine electro-concentration has not been modelled previously using a full physico-chemical model.

2.6 Electro-oxidation

In an electrochemical cell, the anode acts as an electron acceptor, forming an electron sink for oxidation reactions on its surface. A terminal electron acceptor is reduced at the cathode, acting as a sink for electrons produced at the anode. Oxygen is considered an excellent sustainable choice for a terminal electron acceptor as it is readily available from atmosphere, has a positive redox potential (1.23V vs SHE at pH 0), is non-toxic and results in water as the end product (Bratsch, 1989; Kannan

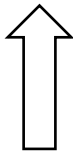
and Gnana kumar, 2015; Logan and Wiley, 2008; Rabaey et al., 2010). However, the solubility of oxygen may be limiting. Another option is to use water as an electron acceptor, resulting in hydrogen gas as an end product. Electro-oxidation reaction pathways at the anode are a function of the electrode material, applied potential, current density, and the electrolyte medium (Martínez-Huitle et al., 2015). Electro-oxidation can proceed through various pathways including (i) via direct electron transfer at the electrode surface, (ii) oxidation with chemisorbed (active anode) or physically sorbed (passive anode) hydroxyl radical, created from water electrolysis at the anode ($M(OH\cdot)$), (iii) oxidation through ROS, and (iv) oxidation through RCS, most notably hypochlorite, when chloride is present (Brillas and Martínez-Huitle, 2015). The ROS are formed as physi-sorbed ($M(OH\cdot)$) reacts with water and include H_2O_2 and O_3 , which have longer lifetimes and can diffuse away from the boundary layer. (Brillas and Martínez-Huitle, 2015)

Anode materials have a large effect on the anodic reactions and experienced oxygen evolution. Most metals and materials (such as iron, copper, aluminium, etc.) are excluded as anodic materials in oxidative electrochemistry as they are not stable but release cations in exchange for electrons - these metals can be used in applications utilizing sacrificial anodes, such as electroplating (Faulkner and Bard, 2008). Most common anodic materials are dimensionally stable materials, that can support oxygen evolution on their surface without degradation of the anode material, and these include e.g. titanium, platinum, different forms of pure carbon, iridium and ruthenium oxides (often grouped as Dimensionally Stable Anodes DSAs), lead oxides, tin and antimony oxides and boron doped diamond (BDD). Electrode materials are divided into active and passive anodic materials based on the behaviour and adsorption energy of formed hydroxyl radicals during water oxidation. Active anodes interact more strongly (chemisorption) with the formed $OH\cdot$ -radical, resulting often in more selective oxidation paths of e.g. organic molecules on the electrode surface. Passive anodes interact less strongly with the hydroxyl radical (physisorption), and can allow nonselective oxidation of organics and result in complete oxidation of organics to CO_2 (Martínez-Huitle et al., 2015). This non-selective nature of BDD and other passive anodes has granted BDD-oxidation the nomenclature Advanced Electrochemical Oxidation Process (EAOP) compared to traditional Electrochemical Oxidation (EO) (Brillas and Martínez-Huitle, 2015). A list of the most common anode materials used in electro-oxidation is presented in Table 3.

In addition to the anode material, also the electrolyte media has a strong effect on electro-oxidation pathways. Firstly, the overall conductivity of the media

determines the overall applicability of electrochemical technologies as low conductivity increases electrode potentials and energy demand. Conductivity can also change the current densities applicable and the resulting reaction regimes which can be mass transfer limited or current density limited, depending on the availability of ions on the surface. The buffer capacity and pH of the media determines the pH at the anode surface, which is an important parameter in the speciation of radicals and effects the resulting oxidative pathways. Finally, the composition of the media determines the formation of radicals that can dominate electrochemical oxidation. Especially chloride and bromide form reactive species (specifically RCS) that are extremely powerful oxidants and biocides. (Brillas and Martínez-Huitle, 2015; Comninellis and Chen, 2010; Ganiyu et al., 2019; Martínez-Huitle et al., 2015) While DSAs are used frequently in electro-oxidation, the following chapters focus on the oxidation chemistry on BDD-electrodes.

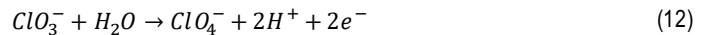
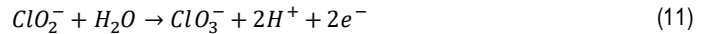
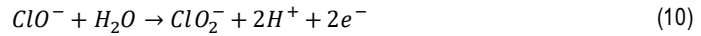
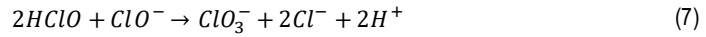
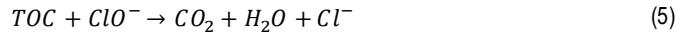
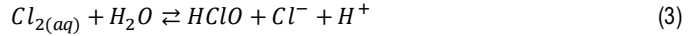
Table 3. Active and passive anode materials based on their oxygen evolution potential in acidic media. The arrow in the rightmost column represents a gradual change from physisorption to chemisorption. (Comninellis and Chen, 2010; Martínez-Huitle et al., 2015).

Anode Type	Composition	Oxygen evolution potential (V vs. SHE)	Adsorption enthalpy of M(OH·)
Active	DSA, RuO ₂ -TiO ₂	1.4-1.7	
	DSA, IrO ₂ – Ta ₂ O ₅	1.5-1.8	
	Ti/Pt	1.7-1.9	
	Carbon and Graphite	1.7	
Passive	Ti/PbO ₂	1.8-2.0	
	Ti/SnO ₂ -Sb ₂ O ₅	1.9-2.2	
	p-Si/BDD	2.2-2.6	
			Physisorption of M(OH·)

2.6.1 Electro-oxidation of chloride

While the specific oxidation pathways of chloride in different pH levels in varied media is a subject of ongoing research, a generally agreed outline can be defined based on existing literature. Urine contains an inherently high concentration of chloride, and thus chloride oxidation chemistry is an integral part of urine oxidation chemistry. Chloride ion is first directly oxidized at the anode to yield soluble chlorine (Eq. 1). If the local equilibrium concentration is exceeded, bubbles of chlorine gas can form. Otherwise, chlorine diffuses to the solution and reacts with chloride to form trichloride ion (Eq. 2) and with water to form hypochlorite (also called active chlorine AC) (Eq. 3). Active chlorine can further oxidize other species in the media

(Eq. 5), it can be reduced at the cathode (Eq. 6), be reduced by the hydrogen produced at the cathode (Eq. 9) or react with itself to form chloride (Eq. 8). Active chlorine can also further oxidize on the anode to form ClO_2^- , ClO_3^- and ClO_4^- ions (Eqs. 10-12). (Brillas and Martínez-Huitle, 2015; Comninellis and Chen, 2010; Ganiyu et al., 2019; Martínez-Huitle et al., 2015)



The chloride oxidation chemistry can be current controlled or mass transport controlled, depending on the applied current density, mixing and chloride concentration in the media. Based on these parameters, the oxidation pathways can be altered significantly. The most typically reported reaction is chloride diffusing as hypochlorite into the bulk, but it can also accumulate as Cl_2 gas and be removed as bubbles or react immediately further on the anode to perchlorates (Comninellis et al., 2008; Martínez-Huitle et al., 2015). The oxidation pathways of chloride in urine in different conditions has not been systematically studied.

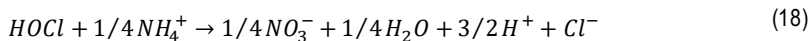
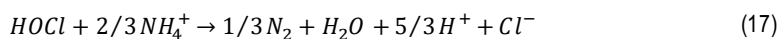
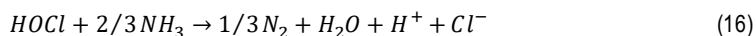
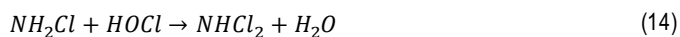
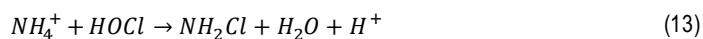
Formation of chlorates: ClO_3^- (chlorate) and ClO_4^- (perchlorate), is a serious impediment to BDD electro-oxidation of chloride containing wastewaters as they both are persistent toxins and harmful to aquatic environment and human health (Garcia-Segura et al., 2015; Radjenovic and Sedlak, 2015). Methods for electro-oxidation with BDD that would not develop chlorates are investigated, but also

alternative anode materials should be considered (Cotillas et al., 2019; Garcia-Segura et al., 2018; Herraiz-Carboné et al., 2020).

2.6.2 Electro-oxidation of ammonium

TAN can be oxidized on a BDD anode through direct oxidation on the anode surface, and this type of oxidation can be described similarly to oxidation of organic material (see Chapter 2.6.3). Oxidation rate can be limited by the applied current or mass transfer to the surface, depending on the applied current and TAN concentration. If the medium contains chloride, an oxidation pathway titled “breakpoint chlorination” can be observed. Breakpoint chlorination is a chemical oxidation phenomenon for TAN and organics, mostly studied in bulk water with addition of active chlorine in neutral pH. It is often cited as the principle behind RCS-mediated TAN oxidation also in electro-oxidation, but also competing theories have been suggested, and as boundary layer phenomena can dominate electro-oxidation chemistry, the details of TAN electro-oxidation are most likely more complicated than the textbook breakpoint chlorination suggests. Alternatives to breakpoint chlorination mechanisms for electrochemical TAN oxidation in chloride containing media have been suggested with different type of local chemistry and pathways on the BDD anode (Gendel and Lahav, 2012).

In breakpoint chlorination, active chlorine ($\text{Cl}_2/\text{HOCl}/\text{OCl}^-$) reacts with TAN to form chloramines (monochloramine, dichloramine and trichloramine), which can further react to form N_2 , oxidize to NO_3^- or reduce back to TAN at the cathode. Typical breakpoint chlorination pathways are presented in equations 13-18. Breakpoint chlorination only proceeds, if RCS/TAN -ratio is above a water specific threshold (typically 1.5:1 Cl_2/TAN), below which chloramines remain inert in the water (Kobylnski and Bhandari, 2010; Randtke, 2010).



The end product of TAN breakpoint chlorination is N₂ gas. However, nitrite and nitrate are potential by-products of urine electro-oxidation that can have unwanted health effects in drinking water or in aquatic environment (Ward et al., 2005).

TAN electro-oxidation in urine differs from organics electro-oxidation, with occasionally separate reaction rates and affinities that can pose challenges for the practical implementation of electro-oxidation as a treatment technology when aiming to oxidize TAN and organics (Zöllig et al., 2017). A better understanding of the TAN oxidation pathways could enable selective organics oxidation from urine without TAN oxidation, allowing for development of novel simultaneous urine treatment and nutrient recovery technologies.

2.6.3 Electro-oxidation of organic material

Hydroxyl radical is known to be a primary oxidant for most organic molecules, and as BDD favors formation of weakly absorbed BDD(OH·) radicals, they are readily scavenged by organic molecules to form oxidized products (Ganiyu et al., 2019). Organic molecules can also be readily oxidized by variety of RCS on the anode or in the bulk medium (Martínez-Huitle et al., 2015). Due to the variety of oxidation pathways, organic material is expected to be oxidized robustly on BDD whenever the anodic potential is high enough to produce BDD(OH·) radicals regardless of the presence of chloride or other species in the medium, even though they can alter the specific pathways and potentially decay rate. Some recalcitrant organic substances, such as fulvic and humic acids and chlorinated organic substances can remain inoxidized by BDD(OH·) (Zöllig et al., 2017). As an example for organic matter oxidation at BDD, one reaction pattern for pure acetic acid oxidation through BDD(OH·) is presented in equation 19, acetic acid presenting a typically refractory organic compound (Kapalka et al., 2008).



2.7 Electrochemical concentration and oxidation of source-separated urine

Nitrogen capture from source-separated urine using electrochemical technologies can be divided into stripping, electrodialysis, electro-concentration, and microbial

electrochemical technologies (METs). Electrodialysis of human urine has been studied by Pronk et al. (Pronk et al., 2006b) aiming for urine treatment and reaching 93 % ammonium removal into concentrate using a conventional electrodialysis setup. The method was tested also in pilot scale with growth tests in agriculture (Pronk et al., 2007). The focus of these studies was in removal of pharmaceuticals, removal efficiency of ions and long term operation in pilot scale. Electrodialysis has also been studied with human urine using a membrane contactor -type ammonium capture through gas phase (Pronk et al., 2006a) – an approach that has later been applied to other streams, such as swine manure. Electrodialysis has further been studied for chemically and biologically pretreated urine as a proposed method for space station urine treatment, capturing nutrients in a liquid form (De Paepe et al., 2018). Electrodialysis is a mature and well understood technology but as a single technology has limitations for direct applicability for urine treatment and TAN recovery. Urine has large organic content, can contain precipitating salts and can foul membranes (Maurer et al., 2006; Udert et al., 2006). Removal of ionic content from solution to low levels through electrodialysis is difficult as current efficiency decreases and energy demand increases with lower ion concentrations. Electrodialysis does not separate salts in urine but concentrates all ionic components, resulting in a high sodicity product, potentially problematic for sustainable nutrient use.

A two-chamber electro-concentration cell has been used for ammonium recovery from human urine with subsequent gas stripping and acid absorption (Luther et al., 2015) or subsequent transmembrane chemisorption using two reactors (Rodríguez Arredondo et al., 2017). Similar approach for urine has also successfully been used in a single reactor (Liu et al., 2020; Tarpeh et al., 2018). Electro-concentration -type treatment has also been combined with electro-oxidation for treating mixed latrine wastewater: a CEM separated anodic chamber was used for acidic electro-oxidation and TAN was concentrated simultaneously through the membrane to the cathode as a nutrient rich concentrate (Yang et al., 2019).

Microbial electrochemical technologies combine microbially-mediated reactions with electrode interactions and external electrical circuits. The most studied MET is microbial fuel cell (MFC), in which biological redox reactions producing energy through breaking of organic compounds are separated into a biological oxidation reaction at the anode and typically an abiotic reduction reaction at the cathode, linked through an electrochemical cell to produce electrical current. In MFCs, organic molecules are oxidized in anaerobic conditions by electrochemically active micro-organisms that are often physically attached onto an electrode (the anode) and

capable of extracellular electron transfer. The electrons are transported through electrical circuit to the cathode, where a terminal electron acceptor, such as oxygen, accepts them and gets reduced. Equal charge is transported from the anode to the cathode through the electrolyte media as ions to close the circuit. (Freguia, 2007; Ledezma et al., 2015; Logan et al., 2006; Logan, 2008; Rabaey et al., 2010) Urine has been studied as a MFC feed for combined energy production and nutrient capture (or self-powered nutrient capture). The Bristol BioEnergy Centre has a long history in METs and has studied use of urine in several MFC studies (Chouler et al., 2016; Ieropoulos et al., 2012; Ieropoulos et al., 2013; Walter et al., 2016). European centre of excellence for sustainable water technology, WETSUS, are also pioneers in the field and a two chamber MFC has been developed, where ammonium is forced through a CEM to the cathode for subsequent capture (Kuntke et al., 2011; Kuntke et al., 2012; Kuntke et al., 2014; Kuntke et al., 2016b). The bioelectrochemical technologies for nutrient capture from urine have further been applied also in long-term pilot scale experiment (Zamora et al., 2017a; Zamora et al., 2017b). At the University of Queensland urine has been studied in a three chamber concentration MFC setup to retrieve ammonium as a solid from a MFC-produced electro-concentrate produced in the MFC (Ledezma et al., 2015; Ledezma et al., 2017).

Urine electro-concentration systems using transmembrane chemisorption or stripping show promise but have not so far advanced beyond pilot scale or into consumer products. No single technological hurdle can be pointed as multiple methods for ammonium capture and separation are available from urine in the current research literature. Nutrient production and wastewater treatment however pose no serious economic incentives to invest into novel urine infrastructure, and price of electrochemical solutions for urine treatment most likely holds the technology back (Chaplin, 2019).

Wastewater electro-oxidation has been studied especially as a means of rapid technology for a latrine wastewater treatment. This technology shows that both active and passive anodes can be used to sanitize mixed feces and urine (latrine water), and typically both TOC and TAN are oxidized at similar timeframes rapidly decomposing to N_2 and CO_2 , depending on the parameters (Cho et al., 2014a; Cho et al., 2014b; Cho and Hoffmann, 2014; Chung et al., 2018; Cid et al., 2018; Huang et al., 2016; Jasper et al., 2016; Jasper et al., 2017; Yang et al., 2019). Urine electro-oxidation on BDD and DSA electrodes has been studied in a series of experiments (Zöllig et al., 2015c; Zöllig et al., 2015b; Zöllig et al., 2017), where simultaneous TOC and TAN oxidation were detected in most cases, but in some experiments, TOC was oxidized before TAN, due to Cl oxidation. In all the oxidation studies

mentioned, chlorate and perchlorate formation were recognized a major problem facing electro-oxidation up-scaling. There are several suggestions for future research and applications to overcome this problem. These include (i) process design to target electro-oxidation as pre- or post-treatment or as an integrated part to mitigate toxin production; (ii) novel BDD-forms and subsequent BDD-coatings, that inhibit chlorate or perchlorate formation, or (iii) development of new materials, such as $\text{TiO}_{2-x}\text{NTA}$ and Ti_4O_7 which also produce less chlorates. Cathodic chlorate reduction is also viable and happens on, e.g. Rh, Pt, Sn, Cu and Ni, cathodes and reactor configurations utilizing such cathodes can mitigate production of toxins. Chlorate precursor, RCS, can be quenched on the anode before they react further and the most efficient quencher is hydrogen peroxide which can be created at the cathode for instance using the electro-Fenton process. Short treatment times and anodic potential optimization can also mitigate or eliminate chlorate formation, while achieving wanted electro-oxidation results. (Garcia-Segura et al., 2018; Yang, 2020).

3 AIMS AND HYPOTHESES OF THE STUDY

The overall aim of the study was to develop a novel electrochemical process for nitrogen capture from source-separated urine as a nutrient product, which could simultaneously act as a treatment method. The research was built on previous concepts developed in microbial electrochemical technologies research for source-separated urine, which combine biological oxidation and electro-concentration. The objectives included proof-of-concept for electro-concentration of source-separated urine for solid ammonium bicarbonate crystal formation and understanding the limitations of the process through modelling. Additional objectives included development of selective electro-oxidation of organic species in urine over ammonium via reagent-free pH control and combining electro-concentration and electro-oxidation to produce a tailored liquid nutrient product. Based on the background given in Chapter 2, the specific aims and hypotheses of the study are as follows:

To capture ammonium from source-separated urine as solid ammonium bicarbonate through electro-concentration (I)

Ammonium and bicarbonate form the two ionic species in ureolysed urine with the highest concentrations, and it was hypothesized that they could be electro-concentrated to form a solid precipitate that would allow reagent-free nitrogen capture from source-separated urine. The solubility of ammonium bicarbonate in highly saline environments and low temperatures relevant for the process is not known from literature or modelling, and experimental measurements are needed to enable analysis on limits and feasibility of this approach. The results are expected to resolve new ways of utilizing electro-concentration for nitrogen capture from urine and act as a proof-of-concept for recovering solid ammonium bicarbonate as a nutrient product from urine using electro-concentration.

To optimize electro-concentration parameters through modelling for high ammonium bicarbonate concentrations (II)

Mass transport of ions and water, pH, current density, feeding parameters and reactor configuration form a complex relationship in urine electro-concentration. High ionic strengths suppress ionic activities of ammonium and bicarbonate and can increase ion-pairing and diffusive losses through membranes in the system. It was hypothesized that a model-based analysis could reveal the ionic speciation and flows present in the electro-concentration system and allow optimization of parameters to maximize the concentrations of TAN and bicarbonate in the concentrate.

To determine the effect of anodic pH on relative TAN and TOC oxidation rates (III)

Electrochemical oxidation of organic material (TOC) in urine that is required to ensure a safe nutrient product typically also removes nitrogen, present as TAN. It was hypothesized, based on literature and previous experiments, that the oxidation of organics is based on an oxidation pathway that is independent of anodic pH, while the ammonium oxidation is linked with the pH on the anode and that in acidic pH level TAN is preserved. By electrochemical reactor design and optimizing parameter settings, it could be possible to implement electro-oxidation with acidic anodic pH, potentially inhibiting TAN oxidation and preserving TAN for further recovery.

To enable $\text{Na}^+/\text{NH}_4^+$ separation with electrochemical pH control using a double reactor electro-concentration and electro-oxidation system (IV)

TAN is present as an uncharged or charged species ($\text{NH}_3/\text{NH}_4^+$) in water depending on the pH (pK_a 9.25). Uncharged particles, like NH_3 , are inert to movement via the electromotive force. It was hypothesized that by applying alkaline conditions, TAN will not be concentrated by electro-concentration, allowing selective removal of other cations, such as sodium, from source-separated urine and subsequent TAN recovery. The reagent-free operating principles of electrochemical pH-control (III), could enable selective $\text{Na}^+/\text{NH}_4^+$ separation and tailoring of nutrient product properties as well as simultaneous treatment via electro-oxidation.

4 SUMMARY OF MATERIALS AND METHODS

This summary lists the feeds, reactor design, analytical and modelling methods used in this research. A more detailed description of methods used are available in Publications I-IV.

4.1 Feed composition

Synthetic urine was utilized in all the studies (I-IV) and real source-separated urine was also used in one of them (III). A series of synthetic urine solution recipes were used in this study based on investigations at the Swiss Federal Institute of Aquatic Science and Technology (EAWAG), a literature survey of source-separated urine samples (see Table 1), the Human Urine Metabolome and source-separated urine collected at the Advanced Water Management Centre at the University of Queensland, Australia. The different synthetic recipes used (I-IV) are presented in Table 4 and components measured in feeds in different Publications in Table 5. Four different synthetic urine recipes were used: Synthetic urine representing ureolysed urine, where acetate represents organic content (ACE); Synthetic urine representing ureolysed urine, omitting organic content (NO ACE); Synthetic urine representing ureolysed urine where organic matter has been completely digested to carbon dioxide, CO₂ (ABC); and Synthetic urine representing ureolysed urine with organic content as organic species based on the Human Urine Metabolome (FEED).

Table 4. Synthetic urine recipes used in different Publications. Units in g L⁻¹, if not otherwise mentioned. See Chapter 4.1. for explanation on different feed compositions.

Chemical	Formula	ACE (I, II)	NO ACE (I, II)	ABC (I, II)	FEED (III, IV)
Ammonium Hydroxide	NH ₄ OH (25% sol)	13 mL L ⁻¹	13 mL L ⁻¹	3.5 mL L ⁻¹	13.8 mL L ⁻¹
Ammonium Bicarbonate	NH ₄ HCO ₃	21.4	21.4	41.2	22.14
Ammonium Chloride	NH ₄ Cl	n.a.	n.a.	n.a.	0.48
Sodium Chloride	NaCl	3.6	3.6	3.6	2.69
Potassium Chloride	KCl	4.2	4.2	4.2	4.1
Sodium Dihydrogen Phosphate	NaH ₂ PO ₄ (anhyd)	2.1	2.1	2.1	2.4
Disodium Sulphate	Na ₂ SO ₄ (anhyd)	2.3	2.3	2.3	2.41
Creatinine	C ₄ H ₇ N ₃ O	n.a.	n.a.	n.a.	2.3
Hippuric Acid	C ₉ H ₉ NO ₃	n.a.	n.a.	n.a.	0.88
Citric Acid	C ₆ H ₈ O ₇	n.a.	n.a.	n.a.	0.88
Glycine	C ₂ H ₅ NO ₂	n.a.	n.a.	n.a.	0.17
Ammonium Acetate	NH ₄ CH ₃ COO	9.6	n.a.	n.a.	2.06

n.a. = not added

Table 5. The real concentrations in synthetic and real urine feed used in different Publications, units in mmol L⁻¹.

Component	NO ACE (I, II)	ACE (I, II)	ABC (I, II)	FEED III (III)	FEED IV (IV)	REAL URINE (III)
TAN	444	568	568	522±40	470±35	197±3
PO ₄ ³⁻	18	18	18	18±2	29±1	5.1±0.9
K ⁺	56	56	56	70±6	70±3	10.4±0.3
Na ⁺	111	111	111	117±8	113±4	27.6±1.0
Cl ⁻	118	118	118	92±5	164±7	24.7±0.8
SO ₄ ²⁻	16	16	16	15±2	19±1	3.7±0.3
TOC	n.a.	n.a.	n.a.	286±46	187±11	114±17

n.a. = not added

4.2 Reactor design and equipment

The laboratory experiments for all Publications were conducted using the same set of six custom built acrylic reactors (constructed by University of Queensland engineering workshop) consisting of three or two acrylic frames, forming three or two parallel compartments, anodic, (middle), and cathodic, of 70 mm x 50 mm x 70 mm each (see Figure 4). CEM (CMI-7000 Membrane International Inc.) was used in all Publications to close the anodic compartment, and AEM (AMI-7001, Membrane International Inc.) was used in Publications I, II and IV to close the cathodic compartment. A Biologic VMP-3 potentiostat was used in all Publications to power and measure the experiments. A graphite rod (Element14, Australia) and graphite granule (Graphite Sales Inc., USA) anode was used in Publications I and II, and a BDD plate anode (Condias Diachem) in Publications III and IV. A stainless-steel mesh cathode was used in all experiments. An Ag/AgCl 3M NaCl reference electrode (BASi, USA) was used in the anodic chamber in Publications III and IV. Online pH sensors were used to monitor anodic and cathodic pH levels: Endress+Hauser Liquisys CPM253 for Publications I and II and Endress+Hauser Liquiline CM448 with Orbisint CPS11D for Publications III and IV). Table 6 lists differences in experimental setups between the Publications. Figure 3 presents reactor schematic diagrams utilized in Publications III and IV.

Table 6. Differences in experimental design between Publications.

Parameter	Publication I	Publication II	Publication III	Publication IV
Number of chambers	3	3	2	3
Number of experiments	13	3 + simulations	19	28 (6 settings)
Applied current density, A m ⁻²	40-100	0-150	100	40-100 and 0-23
Feed	3 different synthetic urines	2 synthetic urines + simulations	Synthetic urine and real urine	Synthetic urine

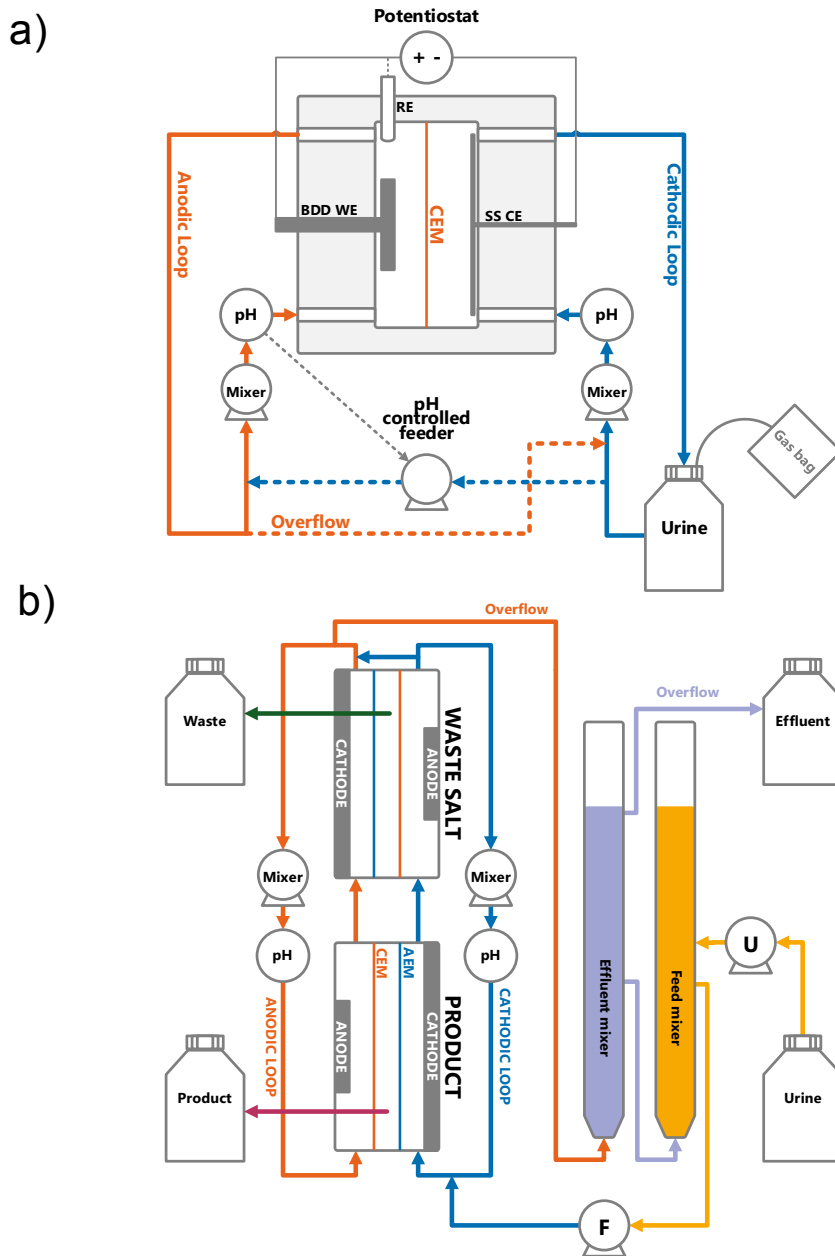


Figure 3. a) Flow diagram of the two-chamber reactor utilized in Publication III (Publication III, Fig 1a), and b) Flow diagram of the double three-chamber reactor utilized in Publication IV (Publication IV, Fig 1). CEM = Cation Exchange Membrane, AEM = Anion Exchange Membrane, BDD = Boron Doped Diamond, WE = Working Electrode, SS = Stainless Steel, CE = Counter Electrode. U = Urine Feed Pump, F = Loop Feed Pump.

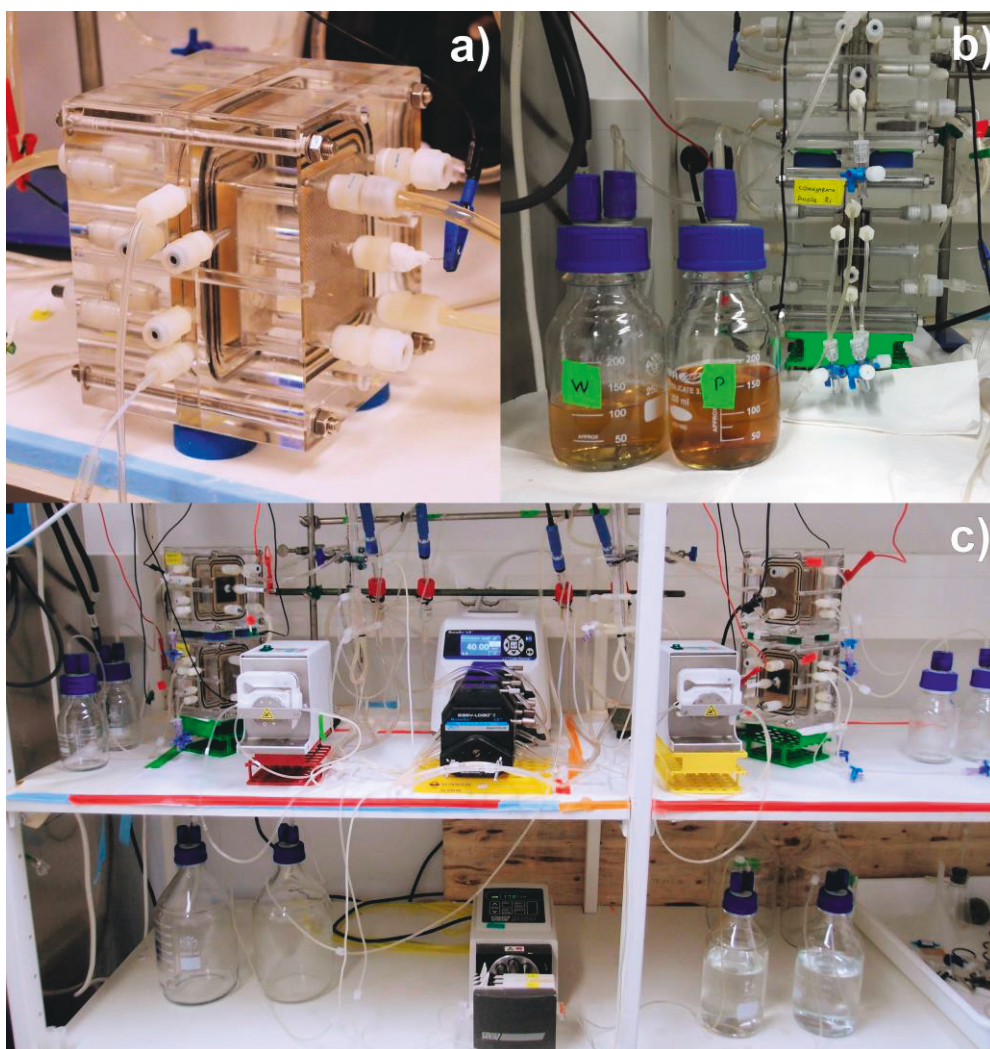


Figure 4. a) Assembled three chamber reactor used in Publications I, II and IV (the same reactor was used without the middle chamber in Publication III), b) close-up of a double-reactor configuration showing collected product and waste concentrates in Publication IV, and c) overview of laboratory setup used in experiments done for Publication IV showing two parallel double reactor configurations.

4.3 Sample analysis

Samples were analyzed for pH and conductivity using sampling probes (all Publications) and for daily monitoring (Publications I and II) using chloride and ammonium test kits (Merck 101807, Merck 114752). Samples were analyzed for Publications I and II by University of Queensland Advanced Water Management Centre Analytical Services Laboratory using Inductively Coupled Plasma Optical Emission Spectroscopy (ICP-OES) for Na, K, Ca and Mg (Perkin Elmer optima 7300DV); Flow Injection Analysis (FIA) for NH₄, NO₃, NO₂ and PO₄ (Lachat QuickChem8500), Ion Chromatograph for Cl (Dionex ICS-2100) and Total Organic Carbon analysis for TOC and TIC (Shimadzu TOC-L CSH TNM-L TN). For Publications III and IV samples were analyzed using ion chromatography for cations and anions (Dionex IC-120 and Thermo Scientific ICS-1600) and Total Organic Carbon analysis for TOC and TIC (Shimadzu TOC-5000 in Publication III and TOC-V CPH in Publication IV). For analysis, samples were filtered using a 0.45 µm syringe filter and stored in a fridge for maximum of 4-7 days either diluted (Publications I and II) or undiluted (Publications III and IV).

4.4 Modelling

The model used in Publication II was operated on Matlab 2014b, combining C-code executable functions (MEX-files) with Matlab ordinary differential equations (ODEs), and is based on earlier work by Thompson Brewster et al. (2017b) and Flores-Alsina et al. (2015). The model comprised of 10 components: sodium, potassium, ammonium, chloride, acetate, calcium, magnesium, carbonate, sulphate and phosphate, and 71 possible ionic species from these components. For more detailed information on the model execution and function, please see Publication II and its supplementary materials.

The model was calibrated based on one set of results from the laboratory experiments and the calibrated model was validated on a parallel set of results from the laboratory experiments with altered parameters. A sensitivity analysis was performed to the validated model to evaluate its stability for parameter change.

5 SUMMARY OF RESULTS AND DISCUSSION

To treat source-separated urine and create a nutrient product of the nitrogen within, several separate challenges need to be addressed. Nitrogen needs to be concentrated or ideally separated as a pure substance. Urine also contains organic loading that should be removed to lower environmental impact of the effluent, and salinity, that is not wanted in a nutrient product. Electro-concentration can separate nitrogen into a concentrate product and in ideal cases also achieve conditions for supersaturations for ammonium separation as a solid salt. Electro-oxidation can remove organic loading in urine, and optimization of the reactor configuration and operation allows methods for selective organics oxidation without nitrogen destruction. Combined electro-oxidation and electro-concentration can form a urine treatment process, concentrating nitrogen into a nutrient product simultaneously reducing the product salinity through selective sodium diversion using reagent-free pH-controlled electro-concentration. The following chapters summarize the results and main findings in Publications I-IV in relation to the aims and hypothesis of the thesis described in chapter 3. More detailed description of the findings can be found from the original Publications (I-IV). This section also provides discussion on the topic.

5.1 Electro-concentration and ammonium precipitation

Urine electro-concentration is a form of electrodialysis and faces similar potential challenges: large concentration gradients, buffer capacity depletion, precipitation and membrane damage, as well as limiting currents (Strathmann, 2010). In Publication I, a series of electro-concentration tests with varied current densities and feed characteristics were performed to find parameters determining limits of electro-concentration and supersaturation for the formation of a solid nutrient product. In Publication II, a similar system was modelled to further find optimal ways and limiting factors of electro-concentration.

5.1.1 Nitrogen recovery via electro-concentration reaches a plateau (I, II)

In the three-chamber cell reactor utilized in Publications I, II and IV, the concentration cell in the center was not stirred or replenished but overflowed freely to a collection bottle. The overflow was due to volume increase due to water flow into the concentration chamber. As explained in Chapter 2, water enters middle chamber through various methods, the two most important of which are osmosis and ion bound water. Osmosis refers to the preferential diffusion of water from dilute to concentrate through a semipermeable membrane, which causes a water flux through the membrane in relation to the concentration difference over the membrane, diluting the concentrate. Ion bound water refers to a hydrated radii around an ion that is transported with the ion through the membrane, creating a mechanistic link with water flux and ion flux to the concentrate (Pronk et al., 2006b). Both mechanisms increase water flux as ion flux increases, reducing the increase in the concentrate chamber concentrations. Additionally, higher concentrations in the concentrate chamber increase also concentrations of uncharged ion-paired species, which can migrate through charged membranes (phenomenon titled back migration or back diffusion) and opposite to the electric field, lowering the attainable peak concentrations in the nutrient product (Thompson Brewster et al., 2016).

As synthetic urine was electro-concentrated and when a steady feed Hydraulic Retention Time (HRT) was used, a similar concentrate strength was formed regardless of the utilized current density (in the range 40 – 100 Am⁻²) or feed composition (Publication I). A representation of the reached electric conductivities and measured ion concentrations in the electro-concentration studies are presented in Figure 5 (Publication I). The ionic conductivity forms a plateau over all experiments, while ionic strength (IS), a compound measure describing the overall salinity, does show an increasing trend as current density is increased. This discrepancy implies that while ion concentration is increasing, the increase does not contribute towards increase in conductivity, which could imply the increase of uncharged species – a result to be verified – as for single salt species much higher concentrations are required for conductivity plateauing (Atkins and de Paula, 2006).

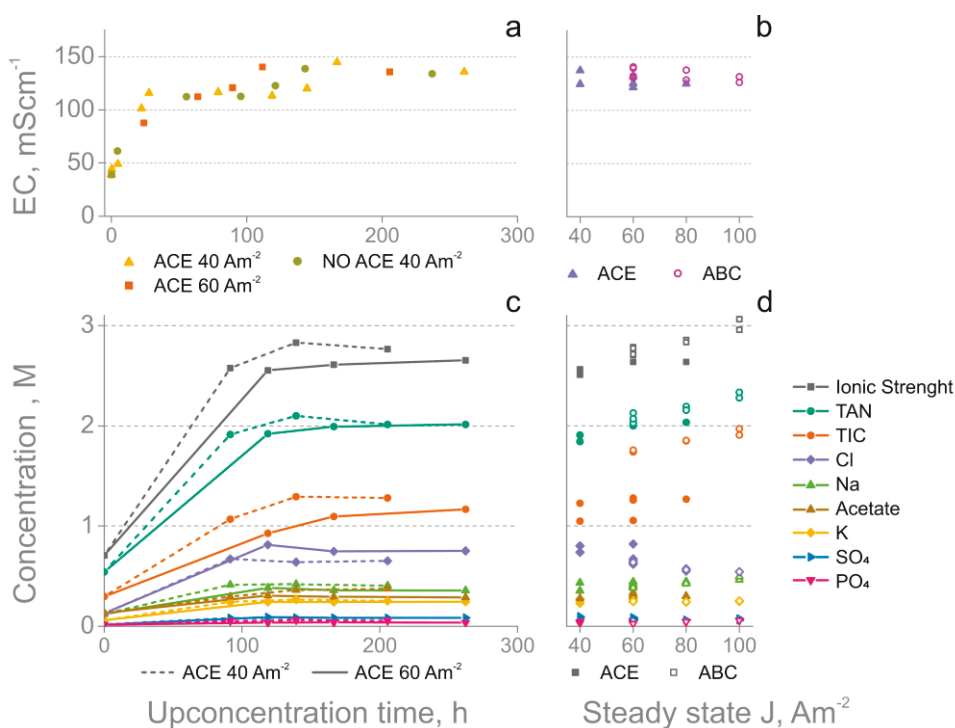


Figure 5. Ion concentrations before (upconcentration) and during steady state. (a) Concentrate conductivity reaching steady state, (b) Concentrate conductivity in steady state, (c) Concentrate ion concentrations reaching steady state, (d) Concentrate ion concentrations in steady state. Upconcentration = phase from start to steady state. Steady state = operational phase with steady concentrations. ACE, NO ACE, ABC = feed characteristics (see Chapter 4.1). (modified from Publication I, Fig. 2)

To better understand the phenomena related to the relation between current density and concentrate concentrations, a modelling study was initiated in parallel. These phenomena were clearly demonstrated in Publication II (See Chapter 5.1.3.).

5.1.2 Parameters dictating ammonium bicarbonate precipitation in the concentrate (I)

As urine is concentrated and subsequently cooled to -18 °C, several species can supersaturate first, depending on their respective concentrations (see Chapter 2.3). Supersaturation cannot currently be modelled as the solubility constants have not been defined at temperature below 0 °C, and the diminishing activities due to competing ions is significant in concentrated urine (Publication I and II). To evaluate

limits for supersaturation conditions, the ammonium bicarbonate ionic strength to total ionic strength ratio (IS_{ABC}/IS) is visualized in relation to the ammonium bicarbonate ionic product (IP_{ABC}) (Figure 6b).

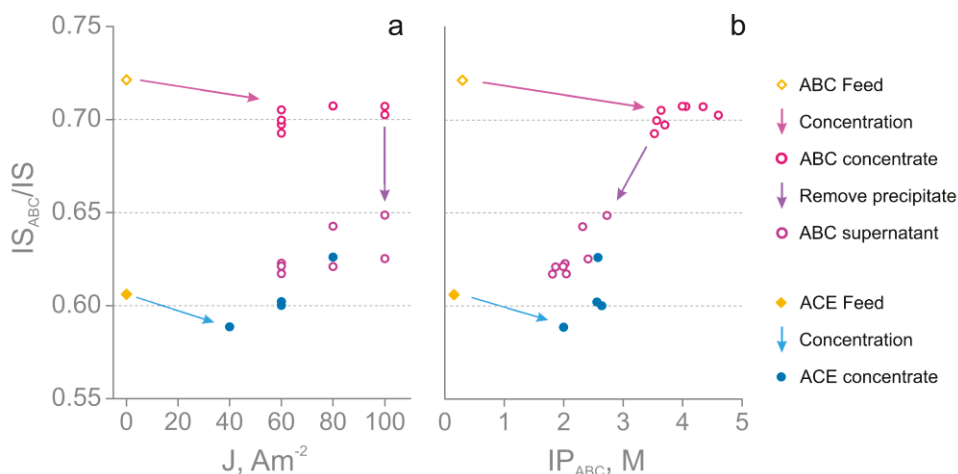


Figure 6. Ratio of ammonium bicarbonate ionic strength and ionic strength (IS_{ABC}/IS) presented in relation to (a) current density (J) and (b) ammonium bicarbonate ionic product (IP_{ABC}). ABC and ACE are synthetic urine feed compositions (see Chapter 4.1.). Supernatant refers to concentrate after cooling and removal of solid crystals. (Publication I, Fig 5)

The analysis of the concentrates of different type of synthetic urine compositions (see Chapter 4.1.) indicated that precipitation at $-18\text{ }^{\circ}C$ occurred only when the ammonium bicarbonate ionic strength constituted more than app. 62 % of the total ionic strength ($IS_{ABC}/IS > 0.62$) and ammonium bicarbonate ionic product (IP_{ABC}) is above 2.25 (mol/L)^2 . These results were obtained by combining measured supernatants after removal of formed crystals and are assumed to be at supersaturation. Feeds simulating urine where organic matter had not been oxidized and thus, where bicarbonate concentration was lower, did not achieve the limits identified for supersaturation and did not produce observable amounts of precipitates.

Maximum of 17 % of feed nitrogen was captured in solid form as ammonium bicarbonate (Publication I). While concentration to even higher ammonium and bicarbonate concentrations is possible (Publication II), larger relative nitrogen capture as solid ammonium bicarbonate would be most likely prohibited by competing ions (sodium and chloride), that inhibit further crystal formation (Publication I).

5.1.3 Electro-concentration is limited by back migration and current leak (II)

Modelling the system in Publication II extrapolated the results beyond experiments performed in Publication I. Sampling could not show fluxes over membranes in the experimental setup (Publication I), but the model provided a method of explaining the results seen in Publication I. The model confirmed the observations of Publication I, that merely increasing current density does not increase ion concentrations in the concentrate (Chapter 5.1.1.). This can be attributed mainly due to two phenomena: current leakage and back migration (for more complete analysis, please refer to Publication II). Current leakage refers to the movement of H^+ and OH^- over the membranes when large current densities are utilized due to the lack of buffer capacity, as other ions are depleted and pH on the membrane surfaces changes. Back migration or back diffusion refers to the diffusion of uncharged ion-pairs and species, the concentrations of which increase as overall concentrations increase in the concentrate and the movement of which is not inhibited by charged membranes or the electric field. Also charged species diffuse through membranes at higher rates as concentration differences over the membrane are larger.

However, modelling results show that by decreasing HRT, the current density can be increased to accommodate higher concentrations of ions in the concentrate. Decreasing the HRT increases concentrations of all species in the reactor, increasing the buffer capacity and lowering the relative difference in concentration over the membranes, decreasing back diffusion. Urine composition affects the concentrate properties, and especially the relative amount of Na and Cl affects the attainable ammonium bicarbonate concentrations as they replace TAN and bicarbonate as concentrate species relative to starting concentrations. Also, membrane properties can impact the concentrate properties affecting diffusion and back migration and membranes with higher resistance to water flux and back diffusion can enable higher concentrations of ions in the concentrate.

Based on the model runs constructed, maximum ion concentrations in the concentrate are achieved by a) increasing feed flow rate to augment the buffer capacity, b) increasing current density when buffer capacity is maintained, c) selecting urine feed with high ammonium and carbonate concentrations and low sodium and chloride concentrations (this is considered unfeasible as collected real urine composition cannot typically be selected), and d) selecting ion exchange membranes with high resistance to water fluxes and ion back diffusion. In an optimal case, a 250 % increase in ammonium and carbonate concentrations was observed in the model for the concentrate ion concentrations. However, optimizing for high ion

concentrations in the concentrate does decrease the overall recovery percentage of ammonium as it requires shorter HRT's to accommodate for added buffer capacity requirements. The model reproduced measured experiments well.

This modelling did consider the electro-concentration cell as a purely electro-dialysis application without oxidation losses and did not consider the added effect of potentially affiliated electro-oxidation processes, which are more deeply analyzed in Publications III and IV.

5.2 Electro-oxidation of source-separated urine on Boron-Doped-Diamond anode

BDD electrode is widely studied and utilized for electro-oxidation as it is extremely durable in acidic and alkaline conditions and favors complete oxidation of waste organic compounds due to low strength of $M(OH\cdot)$ -radical interaction (See Chapter 2.6.). Publication III examined the oxidation of organics, chloride, and ammonium on BDD and the potential for selective oxidation of organics over TAN.

5.2.1 TAN electro-oxidation depends on the Cl/TAN ratio (III)

Two different TAN oxidation regimes were identified in electro-oxidation studies with synthetic and real urine with zero-order decay rates. Zero-order decay implies that TAN oxidation in both regimes was limited by the applied current density, not by TAN concentration. The defining parameter for regime change was found to be the chloride to TAN ratio in the medium. If Cl/TAN was above app. 0.2 M/M, a higher TAN oxidation rate was observed, and below 0.2 M/M, lower TAN oxidation rate was observed. The higher decay rate was measured to be one order of magnitude faster than the slower decay rate (-0.020 h^{-1} and -0.002 h^{-1} , respectively).

In synthetic urine, the change between these regimes could be instigated by changing the anodic pH electrochemically (Figure 7). The reason can be found in the underlying TAN oxidation chemistry, that is linked to the breakpoint chlorination pathway. In low pH, the local oxidation pathway for chloride favors rapid formation of perchlorate, reducing the medium Cl/TAN ratio rapidly to below 0.2 M/M. At neutral pH, the chloride remains as hypochlorite and is available for TAN oxidation through breakpoint chlorination, where it is returned to chloride and can further be oxidized into hypochlorite. In these conditions, Cl/TAN ratio never

descends below 0.2 M/M and TAN is oxidized rapidly. At pH 5, some TAN is oxidized rapidly, but Cl is oxidized even faster, and a change in the oxidation regime is detected at 0.2 M/M, after which only slow TAN oxidation rate is observed. The slower TAN oxidation rate corresponds to oxidation through direct oxidation at the BDD surface (Michels et al., 2010).

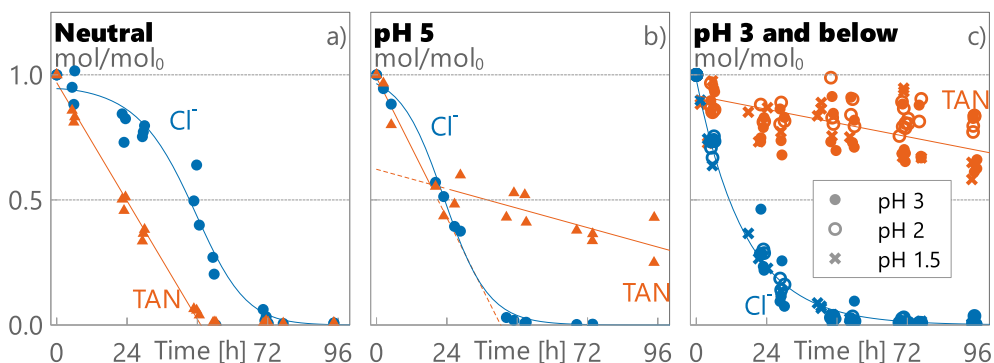


Figure 7. Measured TAN and chloride amount relative to their initial amounts (mol/mol₀) in synthetic urine in a) neutral pH, b) pH 5, and c) pH 3 and below. (Modified from Publication III, Fig 2)

The observations of Cl/TAN ratio affecting the TAN and Cl, but not TOC decay rates form a basis for a hypothesis, based on the results from Publication III and literature, which is summarized in Figure 8. It can be hypothesised that in neutral pH, BDD(OH·) is scavenged rapidly to a low level from the anode surface, and the formed hypochlorite has time to diffuse away and instigate TAN oxidation pathways in the bulk liquid. In low pH, BDD(OH·) are more readily available and oxidation pathways from hypochlorite to chlorite dominate and thus, chloride concentration drops rapidly. RCS concentrations to instigate TAN breakpoint chlorination are not reached. (Brito et al., 2015; Czarnetzki and Janssen, 1992; Martínez-Huitile et al., 2015; Zöllig et al., 2015c).

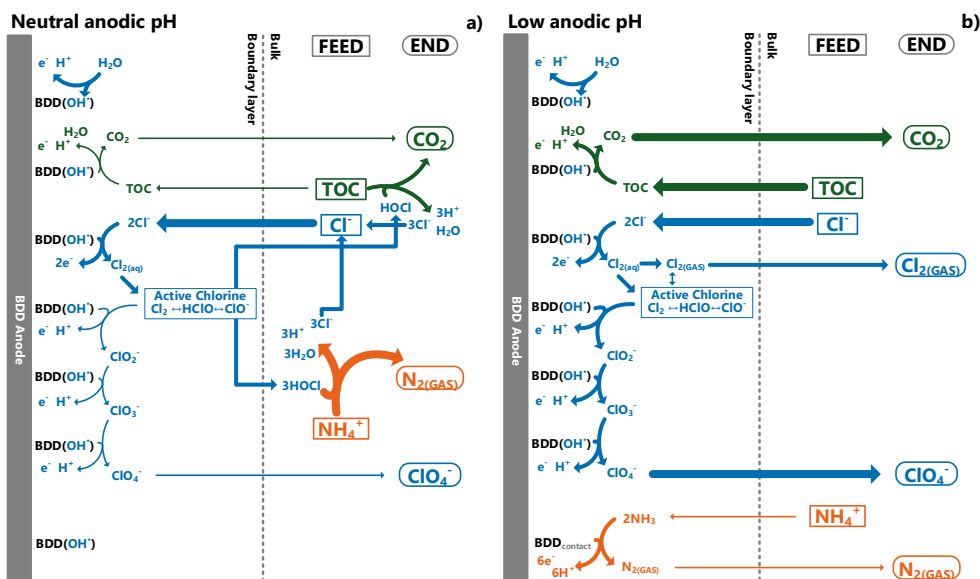


Figure 8. Hypothesised pathways (simplified) dominating TOC and TAN oxidation under a) neutral and b) low anodic pH-conditions. Boxes indicate feed substances, bubbles end products and arrow widths relative scale of reaction rates. In neutral conditions, active chlorine diffuses to bulk and is responsible for most of TOC and TAN decay measured. At low pH, formed chloride radicals (RCS) have reaction pathways with competitive reaction rates including further oxidation and removal as gaseous chlorine, and diffusion of active chlorine to bulk is low and cannot induce breakpoint chlorination -type TAN decay. (Publication III, Fig 7)

5.2.2 TOC electro-oxidation proceeds with constant rate (III, IV)

The oxidation of organic matter, and TOC decay followed 1st order kinetics in all experiments (Publications III, IV), irrespective of the anodic pH (for an example, see Fig. 9). Organic molecules in synthetic urine are known to electro-oxidize via both ROS and RCS species (Brito et al., 2015; Ganiyu et al., 2019), but RCS typically result in a more rapid and efficient oxidant. In this study, no change was detected in the TOC decay rates between experiments with different Cl concentrations, but this can be due to the relative similarity: all experiments started with chloride present and ended with all chloride oxidized. Slightly higher residual organic material was observed in experiments in pH ≤ 5 than at neutral pH, and this can be due to the more general oxidative power of RCS than ROS. The 1st order decay implies mass-transfer-limited reaction kinetics and matches previously reported organics oxidation

behavior at high applied currents on BDD, where current is not limiting the oxidation (Brito et al., 2015; Ganiyu et al., 2019; Martínez-Huitle et al., 2015).

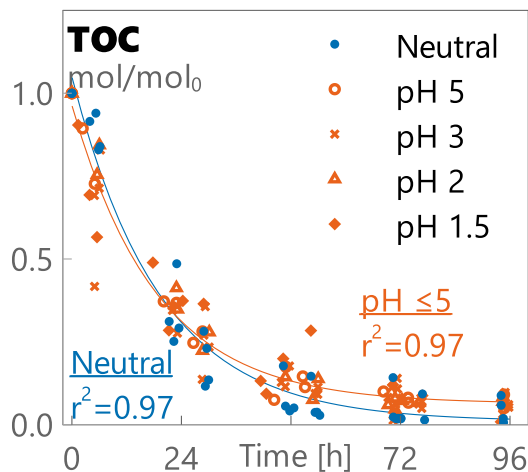


Figure 9. Total Organic Carbon (TOC) amount relative to the initial amount in the feed (mol/mol₀) during electro-oxidation of synthetic urine at different pH values. (Publication III, Fig 3)

5.2.3 Anodic pH control allows selective TOC electro-oxidation in source-separated urine (III)

In source-separated urine, Cl/TAN ratio is naturally close to 0.2 M/M, depending on collection, demographics and storage. Previously in literature (Zöllig et al., 2017), the occasionally observed TOC oxidation over TAN has been considered a nuisance. However, for simultaneous urine treatment and nutrient recovery, simultaneous TOC removal and TAN survival are strived for. By electrochemically controlling the anodic pH, this proof-of-concept study (Publication III) showed, that it is possible to oxidize organics without simultaneously losing a significant fraction of TAN. Chloride chemistry is an integral part of urine electrochemistry and integration of chloride electrochemistry into urine treatment could yield new innovations. By integrating the notion of Cl/TAN ratio as a starting point, it might be possible to develop other means to adjust the Cl/TAN ratio, that do not require the use of extreme pH's and oxidation of chloride into perchlorates.

While encouraging result on the preservation of TAN, the anode used in this study readily oxidizes chloride into chlorate and perchlorate, that are toxic and persistent substances that are a serious impediment to the implementation of BDD

based electro-oxidation technologies for the treatment of source-separated urine (Radjenovic and Sedlak, 2015). Development of new electrode materials (such as $\text{TiO}_{2-x}\text{NTA}$ and Ti_4O_7), chlorate reduction at the cathode, RCS quenching by hydrogen peroxide, operational parameters for minimizing chlorate concentration or selection of operational methods (such as pre-, post- or integrated treatment) could allow for safe electro-oxidation even in chlorine-rich media in the future (Cotillas et al., 2019; Garcia-Segura et al., 2018; Herraiz-Carboné et al., 2020; Santos et al., 2020; Yang, 2020).

5.3 Combined electro-concentration and electro-oxidation for formation of nutrient product with reduced sodicity (IV)

The themes of the three first Publications (I-III) are electro-concentration, chemical speciation, reagent-free pH-control, and pH-dependent electro-oxidation of source-separated urine, all aiming for nitrogen recovery. Publication IV encapsulates all these themes in full by utilizing chemical free pH-control to enact selective electro-concentration to produce a low sodicity nutrient product from source-separated urine, simultaneously treating the urine by removing organic content and recovering nutrients. Sodicity refers to the sodium content of soil or solution, while salinity is typically defined as seawater salinity encompassing all ions including sodium and chloride, but also e.g. sulphate, phosphate, potassium, magnesium, calcium, nitrate and bicarbonate (Daliakopoulos et al., 2016). Urine as a fertilizer can cause high soil salinity or sodicity due to the sodium and chloride in urine (Boh and Sauerborn, 2014). In this study, the aim was to reduce the sodium content of produced nutrient product.

5.3.1 Reagent-free pH control allows Na/TAN separation and adjustment of product sodicity (IV)

When pH rises above pK_a (9.25) of $\text{NH}_4^+/\text{NH}_3$, most TAN is in ammonia form (NH_3) and does not respond to the electromotive force used for ion movement in electro-concentration (there is still movement through diffusion). In electrochemical pH control, the cathode pH increases (through reductive reactions) and imparts an electromotive force that attracts cations and repels anions. To utilize the increased pH for ion separation, in this study two reactors were connected together; The anode

of the waste reactor, was connected to the same loop (cathodic loop) of the cathode of the product reactor and vice versa (see Fig. 3). If the product reactor cathode holds the pH of the loop high enough ($\geq \text{pH } 10$), a significant fraction of the TAN remains as uncharged ammonia and does not respond to the electromotive force in the waste reactor, and does not move to the waste concentrate. This way, the waste reactor effectively removes other ions (waste ions), such as Na and Cl from the system. In addition, the product reactor is left with a larger fraction of TAN to harvest into the product concentrate from the anodic loop with a lower pH.

The above described principle was tested by comparing five different case study experiments to a control case with only one three chamber reactor in operation. Different product and waste reactor current densities were applied to see their effects on the properties of the concentrates from the product and waste reactors and on the energy consumption. The experiments explored (i) the properties of a very small and maximum waste concentrate production (ii) the effects of different loop pH levels for ion separation; (iii) the effects of different combined levels of product and waste reactor current densities; and (iv) an alternative feeding pattern. The product sodicity and specific energy in different experiments are presented in Figure 10.

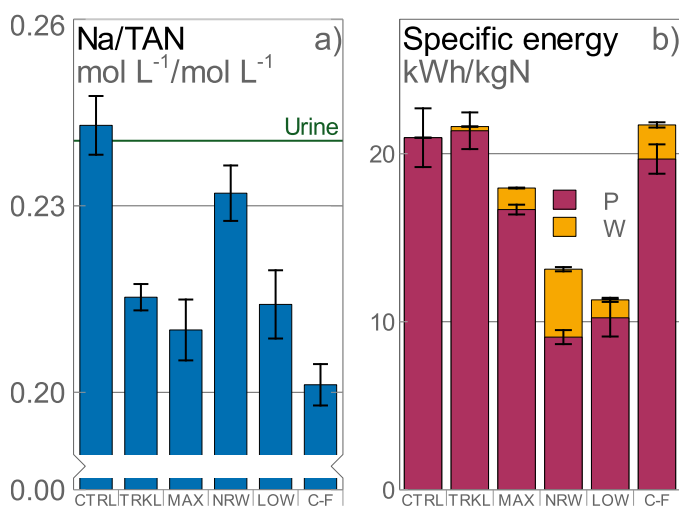


Figure 10. a) Product sodicity indicated by Na/TAN concentration ratio, and b) specific energy consumption in product reactor (P) and waste reactor (W) against TAN captured in the product in different experiments. CTRL=Control, TRKL=Trickle, MAX=Maximum volume, NRW=Narrow Gap, LOW=Low Potential, C-F=Cathodic Feed. (modified from Publication IV, Fig 2)

The results are a proof-of-concept for the selective separation of Na and TAN using a reagent-free pH-control: in one experiment 14 %-mass of Na and only 1 %-mass of TAN were diverted in the waste, comprising of 4 % of the feed volume. Using this separation principle, the sodicity (Na/TAN concentration ratio) was lowered compared to the control experiment by 12 to 17 % in experiments, where the cathodic loop pH was at least 10, with a corresponding specific energy consumptions of 11 to 22 kWh/kgNH₄-N and 68 and 76 % TAN recovery rate, respectively. The waste reactor had a small total energy consumption in comparison to the product reactor, and the movement of Na (and K) in the reactor corresponded to only a small fraction of the total energy used for ion movement. Extreme anodic pH levels and/or lack of buffer capacity caused large current leaks in some experiments (movement of H⁺), reducing energy efficiencies and increasing specific energy consumption. The lowest energy consumption was measured where combined current density and resulting buffer capacity depletion was the lowest resulting in low potentials on electrodes – result that was in line with predictions from Publication II.

The energy consumption depends on the applied current and cell voltage. The cell voltage in turn depends on the buffer capacity depletion and chamber pH, which both affect the cell conductivity. The energy consumption results in Publication IV, as well as modelling results in Publication II guide towards finding an optimal operational point with low current density and electrode potential. Parameters governing energy use are separated from parameters governing sodicity reduction, potentially allowing for their simultaneous optimization. Further understanding the parameters controlling Na/TAN separation and oxidation pathways can allow the tailoring of the sodicity of produced nutrient product and other product characteristics and energy consumption of the system.

5.3.2 TAN and Cl losses depend on sequential oxidation and reduction within the reactor chambers (IV)

Publication III described the TAN oxidation rates experienced at the anode in relation to the Cl/TAN ratio. In the presence of chloride, TAN oxidation is not immediate, but takes place through the breakpoint chlorination -mechanism in which hypochlorite reacts with ammonium to form chloramines, which further react to form nitrogen gas (Publication III). The intermediate oxidative products, hypochlorite and chloramines, can however also go through various reductive

pathways - directly at the cathode or via reduced products such as hydrogen - to reduce back to chloride and ammonium (Kobylinski and Bhandari, 2010; Randtke, 2010). In all experiments in Publication IV, the anodic potentials in the product reactor were high enough (3.4 – 3.9 V vs. SHE) to produce hypochlorite and enable significant TAN loss through breakpoint chlorination (Brillas and Martínez-Huitle, 2015; Martínez-Huitle et al., 2015). However, large differences in TAN and Cl losses were measured, which could be linked to the differences in the applied anodic potentials between the product and waste reactors (see Figure 11), a proximate measure for the difference in oxidation and reduction potential within the reactor loops. This result implies that there is a breakpoint chlorination balance within the reactor loops: chloride is oxidized at the BDD anode and reduced at the stainless steel cathode, both in the same mixing loop with ~ 1 min HRT. The specific parameters of each electrode potential, as well as the reactor loop composition (pH, buffer capacity, ionic composition) determines the extent of breakpoint chlorination observed. In experiments where the product reactor had high cell voltage and anodic potential, but waste reactor had significantly lower cell voltage and anodic potential, a large TAN loss was measured implying larger production of oxidated chloride at the anode than corresponding reduction at the cathode in the same loop. In experiments with a smaller difference between the cell voltages and anode potentials, a smaller TAN loss was detected (Fig. 11).

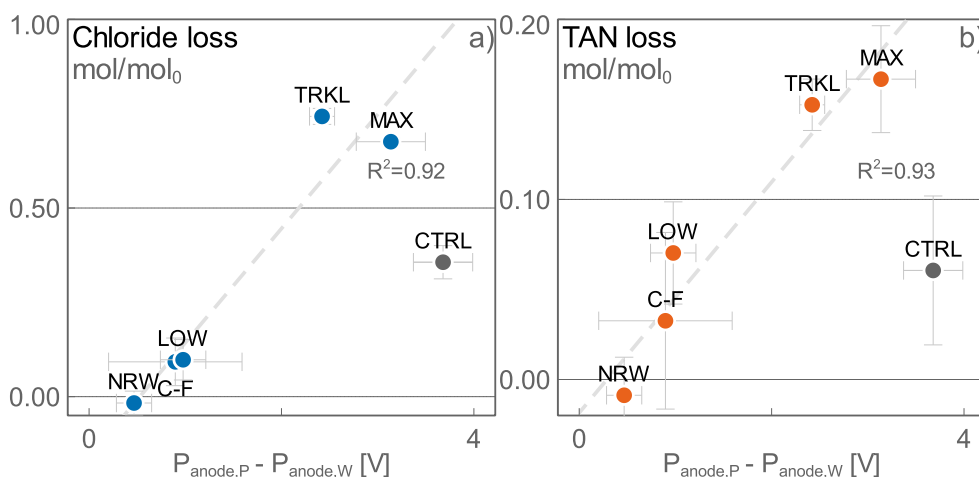


Figure 11. a) Chloride and b) total ammonium nitrogen (TAN) losses (mol/mol₀) plotted against the difference of product and waste reactor anode potentials in different experiments, an indicator of the oxidation and reduction potential for chloride compounds in the reactor. CTRL=Control, TRKL=Trickle, MAX=Maximum volume, NRW=Narrow Gap, LOW=Low Potential, C-F=Cathodic Feed. (Publication IV, Fig 4)

The result shows the subtle balance of the breakpoint chlorination on BDD and demonstrates how it is possible to adjust and counter the TAN and Cl oxidation pathways and TAN oxidation can be decreased by simultaneous application of oxidation and reduction potentials. TAN losses have a significant effect on TAN capture, product sodicity and specific energy efficiency, and thus reducing TAN losses is an important aim in optimizing the process. The understanding of phenomena affecting TAN and Cl losses allows for tailoring of nutrient products, as by selecting operational parameters it is possible to either remove or retain TAN and/or Cl from the product.

5.4 TAN recovery from source-separated urine in electrochemical systems

TAN recovery is often considered as an energy balance: energy is required to capture TAN from a waste stream and this energy is compared to the energy required for equivalent nutrient production through Haber-Bosch method and/or nitrogen removal from the waste stream. Focusing on energy is simple and allows comparison between different technologies and systems but can overshadow other driving aspects for nutrient recovery. The energy sources can differ for produced nutrients and recycled nutrients from waste streams: industrial TAN fixation from the atmosphere is based on fossil fuel incineration, while electricity used for TAN recovery can be renewable. Redirection of waste stream nutrients into reuse can also decrease the amount of excess nutrients present in the surrounding environment, improving environmental conditions and decreasing eutrophication in waterways. Thus, it is important to note that when comparing and selecting for technologies for circular nutrient economy, energy is not the only parameter to consider.

In a traditional wastewater treatment plant, nitrogen removal through nitrification and denitrification contributes a major fraction of the total energy consumption of the process, estimated at 6 – 14 kWh kgN⁻¹ (shortened from kWh kgNH₄-N⁻¹) (Maurer et al., 2003; Ward et al., 2018). Similar level of energy is consumed for nitrogen fixation through the Haber-Bosch process – about 19 kWh kgN⁻¹ (McCarty et al., 2011). In laboratory studies the measured energy use cover only electrochemical energy use, while auxiliary power consumption, such as pumping, is not measured. In a typical case, pumping is measured to contribute ≥ 5 % of a system energy consumption (Tarpeh et al., 2018), but consumption can vary depending on the operational method. Different technologies attempt and achieve different levels

of TAN removal and recovery. Many laboratory studies focus on other aspects than TAN removal or capture rate or they are not reported and thus cannot be compared. Table 7 compiles common key parameters used in TAN recovery studies and the results from these studies and compares them for results of this thesis.

Table 7. Compilation of current densities used in electrochemical TAN capture from source-separated urine and percentual TAN recovery, specific energy consumption and current efficiency (CE) obtained in these experiments. Adapted from reviews (Kuntke et al., 2018; Liu et al., 2020) and other sources in the reference-column. EC=electro-concentration, MFC = Microbial Fuel Cell, MEC = Microbial Electrolysis Cell, TMCS = Transmembrane Chemisorption, C = Concentration, CE = Current Efficiency.

Separation	Capture	Current A m ⁻²	TAN recovery %	Energy kWh kgN ⁻¹	TAN CE %	Reference
EC	C	3-20	93	n.r.	38	(Pronk et al., 2006b)
EC	TMCS	10	64	8.5	57	(Kuntke et al., 2017)
EC	TMCS	20	73	7.3	58	(Kuntke et al., 2017)
EC	TMCS	50	60	15.6	55	(Kuntke et al., 2017)
EC	TMCS	20	89	18	33	(Rodríguez Arredondo et al., 2017)
EC	TMCS	50	63	13.6	53	(Rodríguez Arredondo et al., 2017)
EC	TMCS	50	92	46.3	13	(Rodríguez Arredondo et al., 2017)
EC	Stripping	30	53	9.5	67	(Luther et al., 2015)
EC	Stripping	50	81	12.4	61	(Luther et al., 2015)
EC	Stripping	40	75	14.7	58	(Luther et al., 2015)
EC	Stripping	30	41	16.8	38	(Gildemyn et al., 2015)
EC	Stripping	20	87	2.9*	n.r.	(Christiaens et al., 2017)
EC	Stripping	20	67	3.9*	n.r.	(Christiaens et al., 2017)
MFC	Stripping	2.6*	1.6*	-2.8*	29*	(Kuntke, 2013)
MEC	C	14.6	33.4	2.3	89	(Kuntke et al., 2014)
MEC	TMCS	1.6	46	2.6	69	(Kuntke et al., 2016a)
MEC	TMCS	1.6	26.5	1.1	96	(Zamora et al., 2017a)
MEC	C	29.3	49.5	2.38	95	(Ledezma et al., 2017)
EC	TMCS	100	49.6	8.5	n.r.	(Tarpeh et al., 2018)
EC	TMCS	100	59*	8.9*	n.r.	(Liu et al., 2020)
EC	C	n.r.	64-70	n.r.	n.r.	(De Paepe et al., 2018)
EC	C	60	40	9.7	67	Publication I
EC	C	80	60	10.8	67	Publication I
EC	C	100	72	13.0	67	Publication I
EC	C	10-150	43-57	n.r.	n.r.	Publication II
EC	C	100	76	21.0	34	Publication IV
EC	C	100	70	21.6	36	Publication IV
EC	C	57	62	18.0	60	Publication IV
EC	C	43	56	13.1	68	Publication IV
EC	C	49	68	11.3	61	Publication IV
EC	C	86	76	21.7	39	Publication IV

*n.r. not reported, *calculated or modelled from data provided. Current efficiency refers to the charge passing as TAN through CEM relative to the current passing through the potentiostat.

The range of parameters utilized and the obtained results for electrochemical TAN recovery (Table 7) reflect the varied nature of electrochemical technologies. Some general trends can be noticed: usually when a high TAN recovery is aimed for, a lower current efficiency is achieved due to lower buffering capacity and depletion of ions and conductivity (Thompson Brewster et al., 2017a). This usually also increases the specific energy demand. In electrodialysis, current density is usually limited below the limiting current, but in electro-concentration laboratory studies, currents up to 100 A m^{-2} are utilized, without separately measuring the limiting current. TAN recovery results in the literature range from 1.6 % to 93 %, averaging at 60 %. This reflects the general electrochemical research aim, which is not to treat wastewater and remove all ammonium, but to capture a nutrient product at a reasonable energy expense. Modest TAN recovery also reflects the difficulty of achieving high rates of TAN removal from urine as TAN removal through electrochemistry requires removal of most buffering capacity, after which current efficiency gets lower. The removal of lower ion concentrations is more difficult and would require additional operational steps and higher energy consumption. The maximum results achieved in this thesis for TAN recovery, TAN capture rates of 72 % (Publication I), 57 % (Publication II) and 76 % (Publication IV) are within the upper half to the reported results in the literature, while comparison is not straightforward as operational methods vary.

The specific energy utilized for TAN recovery has varied between -2.8 and 49.3 kWh kgN⁻¹, averaging at 10 kWh kgN⁻¹ (Table 7). There is a wide variety in the energy consumptions reported as microbial systems typically are run at low current and are energy sensitive, while some aspects of energy consumption, such as gas flow in stripping, are not necessarily accounted for. The specific energy consumption for TAN recovery achieved in this thesis varied between 9.7 – 13.0 kWh kgN⁻¹ in the electro-concentration study (Publication I) and between 11.3 – 21.7 kWh kgN⁻¹ in the combined electro-concentration and electro-oxidation study with Na/TAN separation (Publication IV). The energy consumption values measured in this thesis (Publications I and IV) are comparable in magnitude to other processes for nitrogen recovery and removal and can compete in scale of energy use with current nitrogen production and removal infrastructure. The focus of this study was not to optimize the energy use, and it is expected that significantly lower specific energy consumptions can be achieved with the processes developed in this study through optimization.

6 CONCLUSIONS AND FUTURE OUTLOOK

This doctoral thesis shows that electro-oxidation and electro-concentration can be combined to form a novel electrochemical process that allows for simultaneous treatment and formation of a nutrient product with decreased salinity from source-separated urine. This conclusion meets the overall aim set for this thesis.

Electro-concentration can be used to produce solid ammonium bicarbonate crystals from synthetic, ureolysed source-separated urine. 17 % of TAN was captured in solid crystals, with 72 % of total TAN recovered (Publication I). Larger TAN capture into solid crystals was shown to be inhibited by competing salt ions (Na, Cl). Reaching higher ion concentrations in the concentrate are inhibited by buffer capacity depletion in the feed and back migration of uncharged species from the concentrate (Publications I and II). To reach maximum TAN concentration in the concentrate, feed flow rate and current density can be increased as well as selecting feed with higher TAN and membrane materials with higher resistance to back diffusion of ions (Publication II).

Urine electro-oxidation in low pH (anodic $\text{pH} \leq 3$) at BDD electrodes allows for the selective oxidation of organic matter, while retaining TAN. Organics removal is required as a treatment step, while TAN preservation is required for nitrogen recovery. Unlike hypothesized, the decrease in TAN oxidation is due to rapid Cl electro-oxidation in low pH at the anode. Cl to TAN ratio defines the oxidation pathway of TAN in electro-chemical oxidation: when Cl/TAN ratio is above 0.2 mol/mol, rapid breakpoint chlorination -type oxidation of TAN is observed, as is observed at neutral pH. Below this ratio, only slow, direct TAN oxidation is observed. The original hypothesis expected that TAN preservation was related to TAN speciation ($\text{NH}_4^+/\text{NH}_3$). (Publication III)

Electrochemical Na/TAN separation is possible by using reagent-free pH-control in a double reactor electro-concentration setup that forms two separate concentrate products and is based on the NH_3 inertness to electromotive force at high pH (cathodic $\text{pH} \geq 10$). Double reactor electro-concentration resulted in 17 % lower nutrient product sodicity (Na/TAN -ratio) compared to single reactor control, while achieving 76 % TAN recovery into nutrient product. Application of double

reactor setup allows tailoring of the nutrient product composition through operational parameters. (Publication IV)

The study described in this thesis compliments and binds together several separate but intertwined research fields. It gets its motivation from the urine fertilizer research that hopes to simultaneously improve safe and sustainable sanitation availability in the Global South and close the nutrient loop, and builds on the strong agricultural and research background using non-treated, stored, human urine for crops (Bonvin et al., 2015; Heinonen-Tanski et al., 2007; Jönsson and Vinnerås, 2013; Pronk and Koné, 2009; Richert et al., 2010; Vinnerås and Jönsson, 2013) From electrochemistry, electro-oxidation builds from studies that aim for local treatment of wastewater for disposal or water reuse (Cho et al., 2014a; Cid et al., 2018; Huang et al., 2016; Jasper et al., 2016), while electro-concentration grows from membrane technologies that aim at recovery of nutrients, especially nitrogen, from urine and other waste streams (Kuntke et al., 2018; Luther et al., 2015). An important part of nutrient research has been based on bioelectrochemistry and related membrane technologies (Ledezma et al., 2017). The results of this thesis are relevant for all these fields and indicate novel ways for nutrient recycling with electrochemical applications.

From this work, the most obvious questions calling for future research include the following. In the narrow set of parameters studied, only limited sodicity reduction through pH-controlled electro-concentration was achieved (Publication IV), while a proof-of-concept of clear Na/TAN separation was shown. It should be further delineated, how the technology could be improved to achieve increased, or even total sodicity removal. Means of pushing the technology further could involve separation of electro-oxidation and electro-concentration to reduce TAN loss and separation of nutrient product formation from waste salt separation, leaving more buffer capacity and time for Na-removal without simultaneous Na leaching to the product.

The BDD anode produces chlorates, toxic and persistent substances, from source-separated urine that are a serious impediment to application of this technology (Publication III). It should be investigated, which electrode materials can surpass BDD, or which operational methods can eliminate the production of chlorates. This question is under active development as electro-oxidation is a highly promising technology for future water treatment, and new materials and methods are sure to emerge. However, also current technologies can offer solutions for urine treatment through novel applications. Pure electro-concentration or electrodialysis does not need any oxidation chemistry for successful urine treatment. ROS can be

produced in a separate, non-chloride containing water stream, for subsequent oxidation use and this type of unit can be combined as the electrode rinsing chamber of an electro dialysis cell.

This study did not concentrate on the evaluation of effluent quality or optimization of parameters to meet treatment requirements (Publications I-IV), while previous studies imply that electro-oxidation is efficient in sterilizing urine and rendering it safe for disposal (Yang et al., 2019; Zöllig et al., 2017). Thus, it should be determined what are the effects of this technology to the bacteria, viruses, cysts, helminth eggs and microbiota potentially present in urine and other waste streams. Currently it has not yet been determined whether this technology produces unacceptable levels of byproducts, such as chlorates and chlorinated organic compounds, and what are all the compounds that require attention. It is uncertain whether this technology could be optimized to serve as the main treatment option for urine. This requires a meticulous and comprehensive analytical study, with a forward-looking attitude as new legislation and environmental impacts can be still uncovered.

Energy consumption was not optimized in electro-concentration or electro-oxidation (Publication I-IV), but large variability was measured based on different study parameters, indicating plenty of room for optimization. Parameters should be optimized for energy consumption to find out the minimum energy demand for a non-biological source-separated urine treatment and nutrient capture process. These optimal results should be compared to traditional wastewater treatment infrastructure and nutrient production costs amended with the environmental costs caused by environmental damage due to non-recycled nutrient loading. Already from the non-optimized results (Publication IV) it seems plausible, that electrochemical source-separated urine treatment with nutrient capture can be competitive. Finding optimal reactor configurations, materials and methods and adjusting for low current densities and accordingly lower potentials can potentially bring this technology significantly lower in energy consumption.

REFERENCES

- Atkins P, de Paula J. 2006. Physical Chemistry. W. H. Freeman. Physical chemistry.
- Beckmann W. 2013a. Mechanisms of Crystallization. In: . *Crystallization*. Wiley-VCH Verlag GmbH & Co. KGaA, pp. 7–33.
- Beckmann W. 2013b. Precipitation. In: . *Crystallization*. Wiley-VCH Verlag GmbH & Co. KGaA, pp. 235–246.
- Blaszkewicz M, Liesenhoff-Henze K. 2012. Creatinine in urine [Biomonitoring Methods, 2010]. In: . *MAK-Collection Occup. Heal. Saf.* Weinheim, Germany: Wiley-VCH Verlag GmbH & Co. KGaA, pp. 169–184.
- Boh MY, Sauerborn J. 2014. Effect of NaCl-Induced Salinity and Human Urine Fertilization on Substrate Chemical Properties. *Open J. Soil Sci.* **04**:16–25.
- Bonvin C, Etter B, Udert KM, Frossard E, Nanzer S, Tamburini F, Oberson A. 2015. Plant uptake of phosphorus and nitrogen recycled from synthetic source-separated urine. *Ambio* **44**:217–227.
- Bouatra S, Aziat F, Mandal R, Guo AC, Wilson MR, Knox C, Bjorndahl TC, Krishnamurthy R, Saleem F, Liu P, Dame ZT, Poelzer J, Huynh J, Yallou FS, Psychogios N, Dong E, Bogumil R, Roehring C, Wishart DS. 2013. The Human Urine Metabolome. *PLoS One* **8**.
- Bratsch SG. 1989. Standard Electrode Potentials and Temperature Coefficients in Water at 298.15 K. *J. Phys. Chem. Ref. Data* **18**:1–21.
- Brillas E, Martínez-Huitle CA. 2015. Decontamination of wastewaters containing synthetic organic dyes by electrochemical methods. An updated review. *Appl. Catal. B Environ.* Elsevier.
- Brito CDN, De Araújo DM, Martínez-Huitle CA, Rodrigo MA. 2015. Understanding active chlorine species production using boron doped

- diamond films with lower and higher sp^3/sp^2 ratio. *Electrochem. commun.* **55**:34–38.
- Capdevila-Cortada M. 2019. Electrifying the Haber–Bosch. *Nat. Catal.* Nature Research.
- Chaplin BP. 2019. The Prospect of Electrochemical Technologies Advancing Worldwide Water Treatment. *Acc. Chem. Res.* **52**:596–604.
- Chipako TL, Randall DG. 2020. Urine treatment technologies and the importance of pH. *J. Environ. Chem. Eng.* **8**:103622.
- Cho K, Hoffmann MR. 2014. Urea degradation by electrochemically generated reactive chlorine species: Products and reaction pathways. *Environ. Sci. Technol.* **48**:11504–11511.
- Cho K, Kwon D, Hoffmann MR. 2014a. Electrochemical treatment of human waste coupled with molecular hydrogen production. *RSC Adv.* **4**:4596–4608.
- Cho K, Qu Y, Kwon D, Zhang H, Cid CA, Aryanfar A, Hoffmann MR. 2014b. Effects of anodic potential and chloride ion on overall reactivity in electrochemical reactors designed for solar-powered wastewater treatment. *Environ. Sci. Technol.* **48**:2377–2384.
- Chouler J, Padgett GA, Cameron PJ, Preuss K, Titirici M-M, Ieropoulos I, Di Lorenzo M. 2016. Towards effective small scale microbial fuel cells for energy generation from urine. *Electrochim. Acta* **192**:89–98.
- Christiaens MERR, Gildemyn S, Matassa S, Ysebaert T, De Vrieze J, Rabaey K. 2017. Electrochemical Ammonia Recovery from Source-Separated Urine for Microbial Protein Production. *Environ. Sci. Technol.* **51**:13143–13150.
- Chung CM, Hong SW, Cho K, Hoffmann MR. 2018. Degradation of organic compounds in wastewater matrix by electrochemically generated reactive chlorine species: Kinetics and selectivity. *Catal. Today* **313**:189–195.
- Ciba-Geigy. 1977. Wissenschaftliche Tabellen Geigy. Teilband Körperflüssigkeiten (Scientific tables Geigy. volume body fluids). 8th ed. Basel.

- Cid CA, Qu Y, Hoffmann MR. 2018. Design and preliminary implementation of onsite electrochemical wastewater treatment and recycling toilets for the developing world. *Environ. Sci. Water Res. Technol.* **4**:1439–1450.
- Comninellis C, Chen G. 2010. Electrochemistry for the environment. *Electrochem. Environ.* Springer New York 1–563 p.
- Comninellis C, Kapalka A, Malato S, Parsons SA, Poullos I, Mantzavinos D. 2008. Advanced oxidation processes for water treatment: Advances and trends for R&D. *J. Chem. Technol. Biotechnol.* **83**:769–776.
- Coquerel GG. 2014. Crystallization of molecular systems from solution: phase diagrams, supersaturation and other basic concepts. *Chem. Soc. Rev.* **43**:2286–2300.
- Cotillas S, Lacasa E, Herraiz M, Sáez C, Cañizares P, Rodrigo MA. 2019. The Role of the Anode Material in Selective Penicillin G Oxidation in Urine. *ChemElectroChem* **6**:1376–1384.
- Czarnetzki LR, Janssen LJJ. 1992. Formation of hypochlorite, chlorate and oxygen during NaCl electrolysis from alkaline solutions at an RuO₂/TiO₂ anode. *J. Appl. Electrochem.* **22**:315–324.
- Daliakopoulos IN, Tsanis IK, Koutroulis A, Kourgialas NN, Varouchakis AE, Karatzas GP, Ritsema CJ. 2016. The threat of soil salinity: A European scale review. *Sci. Total Environ.* Elsevier B.V.
- Darde V, van Well WJM, Stenby EH, Thomsen K. 2010. Modeling of Carbon Dioxide Absorption by Aqueous Ammonia Solutions Using the Extended UNIQUAC Model. *Ind. Eng. Chem. Res.* **49**:12663–12674.
- Erisman JW, Sutton M a., Galloway J, Klimont Z, Winiwarter W. 2008. How a century of ammonia synthesis changed the world. *Nat. Geosci* **1**:636–639.
- Etter B, Hug A, Udert KM. 2013. Total Nutrient Recovery from Urine – Operation of a Pilot-Scale Nitrification Reactor. *WEF/IWA Int. Conf. Nutr. Remov. Recover.*:1–4.
- FAO. 2012. Current world fertilizer trends and outlook to 2016.
- FAO. 2017. FAOSTAT statistical database. [Rome] : FAO, c1997-.

- Faulkner AJ, Bard LR. 2008. *Electrochemical Methods: Fundamentals and Applications*, 2nd Edition. *Wiley* 1–864 p.
- Flores-Alsina X, Kazadi Mbamba C, Solon K, Vrecko D, Tait S, Batstone DJ, Jeppsson U, Gernaey K V. 2015. A plant-wide aqueous phase chemistry module describing pH variations and ion speciation/pairing in wastewater treatment process models. *Water Res.* **85**:255–265.
- Freguia S. 2007. *Fundamental studies of anodic and cathodic processes in microbial fuel cells*; The University of Queensland.
- Friedler E, Butler D, Alfiya Y. 2013. Wastewater composition. In: Larsen, TA, Udert, KM, Lienert, J, editors. *Source Sep. Decentralization Wastewater Manag* Oxford: IWA Publishing, pp. 241–258.
- Galama AH, Daubaras G, Burheim OS, Rijnaarts HHM, Post JW. 2014. Seawater electro dialysis with preferential removal of divalent ions. *J. Memb. Sci.* **452**:219–228.
- Galloway JN, Dentener FJ, Capone DG, Boyer EW, Howarth RW, Seitzinger SP, Asner GP, Cleveland CC, Green PA, Holland EA, Karl DM, Michaels AF, Porter JH, Townsend AR, Vöosmarty CJ. 2004. Nitrogen Cycles: Past, Present, and Future. *Biogeochemistry* **70**:153–226.
- Ganiyu SO, Martínez-Huitle CA, Martínez-Huitle CA. 2019. Nature, Mechanisms and Reactivity of Electrogenenerated Reactive Species at Thin-Film Boron-Doped Diamond (BDD) Electrodes During Electrochemical Wastewater Treatment. *ChemElectroChem*. Wiley-VCH Verlag. Vol. 6.
- Garcia-Segura S, Keller J, Brillas E, Radjenovic J. 2015. Removal of organic contaminants from secondary effluent by anodic oxidation with a boron-doped diamond anode as tertiary treatment. *J. Hazard. Mater.* **283**:551–557.
- Garcia-Segura S, Ocon JD, Chong MN. 2018. Electrochemical oxidation remediation of real wastewater effluents — A review. *Process Saf. Environ. Prot.* Institution of Chemical Engineers.
- Gendel Y, Lahav O. 2012. Revealing the mechanism of indirect ammonia electrooxidation. *Electrochim. Acta* **63**:209–219.
- Gildemyn S, Luther AK, Andersen SJ, Desloover J, Rabaey K. 2015.

Electrochemically and bioelectrochemically induced ammonium recovery. *J. Vis. Exp.*:52405.

Haynes WM. 2012. CRC Handbook of Chemistry and Physics. 92nd Edition. Greece. Vol. 32 2220 p.

Heinonen-Tanski H, van Wijk-Sijbesma C. 2005. Human excreta for plant production. *Bioresour Technol* **96**:403–411.

Heinonen-Tanski H, Sjöblom A, Fabritius H, Karinen P. 2007. Pure human urine is a good fertiliser for cucumbers. *Bioresour. Technol.* **98**:214–217.

Herraiz-Carboné M, Cotillas S, Lacasa E, Moratalla Á, Cañizares P, Rodrigo MA, Sáez C. 2020. Improving the biodegradability of hospital urines polluted with chloramphenicol by the application of electrochemical oxidation. *Sci Total Environ.* **725**:138430.

Huang X, Qu Y, Ement Cid CA, Finke C, Hoffmann MR, Lim K, Jiang SC. 2016. Electrochemical disinfection of toilet wastewater using wastewater electrolysis cell.

Ieropoulos IA, Greenman J, Melhuish C. 2012. Urine utilisation by microbial fuel cells; energy fuel for the future. *Phys. Chem. Chem. Phys.* **14**:94–98.

Ieropoulos I a., Ledezma P, Stinchcombe A, Papaharalabos G, Melhuish C, Greenman J. 2013. Waste to real energy: the first MFC powered mobile phone. *Phys. Chem. Chem. Phys.* **15**:15312–15316.

Ippersiel D, Mondor M, Lamarche F, Tremblay F, Dubreuil J, Masse L. 2012. Nitrogen potential recovery and concentration of ammonia from swine manure using electro dialysis coupled with air stripping. *J. Environ. Manage.* **95**:S165–S169.

Jaatinen S, Lakaniemi AM, Rintala J. 2016. Use of diluted urine for cultivation of *Chlorella vulgaris*. *Environ. Technol. (United Kingdom)* **37**:1159–1170.

Jasper JT, Shafaat OS, Hoffmann MR. 2016. Electrochemical Transformation of Trace Organic Contaminants in Latrine Wastewater.

Jasper JT, Yang Y, Hoffmann MR. 2017. Toxic Byproduct Formation during Electrochemical Treatment of Latrine Wastewater. *Environ. Sci. Technol.*

51:7111–7119.

- Johansson M, Jönsson H, Höglund C, Richert Stintzing A, Rodhe L. 2001. Final Report for Source-Separated Human Urine: A Future Source of Fertilizer for Agriculture in the Stockholm Region. Stockholm, Sweden: Stockholm Vatten, Stockholmshem & HSB National Federation.
- Jönsson H, Vinnerås B. 2013. Closing the loop: Recycling nutrients to agriculture. In: Larsen, TA, Udert, KM, Lienert, J, editors. *Source Sep. Decentralization Wastewater Manag.* Oxford: IWA Publishing, pp. 163–178.
- Jönsson H, Stenström TA, Svensson J, Sundin A. 1997. Source separated urine-nutrient and heavy metal content, water saving and faecal contamination. *Water Sci. Technol.* **35**:145–152.
- Kannan MV, Gnana kumar G. 2015. Current status, key challenges and its solutions in the design and development of graphene based ORR catalysts for the microbial fuel cell applications. *Biosens. Bioelectron.* **77**:1208–1220.
- Kapalka A, Lanova B, Baltruschat H, Fóti G, Comninellis C. 2008. DEMS Study of the Acetic Acid Oxidation on Boron-Doped Diamond Electrode. *J. Electrochem. Soc.* **155**:E96.
- Keeney DR, Hatfield JL. 2008. The Nitrogen Cycle, Historical Perspective, and Current and Potential Future Concerns. In: . *Nitrogen Environ. Sources, Probl. Manag.*
- Kim Y, Walker WS, Lawler DF. 2012. Competitive separation of di- vs. monovalent cations in electrodialysis: Effects of the boundary layer properties. *Water Res.* **46**:2042–2056.
- Kirchmann H, Pettersson S. 1994. Human urine - Chemical composition and fertilizer use efficiency. *Fertil. Res.* **40**:149–154.
- Kobylinski EA, Bhandari A. 2010. Chlorination of Wastewater. *White's Handb. Chlorination Altern. Disinfect. Fifth Ed.*:326–362.
- Kraaijeveld G, Sumberova V, Kuindersma S, Wesselingh H. 1995. Modelling electrodialysis using the Maxwell-Stefan description. *Chem. Eng. J. Biochem. Eng. J.* **57**:163–176.

- Kroschwitz JI, Seidel A. 2004. Kirk-Othmer encyclopedia of chemical technology. Hoboken, N.J: Wiley-Interscience. Vol. 5th.
- Kuntke P, Sleutels THJA, Rodríguez Arredondo M, Georg S, Barbosa SG, ter Heijne A, Hamelers HVM, Buisman CJN. 2018. (Bio)electrochemical ammonia recovery: progress and perspectives. *Appl. Microbiol. Biotechnol.* **102**:3865–3878.
- Kuntke P, Śmiech KM, Bruning H, Zeeman G, Saakes M, Sleutels THJA, Hamelers HVM, Buisman CJN. 2012. Ammonium recovery and energy production from urine by a microbial fuel cell. *Water Res.* **46**:2627–2636.
- Kuntke P, Zamora P, Saakes M, Buisman CJN, Hamelers HVM. 2016a. Gas-permeable hydrophobic tubular membranes for ammonia recovery in bio-electrochemical systems. *Environ. Sci. Water Res. Technol.* **2**:261–265.
- Kuntke P. 2013. Nutrient and energy recovery from urine; [S.l.: PhD Thesis.
- Kuntke P, Geleji M, Bruning H, Zeeman G, Hamelers HVM, Buisman CJN. 2011. Effects of ammonium concentration and charge exchange on ammonium recovery from high strength wastewater using a microbial fuel cell. *Bioresour. Technol.* **102**:4376–4382.
- Kuntke P, Sleutels THJA, Saakes M, Buisman CJN. 2014. Hydrogen production and ammonium recovery from urine by a Microbial Electrolysis Cell. *Int. J. Hydrogen Energy* **39**:4771–4778.
- Kuntke P, Rodríguez Arredondo M, Widyakristi L, Ter Heijne A, Sleutels THJA, Hamelers HVM, Buisman CJN. 2017. Hydrogen Gas Recycling for Energy Efficient Ammonia Recovery in Electrochemical Systems. *Environ. Sci. Technol.* **51**:3110–3116.
- Kuntke P, Zamora P, Saakes M, Buisman CJN, Hamelers HVMMV. 2016b. Gas-permeable hydrophobic tubular membranes for ammonia recovery in bio-electrochemical systems. *Environ. Sci. Water Res. Technol.* **2**:261–265.
- Larsen TA, Udert KM, Lienert J. 2013. Source separation and decentralization for wastewater management. London: IWA.
- Ledezma P, Jermakka J, Keller J, Freguia S. 2017. Recovering Nitrogen as a Solid without Chemical Dosing: Bio-Electroconcentration for Recovery of

Nutrients from Urine. *Environ. Sci. Technol. Lett.* **4**:acs.estlett.7b00024.

- Ledezma P, Kuntke P, Buisman CJNN, Keller J, Freguia S. 2015. Source-separated urine opens golden opportunities for microbial electrochemical technologies. *Trends Biotechnol.* **33**:214–220.
- Lee HJ, Strathmann H, Moon SH. 2006. Determination of the limiting current density in electrodialysis desalination as an empirical function of linear velocity. *Desalination* **190**:43–50.
- Liu MJ, Neo BS, Tarpah WA. 2020. Building an operational framework for selective nitrogen recovery via electrochemical stripping. *Water Res.* **169**:115226.
- Logan BE. 2008. MFCs for Wastewater Treatment. In: . *Microb. Fuel Cells*. John Wiley & Sons, Inc., pp. 146–161.
- Logan BE, Wiley J. 2008. Materials. In: . *Microb. Fuel Cells*. John Wiley & Sons, Inc., pp. 61–84.
- Logan BE, Hamelers B, Rozendal R, Schröder U, Keller J, Freguia S, Aelterman P, Verstraete W, Rabaey K. 2006. Microbial Fuel Cells: Methodology and Technology. *Environ. Sci. Technol.* **40**:5181–5192.
- Luther AK, Desloover J, Fennell DE, Rabaey K. 2015. Electrochemically driven extraction and recovery of ammonia from human urine. *Water Res.* **87**:367–377.
- Ma P, Ma H, Sabatino S, Galia A, Scialdone O. 2018. Electrochemical treatment of real wastewater. Part 1: Effluents with low conductivity. *Chem. Eng. J.* **336**:133–140.
- Martínez-Huitle CA, Rodrigo MA, Sirés I, Scialdone O. 2015. Single and Coupled Electrochemical Processes and Reactors for the Abatement of Organic Water Pollutants: A Critical Review. *Chem. Rev.* American Chemical Society.
- Maurer M, Pronk W, Larsen TA. 2006. Treatment processes for source-separated urine. *Water Res.* **40**:3151–3166.
- Maurer M, Schwegler P, Larsen TA. 2003. Nutrients in urine: Energetic aspects of removal and recovery. *Water Sci. Technol.* **48**:37–46.

- McCarty PL, Bae J, Kim J. 2011. Domestic wastewater treatment as a net energy producer-can this be achieved? *Environ. Sci. Technol.* **45**:7100–7106.
- Michels NL, Kapalka A, Abd-El-Latif AA, Baltruschat H, Comninellis C. 2010. Enhanced ammonia oxidation on BDD induced by inhibition of oxygen evolution reaction. *Electrochem. commun.* **12**:1199–1202.
- Mohammadi T, Moheb A, Sadrzadeh M, Razmi A. 2005. Modeling of metal ion removal from wastewater by electrodialysis. *Sep. Purif. Technol.* **41**:73–82.
- Mondor M, Masse L, Ippersiel D, Lamarche F, Massé DI. 2008. Use of electrodialysis and reverse osmosis for the recovery and concentration of ammonia from swine manure. *Bioresour. Technol.* **99**:7363–7368.
- Moon P, Sandí G, Stevens D, Kizilel R. 2004. Computational modeling of ionic transport in continuous and batch electrodialysis. *Sep. Sci. Technol.* **39**:2531–2555.
- Myerson AS. 2001. Handbook of industrial crystallization. Boston: Butterworth-Heinemann. Vol. 2nd.
- Nikonenko V, Lebedev K, Manzanares JA, Pourcelly G. 2003. Modelling the transport of carbonic acid anions through anion-exchange membranes. *Electrochim. Acta* **48**:3639–3650.
- Nikonenko V, Zabolotsky V, Larchet C, Auclair B, Pourcelly G. 2002. Mathematical description of ion transport in membrane systems. *Desalination* **147**:369–374.
- Nikonenko V V., Pismenskaya ND, Belova EI, Sifat P, Huguet P, Pourcelly G, Larchet C. 2010. Intensive current transfer in membrane systems: Modelling, mechanisms and application in electrodialysis. *Adv. Colloid Interface Sci.* Elsevier B.V.
- Ortiz JM, Sotoca JA, Expósito E, Gallud F, García-García V, Montiel V, Aldaz A. 2005. Brackish water desalination by electrodialysis: Batch recirculation operation modeling. *J. Memb. Sci.* **252**:65–75.
- De Paepe J, Lindeboom REF, Vanoppen M, De Paepe K, Demey D, Coessens W, Lamaze B, Verliefe ARD, Clauwaert P, Vlaeminck SE. 2018. Refinery and concentration of nutrients from urine with electrodialysis enabled by

- upstream precipitation and nitrification. *Water Res.* **144**:76–86.
- Patel A, Mungray AA, Mungray AK. 2020. Technologies for the recovery of nutrients, water and energy from human urine: A review. *Chemosphere*. Elsevier Ltd.
- Perera MK, Englehardt JD, Dvorak AC. 2019. Technologies for Recovering Nutrients from Wastewater: A Critical Review. *Environ. Eng. Sci.* Vol. 36.
- Perry RH, Green DW, Ackers DE. 2008. Perry's chemical engineers' handbook. New York;London; McGraw-Hill Professional. Vol. 8th.
- Pronk W, Koné D. 2009. Options for urine treatment in developing countries. *Desalination* **248**:360–368.
- Pronk W, Zuleeg S, Lienert J, Escher B, Koller M, Berner A, Koch G, Boller M. 2007. Pilot experiments with electrodialysis and ozonation for the production of a fertiliser from urine. *Water Sci. Technol.*
- Pronk W, Biebow M, Boller M. 2006a. Treatment of source-separated urine by a combination of bipolar electrodialysis and a gas transfer membrane. *Water Sci. Technol.* **53**:139–146.
- Pronk W, Biebow M, Boller M. 2006b. Electrodialysis for recovering salts from a urine solution containing micropollutants. *Environ. Sci. Technol.* **40**:2414–2420.
- Rabaey K, Angenent L, Schröder U, Keller J. 2010. Bioelectrochemical systems : from extracellular electron transfer to biotechnological application. *Integr. Environ. Technol. Ser.*:488.
- Radjenovic J, Sedlak DL. 2015. Challenges and Opportunities for Electrochemical Processes as Next-Generation Technologies for the Treatment of Contaminated Water. *Environ. Sci. Technol.* **49**:11292–11302.
- Randall DG, Naidoo V. 2018. Urine: The liquid gold of wastewater. *J. Environ. Chem. Eng.* **6**:2627–2635.
- Randtke SJ. 2010. Chemistry of Aqueous Chlorine. *White's Handb. Chlorination Altern. Disinfect. Fifth Ed.* **2**:68–173.

- Richert A, Gensch R, Jönsson H, Stenström T-A, Dagerskog L. 2010. Practical Guidance on the Use of Urine in Crop Production. *Stock. Environ. Inst.* 69 p.
- Rodríguez Arredondo M, Kuntke P, ter Heijne A, Hamelers HVM, Buisman CJN. 2017. Load ratio determines the ammonia recovery and energy input of an electrochemical system. *Water Res.* **111**:330–337.
- Rosca V, Duca M, DeGroot MT, Koper MTM. 2009. Nitrogen Cycle Electrocatalysis. *Chem. Rev.* **109**:2209–2244.
- Santos GOS, Eguiluz KIB, Salazar-Banda GR, Sáez C, Rodrigo MA. 2020. Understanding the electrolytic generation of sulfate and chlorine oxidative species with different boron-doped diamond anodes. *J. Electroanal. Chem.* **857**:113756.
- Solon K, Flores-Alsina X, Mbamba CK, Volcke EIP, Tait S, Batstone D, Gernaey K V., Jeppsson U. 2015. Effects of ionic strength and ion pairing on (plant-wide) modelling of anaerobic digestion. *Water Res.* **70**:235–245.
- Strathmann H. 2010. Electrodialysis, a mature technology with a multitude of new applications. *Desalination* **264**:268–288.
- Strathmann H. 2004. Ion-exchange membrane separation processes. In: Heiner, S, editor. *Membr. Sci. Technol.* Elsevier, Vol. Volume 9, pp. v–vi.
- Stumm W, Morgan JJ. 1996. Aquatic chemistry: chemical equilibria and rates in natural waters. *Choice Rev. Online* **33**:33-6312-33–6312.
- Sutton MA, Bleeker A, Howard CM, Bekunda M, Grizzetti B, de Vries W, van Grinsven HJM, Abrol YP, Adhya TK, Billen G, Davidson EA, Datta A, Diaz R, Erisman JW, Liu XJ, Oenema O, Palm C, Raghuram N, Reis S, Scholz RW, Sims T, Westhoek H, Zhang FS. 2013. Our Nutrient World: The challenge to produce more food and energy with less pollution. Global Overview of Nutrient Management.
- Takiyama H. 2012. Supersaturation operation for quality control of crystalline particles in solution crystallization. *Adv. Powder Technol.* **23**:273–278.
- Tanaka Y. 2013. Development of a computer simulation program of batch ion-exchange membrane electrodialysis for saline water desalination. *Desalination*

320:118–133.

Tarpeh WA, Barazesh JM, Cath TY, Nelson KL. 2018. Electrochemical Stripping to Recover Nitrogen from Source-Separated Urine. *Environ. Sci. Technol.* **52**:1453–1460.

Tettenborn F, Behrendt J, Otterpohl R. 2007. Final report for task 7 of the demonstration project "Sanitation Concepts for Separate Treatment of Urine, Faeces and Greywater " (SCST) Resource recovery and removal of pharmaceutical residues Treatment of separate collected urine.

Thompson Brewster E, Jermakka J, Freguia S, Batstone DJDJ. 2017a. Modelling recovery of ammonium from urine by electro-concentration in a 3-chamber cell. *Water Res.* **124**.

Thompson Brewster E, Mehta CM, Radjenovic J, Batstone DJ. 2016. A mechanistic model for electrochemical nutrient recovery systems. *Water Res.* **94**:176–186.

Thompson Brewster E, Ward AJ, Mehta CM, Radjenovic J, Batstone DJ. 2017b. Predicting scale formation during electro-dialytic nutrient recovery. *Water Res.* **110**:202–210.

Udert KM, Wachter M, Wächter M. 2012. Complete nutrient recovery from source-separated urine by nitrification and distillation. *Water Res.* **46**:453–464.

Udert KM, Larsen TA, Gujer W. 2006. Fate of major compounds in source-separated urine. *Water Sci. Technol.* **54**:413–420.

Udert K, Sarina J. 2013. Biological nitrogen conversion processes. In: Larsen, TA, Udert, KM, Lienert, J, editors. *Source Sep. Decentralization Wastewater Manag.* Oxford: IWA Publishing, pp. 291–306.

Udert KM, Larsen TA, Biebow M, Gujer W. 2003. Urea hydrolysis and precipitation dynamics in a urine-collecting system. *Water Res.* **37**:2571–2582.

Vinnerås B, Jönsson H. 2013. The Swedish experience with source separation. In: Larsen, TA, Udert, KM, Lienert, J, editors. *Source Sep. Decentralization Wastewater Manag.* Oxford: IWA Publishing, pp. 415–422.

- Walter XA, Forbes S, Greenman J, Ieropoulos IA. 2016. From single MFC to cascade configuration: The relationship between size, hydraulic retention time and power density. *Sustain. Energy Technol. Assessments* **14**:74–79.
- Ward AJ, Arola K, Thompson Brewster E, Mehta CM, Batstone DJ. 2018. Nutrient recovery from wastewater through pilot scale electro dialysis. *Water Res.* **135**:57–65.
- Ward MH, deKok TM, Levallois P, Brender J, Gulis G, Nolan BT, VanDerslice J. 2005. Workgroup report: Drinking-water nitrate and health - Recent findings and research needs. *Environ. Health Perspect.* **113**:1607–1614.
- Yang Y. 2020. Recent advances in the electrochemical oxidation water treatment: Spotlight on byproduct control. *Front. Environ. Sci. Eng.* **14**.
- Yang Y, Lin L, Tse LK, Dong H, Yu S, Hoffmann MR. 2019. Membrane-separated electrochemical latrine wastewater treatment. *Environ. Sci. Water Res. Technol.* **5**:51–59.
- Zabolotskii VI, Lebedev KA, Urtenov MK, Nikonenko V V., Vasilenko PA, Shaposhnik VA, Vasil'Eva VI. 2013. Mathematical model describing voltammograms and transport numbers under intensive electro dialysis modes. *Russ. J. Electrochem.* **49**:369–380.
- Zamora P, Georgieva T, Ter Heijne A, Sleutels THJA, Jeremiasse AW, Saakes M, Buisman CJN, Kuntke P. 2017a. Ammonia recovery from urine in a scaled-up Microbial Electrolysis Cell. *J. Power Sources* **356**:491–499.
- Zamora P, Georgieva T, Salcedo I, Elzinga N, Kuntke P, Buisman CJN. 2017b. Long-term operation of a pilot-scale reactor for phosphorus recovery as struvite from source-separated urine. *J. Chem. Technol. Biotechnol.* **92**:1035–1045.
- Zöllig H, Fritzsche C, Morgenroth E, Udert KM, Zöllig H, Fritzsche C, Morgenroth E, Udert KM. 2015a. Direct electrochemical oxidation of ammonia on graphite as a treatment option for stored source-separated urine. *Water Res.* **69**:284–294.
- Zöllig H, Morgenroth E, Udert KM. 2015b. Inhibition of direct electrolytic ammonia oxidation due to a change in local pH. *Electrochim. Acta* **165**:348–355.

Zöllig H, Remmele A, Fritzsche C, Morgenroth E, Udert KM. 2015c. Formation of Chlorination Byproducts and Their Emission Pathways in Chlorine Mediated Electro-Oxidation of Urine on Active and Nonactive Type Anodes. *Environ. Sci. Technol.* **49**:11062–11069.

Zöllig H, Remmele A, Morgenroth E, Udert KM. 2017. Removal rates and energy demand of the electrochemical oxidation of ammonia and organic substances in real stored urine. *Environ. Sci. Water Res. Technol.* **3**:480–491.

Zumdahl S, DeCoste. 2012. Chemical Principles.

PUBLICATIONS

- Publication I Jermakka, J., Thompson Brewster, E., Ledezma, P., Freguia, S. Electro-concentration for chemical-free nitrogen capture as solid ammonium bicarbonate. *Separation and Purification Technology* 203 (2018) 48-55.
- Publication II Thompson Brewster, E., Jermakka, J., Freguia, S., Batstone, D. J. Modelling recovery of ammonium from urine by electro-concentration in a 3-chamber cell. *Water Research* 124 (2017) 210-218.
- Publication III Jermakka, J., Freguia, S., Kokko, M., Ledezma, P. Electrochemical system for selective oxidation of organics over ammonia in urine. *Environmental Science: Water Research & Technology* 7 (2021) 942-955.
- Publication IV Jermakka, J., Thompson Brewster, E., Freguia, S., Ledezma, P., Kokko, M. Electro-concentration of urine designed for separation of sodium from nitrogen. *Separation and Purification Technology* 276 (2021) 119275.

PUBLICATION

I

Electro-concentration for chemical-free nitrogen capture as solid ammonium bicarbonate

Johannes Jermakka, Emma Thompson Brewster, Pablo Ledezma, Stefano Freguia

Separation and Purification Technology 203 (2018) 48-55
<https://doi.org/10.1016/j.seppur.2018.04.023>

Publication reprinted with the permission of the copyright holders.



ELSEVIER

Contents lists available at ScienceDirect

Separation and Purification Technology

journal homepage: www.elsevier.com/locate/seppur

Electro-concentration for chemical-free nitrogen capture as solid ammonium bicarbonate

Johannes Jermakka^{a,b,*}, Emma Thompson Brewster^c, Pablo Ledezma^c, Stefano Freguia^c^a Work Conducted at Advanced Water Management Centre, The University of Queensland, Australia^b Laboratory of Chemistry and Bioengineering, Tampere University of Technology, Finland^c Advanced Water Management Centre, The University of Queensland, Australia

ARTICLE INFO

Keywords:

Nutrient recovery

Urine

Electro-concentration

Ammonium bicarbonate precipitation

ABSTRACT

Source-separated urine is a promising stream for nutrient capture using electrochemical technologies. It contains the majority of macronutrients present in municipal wastewater in a concentrated, high ionic conductivity liquid and in N:P:K ratios suitable for agricultural application. The purpose of this study was to recover nutrients from urine, and particularly nitrogen as a solid without any chemical addition. Simulated source-separated urine was concentrated using a three-compartment electrochemical system, applying a range of current densities and feed compositions. Electro-concentration into a liquid concentrate reached maximum recovery of 72:61:79% for N:P:K, respectively, from a synthetic feed simulating ureolysed and digested urine, with a specific electrical energy consumption of 47 MJ/kg N and current efficiency of 67% for ammonium. Cooling the concentrate to -18°C resulted in solid ammonium bicarbonate crystal formation in samples with high ammonium bicarbonate ionic product and high relative ammonium bicarbonate ionic strength. Precipitation started to occur when ammonium bicarbonate ionic product was higher than 2.25 M^2 and ammonium bicarbonate accounted for more than 62% of the total ionic strength of the feed. The maximum observed nitrogen recovery into solid ammonium bicarbonate reached 17% using a current density of 100 A m^{-2} . Based on these results, electro-concentration is a promising technology for urine nutrient capture. However, capture as solid ammonium bicarbonate is feasible only if higher recovery efficiencies are achieved by removing competing ions.

1. Introduction

Source-separated, decentralized systems offer promising alternatives for the future of human sanitation enabling localised recovery of nutrients and water resources [1]. While planetary boundaries of Earth are under unprecedented stress by population growth and climate change [2], source separation can provide means of reducing community energy and water consumption by enabling water and nutrient recovery and reuse, even in situations of inadequate infrastructure [1]. Of source-separated domestic wastewater streams, greywater contains most of the recoverable water. Faecal matter (0.1% of wastewater stream) in turn contains most of the organic loading and almost all pathogens, while urine contains the majority of nutrients (79–47–71% and 86–65–76% of N:P:K in total domestic wastewater and excreta, respectively) [3]. This renders source-separated urine the most promising domestic stream for nutrient recovery [4].

Nutrients in urine are typically found in ratios suitable for direct reuse as fertiliser [5] but, while use of human urine for agriculture is

well known, direct reuse is not always feasible due to liquid transportation costs, handling, salinity and health and safety issues [6]. However, technologies enabling recovery of nutrients from source-separated urine as separate streams are not widely applied [7]. Phosphorus is the most studied nutrient for recovery from source-separated urine, typically captured as solid struvite precipitate [8–11], while no references for selective potassium recovery are found. Nitrogen capture from urine has been studied through several methods including stripping [12,13], electro dialysis [14–16], electro-concentration [17–19] and microbial electrochemical technologies (METs) [20–24]. Nitrogen recovery as solid ammonium bicarbonate without chemical addition has been proposed by means of a combined microbial electrochemical cell and electro-concentration [25].

Urine is an excellent feed for electrochemical treatment being (i) highly conductive, avoiding Ohmic losses problematic in normal sewage, (ii) well buffered, enabling operation with low pH differences and thus lower thermodynamic voltage requirements between anode and cathode, (iii) and highly concentrated in nutrients [4]. For instance,

* Corresponding author at: Tampere University of Technology, Laboratory of Chemistry and Bioengineering, PO Box 541, 33101 Tampere, Finland.

E-mail addresses: johannes.jermakka@tut.fi (J. Jermakka), emmathompsonbrewster@gmail.com (E. Thompson Brewster), p.ledezma@awmc.uq.edu.au (P. Ledezma), s.freguia@awmc.uq.edu.au (S. Freguia).<https://doi.org/10.1016/j.seppur.2018.04.023>

Received 11 December 2017; Received in revised form 6 April 2018; Accepted 6 April 2018

Available online 07 April 2018

1383-5866/ © 2018 Elsevier B.V. All rights reserved.

electrodialysis of human urine was studied by Pronk et al. (2006b) reaching high degrees of desalination (e.g. N, P and K recoveries of 93, 74 and 94%, respectively). Electrodialysis was further studied with alternative settings with a membrane contactor ammonium capture device [26] and also in pilot scale [27]. Electrodialysis has similarly been applied for nitrogen recovery from a similar waste stream, swine manure [28,29]. Also, electro-concentration using a two chamber electrochemical cell has been studied for ammonium removal and recovery from anaerobic digestate, enabling reasonable ammonium capture at low energy consumption measured approximately 18–150 MJ/kg N [18,19]. The same technology has been applied also for human urine [15,17], with subsequent ammonia stripping measured at 43 MJ/kg N. A similar three-cell system, as used in this article, has been used to model and evaluate the limiting factors of electro-concentration [30]. These studies demonstrate that electro-concentration is technically feasible and also an economically promising solution for different feeds.

Most of the aforementioned nitrogen-specific technologies use ammonia gas stripping followed by capture into strong acid solutions (e.g. sulfuric acid). This is effective, but the use of strong acids is a disadvantage adding to the cost and risk of operation, especially in decentralized scenarios.

Sufficiently concentrated urine has the potential to become saturated in ammonium bicarbonate when cooled, as the solubility of ammonium bicarbonate reduces with temperature. This can induce precipitation of solid ammonium bicarbonate crystals allowing for chemical free recovery of nitrogen as a solid [25]. Precipitation of ammonium bicarbonate from concentrated urine is not widely discussed in the literature. It is highly soluble (17.6 g/100 g H₂O at 20 °C [31]) but its actual solubility in high strength salt solutions, such as urine, is unknown as generalised wastewater physico-chemical speciation models do not exist for solutions with many components and high ionic strength [30]. Other species with similar range solubilities include potassium bicarbonate and sodium bicarbonate (24.9 and 8.7 g/100 g H₂O at 20 °C, respectively [31]). As temperature is lowered, the solubility of ammonium bicarbonate decreases relatively more than other bicarbonates (10.6, 18.6 and 6.5 g/100 g H₂O at 0 °C for ammonium, potassium and sodium bicarbonate, respectively [31]). As potassium and sodium are present in lower concentrations in urine to ammonium, ammonium bicarbonate is expected to precipitate first when urine is cooled. Commonly used speciation models such as PHREEQC 3 and Visual MINTEQ 3.1 do not currently extend to highly concentrated solutions such as concentrated urine [30], and experimental results are required to confirm this hypothesis.

In this paper, changes in urine concentrate composition correlating to the feed composition and the applied current density are demonstrated by means of a three compartment abiotic electro-concentration cell fed with synthetic urine. Inspired by a bio-electrochemical concept demonstrated by Ledezma et al. [25], the abiotic approach allows rapid mapping of parameters beyond the limitations of microbiological constraints. Synthetic urine was chosen to enable consistency when systematically varying the experimental factors of applied current density and feed composition [32,33]. Nitrogen recovery is achieved as solid ammonium bicarbonate via cooling, and the limits for recovery as a solid are identified.

2. Materials and methods

2.1. Medium composition

A synthetic urine solution (referred to as ACE as it contains acetate as representative of the organic fraction) representing ureolysed urine was selected based on work done at the Swiss Federal Institute of Aquatic Science and Technology (EAWAG) [33,34] consisting of (g L⁻¹) Na₂SO₄ (2.3), NaH₂PO₄ (2.1), NaCl (3.6), KCl, (4.2), NH₄CH₃CO₂ (9.6), NH₄OH (25% liquid, 13 mL L⁻¹), NH₄HCO₃ (21.4). This recipe simulates urine after complete removal of Mg and Ca through precipitation

with phosphate during ureolysis, and models organic content with acetate. A composition without ammonium acetate was tested (referred to as NO ACE) identical to ACE, except without addition of NH₄CH₃CO₂. A further medium was developed in which all acetate was assumed to be digested into carbon dioxide, modelling fully digested ureolysed urine. This digested urine recipe (referred to as ABC for ammonium bicarbonate) consisted of (g L⁻¹) Na₂SO₄ (2.3), NaH₂PO₄ (2.1), NaCl (3.6), KCl, (4.2), NH₄OH (25% liquid, 3.5 mL L⁻¹), NH₄HCO₃ (41.2). The feeds were prepared as used and feed composition was monitored through sampling when changing the feed. Synthetic urine was chosen to enable consistency when systematically varying the experimental factors.

2.2. Reactor and equipment

Custom reactors were used consisting of three acrylic plates forming three parallel compartments (anodic, middle and cathodic) of 70 mm × 50 mm × 10 mm each (see Fig. 1). Four identical reactors were used as replicates. The anodic compartment was filled with a packed bed of acid and alkaline washed graphite granules (granule size 2–10 mm; EC-100, Graphite Sales Inc., USA) with a graphite rod (Ø5 mm; Element14, Australia) acting as a current collector. The anode was separated from a middle compartment by a Cation Exchange Membrane (CEM) (CMI-7000 Membrane International Inc., USA). The cathodic compartment contained a 70 mm × 50 mm stainless steel mesh as a cathode and was separated from the middle compartment by an Anion Exchange Membrane (AEM) (Membrane International Inc. AMI-7001). The projected surface area of both membranes and electrodes was 35 cm² and the volume of each chamber was 35 mL, rendering the reactor effective volume as 105 mL. The anodic and cathodic compartments were hydraulically connected forming a loop including an online pH meter (Endress + Hauser Liquisys CPM253) and a circulation pump. The middle compartment was connected to an overflow bottle with a gas bag and was not open to the atmosphere. A potentiostat (Bio-Logic VMP-3) was used as a power source in two electrode mode, applying constant current and recording the voltage applied and electrical energy used. Current densities of 40–100 A m⁻² were applied. A cooling coil system (RC1, Ratek, Australia) was used to lower the temperature of a thermally-isolated container to +4 °C to store the collected concentrate. A freezer set to -18 °C was used to cool the collected concentrate.

2.3. Operation

Feed was pumped into each reactor at a constant rate of 20.9 ± 0.4 mL h⁻¹ to the anodic chamber of the reactor. The anodic chamber and the cathodic chamber were connected and constantly circulated at 2100 mL h⁻¹. Effluent was collected from the cathodic chamber. A concentrate was formed as the middle chamber overflow and was collected into a 250 mL bottle kept at 4 °C. Flow schematics are presented in Fig. 1a. A constant current density, J [A m⁻²], between the electrodes was applied and the voltage required for this current was logged by the potentiostat. All runs were initiated with feed in all compartments and monitored until steady state was reached and no change in composition in the middle chamber was detected. All experimental runs showed a clear concentration phase and subsequent steady state phase. Samples from three runs were analysed during the concentration phase, all other runs were sampled and analysed only during steady state - a list of experiments can be found in the results section (Table 1). In steady state operation, empty overflow collection bottles were used to collect the overflow over a set time period. 1.5 mL samples were taken from the feed, the anodic chamber, the middle chamber, and the effluent. Samples were taken at the start and end of a steady state phase. At the end of a steady state experiment, the concentrate collection bottle was removed, sampled, measured for volume and set in a freezer (-18 °C). After 18 h the supernatant was filtered

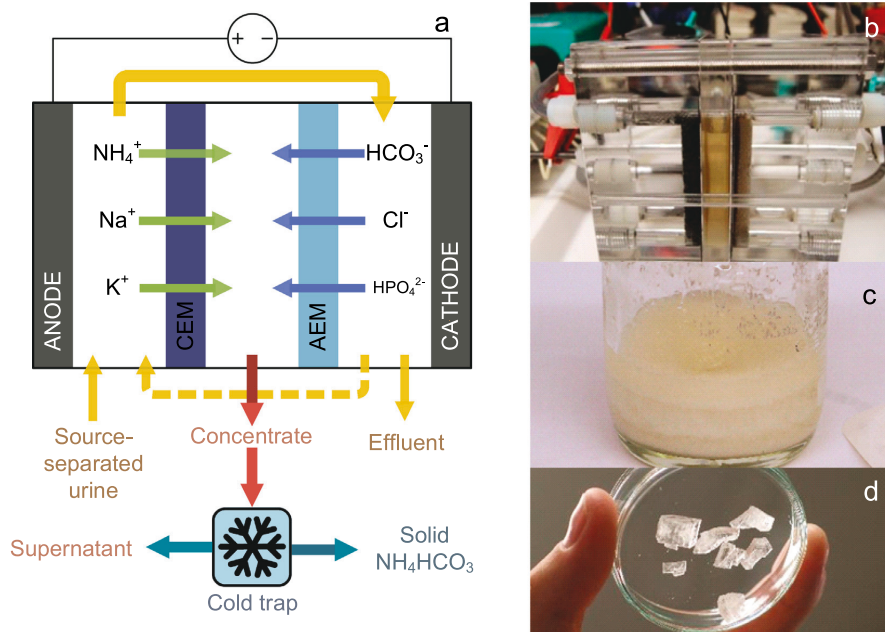


Fig. 1. Experiment illustrations. (a) Schematic flow chart, (b) three compartment reactor, (c) precipitated solids after cooling and decanting, and (d) air dried solid ammonium bicarbonate crystals from the precipitated solids. CEM: cation-exchange membrane. AEM: anion-exchange membrane.

(0.45 μm) to separate the formed crystals and measured for volume, with precipitated solids collected for reference. The collected solids were redissolved in 2000 mL deionized water and sampled. All samples were filtered (0.45 μm) and diluted with deionized water for analysis. Results presented with 95% confidence intervals represent parallel results from repeated experiments. Repetitions were done 1, 2 or 4 times, depending on the experiment (see Table 1).

2.4. Sample analysis

Samples were analysed for pH, conductivity (EC), chloride and TAN (Total Ammonium Nitrogen) with Horiba B-712 pH meter, Horiba B-771 EC meter, Merck Spectroquant Chloride Test (101807), and Merck Spectroquant Ammonium Test (114752), respectively. These results confirmed the formation of steady state conditions and ruled out leaks or other problems. Samples from three concentration stages and 13 steady state samples were further analysed, respectively, for elemental analysis, ammonia species, anions and carbon species using Inductively Coupled Plasma Optical Emission Spectroscopy (ICP-OES) (Perkin Elmer Optima 7300DV, Waltham, MA, USA) after nitric acid digestion (calcium, sodium, potassium, magnesium); Flow Injection Analysis (FIA) Lachat QuickChem8500 (Lachat Instruments, Loveland, CO, USA); Ion Chromatography Dionex ICS-2100 (Dionex, CA, USA); and Total Organic Carbon Analyser Shimadzu TOC-L CSH with TNM-L TN unit (Kyoto, Japan).

Raman spectroscopy was taken from sample of formed crystals employing an Alpha 300 (WITec GmbH, Ulm, Germany) equipped with a 40x collar corrected (Nikon) objective. A frequency doubled continuous-wave Nd:YAG laser stabilized at 532 nm was used for excitation. Raman signals were collected with a 50 mm optical fibre with a resolution of 4 cm^{-1} . For all the measurements the laser power at the sample was less than 10 mW.

2.5. Calculations

Ionic strength to compare salinities of samples was calculated using Eq. (1).

$$IS = \frac{1}{2} \sum_{i=1}^n c_i z_i^2 = \frac{1}{2} ([\text{NH}_4^+] + [\text{Na}^+] + [\text{K}^+] + [\text{Cl}^-] + [\text{HCO}_3^-] + [\text{SO}_4^{2-}] [-2]^2 + [\text{HPO}_4^{2-}] [-2]^2) \quad (1)$$

where IS is ionic strength, c_i is molarity (mol L^{-1}) and z_i is charge. No corrections for activities were applied [35].

The ionic strength of ammonium bicarbonate was calculated using Eq. (2).

$$IS_{ABC} = 1/2([\text{NH}_4^+] + [\text{HCO}_3^-]) \quad (2)$$

where $[\text{NH}_4^+]$ and $[\text{HCO}_3^-]$ are ammonium and bicarbonate concentrations. This represents the share of ammonium bicarbonate of the total ionic content of the solution. Activity coefficients were assumed to be 1. This formula was mainly used to calculate the relative fraction of ammonium bicarbonate in ionic strength IS_{ABC}/IS .

Ammonium bicarbonate ionic product was calculated using Eq. (3).

$$IP_{ABC} = [\text{NH}_4^+][\text{HCO}_3^-] \quad (3)$$

where $[\text{NH}_4^+]$ and $[\text{HCO}_3^-]$ are ammonium and bicarbonate concentrations [36]. Activity coefficients were assumed to be 1. Ionic product is used to determine saturation of species for precipitation.

The Coulombic efficiency for ammonium transfer was calculated according to Eq. (4).

$$CE = \frac{n_{\text{NH}_4} \times z_{\text{NH}_4}}{Q \times F} \quad (4)$$

where CE is Coulombic efficiency, n_{NH_4} is moles of ammonium ions transferred (mol), and z_{NH_4} is charge of ammonium ion (1), Q is the

Table 1

Feed, concentrate and filtered precipitated concentrate main ionic components. NO ACE and ABC feeds do not contain acetate. N = number of parallel experiments. If multiple experiments, values are averages with 95% confidence intervals. All values in mM expect current density J in $A\ m^{-2}$.

Feed	J	N	TAN ^a	Na	K	TiC ^b	Cl	Acetate	SO ₄	PO ₄
NO ACE	Feed		444	111	56	271	118	NA	16	18
	40	1	1842	434	270	1226	801	NA	97	42
ACE	Feed		568	111	56	271	118	125	16	18
	40	1	1906	353	230	1047	739	277	83	33
	60	2	2049 ± 20	428 ± 21	255 ± 11	1268 ± 15	669 ± 4	332	82 ± 5	51 ± 7
	80	1	2035	444	240	1266	550	Err ^c	62	48
ABC	Feed		568	111	56	521	118	NA	16	18
	60	4	2065 ± 39	399 ± 11	250 ± 3	1747 ± 8	632 ± 12	NA	66 ± 5	25 ± 1
	80	2	2174 ± 25	428 ± 4	245 ± 2	1852 ± 3	568 ± 7	NA	61 ± 1	45 ± 1
	100	2	2306 ± 40	480 ± 23	250 ± 3	1939 ± 45	544 ± 1	NA	68 ± 9	58 ± 1
Supernatant after solids precipitation										
ABC	60	4	1606 ± 54	429 ± 10	253 ± 4	1223 ± 30	669 ± 7	NA	69 ± 5	28 ± 2
	80	2	1585 ± 140	437 ± 1	239 ± 1	1315 ± 85	582 ± 12	NA	63 ± 1	44 ± 2
	100	2	1817 ± 55	500 ± 20	250 ± 1	1413 ± 80	563 ± 4	NA	71 ± 10	61 ± 1

^a Total ammonia nitrogen, $NH_4^+ + NH_3$.

^b Total inorganic carbon, $CO_2 + HCO_3^- + CO_3^{2-}$.

^c Error in sample preparation.

charge passed by the potentiostat (C) and F the Faraday constant ($96\ 485\ C\ mol^{-1}$) [36].

Statistical tests were conducted using MathWorks MATLAB R2017 and Microsoft Excel 2016 Data Analysis. The analysis included one-way and multivariable analysis of variance (ANOVA), and coefficients of correlation using MATLAB, and regression analysis using Microsoft Excel. A significance threshold of 5% was used for all statistical tests and error margins given for values represent 95% confidence intervals for all values presented.

3. Results and discussion

3.1. Concentrate strength remains similar with varied applied current and feed composition

During the concentration stage the middle compartment concentration increases as ions migrate through the ion selective membranes due to the applied potential. The consequent higher concentration gradient across the membrane increases water osmosis through the membrane. In addition, the concentration gradient causes back migration of ionic species from the middle chamber to the catholyte and anolyte due to non-ideal membrane permselectivity, and uncharged ion pairs diffuse across the ion exchange membranes, resulting in a concentration plateau of the concentrate [37]. Electro-osmosis also contributes to water flow into middle chamber [38].

Measured ionic conductivities and ionic concentrations during concentration and steady state phases are presented in Fig. 2. The plateau concentrations reached for each feed and current density (J) applied are found in Table 1. No membrane fouling or scaling was detected during the duration of experiments and no difference in results was seen between runs with fresh and used membranes (results not shown).

In order to study the saturation in large concentrations, a speciation model is commonly used to find out activities of different species. However, high concentrations and large number of components found in our concentrate render it unsuitable for currently existing speciation models [30]. Thus saturation was studied experimentally using conductivity and measured concentrations.

As current density was increased, water flux into concentrate at steady state was found to be proportional to the current density within the studied current density range (a linear regression analysis using MS Excel fitted the model $Q_w = 0.147\%/A\ m^{-2}\ J + 3.66\%$ with a p-value of 0.001, where Q_w is the portion of water in the feed to flow to the

concentrate) (Table 2). This supports the notion that as more ions cross the membrane, more ion-bound water is transported while the higher concentration gradient also induces higher water current through osmosis.

As water flux increases, the measured ionic conductivity forms a plateau averaging $131 \pm 4\ mS\ cm^{-1}$ (see Fig. 2a and b). Applied current density or feed do not affect the conductivity within the limits of the experiments considering a 5% significance threshold (one-way ANOVA using MATLAB gives p-values 0.96 and 0.20 for current density and feed, respectively).

While conductivity was unaffected by the applied current density, the ionic strength, calculated as shown in Eq. (1), was observed to increase as current density J increased. Linear regression using Microsoft Excel 2016 fitted the model $IS = 0.0068\ M/A\ m^{-2}\ J + 2.2961\ M$ with a p-value of $1.1 \cdot 10^{-4}$, less than 5%, indicating a significant relationship (see Fig. 2d). This result suggests that current density correlates with the ionic strength of the concentrate linearly within the limits of the experiment. The increase in ionic strength observed was statistically significant but small, increasing only 16%, while current density more than doubled from 40 to $100\ A\ m^{-2}$.

The discrepancy between plateauing of ionic conductivity and the small increase of ionic strength with current density is an interesting finding. A plausible explanation is that the proportion of chargeless species can increase with increasing concentration, thus not increasing the actual activities of charged species. As full speciation is not available, this remains a result to be verified. For single salt solutions, it has been shown that ionic conductivity can plateau and drop in high concentrations due to a larger portion of the salt remaining in non-ionic form [36]. This however typically happens only at salinities in the range of tens of percent's in mass, which were not reached here.

Considering energy efficiency during electro-concentration at different current densities, current efficiency for ammonium transport over the CEM from anode to concentrate was 63–72% (average $67 \pm 2\%$) in all experiments without a statistically significant dependence on current density or feed type (a two-factor ANOVA using MATLAB gives p-values of 0.453 and 0.169 for current density and feed, respectively).

The relative ionic concentrations for different current densities are presented in Fig. 3 for the concentrate and the diluate for ACE and ABC feeds. Increase in current density increases the extent of salt removal from the feed (one-way ANOVA gives p-value of 0.0004 for current density), which is reflected in the diminishing diluate concentrations. Different ions concentrate with different ease through the membranes

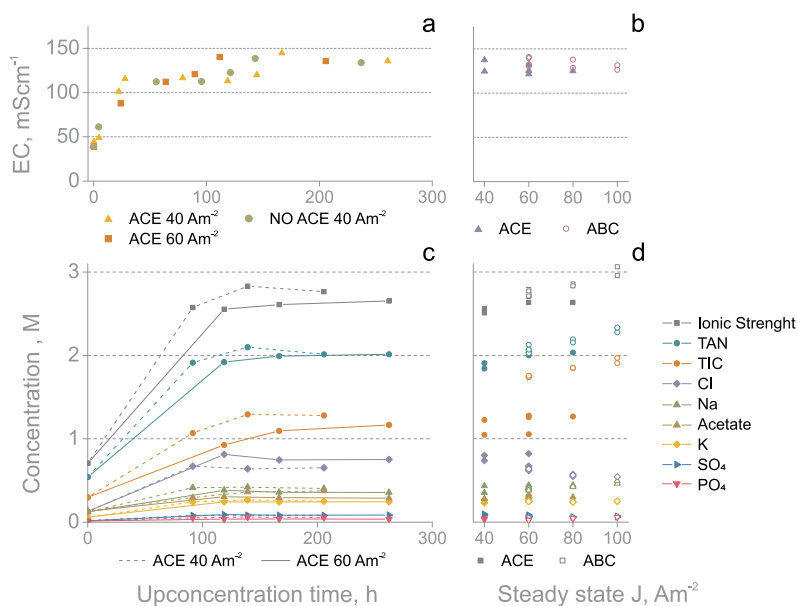


Fig. 2. Concentration and steady state characteristics. (a) Increase of concentrate conductivity during concentration phase. (b) Concentrate conductivity in steady state for different feeds and different current densities. (c) Increase of concentrate concentrations during concentration phase. (d) Concentrate concentrations in steady state for different feeds and current densities. The ionic conductivity of concentrate is constant with different feeds and current densities while ionic strength and concentrations are affected by feed and current density.

based on their diffusion coefficients, also referred as ion mobility. The diffusion coefficients for diffusion at infinitely small concentrations for Cl^- , K^+ , NH_4^+ , Na^+ , HCO_3^- , CH_3CO_2^- and H_2PO_3^- are (in $10^{-5} \text{ cm}^2 \text{ mol}^{-1}$) 2.03, 1.96, 1.96, 1.33, 1.19, 1.09 and 0.96 [31], respectively. The diffusion coefficients match the order of relative concentration for ABC feed. For ACE feed, the order at 40 A m^{-2} matches for all ions except HCO_3^- , while variation is found at higher current densities. At low current densities, a high fraction of current goes through the membranes as ions with high mobility. At higher current densities correlating to high extent of salt removal, this effect is countered as ions with high mobility get depleted and ions with lower mobility take a larger fraction of the current. As extent of salt recovery increases towards maximum, all salts should converge towards the same concentration factor. This trend can be seen in Fig. 3 for ABC feed, while not yet clearly for ACE feed.

The effect of changing relative concentrations with changing current density is relatively small, but has potential for optimizing nutrient recovery technologies for targeted ions. At lower current densities (correlating to lower extent of salt removal) relatively stronger chloride and potassium concentrate can be obtained - at higher current densities relative composition converges towards feed relative composition.

Table 2

Recovery percentage of main components and total volume into concentrate, and recovered nitrogen in subsequent solid precipitate. NO ACE and ABC feeds do not contain acetate. N = number of parallel experiments. If multiple experiments, values are averages with 95% confidence intervals. All units in percent expect current density J in A m^{-2} .

Feed	J	N	TAN ^a	Na	K	TIC ^b	Cl	Ac	SO ₄	PO ₄	H ₂ O	Solid NH ₄ HCO ₃ ^c
NO ACE	40	1	38	33	41	37	60	NA	57	21	9.3	Not detected
ACE	40	1	33	28	37	34	55	21	47	19	9.6	Not detected
	60	2	49 ± 2	47 ± 2	56 ± 2	57 ± 1	69 ± 1	34	66 ± 1	39 ± 6	12.9 ± 0.6	Not detected
	80	1	62	63	69	74	74	Err ^d	67	47	16.4	Not detected
ABC	60	4	40 ± 1	37 ± 3	47 ± 4	37 ± 2	58 ± 6	NA	47 ± 6	16 ± 1	11.4 ± 0.3	11 ± 1
	80	2	60 ± 1	57 ± 1	66 ± 2	55 ± 2	75 ± 1	NA	63 ± 2	42 ± 2	15.7 ± 0.4	16 ± 4
	100	2	72 ± 1	76 ± 2	79 ± 2	64 ± 1	87 ± 3	NA	84 ± 9	61 ± 2	17.8 ± 0.6	17 ± 3

^a Total ammonia nitrogen, $\text{NH}_4^+ + \text{NH}_3$.

^b Total inorganic carbon, $\text{CO}_2 + \text{HCO}_3^- + \text{CO}_3^{2-}$.

^c Total ammonia nitrogen in solid ammonium bicarbonate after precipitation.

^d Error in sample preparation.

3.2. Concentrate precipitation

The collected concentrate was cooled to $-18 \text{ }^\circ\text{C}$ for 20 h, and salt precipitation occurred as mixture of small and large crystals, forming layer-like structures in runs using ABC feed. No freezing of water was observed probably due to the very high salinity. Formed crystals were identified as pure ammonium bicarbonate through Raman spectroscopy (see Fig. 4) and mass balances support this observation as only ammonium and bicarbonate show significant change in liquid concentration during precipitation (see Table 1). The fractions captured in the concentrate and further in the precipitated solid are presented in Table 2. Maximum recovery rate of 72–61–79% of N:P:K, respectively, into liquid concentrate, and 17% recovery of N into ammonium bicarbonate solid were achieved from ABC feed at 100 A m^{-2} .

Ammonium bicarbonate can precipitate if there are favourable conditions for nucleation under supersaturation [39]. For cooled concentrates, supersaturation cannot currently be modelled as the solubility constant of ammonium bicarbonate has not been defined at temperatures below $0 \text{ }^\circ\text{C}$, and the salt effect (diminishing activities due to competing ions) is significant.

To evaluate limits for saturation conditions, ionic strength (IS),

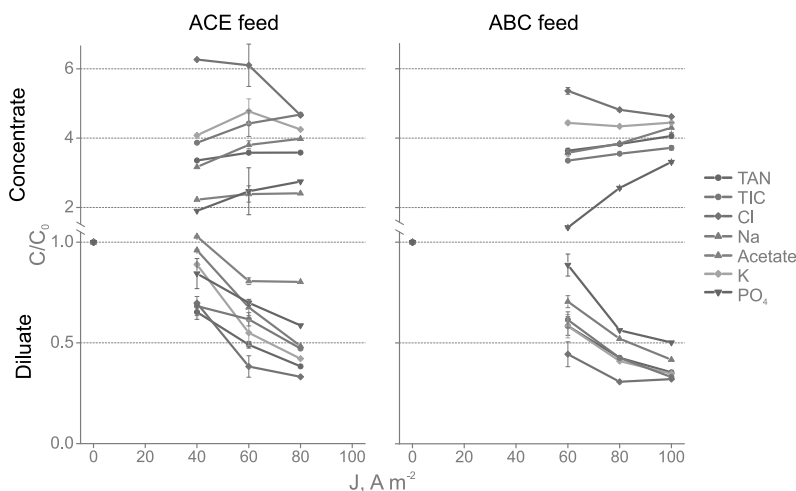


Fig. 3. Relative concentrate and dilute concentrations. Synthetic ureolysed urine feed (ACE feed) and synthetic ureolysed digested urine feed (ABC feed) are presented at different current densities.

ammonium bicarbonate ionic strength (IS_{ABC}), the ratio of these two (IS_{ABC}/IS), and ammonium bicarbonate ionic product (IP_{ABC}) are compared (see Fig. 5 and Table 3). These variables are calculated from measured concentrations.

As concentrate from ABC feed is cooled, precipitation occurred in all ABC concentrate samples and a residual ABC supernatant can be expected to be close to saturation conditions of solid ammonium bicarbonate. We examined the statistics of different liquids, namely ACE concentrate, ABC concentrate and ABC supernatant to find relevant differences. Averages of both IP_{ABC} and IS_{ABC} were higher for ACE concentrate than ABC supernatant ($2.44 M^2$ and $2.15 M^2$, and $1.58 M$ and $1.47 M$, respectively), suggesting a more saturated solution. However, no precipitation was detected in ACE concentrates. As competing ions can lower the activities of precipitating ions, we then looked at the relative ionic strength of ammonium bicarbonate (IS_{ABC}/IS). The average IS_{ABC}/IS was lower for ACE concentrate compared to ABC supernatant (60% and 63%, respectively). Otherwise the samples from ABC supernatant and ACE concentrate have similar ionic properties. One-way ANOVA for IS_{ABC} , IP_{ABC} and IS_{ABC}/IS between ABC

supernatant and ACE concentrate gives p-values of 0.05, 0.15 and 0.02, respectively, implicating weak or no statistical difference when using a 5% confidence interval. ABC supernatant and ACE concentrate as a combined group however differ very significantly from supersaturated ABC concentrate (one-way ANOVA for IS_{ABC} , IP_{ABC} and IS_{ABC}/IS between combined ABC supernatant and ACE concentrate and ABC concentrate gives p-values of $2.9 \cdot 10^{-8}$, $4.8 \cdot 10^{-9}$ and $8.6 \cdot 10^{-11}$, respectively, indicating significant difference using a 5% confidence interval). These results indicate that both ABC supernatant and ACE concentrate are close to saturation, while ABC concentrate is supersaturated. The limiting conditions for forming a solid precipitate in this experiment occur close to the conditions measured for ABC supernatant and ACE concentrate, towards the conditions found in ABC concentrate. In separate short term experiments with concentrate feed recycled to the feed (data not presented), trace amounts of ammonium bicarbonate precipitate has been successfully collected also when using ACE feed in a concentrate with similar composition to the ACE concentrate shown here, further supporting that the notion that ACE concentrate is close to saturation (at $-18^\circ C$).

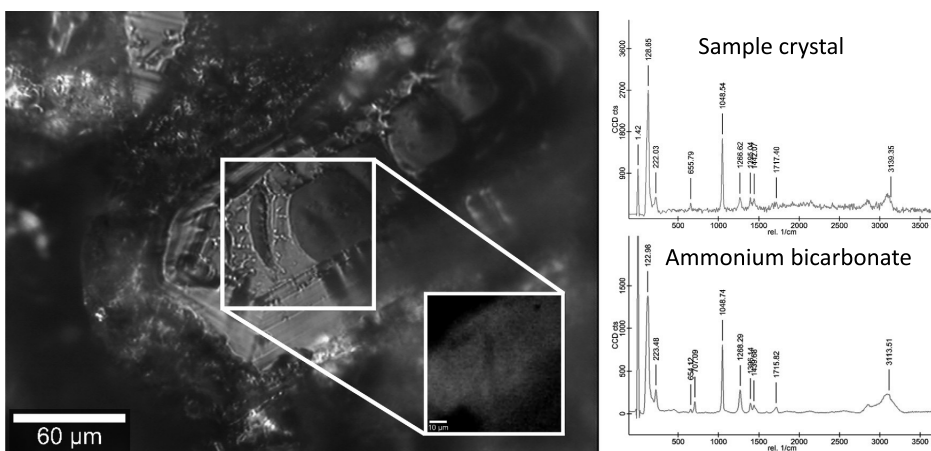


Fig. 4. Solid crystals. Crystals were identified as pure ammonium bicarbonate by Raman spectroscopy.

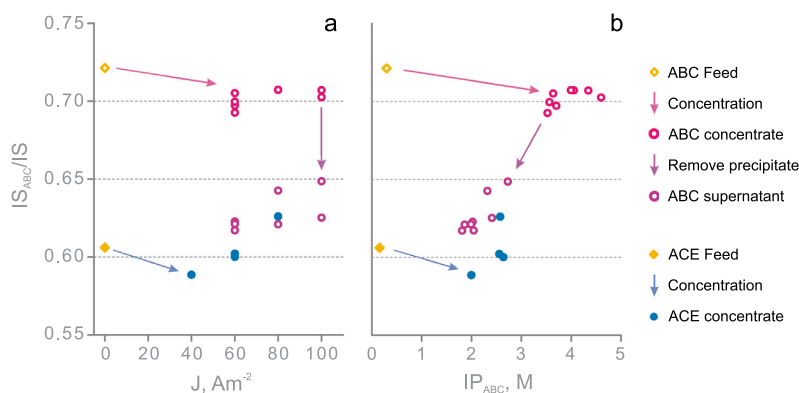


Fig. 5. Relative ammonium bicarbonate ionic strength. Presented in relation to (a) current density and (b) ionic strength, for feeds, concentrates and precipitation supernatants. When feeds are concentrated, IS_{ABC}/IS remains on a similar level to feed and ionic strength increases. Precipitation at $-18^{\circ}C$ for ABC feed decreases IS_{ABC}/IS to a similar level found at ACE feed.

Table 3

Average parameters of liquids. Ionic strength (IP), ammonium bicarbonate ionic strength (IP_{ABC}), and ammonium bicarbonate ionic product (IP_{ABC}) of ACE and ABC feed, their concentrates and ABC supernatant after precipitation. N = number of parallel experiments. If multiple experiments, values are averages with 95% confidence intervals.

		N	IS, M	IS_{ABC}, M	IP_{ABC}, M^2	$IS_{ABC}/IS, \%$
ACE	Feed	1	0.69	0.42	0.15	60.9
	Concentrate	4	2.67 ± 0.19	1.61 ± 0.14	2.44 ± 0.48	60.4 ± 2.5
ABC	Feed	1	0.75	0.54	0.30	72.1
	Concentrate	8	2.83 ± 0.11	1.99 ± 0.08	3.93 ± 0.33	70.2 ± 0.5
	Supernatant	8	2.35 ± 0.11	1.47 ± 0.09	2.15 ± 0.26	62.7 ± 1.0

From these data sets, we can thus hypothesise that to reach precipitation of ammonium bicarbonate from concentrated urine at $-18^{\circ}C$, minimum threshold values for both IP_{ABC} and IS_{ABC}/IS must be satisfied. These values are estimated at around $2.25 M^2$ for IP_{ABC} and $\sim 62\%$ for IS_{ABC}/IS , these being combined averages for ABC supernatant and ACE concentrate from our experiments.

These results suggest that the limiting factor for further precipitation is the relative ammonium bicarbonate concentration to the total ionic strength. This means that other ions in the concentrate block further precipitation and to reach higher capture through precipitation, alternate ways of ion separation are required.

3.3. Feasibility of nitrogen capture through electro-concentration

The energy used for electro-concentration was measured by the potentiostat as an integrated product of applied potential and resulting current. The system produced oxygen at the anode and hydrogen on the cathode with applied total cell voltages of 3–5 V, depending on the current density. Specific electrical energy consumption was measured as $30, 35 \pm 1$ and $46 MJ kg N^{-1}$ for ACE feed at 40, 60 and $80 A m^{-2}$, and $35 \pm 1, 39 \pm 2$ and $47 \pm 3 MJ kg N^{-1}$ for ABC feed at 60, 80 and $100 A m^{-2}$, respectively. This energy consumption is high compared to bio-electroconcentration systems applying bioanodes running on urine ($8.6 MJ/kg N$ [25], and $4.9 MJ/kg N$ [40]). The use of bioanodes and oxygen reducing cathodes holds promise to reach current densities similar to those used in this study [4,25] with significantly lower energy demands, potentially even reaching positive energy outputs [4,41].

Capture of nitrogen as solid ammonium bicarbonate without chemical addition by cooling the concentrate is found possible for ABC feed (simulated ureolysed and digested feed) reaching up to 17% capture. The ACE feed (simulated ureolysed feed) did not show capacity for capture as solid via cooling due to low IP_{ABC}/IS ratio. Limited methods are available to increase the portion that can be captured as solid due to the large concentrations of competing ions, especially sodium,

potassium and chloride. Concentrate refeeding or serial reactor systems can be applied to the concentrate to reach higher concentrations and liquid capture rates. However, these methods will not significantly change the total fraction of nitrogen that can be captured as solid ammonium bicarbonate as they don't remove competing ions which will also concentrate, further inhibiting ammonium bicarbonate precipitation (for more detailed evaluation of competitive ion transport, see Thompson Brewster et al. 2017). This limitation renders capture by cooling non-feasible as a primary means of nitrogen separation from the concentrate in the studied settings. Selective membranes or other methods of removing competing salts could change this conclusion and could enable precipitation by cooling as a viable option. For specific ammonium bicarbonate removal, other methods such as thermal evaporation or stripping are seen more appropriate as ammonium and bicarbonate are the only readily evaporative species.

Acknowledgements

The authors acknowledge the facilities, and the scientific and technical assistance of the Analytical Services Laboratory at the Advanced Water Management Centre, The University of Queensland and Dr B. C. Donose for help with the spectroscopic analyses. This work was performed in part at the Queensland node of the Australian National Fabrication Facility, a company established under the National Collaborative Research Infrastructure Strategy to provide nano and microfabrication facilities for Australia's researchers.

Funding

This research was supported financially by Maj and Tor Nessling foundation and Walter Ahlström foundation supporting Johannes Jermakka; and the Australian Research Council Project LP 150100402 in partnership with Queensland Urban Utilities (QUU) and ABR Process Development; the Australian Grain Research & Development Corporation Grain Research Scholarship (GRS10661) supporting

Emma Thompson Brewster. Pablo Ledezma acknowledges an ECR Development Fellowship from The University of Queensland.

References

- [1] T.A. Larsen, K.M. Udert, J. Lienert, Source separation and decentralization for wastewater management, IWA, London, 2013.
- [2] J. Rockström, W. Steffen, K. Noone, Å. Persson, F.S. Chapin, E. Lambin, T.M. Lenton, M. Scheffer, C. Folke, H.J. Schellnhuber, B. Nykvist, C.A. de Wit, T. Hughes, S. van der Leeuw, H. Rodhe, S. Sörlin, P.K. Snyder, R. Costanza, U. Svedin, M. Falkenmark, L. Karlberg, R.W. Corell, V.J. Fabry, J. Hansen, B. Walker, D. Liverman, K. Richardson, P. Crutzen, J. Foley, Planetary boundaries: Exploring the safe operating space for humanity, *Ecol. Soc.* 14 (2009), <http://dx.doi.org/10.1038/461472a>.
- [3] E. Friedler, D. Butler, Y. Alfiya, Wastewater composition, in: T.A. Larsen, K.M. Udert, J. Lienert (Eds.), *Source Sep. Decentralization Wastewater Manag.* IWA Publishing, Oxford, 2013, pp. 241–258.
- [4] P. Ledezma, P. Kuntke, C.J.N. Buisman, J. Keller, S. Freguia, Source-separated urine opens golden opportunities for microbial electrochemical technologies, *Trends Biotechnol.* 33 (2015) 214–220, <http://dx.doi.org/10.1016/j.tibtech.2015.01.007>.
- [5] H. Jönsson, B. Vinnerås, Closing the loop: Recycling nutrients to agriculture, in: T.A. Larsen, K.M. Udert, J. Lienert (Eds.), *Source Sep. Decentralization Wastewater Manag.* IWA Publishing, Oxford, 2013, pp. 163–178.
- [6] T.A. Larsen, K.M. Udert, J. Lienert, Editorial, in: T.A. Larsen, K.M. Udert, J. Lienert (Eds.), *Source Sep. Decentralization Wastewater Manag.* IWA Publishing, Oxford, 2013, pp. 1–11.
- [7] M. Maurer, W. Pronk, T.A. Larsen, Treatment processes for source-separated urine, *Water Res.* 40 (2006) 3151–3166, <http://dx.doi.org/10.1016/j.watres.2006.07.012>.
- [8] S. Antonini, S. Paris, T. Eichert, J. Clemens, Nitrogen and phosphorus recovery from human urine by struvite precipitation and air stripping in Vietnam, *Clean - Soil, Air, Water* 39 (2011) 1099–1104, <http://dx.doi.org/10.1002/clen.201100036>.
- [9] B. Etter, E. Tilley, R. Khadka, K.M. Udert, Low-cost struvite production using source-separated urine in Nepal, *Water Res.* 45 (2011) 852–862, <http://dx.doi.org/10.1016/j.watres.2010.10.007>.
- [10] A. Hug, K.M. Udert, Struvite precipitation from urine with electrochemical magnesium dosage, *Water Res.* 47 (2013) 289–299, <http://dx.doi.org/10.1016/j.watres.2012.09.036>.
- [11] J.A. Wilsenach, C.A. Schuurbierts, M.C. van Loosdrecht, Phosphate and potassium recovery from source separated urine through struvite precipitation, *Water Res.* 41 (2007) 458–466, <http://dx.doi.org/10.1016/j.watres.2006.10.014>.
- [12] T. Duong, Z.L. Xie, D. Ng, M. Hoang, Ammonia removal from aqueous solution by membrane distillation, *Water Environ. J.* 27 (2013) 425–434, <http://dx.doi.org/10.1111/j.1747-6593.2012.00364.x>.
- [13] A. Zarebska, K.V. Christensen, B. Norddahl, The application of membrane contactors for ammonia recovery from pig slurry, *Procedia Eng.* 44 (2012) 1642–1645, <http://dx.doi.org/10.1016/j.proeng.2012.08.895>.
- [14] M. Ronteltap, M. Maurer, W. Gujer, Struvite precipitation thermodynamics in source-separated urine, *Water Res.* 41 (2007) 977–984, <http://dx.doi.org/10.1016/j.watres.2006.11.046>.
- [15] M. Rodríguez Arredondo, P. Kuntke, A. ter Heijne, H.V.M. Hamelers, C.J.N. Buisman, Load ratio determines the ammonia recovery and energy input of an electrochemical system, *Submitted*. 111 (2017) 330–337. doi:10.1016/j.watres.2016.12.051.
- [16] P. Kuntke, M. Rodríguez Arredondo, L. Widayakristi, A. Ter Heijne, T.H.J.A. Sleutels, H.V.M. Hamelers, C.J.N. Buisman, Hydrogen gas recycling for energy efficient ammonia recovery in electrochemical systems, *Environ. Sci. Technol.* (2017), <http://dx.doi.org/10.1021/acs.est.6b06097>.
- [17] A.K. Luther, J. Desloover, D.E. Fennell, K. Rabaey, Electrochemically driven extraction and recovery of ammonia from human urine, *Water Res.* 87 (2015) 367–377, <http://dx.doi.org/10.1016/j.watres.2015.09.041>.
- [18] J. Desloover, A. Abate Woldeyohannis, W. Verstraete, N. Boon, K. Rabaey, Electrochemical resource recovery from digestate to prevent ammonia toxicity during anaerobic digestion, *Environ. Sci. Technol.* 46 (2012) 12209–12216, <http://dx.doi.org/10.1021/es3028154>.
- [19] J. Desloover, J. De Vrieze, M. Van De Vijver, J. Mortelmans, R. Rozendal, K. Rabaey, Electrochemical nutrient recovery enables ammonia toxicity control and biogas desulfurization in anaerobic digestion, *Environ. Sci. Technol.* 49 (2015) 948–955, <http://dx.doi.org/10.1021/es504811a>.
- [20] P. Kuntke, Nutrient and energy recovery from urine, PhD Thesis, 2013. <http://edepot.wur.nl/254782>.
- [21] M. Rodríguez Arredondo, P. Kuntke, A.W. Jeremiasse, T.H.J.A. Sleutels, C.J.N. Buisman, A. ter Heijne, Bioelectrochemical systems for nitrogen removal and recovery from wastewater, *R. Soc. Chem.* 1 (2014) 22–33, <http://dx.doi.org/10.1039/C4EW00066H>.
- [22] S. Gildemyn, A.K. Luther, S.J. Andersen, J. Desloover, K. Rabaey, Electrochemically and bioelectrochemically induced ammonium recovery, *J. Vis. Exp.* (2015), <http://dx.doi.org/10.3791/52405>.
- [23] P. Kuntke, P. Zamora, M. Saakes, C.J.N. Buisman, H.V.M. Hamelers, Gas-permeable hydrophobic tubular membranes for ammonia recovery in bio-electrochemical systems, *Environ. Sci. Water Res. Technol.* (2016), <http://dx.doi.org/10.1039/c5ew00299k>.
- [24] R.C. Tice, Y. Kim, Energy efficient reconcentration of diluted human urine using ion exchange membranes in bioelectrochemical systems, *Water Res.* 64 (2014) 61–72, <http://dx.doi.org/10.1016/j.watres.2014.06.037>.
- [25] P. Ledezma, J. Jermakka, J. Keller, S. Freguia, Recovering nitrogen as a solid without chemical dosing: bio-electroconcentration for recovery of nutrients from urine, *Environ. Sci. Technol. Lett.* (2017), <http://dx.doi.org/10.1021/acs.estlett.7b00024>.
- [26] W. Pronk, M. Biebow, M. Boller, Treatment of source-separated urine by a combination of bipolar electro dialysis and a gas transfer membrane, *Water Sci. Technol.* 53 (2006) 139–146, <http://dx.doi.org/10.2166/wst.2006.086>.
- [27] W. Pronk, S. Zuleeg, J. Lienert, B. Escher, M. Koller, A. Berner, G. Koch, M. Boller, Pilot experiments with electro dialysis and ozonation for the production of a fertilizer from urine, *Water Sci. Technol.* 56 (2007) 219–227, <http://dx.doi.org/10.2166/wst.2007.575>.
- [28] M. Mondor, L. Masse, D. Ippersiel, F. Lamarche, D.I. Massé, Use of electro dialysis and reverse osmosis for the recovery and concentration of ammonia from swine manure, *Bioresour. Technol.* 99 (2008) 7363–7368, <http://dx.doi.org/10.1016/j.biortech.2006.12.039>.
- [29] D. Ippersiel, M. Mondor, F. Lamarche, F. Tremblay, J. Dubreuil, L. Masse, Nitrogen potential recovery and concentration of ammonia from swine manure using electro dialysis coupled with air stripping, *J. Environ. Manage.* 95 (2012) S165–S169, <http://dx.doi.org/10.1016/j.jenvman.2011.05.026>.
- [30] E. Thompson Brewster, J. Jermakka, S. Freguia, D.J. Batstone, Modelling recovery of ammonium from urine by electro-concentration in a 3-chamber cell, *Water Res.* (2017), <http://dx.doi.org/10.1016/j.watres.2017.07.043>.
- [31] W.M. Haynes, *CRC Handbook of Chemistry and Physics*, 92nd ed., Greece, 2012.
- [32] K. Xu, J. Li, M. Zheng, C. Zhang, T. Xie, C. Wang, The precipitation of magnesium potassium phosphate hexahydrate for P and K recovery from synthetic urine, *Water Res.* 80 (2015) 71–79, <http://dx.doi.org/10.1016/j.watres.2015.05.026>.
- [33] K.M. Udert, T.A. Larsen, W. Gujer, Fate of major compounds in source-separated urine, *Water Sci. Technol.* 54 (2006) 413–420, <http://dx.doi.org/10.2166/wst.2006.921>.
- [34] K.M. Udert, T.A. Larsen, M. Biebow, W. Gujer, Urea hydrolysis and precipitation dynamics in a urine-collecting system, *Water Res.* 37 (2003) 2571–2582, [http://dx.doi.org/10.1016/S0043-1354\(03\)00065-4](http://dx.doi.org/10.1016/S0043-1354(03)00065-4).
- [35] K. Solon, X. Flores-Alsina, C.K. Mbamba, E.I.P. Volcke, S. Tait, D. Batstone, K.V. Gernaey, U. Jeppsson, Effects of ionic strength and ion pairing on (plant-wide) modelling of anaerobic digestion, *Water Res.* 70 (2015) 235–245, <http://dx.doi.org/10.1016/j.watres.2014.11.035>.
- [36] P. Atkins, J. de Paula, *Physical Chemistry*, W. H. Freeman, 2006. <https://books.google.fi/books?id=Ik2PzH9LmS8C>.
- [37] H. Strathmann, Ion-exchange membrane separation processes, in: S. Heiner (Ed.), *Membr. Sci. Technol.*, Elsevier, 2004: pp. v–vi. doi:[http://dx.doi.org/10.1016/S0927-5193\(04\)80031-7](http://dx.doi.org/10.1016/S0927-5193(04)80031-7).
- [38] W. Pronk, M. Biebow, M. Boller, Electro dialysis for recovering salts from a urine solution containing micropollutants, *Environ. Sci. Technol.* 40 (2006) 2414–2420, <http://dx.doi.org/10.1021/es051921i>.
- [39] J.I. Kroschwitz, A. Seidel, *Kirk-Othmer Encyclopedia of Chemical Technology*, Wiley-Interscience, Hoboken, N.J., 2004.
- [40] P. Zamora, T. Georgieva, A. Ter Heijne, T. Sleutels, A. Jeremiasse, Ammonia recovery from urine in a scaled-up Microbial Electrolysis, *Cell* (2017) 1–9, <http://dx.doi.org/10.1016/j.jpowsour.2017.02.089>.
- [41] P. Kuntke, K.M. Smiech, H. Bruning, G. Zeeman, M. Saakes, T.H.J.A. Sleutels, H.V.M. Hamelers, C.J.N. Buisman, K.M. Smiech, H. Bruning, G. Zeeman, M. Saakes, T.H.J.A. Sleutels, H.V.M. Hamelers, C.J.N. Buisman, Ammonium recovery and energy production from urine by a microbial fuel cell, *Water Res.* 46 (2012) 2627–2636, <http://dx.doi.org/10.1016/j.watres.2012.02.025>.

PUBLICATION
II

**Modelling recovery of ammonium from urine by electro-concentration in a
3-chamber cell**

Emma Thompson Brewster, Johannes Jermakka, Stefano Freguia, Damien J.
Batstone

Water Research 124 (2017) 210-218
<https://dx.doi.org/10.1016/j.watres.2017.07.043>

Publication reprinted with the permission of the copyright holders.



Modelling recovery of ammonium from urine by electro-concentration in a 3-chamber cell

Emma Thompson Brewster^a, Johannes Jermakka^{a, b}, Stefano Freguia^a,
Damien J. Batstone^{a, *}

^a Advanced Water Management Centre, The University of Queensland, St Lucia, QLD 4072, Australia

^b Department of Chemistry and Bioengineering, Tampere University of Technology, P.O. Box 541, 33101 Tampere, Finland

ARTICLE INFO

Article history:

Received 5 March 2017

Received in revised form

10 July 2017

Accepted 18 July 2017

Available online 20 July 2017

Keywords:

Electro-concentration

Nutrient recovery

Urine

Electrochemical model

Ammonium bicarbonate

Physicochemical model

ABSTRACT

Electro-concentration enables treatment and nutrient recovery from source-separated urine, and is a potential technology for on-site treatment using a 3 compartment configuration that has anode, cathode and middle concentrate compartments. There is a particular focus on driving concentration towards the precipitation threshold in the concentrate compartment to generate solid ammonium salts, including ammonium bicarbonate. To evaluate controlling mechanisms and the feasibility of achieving high concentrations, a dynamic mechanistic model was developed and validated using experiments with synthetic urine. It was identified that high concentrations are prevented by increased back diffusion (diffusion from the middle chamber to the anolyte and catholyte) due to large concentration gradients, and the preferential migration of protons or hydroxide ions due to a loss of buffering capacity in the anolyte and catholyte (due to pH extremes). Model-based sensitivity analysis also identified that electrolyte ion concentrations (including buffer capacity) were the main controlling mechanisms, rather than membrane or electrolyte current transfer capacity. To attain high concentrations, operation should be done using a) a high current density (however there is a maximum efficient current density); b) feed at short hydraulic retention time to ensure sufficient buffer capacity; and c) a feed high in ammonium and carbonate, not diluted, and not contaminated with other salts, such as pure ureolysed urine. Taking into account electron supply and bio-anodic buffer limitations, model testing shows at least double the aqueous concentrations observed in the experiments may be achieved by optimising simple process and operational parameters such as flow rate, current density and feed solution composition. Removal of total ammonium nitrogen (TAN) and total carbonate carbon (TCC) was between 43–57% and 39–53%, respectively. Balancing the sometimes conflicting process goals of high concentrations and removal percentage will need to be considered in further application. Future experimental work should be directed towards developing electrodes capable of higher current densities. In addition it would be desirable to use ion exchange membranes with higher resistance to water fluxes and which limit back diffusion. Future modelling work should describe osmotic and electro-osmotic water fluxes as a function of the concentration gradient across the membranes and ionic fluxes, respectively. More generalised wastewater physico-chemistry speciation models should identify best methods where relatively simple Davies activity corrections do not apply.

© 2017 Elsevier Ltd. All rights reserved.

1. Introduction

There are benefits in source separating and separately treating urine and faeces from domestic sources (Larsen et al., 2013). In particular, urine treatment may be focused on nutrient removal,

while faecal and flush water treatment may be focused on pathogen and organics removal. In addition, the high quantities and concentrations of nutrients in undiluted urine make it an ideal feed stream for nutrient recovery (Maurer et al., 2003).

A promising technology for decentralised nutrient recovery from urine after urea hydrolysis (ureolysed urine) is bioelectrolysis in a three-compartment system, see Fig. 1 (Tice and Kim, 2014; Ledezma et al., 2017). Pre-ureolysed urine passes through a bio-

* Corresponding author.

E-mail address: d.batstone@awmc.uq.edu.au (D.J. Batstone).

Nomenclature

ABC	Solid phase ammonium bicarbonate
IEM	Ion exchange membrane
ODE	Ordinary differential equation
DAE	Differential algebraic equation
DBL	Diffusion boundary layer
AEM	Anion exchange membrane
CEM	Cation exchange membrane
BES	Bio-electrochemical systems
RSM	Response surface model
TAN	Total ammonium nitrogen
TCC	Total carbonate carbon
p	The p -value for the probability model
pK_a	Acid dissociation constant
Q	Convective flow rate (mL min^{-1})
$k_f a$	The overall film mass transfer coefficient (s^{-1})
I	Current density (A m^{-2})
Re%	Recovery percentage (%)
C	Concentration (M)

across ion exchange membranes (IEMs) into the concentrate, but will still diffuse across IEMs due to the concentration gradient (Kuntke et al., 2012a; Dykstra et al., 2014; Pronk et al., 2006). Thirdly, competitive current transport of other ions in urine, such as sodium, chloride, potassium and acetate, will limit the current efficiency for ammonium and bicarbonate transfer (Kelly and He, 2014; Liu et al., 2016), as well as increasing the ionic strength of solution, effectively decreasing the ionic activity of ammonium and bicarbonate. This further limits the ability to achieve supersaturation (Tait et al., 2009). Finally, maximum concentrate concentrations are restricted by back diffusion, that is, the diffusion of ions from the middle chamber to the anolyte and/or catholyte, as well as water flux into the concentrate due to osmosis and electro-osmosis (Pronk et al., 2006).

Model-based analysis using the framework developed in Thompson Brewster et al. (2016) has been adapted for the two IEM, three-chamber system corresponding to the configuration shown in Fig. 1. The model is validated using laboratory scale experiments with synthetic urine. Sensitivity analysis on operational and membrane parameters is undertaken to analyse the product concentrations of ammonium and bicarbonate in relation to the fluxes of ions in and out of the middle chamber.

Bioelectrolytic ABC recovery is intended to be a microbial process, which utilises current generated at a bio-anode. However, the biological aspect is modelled here assuming that the microbial biomass is not limiting, as suggested in the experiments of Ledezma et al. (2017). In addition, only aqueous and gas phases are included in the model as no solid ABC formation occurs at these conditions of ambient temperature and pressure. The focus here is an electrochemical approach to investigate the complex relationship between pH, current density, mass transport and other electrochemical operational parameters enabling high concentrate concentrations during electro-concentration processes. As ammonium and carbonate species are concentrated in the middle chamber, so too are many other ions. The already high ionic strength of urine (compared to other wastewater streams) is further increased in the middle chamber and product. With increasing ionic strength the ionic activity of ammonium and bicarbonate species becomes suppressed. This may prevent saturation of ABC, even using a completely optimised system in this configuration. Hence, the objective of this work was to assess the ability of microbial electrodesalination systems to achieve maximum aqueous concentrations of ammonium and bicarbonate, such that precipitation potential of ABC solid is maximised in the concentrate stream.

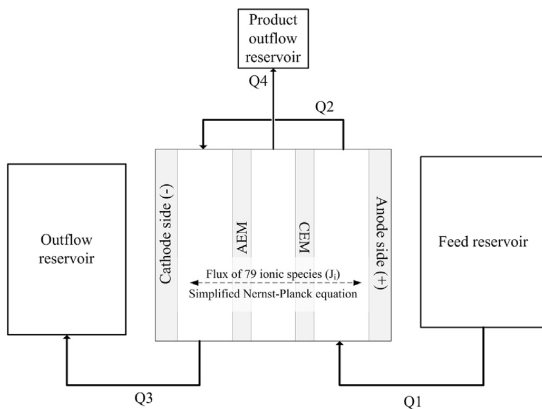


Fig. 1. Configuration of the system studied. The anion exchange membrane (AEM) and cation exchange membrane (CEM) are shown, as are modelled streams including convective flows (Q1–Q4).

anodic chamber, then into a cathodic chamber, with ammonium (and other cations) passing from the bioanodic chamber into a middle chamber, and bicarbonate (and other anions) passing from the cathodic chamber to a middle chamber. Ammonium and bicarbonate ions are concentrated in the middle chamber in preparation for precipitation of solid ammonium bicarbonate (ABC), a desirable product suitable for use in fertiliser production.

Several fundamental challenges make supersaturation of ABC from urine difficult. Firstly, ABC is highly soluble, 24.8 g/100gH₂O at 25 °C (Haynes, 2014). Low temperature or vacuum concentration processes are required for crystallisation to occur. Secondly, the speciation of ammonium and bicarbonate in electrochemical systems is necessary to consider relating to the respective (and for carbonate multiple) acid-base dissociation points (associated with pK_a values). This particularly affects electro-concentration processes as non-charged species ($\text{NH}_3(\text{aq})$, $\text{H}_2\text{CO}_3(\text{aq})$) will not migrate

2. Methods

2.1. Modelling methods

The modelling framework in Thompson Brewster et al. (2016) provides a 2D simulation platform incorporating migrative-diffusive, and convective fluxes using a series of ordinary differential equations (ODEs), coupled with fast acid-base and ion pairing reactions assumed to always be at equilibrium. The acid-base and ion-pairing equilibrium reactions use the model described in Flores-Alsina et al. (2015) (including all equilibrium constants). This is done by combining the ODEs in MATLAB 2014b with C code modified from Flores-Alsina et al. (2015) to compile to a matlab executable (MEX) function. The method used here uses a similarly fast acid-base dissociation equilibria approach to Dykstra et al. (2014) and Liu et al. (2016), who studied ammonium mass transport in urine and synthetic digestion effluent of livestock waste, respectively. However, incorporated here is a larger set of components and species, including ion-pairing. In addition, the dynamic and experimentally validated combined system of differential algebraic equations

(DAEs) and ODEs describes speciation and mechanistic mass transport across the whole experimental domain, including flows and reservoirs. The integration of the speciation, pH and ion-pairing code in Flores-Alsina et al. (2015), means this model is more generalizable and versatile than previously described models.

A difference from Thompson Brewster et al. (2016), using the speciation code from Flores-Alsina et al. (2015), is that an ideal activity model was used here. That is, the activity coefficient was set equal to 1. This is because the Davies activity correction has a validity range of up to 0.5–0.7 M and the middle chamber approaches 2 M, well exceeding the validity of the Davies activity model (and indeed, the Davies model produces substantially more erroneous results, including activity corrections greater than 1.0, compared with an ideal assumption based on calculations provided in supplementary information 1). The effect of an ideal assumption was shown to not be a significant factor in this specific instance (see supplementary information 1), but activity models at very high ionic strengths, applied to generalised wastewater models remains a challenge as discussed further in this paper. In this case assuming ideal activity was acceptable because no precipitation was modelled, and because the dominant migratory fluxes into the middle chamber are based on the catholyte and anolyte concentrations, which are less influenced by non-ideality than the middle chamber. See supplementary information 1 for analysis of the effect of an ideal activity assumption (note ion pairing has been retained).

The system shown in Fig. 1 was implemented in the model, corresponding to the experimental configuration described in Section 2.2. This has 6 control volumes, including constant volume catholyte, anolyte and middle reactor chambers; and varying volume feed inflow, feed outflow and product overflow reservoir chambers. No diffusion boundary layers (DBLs) were included in the model as at the reactor size and flows in Thompson Brewster et al. (2016) they were not a controlling factor. In this case, flow rates are slower than Thompson Brewster et al. (2016) and granular electrodes are used, making boundary layer limitations less prevalent. Diffusion and migratory fluxes occur across the anion exchange membrane (AEM) and cation exchange membrane (CEM) according to the simplified Nernst-Planck equation and taking in account 71 possible ionic species based on the 10 components: sodium, potassium, ammonium, chloride, acetate, calcium, magnesium, carbonate, sulphate and phosphate. $\text{CO}_2(\text{g})$ stripping in the anode (low pH), with conjugate reabsorption into the aqueous phase in the cathode, was also included. The anode overall film mass transfer coefficient, the k_a constant (s^{-1}), was fitted during calibration, and cathode gas transfer assumed instantaneous. This mechanism was shown to be necessary during calibration of pH and carbonate concentrations against measured data.

The differential equations forming the model are provided in supplementary information 2. Initial concentration conditions were set to the initial concentrations of the feed for the feed and outflow reservoirs, and the catholyte, middle and anolyte chambers (see Table 1). The initial overflow reservoir concentrations were set to 10^{-21} mM. Initial volume conditions were 10^{-21} m³ for the overflow reservoir, 1 m³ for the anode feed reservoir and 10^{-6} m³ for the cathode outlet reservoir. Spatial boundary conditions are zero flux and zero concentration gradient at the electrode compartment domain limits. It is noted that there are lateral advective flows through catholyte and anolyte chambers, but these act on bulk compartments only. The system of ODE equations was solved by ODE45, while the algebraic equations were solved using an annealing Newton's method as in Flores-Alsina et al. (2015).

As discussed and evaluated in Thompson Brewster et al. (2016), the membrane resistance to all ions is artificially accounted for in the model by reducing the diffusion coefficient in the membrane by one order of magnitude for counter-ions and two orders of

Table 1

Feed concentration for the feed urine recipe and the feed with no acetate.

Component (M)	Urine	No acetate
Sodium	0.111	0.111
Potassium	0.056	0.056
Ammonium	0.568	0.444
Chloride	0.118	0.118
Acetate	0.125	0
Calcium	0	0
Magnesium	0	0
Carbonate	0.271	0.271
Sulphate	0.016	0.016
Phosphate	0.018	0.018

magnitude for co-ions. The diffusion coefficients for protons and hydroxide ions in the membrane are the same as in solution due to the ions' naturally higher mobility and solvation of the membranes (Thompson Brewster et al., 2016). The diffusion coefficients used in this study can be found in the supplementary information of Thompson Brewster et al. (2017).

Water fluxes from the electrolytes into the middle chamber and overflowing into the reservoir are also taken into account by empirically fitting the rate of water flux to be constant with time and equal to the total amount measured during the experiments.

2.2. Experiments

Three dynamic experiments were performed in a continuous, laboratory scale reactor built on the scheme of Fig. 1, with feed flow path from anode to cathode to effluent, with both cathode and anode circulated internally. The concentrate was collected by gravity to an overflow bottle. Conditions of the three experiments correspond to different operating parameters shown in Table 2. The working (i.e. total liquid solution) volumes of each chamber are shown in Table 2. Working volumes vary due to three different reactors being used, each having slight variations in granule pore volume and tube length. The anolyte feed consisted of synthetic ureolysed urine based on Udert et al. (2006) (hereafter called 'urine'), or a no acetate alternative (hereafter called 'no acetate'). The composition of each is shown in Table 1. The no acetate feed was used to simulate the effect of an ideal bio-electrolytic cell which would convert acetate to carbonate in the bio-anode.

The unit was equipped with one CEM (Membrane International Inc. CMI-7000) and one AEM (Membrane International Inc. AMI-7001), each with an effective area of 70×50 mm (35 cm^2), and a 10 mm spacing for the electrode and middle chambers. A stainless steel mesh cathode and a graphite granular anode with graphite rod current collector were utilised. A potentiostat (BioLogic VSP) was used to supply the current density specified in Table 2. The feed has a flow rate of 0.3 mL min^{-1} . There was only self-sourced convective flow in the middle chamber to an overflow reservoir due to small water fluxes through the membranes. The run was started with all chambers filled with feed solution and run

Table 2

Operating parameters of the three experiments.

	Run 1	Run 2	Run 3
Feed	Urine	Urine	No acetate
Applied current (A m^{-2})	40	60	40
Feed flow rate (mL min^{-1})	0.3	0.3	0.3
Water flux to overflow (mL min^{-1})	0.031	0.038	0.031
Working volume cathode (mL)	41.9	44.1	45.6
Working volume anode (mL)	54.2	52.4	50.4
Working volume middle (mL)	43.5	42.7	45.5

continuously until steady state concentrations were reached in all chambers, around 11 d.

2.3. Analytical techniques

Sampling was done using a sampling port with a syringe from feed and anode recirculation loops; cathode effluent; and middle chamber. 1–1.5 mL samples were taken and diluted with deionised water for analysis. Samples were analysed for Na, K, Ca, Mg and SO_4^{2-} -S using Inductively Coupled Plasma Optical Emission Spectroscopy Perkin Elmer Optima 7300DV. Flow Injection Analysis Lachat QuickChem8500 (Lachat Instruments, Loveland, CO, USA) was used to determine total soluble NH_4^+ -N and PO_4^{3-} -P. Ion Chromatography Dionex ICS-2100 (Dionex, CA, USA) was used to determine Cl, and Total Organic Carbon Analyzer Shimadzu TOC-L CSH with TNM-L TN unit (Kyoto, Japan) to determine total organic carbon (acetate component) and inorganic carbon (carbonate component).

2.4. Sensitivity analysis

2.4.1. Overview of sensitivity analysis

After model validation, a series of simulations were performed to evaluate the impact of different operating conditions on the product reservoir concentrations as outlined below. In all cases the different treatments are compared via the plateau (steady-state) concentrations of aqueous ammonium and bicarbonate in the product overflow reservoir and using the base settings of run 1 (current density, flow rate, feed composition, etc.) unless specified otherwise.

2.4.2. Current density

A key focus of research is improving the current and power density capabilities of bio-electrodes (Guo et al., 2015; Logan and Rabae, 2012). Simulations were done to identify whether there is an optimum current density, or if a greater current density always achieves greater product concentrations. These simulations sweep the current density from 10 to 150 A m^{-2} in increments of 20 A m^{-2} with all other parameters remaining constant.

2.4.3. Retention time

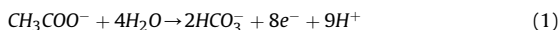
In bio-electrochemical systems (BESs), it is important that the anolyte solutions remain relatively neutral in pH, to avoid biological inhibition (Torres, 2014). In this application, bicarbonate buffer is important to keep the bio-anode at a near neutral pH. To evaluate the minimum operating flowrate (i.e. minimum input of buffer capacity), the impact of feed flow rate, and therefore retention time, on the pH as well as product concentrations is evaluated between 0.1 and 1 mL min^{-1} in increments of 0.1 mL min^{-1} .

2.4.4. Additional NaCl in feed

There will be natural variation in the feed during practical process operation. In addition, competitive current transport may limit the product concentration of ammonium and bicarbonate in the presence of other ions. The impact of excess salt (and therefore higher ionic strength) in the feed is evaluated by varying the feed between 111–611 mM and 118–618 mM increasing in increments of 50 mM of sodium and chloride, respectively.

2.4.5. Acetate

In BESs a key biological reaction is the conversion of organic substrate, commonly modelled as acetate, to bicarbonate at the anode, see Equation (1) (Kuntke et al., 2012b).



The effect of the reaction conversion may be evaluated in terms of ionic fluxes across the membrane because higher bicarbonate concentrations in the anode increase the current efficiency of bicarbonate transport across the membrane (Dykstra et al., 2014). The impact of the acetate concentration in the catholyte is evaluated by running abiotic simulations. The simulations simply vary the amount of acetate in the feed to reflect 0 and 100% acetate conversion using the assumption that 1 M of acetate converts to 2 M carbonate.

2.4.6. Membrane properties

Another avenue of research is on IEM development for emerging wastewater treatment processes (Logan and Elimelech, 2012; Xu, 2005). The following membrane properties were tested to determine if using membranes with different characteristics has an effect on the product concentrations to advise on the direction of membrane research: a) membrane resistance to all ions increased by 10 and 100 times; b) membrane resistance to $\text{NH}_3(\text{aq})$ increased by 10 and 100 times; and c) reduced water flux into the middle chamber by 50% and 33% the original volume in run 1. The large values from increasing membrane resistance to ions by two orders of magnitude are chosen to determine whether there is significant benefit to pursuing this avenue of research.

3. Results and discussion

3.1. Calibration & validation

Calibration was done on run 1 (40 A m^{-2} , acetate present) to determine the k_a constant for CO_2 stripping in the anode to be 1.8 h^{-1} . Based on the model fit to experimentally observed nitrogen component concentrations, no NH_3 stripping was observed to occur (see supplementary information 3 for further information). An *F*-test with 5% significance threshold found that there was no significant difference ($p = 0.65$) between a model not including ammonia stripping and a model including ammonia stripping. Fig. S4.2 shows the pH in all chambers to be above 6 during the validation experiments, indicating that little nitrogen would be in form of NH_3 . The high middle chamber concentrations may have provided a driving force for some ammonia losses. However this was not observed to be significant.

Separately, a normalised R^2 value of 0.98 was calculated based on 351 measurements, across the 3 experiments, measuring 9 components (NH_4 -N, K, PO_4 -P, Ac, SO_4 , Na, CO_3 , Cl and pH) and comparing them with modelled values. See Fig. S4.1 and S4.2 for time-series data corresponding to this analysis.

3.2. Current density and retention time

The product concentrations are asymptotic with increasing applied current (Fig S5.1). Above 90 A m^{-2} with feed flow of 0.3 mL min^{-1} , increased current no longer improves the product concentrations. At this point extreme pH levels occur in the cathodic and anodic chambers due to depletion of major cations and anions in the electrolytes. Above 90 A m^{-2} H^+ preferentially transports the additional current density over NH_4^+ (and other cations), and similarly OH^- preferentially transports over bicarbonate (and other anions) (see Fig. S6.1–S6.3). The relationship between leakage rate and pH can be seen in Fig. 2. Fig. 2 displays the dominant species which carry charge across the CEM (left hand side) and AEM (right hand side) at steady state when the pH of the anolyte (left hand side) or catholyte (right hand side) varies. In

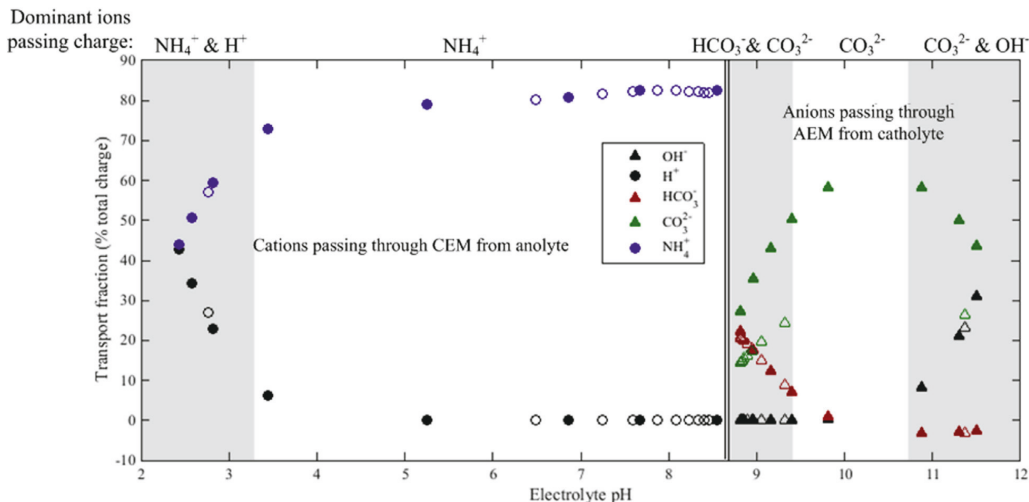


Fig. 2. Current density parameter sweeps from 10 to 150 A m⁻² with flow rate 0.3 mL min⁻¹ (filled markers) and flow rate parameter sweeps from 0.1 to 1 mL min⁻¹ with current density of 40 A m⁻² (outlined markers), displaying anolyte pH and cation current transport fraction (circles, on the left), and catholyte pH and anion current transport fraction (triangles, on the right).

Fig. 2, the fraction of total charge is the charge flux of the species (mol eq s⁻¹) divided by the equivalent total moles of charge (mol eq s⁻¹) calculated from the applied current. Fig. 2 illustrates the speciation of bicarbonate to carbonate in the catholyte with elevated pH. This could benefit the product concentrations due to carbonate being a divalent species and dominant at high pH, and will transport proportionally more current through the membranes compared to other anions. The rate of transport of current by protons or hydroxide ions (hereafter referred to as current leakage) at values less than pH 6 is much less likely to be an issue in a biological system as the process cannot operate below biological pH limitations of approximately 7.1–7.45 (Ledezma et al., 2017). Fig. 2 does not add to 100% of charge, as not all ions are displayed here. The balance (to 100% of charge) is Na⁺ and K⁺ through the CEM, and Cl⁻ and Ac⁻ through the AEM (see Figs. S6.1–S6.3 and S6.8–S6.10 for flux results of all species).

Fig. 2 also indicates there is a minimum required flow rate to prevent current leakage and achieve optimal product concentrations. For this configuration at 40 A m⁻² and 0.2 mL min⁻¹, the retention time is so great that the buffering capacity of the carbonate system is exhausted, and the pH of the anolyte and cathode deviate from neutral (Fig. S5.1).

A response surface model (RSM) was done through multivariate linear regressions in Microsoft Excel (2010) varying current density and flow rate as factors and using ammonium nitrogen (TAN) and total carbonate carbon (TCC) as the response variables. The regression factor for current density was scaled so the maximum value of 150 A m⁻² was equal to 1. Equations (2) and (3) display the regression output, and Fig. 3 visualises the RSM.

$$Y_{TAN} = -200 + 2289Q + 3841I + -3128Q^2 + -2891I^2 + 7941QI \tag{2}$$

$$Y_{TCC} = -46 + 1030Q + 2115I + -1512Q^2 + -1630I^2 + 3852QI \tag{3}$$

where Q is flow (mL min⁻¹) and I is scaled current density (A m⁻²).

The overall model for both regressions was significant (F-test $p_{TAN} = 2 \times 10^{-12}$, $p_{TCC} = 6 \times 10^{-12}$) with the interaction parameter

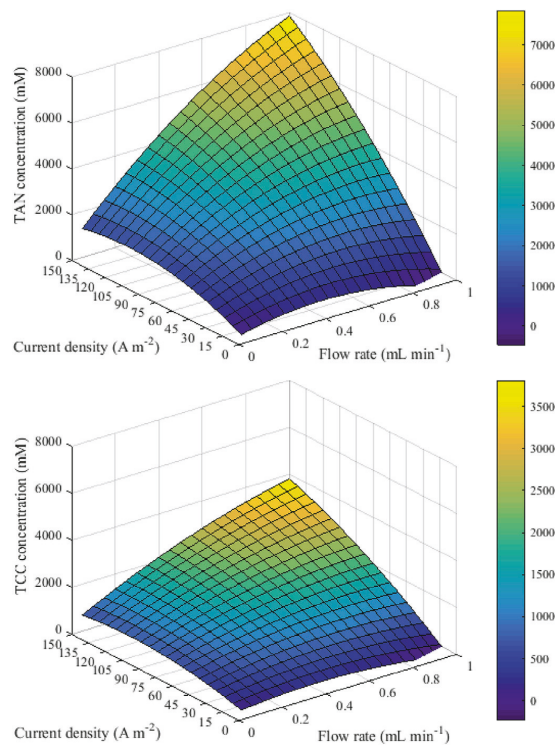


Fig. 3. Response surface modelling (RSM) of total ammonium nitrogen (TAN) and total carbonate carbon (TCC) by varying current density and flow rate.

(the final term of Equations (2) and (3)) having the most significant effect (single parameter two-tailed t -test $p_{X1X2TAN} = 3 \times 10^{-10}$, $p_{X1X2TCC} = 9 \times 10^{-10}$). The RSM shows that with increasing both current density and flow rate, the model developed in this paper does not identify any limiting mechanisms to achieving high concentrate concentrations as long as both factors (current density and flow rate) are increased simultaneously. This indicates the main controlling mechanism to achieving high concentrations in this system is the electrolyte composition, which does not appear to be limited by membrane or electrolyte current carrying capacity. Bioelectrodes are currently incapable of generating such high current densities, and the maximum concentration is at or below the solubility threshold for ABC of 24.8 g/100 g (also needing to consider ionic activity and ion pairing, which in this application will further increase the solubility threshold of ABC) (Thompson Brewster et al., 2017). However, the model nevertheless demonstrates that very high concentrations can be achieved when operating at a suitable TCC loading rate.

Rodríguez Arredondo et al. (2017) defined of loading rate as the current density divided by influent TAN, and demonstrated with high loading rate that 100% TAN recovery can be achieved. The model developed here extends this way of thinking to mechanistically describe maximum product concentrations of TAN and TCC and recovery percentage based on feed composition and current density. In the system studied here it is not possible to only study TAN loading because bicarbonate is the limiting component in this configuration.

3.3. Acetate conversion

The simulated conversion of acetate to bicarbonate increases the plateau concentrations of bicarbonate in the product (Fig. S5.1). This is due to the resulting bicarbonate flux increase across the AEM into the middle chamber due to higher overall concentrations in the cathode and anode. Higher concentrations result in the preferential proportioning of current transported by bicarbonate according to the Nernst-Planck equation (Thompson Brewster et al., 2016) (Fig. S6.4 and S6.5). The naturally occurring concentration of bicarbonate in ureolysed urine is less than ammonium (about half). If the bio-anode achieves high acetate to carbonate conversion, this is effectively increasing the current available, which will increase product concentrations (due to acetate conversion). However, increased current density will more quickly deplete (due to increased migration) the buffering capacity of the cathode chamber.

3.4. Salinity

Additional sodium and chloride added to the feed had the effect of proportionally decreasing the ammonium and carbonate in the product (Fig. S5.1). This was attributed to the preferential proportioning of current to sodium and chloride due to their higher concentrations in the anolyte and catholyte (Fig. S6.6 and S6.7).

3.5. Membrane properties

3.5.1. Membrane resistance to all ions

Increasing the membrane resistance by one order of magnitude to all ions slightly increased the plateau concentrations of all components, but did not affect pH and further increase to two orders of magnitude had minimal additional effect (Fig. S5.1). Less back diffusion was observed with increasing membrane resistance (Fig. S6.11–S6.13)

3.5.2. Membrane resistance to ammonia

Increasing the membrane resistance to ammonia by one order of

magnitude slightly increased the plateau concentrations of nitrogen in the product, but it did not affect pH. A further increase to two orders of magnitude higher had minimal additional effect (Fig. S5.1). Increasing the membrane resistance to ammonia slightly reduced the steady-state value of the ammonia back diffusive flux (Fig. S6.14–S6.16).

3.5.3. Water flux into middle chamber

Decreasing water flux increases the time to reach a plateau concentration, but also proportionally increases the product concentrations (Fig. S5.1). For this study, simulations were run for 100 d, increased from the 11 d used for all other simulations, to ensure the final concentrations were at steady-state. The product concentrations increase as the water flux to the middle chamber decreases. This is expected, as less water flux means less water to dilute the middle chamber concentrations. The ionic fluxes into the middle chamber do not change significantly as the rate of water flux decreases. However, the rates of ionic flux out of the middle chamber do increase slightly with the decrease in water flux (Fig. S6.17–S6.19). Lowering water flux into the middle chamber had a much greater effect on product concentrations than either membrane resistance sensitivity analysis. Mechanistically, osmotic and electro-osmotic water fluxes will be proportional to the concentration gradient and current density, and using membranes with high steric hindrance is the only way to reduce the water flows (Rottiers et al., 2014) Therefore, further membrane development for this application should involve developing membranes with high steric hindrance.

3.6. Key factors

3.6.1. Bicarbonate

Bicarbonate is important to system efficiency and maximum concentration for two reasons: enabling increased product concentrations of ammonium bicarbonate, and functioning as buffer. For the latter reason, it is important that the system is run at an appropriate current density and flow rate that there is sufficient buffer capacity to ensure the pH remains close to neutral in all streams, while still maximising product concentration of carbonate. This is essential to prevent current leakage from protons and hydroxide ions, as well as ensuring the functioning of the bio-anode in a bioelectrochemical application. At pilot or full scale, the retention time and applied current will need to be balanced for different reactor sizing. A feedback controller which controls the anode feed pump rate would largely address the buffer capacity and bicarbonate availability issue. The model developed here could be used to evaluate appropriate reactor sizing based on the possible current densities and minimum available urine flow rates. It is intuitive that the bio-anode should be operated to ensure optimum conversion of organics in the feed to bicarbonate to increase the bicarbonate concentration in the cathodic chamber. However, in practice, increased conversion is proportional to increased current which must be coupled with increased carbonate loading to ensure buffer capacity is not exhausted. Another process option if nutrient removal from urine is a key target as opposed to high product concentrations, is to recirculate the cathode effluent back to the anodic chamber.

3.6.2. Optimum configuration

The abiotic model developed here is able to operate under more extreme conditions compared to a biotic system. In particular, the acetate conversion to bicarbonate is linked to current production, and the anolyte pH must remain within the biological range (pH 7.1–7.45, Ledezma et al., 2017). Two scenarios which balance these considerations with improved operational settings are proposed.

These scenarios take into account that 8 electrons are produced to convert acetate to carbonate (Equation (1)). The electron consumption is taken into account to provide a realistic relationship between current density and acetate conversion to bicarbonate based on the electron balance. This is simulated by varying the feed composition concentrations of acetate and bicarbonate proportional to the current density being used. Proposed option 1 uses a current density of 60 A m^{-2} , 50% acetate conversion, and the same flow rate as run 1 (0.3 mL min^{-1}). Proposed option 2 evaluated a higher current density of 90 A m^{-2} , double the feed flow of 0.6 mL min^{-1} and 30% acetate conversion. These operational scenarios use the same feed as in run 1 (apart from where specified), no additional salt and 10% reduction of the osmotic and electroosmotic water flux observed in run 1.

Table 3 shows the steady-state concentrations of ammonium and carbonate components. It shows higher product concentrations can be achieved compared to the validation run, while maintaining adequate buffering capacity. Recovery percentages for ammonium and carbonate were calculated using Equation (4).

$$\text{Re}\% = 1 - \frac{C_{\text{out}}Q_{\text{out}}}{C_{\text{in}}Q_{\text{in}}} \quad (4)$$

where Re% is the recovered percentage, C is the concentration (M), Q is the flow rate (mL min^{-1}) and subscripts in and out refers to the anolyte feed stream and catholyte outflow stream, respectively. Load ratios for TAN according to the method in Rodríguez Arredondo et al. (2017) were calculated and are shown in Table 3. These are the ratio of applied current over the influent TAN. Load ratios less than 1 indicate there is more TAN being fed than may be transported to the middle chamber. The low values displayed here may appear that the system is inefficient, but balance is needed to maintain a neutral pH and prevent current leakage as illustrated in Fig. 2. As bicarbonate is limiting compared to ammonium, there will always be a loading ratio less than 1 for TAN. However, of interest is that the load ratios are equal to the recovery percentages. Future work should study the greatest loading ratio possible while maintaining adequate buffer capacity in the system.

These results indicate that realistic operating strategies can significantly increase ammonium and bicarbonate concentrations in the product, while maintaining effective buffer capacity through the system. A recommended method to ensure high product concentrations within realistic operational conditions is by increasing the feed flow rate; however this may be limited by urine supply in a pilot scenario. Table 3 indicates that higher concentrations in the product results in lower recovery for TCC. However, no similarly obvious relationship was observable for TAN in this system, with Option 1 having higher TAN recovery than Run 1. This relationship warrants further investigation if both high product concentration

and recovery percentage of TAN (but not TCC) are desired.

Fig. 4 displays steady-state species fluxes for the base case of run 1 and the two optimised scenarios. The suggested options ensure adequate buffering capacity in the chambers and result in larger fluxes into the middle chamber, without current leakage or a proportional difference in the species undergoing the largest fluxes. Fig. 4 displays some cations and anions transporting across the AEM and CEM, respectively. This is because the modelling includes manufacturer's parameters for non-ideal permselectivity fractions of 90% for the AEM and 94% for the CEM (Thompson Brewster et al. 2016).

3.7. Model limitations

3.7.1. Water flux

The model of water fluxes used here is simply determined by estimating a constant water flux over time equal to the total change in overflow reservoir volume measured between the start and the end of the experiments. Pronk et al. (2006) proposes a mechanistic relationship which accounts for the electro-osmosis due to hydrated radii of migrating ions and osmosis due to the concentration gradient across the membrane. This suggests that the ionic transport rates and membrane concentration gradient should be mechanistically linked to the water flux. Future work should experimentally record the overflow volume with time so that the model of water flux can incorporate a mechanistic relationship of osmotic and electroosmotic water fluxes as proposed by Pronk et al. (2006).

3.7.2. Activity correction

As mentioned in Section 2.1, the middle chamber involves a particularly high strength solution with an ionic strength upwards of 1.8 M. The Davies activity correction, used in the speciation code from Flores-Alsina et al. (2015) only has validity up to 0.5 M (Stumm and Morgan, 1996; Tait et al., 2012). While it was shown that a model using an ideal activity assumption (while still including ion-pairing and acid-base dissociation) was not significantly different from a model using the Davies activity correction, it is essential to accurately model activity if saturation and precipitation is to be studied (Mbamba et al., 2015). For example, activity needs to be included to effectively study ABC saturation, or problematic scales such as gypsum or calcite. It is recommended that future model development works towards a generalised physico-chemical model for wastewaters with ionic strengths higher than 0.5 M.

3.7.3. Membrane or electrode scaling

The assumption of only modelling gas and liquid phases meant that supersaturation of common calcium or magnesium scaling precipitants such as calcite and gypsum was not considered. The experiments here did not include calcium or magnesium in the synthetic urine solutions. However, real ureolysed urine will contain calcium and magnesium. Future work should determine the scaling potential of the system using real ureolysed urine, and use a modelling approach such as described in Thompson Brewster et al. (2017).

4. Conclusions

Current density and feed flow rate have the most impact on the steady-state concentrations of ammonium and bicarbonate in the concentrate. In all circumstances the maximum concentrate concentrations were limited by back diffusion of ions from the concentrate to the electrolytes and current leakage due to a depletion of buffer capacity (bicarbonate availability) of the

Table 3
Final steady-state results of testing optimised modelled scenarios.

Parameter	Run 1	Option 1	Option 2
Current density (A m^{-2})	40	60	90
Flow rate (mL min^{-1})	0.3	0.3	0.6
Simulated acetate conversion in feed (%)	0	50	30
Water flux to overflow reservoir (mL min^{-1})	0.031	0.028	0.028
Steady state product TAN (M)	2.0	3.2	4.9
Steady state product TCC (M)	1.0	2.0	2.8
Steady state pH middle chamber	8.6	8.6	8.5
Steady state pH anode chamber	7.3	6.6	6.6
Steady state pH cathode chamber	9.1	9.0	8.9
TAN recovery %	43.0	56.8	46.3
TCC recovery %	52.9	47.9	38.5
TAN load ratio	0.43	0.57	0.46

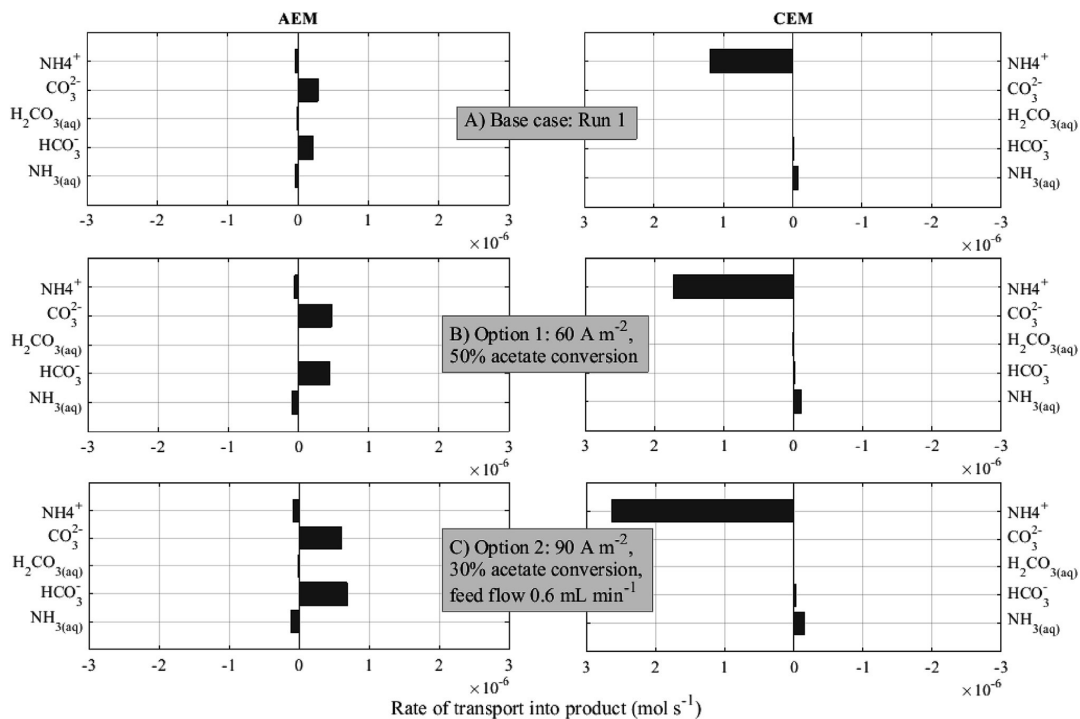


Fig. 4. Steady-state fluxes of ammonium and bicarbonate acid-base dissociation species across the anion exchange membrane (AEM) and cation exchange membrane (CEM) into the middle chamber for Run 1, and two examples of suggested operating conditions. The positive direction indicates fluxes into the middle chamber.

electrolytes. Maximum concentrate concentrations are achieved by utilising: a) sufficient feed flow rate that the bicarbonate buffer capacity is not depleted; b) high current density (noting there is a maximum efficient current density depending on the configuration); c) urine feed high in ammonium and carbonate, with minimal concentrations of other salts or dilution; and d) ion exchange membranes with high resistance to water fluxes and back diffusion of ions. Optimising the operation by decreasing membrane water flux by 10%, increasing current density to 90 A m^{-2} , doubling the flow rate, and including conversion of 30% feed acetate to carbonate based on the stoichiometric relationship of the bioanode reaction results in a 250% increase in aqueous concentrations of ammonium and carbonate. Optimising the concentration of TCC decreased the recovery percentage. However, the same clear trend was not observed for TAN, and further work should be done to optimise both TAN concentration and recovery simultaneously.

Acknowledgements

This research was supported financially by Australian Research Council Project LP 150100402 in partnership with Queensland Urban Utilities (QUU) and ABR Process Development; the Australian Grain Research & Development Corporation Grain Research Scholarship (GRS10661) supporting Emma Thompson Brewster; and the Maj and Tor Nessling foundation and Walter Ahlström foundation supporting Johannes Jermakka. The authors acknowledge the facilities, and the scientific and technical assistance of the Analytical Services Laboratory at the Advanced Water Management Centre, The University of Queensland.

Appendix A. Supplementary data

Supplementary data related to this article can be found at <http://dx.doi.org/10.1016/j.watres.2017.07.043>.

References

- Dykstra, J.E., Biesheuvel, P.M., Bruning, H., Ter Heijne, A., 2014. Theory of ion transport with fast acid-base equilibrations in bioelectrochemical systems. *Phys. Rev. E* 90, 013302.
- Flores-Alsina, X., Mbamba, C.K., Solon, K., Vrecko, D., Tait, S., Batstone, D.J., Jeppsson, U., Gernaey, K.V., 2015. A plant-wide aqueous phase chemistry module describing pH variations and ion speciation/pairing in wastewater treatment process models. *Water Res.* 85, 255–265.
- Guo, K., Prevotau, A., Patil, S.A., Rabaey, K., 2015. Engineering electrodes for microbial electrocatalysis. *Curr. Opin. Biotechnol.* 33, 149–156.
- Haynes, W.M., 2014. *CRC Handbook of Chemistry and Physics*, 95th ed. CRC Press, Boca Raton, Fla.
- Kelly, P.T., He, Z., 2014. Nutrients removal and recovery in bioelectrochemical systems: a review. *Bioresour. Technol.* 153, 351–360.
- Kuntke, P., Smiech, K.M., Bruning, H., Zeeman, G., Saakes, M., Sleutel, T., Hamelers, H.V.M., Buisman, C.J.N., 2012a. Ammonium recovery and energy production from urine by a microbial fuel cell. *Water Res.* 46, 2627–2636.
- Kuntke, P., Smiech, K.M., Bruning, H., Zeeman, G., Saakes, M., Sleutel, T., Hamelers, H.V.M., Buisman, C.J.N., 2012b. Ammonium recovery and energy production from urine by a microbial fuel cell. *Water Res.* 46, 2627–2636.
- Larsen, T.A., Udert, K.M., Lienart, J., 2013. *Source Separation and Decentralization for Wastewater Management*. IWA Publishing, London.
- Ledezma, P., Jermakka, J., Keller, J., Freguia, S., 2017. Recovering nitrogen as a solid without chemical dosing: bio-electroconcentration for recovery of nutrients from urine. *Environ. Sci. Technol. Lett.* 4 (3), 119–124.
- Liu, Y., Qin, M., Luo, S., He, Z., Qiao, R., 2016. Understanding ammonium transport in bioelectrochemical systems towards its recovery. *Sci. Rep.* 6, 22547.
- Logan, B.E., Elimelech, M., 2012. Membrane-based processes for sustainable power generation using water. *Nature* 488 (7411), 313–319.
- Logan, B.E., Rabaey, K., 2012. Conversion of wastes into bioelectricity and chemicals

- by using microbial electrochemical technologies. *Science* 337 (6095), 686–690.
- Maurer, M., Schwegler, P., Larsen, T.A., 2003. Nutrients in urine: energetic aspects of removal and recovery. *Water Sci. Technol.* 48 (1), 37–46.
- Mbamba, C.K., Tait, S., Flores-Alsina, X., Batstone, D.J., 2015. A systematic study of multiple minerals precipitation modelling in wastewater treatment. *Water Res.* 85, 359–370.
- Pronk, W., Biebow, M., Boller, M., 2006. Electrodialysis for recovering salts from a urine solution containing micropollutants. *Environ. Sci. Technol.* 40 (7), 2414–2420.
- Rodríguez Arredondo, M., Kuntke, P., ter Heijne, A., Hamelers, H.V.M., Buisman, C.J.N., 2017. Load ratio determines the ammonia recovery and energy input of an electrochemical system. *Water Res.* 111, 330–337.
- Rottiers, T., Ghyselbrecht, K., Meesschaert, B., Van der Bruggen, B., Pinoy, L., 2014. Influence of the type of anion membrane on solvent flux and back diffusion in electrodialysis of concentration NaCl solutions. *Chem. Eng. Sci.* 113, 95–100.
- Stumm, W., Morgan, J.J., 1996. In Schnoor, J.L., Zehnder, A. (Eds), John Wiley and Sons, New York, USA.
- Tait, S., Clarke, W.P., Keller, J., Batstone, D.J., 2009. Removal of sulfate from high-strength wastewater by crystallisation. *Water Res.* 43, 762–772.
- Tait, S., Solon, K., Volcke, E.I.P., Batstone, D.J., 2012. A Unified Approach to Modelling Wastewater Chemistry: Model Corrections. 3rd Wastewater Treatment Modelling Seminar. Mont-Sainte-Anne, Quebec, Canada.
- Thompson Brewster, E., Mehta, C.M., Radjenovic, J., Batstone, D.J., 2016. A mechanistic model for electrochemical nutrient recovery systems. *Water Res.* 94, 176–186.
- Thompson Brewster, E., Ward, A.J., Mehta, C.M., Radjenovic, J., Batstone, D.J., 2017. Predicting scale formation during electro-dialytic nutrient recovery. *Water Res.* 110, 202–210.
- Tice, R.C., Kim, Y., 2014. Energy efficient reconcentration of diluted human urine using ion exchange membranes in bioelectrochemical systems. *Water Res.* 64, 61–72.
- Torres, C.I., 2014. On the importance of identifying, characterizing, and predicting fundamental phenomena towards microbial electrochemistry applications. *Curr. Opin. Biotechnol.* 27, 107–114.
- Udert, K.M., Larsen, T.A., Gujer, W., 2006. Fate of major compounds in source-separated urine. *Water Sci. Technol.* 54 (11–12), 413–420.
- Xu, T.W., 2005. Ion exchange membranes: state of their development and perspective. *J. Membr. Sci.* 263 (1–2), 1–29.

Supplementary information: Modelling recovery of ammonium from urine by electro-concentration in a 3-chamber cell

Emma Thompson Brewster¹, Johannes Jermakka^{1,2}, Stefano Freguia¹, Damien J. Batstone^{1}*

¹Advanced Water Management Centre, The University of Queensland, St Lucia, QLD 4072, Australia

²Department of Chemistry and Bioengineering, Tampere University of Technology, P.O. Box 541, 33101 Tampere, Finland

**Corresponding Author:*

Prof. Damien J. Batstone, Advanced Water Management Centre, The University of Queensland, St Lucia, QLD 4072, Australia

Phone: +61 (7) 3346 9051;

Fax: +61 (7) 3365 4726;

Email d.batstone@awmc.uq.edu.au

28 pages

2 texts

28 equations

1 table

22 figures

SUPPLEMENTARY INFORMATION 1: Ideal model

Manually increasing the concentration of component inputs confirms that the Davies activity correction is valid up to ionic strength of 0.5-0.7 M. The same trend is observed using the Flores-Alsina et al. (2015) framework and Visual MINTEQ (Version 3.0). After approximately 0.7 M, the activity coefficient begins to increase, rather than decrease, with increasing ionic strength. At approximately 1.8-2.0 M the activity coefficient becomes greater than 1. An activity coefficient greater than one, is a mathematical artifact of using an activity correction inappropriate for the ionic strength of solution. This type of erroneous output was observed to occur when studying the middle chamber concentrations. Table 1 shows the equilibrium concentrations of components in the middle chamber, and the corresponding ionic strength, monovalent activity coefficient and pH using Davies, SIT and Debye-Huckel methods in Visual MINTEQ. Table 1 indicates that only an SIT method would only be appropriate for this system as Davies and Debye-Huckel methods result in activity coefficients greater than 1. The speciation code was adapted to use ideal conditions, meaning the activity coefficient was set to 1 assuming activity is equal to concentration. This allows pH, ion-pairing and acid-base dissociation to still be evaluated across the dynamic ED model, but under the assumption of an activity coefficient equal to 1. Comparing pH, ammonium and carbonate components in the model and experimental chambers, a χ^2 test was performed with 95% confidence to determine whether there was a difference in model output using the Davies activity correction or the ideal model. The F statistic (0.99) was less than the critical F value (1.33), indicating that the models are not significantly different. In addition, the R^2 of both the Davies and ideal models were both 0.98, indicating no difference in their ability to reflect the variance present in the experimental data.

The lack of difference between the ideal and Davies models is because the diffusive and convective transport are functions of the concentrations, and not activities. In addition, the

majority of migratory transport is due to the ratio of activities of species in the anolyte and catholyte. In the anolyte and catholyte the ionic strength is low, and the ratio of activities is unlikely to differ. While an ideal model is not perfect (no models are), it is determined to be a reasonable assumption in this system for studying limiting mechanisms to middle chamber aqueous concentrations. It would be important to include a valid activity correction should the model be used to study super-saturation in the middle chamber as this is dependent on ionic activity and not concentration.

Table 1: Summary of plateau middle chamber concentrations and their calculated ionic strengths using Davies, SIT and Debye-Huckel methods in Visual MINTEQ (version 3.0).

Components and parameters of interest	Run 1	Run 2	Run 3
Na (mM)	280.6	384.7	353.3
K (mM)	192.8	237.3	235.8
NH4 (mM)	2033.9	2444.5	1848.0
Cl (mM)	536.9	575.52	538.2
Ac (mM)	285.43	371.65	0
CO3 (mM)	1002.2	1222.0	1118.6
SO4 (mM)	59.19	70.4	62.4
PO4 (mM)	84.21	90.7	85.3
Davies ionic strength (MINTEQ) (M)	1.9543	2.2546	1.8191
Davies monovalent activity coefficient (MINTEQ)	1.0039	1.0937	0.9670
Davies pH (MINTEQ)	8.732	8.812	8.847
SIT ionic strength (MINTEQ) (M) ¹	2.2443	2.6577	2.2058
SIT monovalent activity coefficient (MINTEQ) (M) ¹	0.6177	0.6178	0.6297
SIT pH (MINTEQ) ¹	9.102	9.064	9.188
Debye-Huckel ionic strength (MINTEQ) (M)	2.3366	2.8125	2.2441
Debye-Huckel monovalent activity coefficient (MINTEQ) (M)	1.1201	1.2912	1.0904
Debye-Huckel pH (MINTEQ)	8.886	8.991	8.966

¹The SIT simulations were performed using pH calculated from a mass balance, not a mass and charge balance as there was difficulty converging on a solution when using a mass and charge balance.

SUPPLEMENTARY INFORMATION 2: Model state equations

Note: Q5 and Q6 represent osmotic flows across the CEM and AEM, respectively. J_a and J_c refer to the ionic flux across the AEM and CEM, respectively.

Catholyte chamber (Cc)

Step 1: changing volume

$$\frac{dV_{Cc}}{dt} = Q_2 - Q_3 - Q_6 = 0 \quad (\text{S2.1})$$

Step 2: Mass differential

$$\frac{dV_{Cc}C_{Cc}}{dt} = Q_2C_2 - Q_3C_{Cc} + J_a \quad (\text{S2.2})$$

Step 3: General expansion term

$$\frac{dVC}{dt} = C \frac{dV}{dt} + V \frac{dC}{dt} \quad (\text{S2.3})$$

Step 4: Sub step 1 into first RHS term and sub step 2 into LHS term

$$V_{Cc} \frac{dC_{Cc}}{dt} = -C_{Cc}(Q_2 - Q_3 - Q_6) + Q_2C_2 - Q_3C_{Cc} + J_a \quad (\text{S2.4})$$

$$\frac{dC_{Cc}}{dt} = \frac{(Q_2 - Q_3 - Q_6)}{V_{Cc}} (-C_{Cc}) + \frac{Q_2}{V_{Cc}} C_2 - \frac{Q_3}{V_{Cc}} C_{Cc} + \frac{1}{V_{Cc}} (J_a) \quad (\text{S2.5})$$

$$\frac{dC_{Cc}}{dt} = \frac{(Q_2 - Q_6)}{V_{Cc}} (-C_{Cc}) + \frac{Q_2}{V_{Cc}} C_2 + \frac{1}{V_{Cc}} (J_a) \quad (\text{S2.6})$$

Product chamber (Pc)

$$\frac{dV_{Pc}}{dt} = Q_6 + Q_5 - Q_4 = 0 \quad (\text{S2.7})$$

$$\frac{dV_{Pc}C_{Pc}}{dt} = 0 - Q_4C_{Pc} + J_a - J_c - R_{p,Pc}V_{Pc} \quad (\text{S2.8})$$

$$V_{Pc} \frac{dC_{Pc}}{dt} = -C_{Pc}(Q_6 + Q_5 - Q_4) - Q_4C_{Pc} + J_a - J_c - R_{p,Pc}V_{Pc} \quad (\text{S2.9})$$

$$\frac{dC_{Pc}}{dt} = -\frac{(Q_6 + Q_5 - Q_4)}{V_{Pc}} (C_{Pc}) - \frac{Q_4}{V_{Pc}} (C_{Pc}) + \frac{1}{V_{Pc}} (J_a - J_c) - R_{p,Pc} \quad (\text{S2.10})$$

$$\frac{dC_{Pc}}{dt} = \frac{(Q_6 + Q_5)}{V_{Pc}} (-C_{Pc}) + \frac{1}{V_{Pc}} (J_a - J_c) - R_{p,Pc} \quad (\text{S2.11})$$

Anolyte chamber (Ac)

$$\frac{dV_{Ac}}{dt} = Q_1 - Q_5 - Q_2 = 0 \quad (\text{S2.12})$$

$$\frac{dV_{Ac}C_{Ac}}{dt} = Q_1C_1 - Q_2C_{Ac} - J_c \quad (S2.13)$$

$$V_{Ac} \frac{dC_{Ac}}{dt} = -C_{Ac}(Q_1 - Q_5 - Q_2) + Q_1C_1 - Q_2C_{Ac} - J_c \quad (S2.14)$$

$$\frac{dC_{Ac}}{dt} = -\frac{Q_1 - Q_5 - Q_2}{V_{Ac}}C_{Ac} + \frac{Q_1}{V_{Ac}}C_1 - \frac{Q_2}{V_{Ac}}C_{Ac} - \frac{J_c}{V_{Ac}} \quad (S2.15)$$

$$\frac{dC_{Ac}}{dt} = \frac{(Q_5 + Q_2)}{V_{Ac}}C_{Ac} - \frac{Q_2}{V_{Ac}}C_{Ac} - \frac{J_c}{V_{Ac}} \quad (S2.16)$$

Product overflow reservoir (Por)

$$\frac{dV_{Por}}{dt} = Q_4 - 0 \neq 0 \quad (S2.17)$$

$$\frac{dV_{Por}C_{Por}}{dt} = Q_4C_4 - 0 \quad (S2.18)$$

$$V_{Por} \frac{dC_{Por}}{dt} = -C_{Por}(Q_4 - 0) + Q_4C_4 \quad (S2.19)$$

$$\frac{dC_{Por}}{dt} = \frac{Q_4}{V_{Por}}(C_4 - C_{Por}) \quad (S2.20)$$

Feed in reservoir (Fir)

$$\frac{dV_{Fir}}{dt} = 0 - Q_1 \neq 0 \quad (S2.21)$$

$$\frac{dV_{Fir}C_{Fir}}{dt} = -Q_1C_{Fir} \quad (S2.22)$$

$$V_{Fir} \frac{dC_{Fir}}{dt} = -C_{Fir}(0 - Q_1) - Q_1C_{Fir} \quad (S2.23)$$

$$\frac{dC_{Fir}}{dt} = \frac{Q_1}{V_{Fir}}(C_{Fir} - C_{Fir}) = 0 \quad (S2.24)$$

Feed out reservoir (For)

$$\frac{dV_{For}}{dt} = Q_3 - 0 \neq 0 \quad (S2.25)$$

$$\frac{dV_{For}C_{For}}{dt} = Q_3C_3 \quad (S2.26)$$

$$V_{For} \frac{dC_{For}}{dt} = -C_{For}(Q_3 - 0) + Q_3C_3 \quad (S2.27)$$

$$\frac{dC_{For}}{dt} = \frac{Q_3}{V_{For}}(C_3 - C_{For}) \quad (S2.28)$$

SUPPLEMENTARY INFORMATION 3: Ammonia stripping test

Visually it was difficult to determine whether including ammonia stripping in the middle chamber improved the model fit to experimental data. Therefore, the same statistical χ^2 -test was performed as in supplementary information 2, to determine whether a model not including ammonia stripping in the middle chamber was different to a model including ammonia stripping in the middle chamber. The best fit k_{1a} value was determined to be 0.11 h^{-1} . The test showed the models are not significantly different with an F statistic of 1.07, which is less than a critical F value of 1.34. In addition, the R^2 values for the no stripping model is 0.976 and with stripping 0.982. Indicating that including an ammonia stripping model only accounts for 0.6% more variance than a model without ammonia stripping. To not add unnecessary complexity to the model, ammonia stripping was not included in the subsequent analysis.

SUPPLEMENTARY INFORMATION 4: Model validation

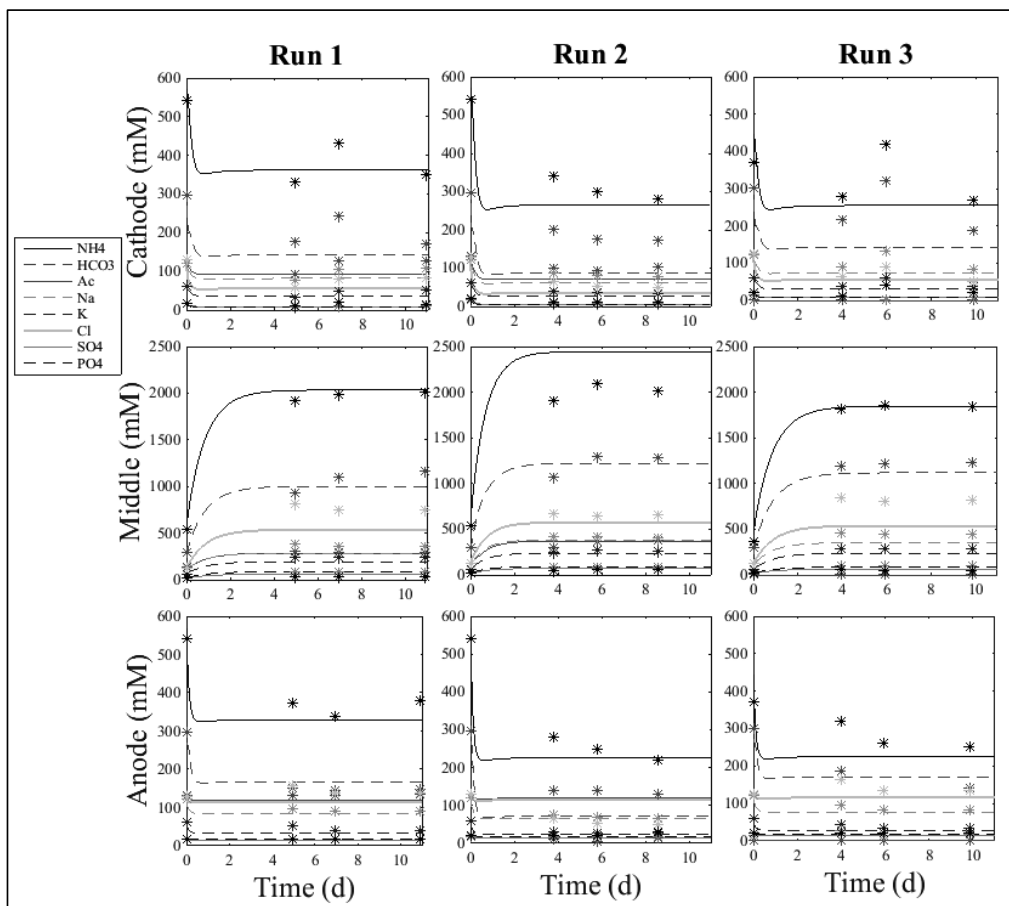


Figure S4.1: Model validation of component concentrations for the three experiments.

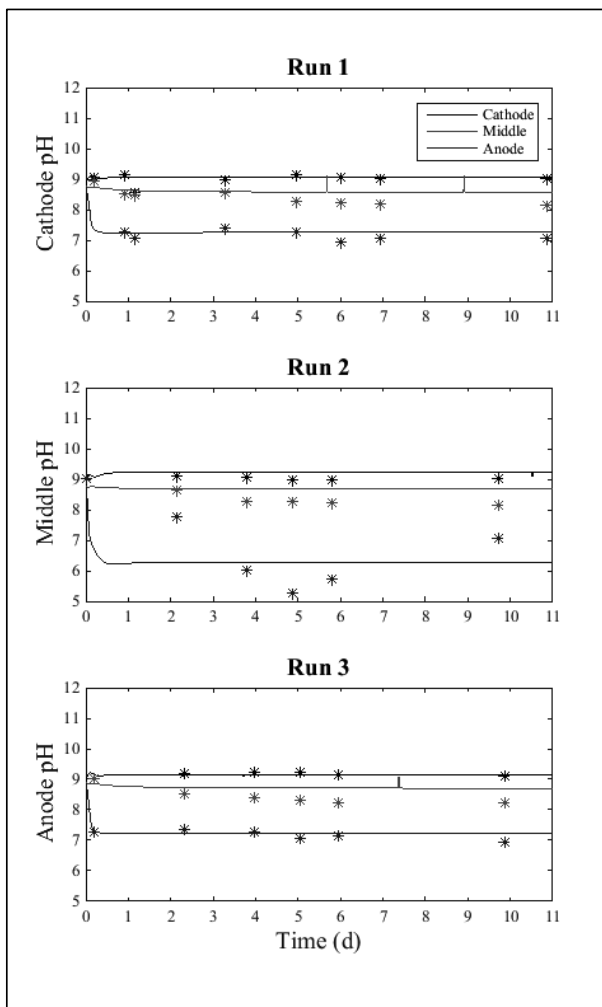


Figure S4.2: Model validation of pH for the three experiments.

SUPPLEMENTARY INFORMATION 5: Model sensitivity analysis

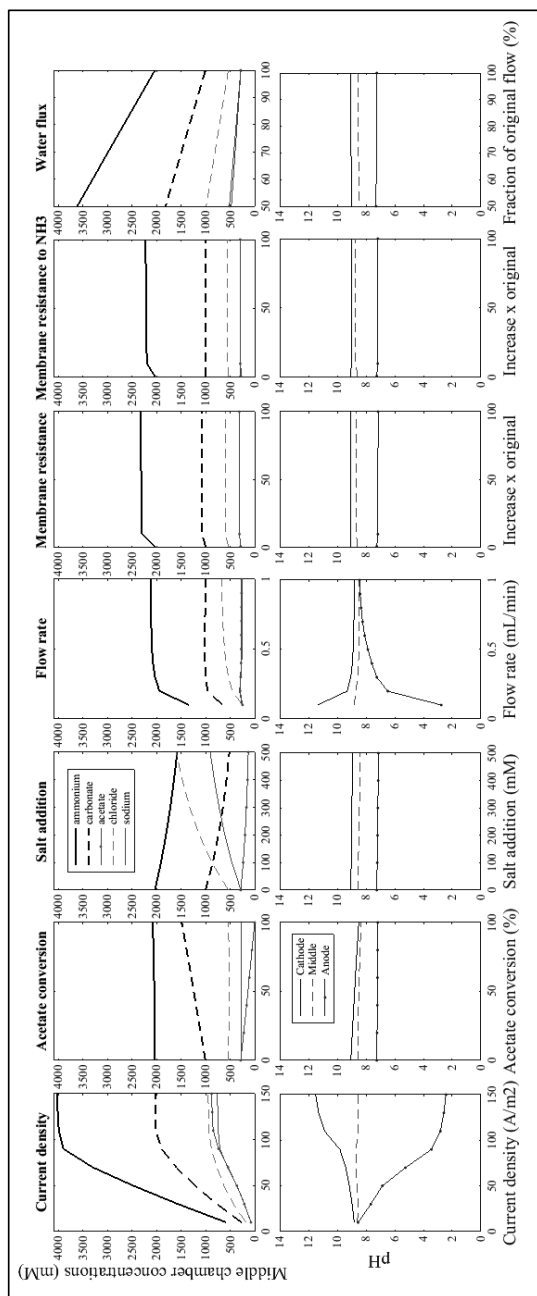


Figure S5.1: Parameter sweeps of current density, acetate conversion, salt addition, flow rate and membrane properties showing middle chamber component concentrations (top row) and pH (bottom row) at equilibrium.

SUPPLEMENTARY INFORMATION 6: Flux results

Current density

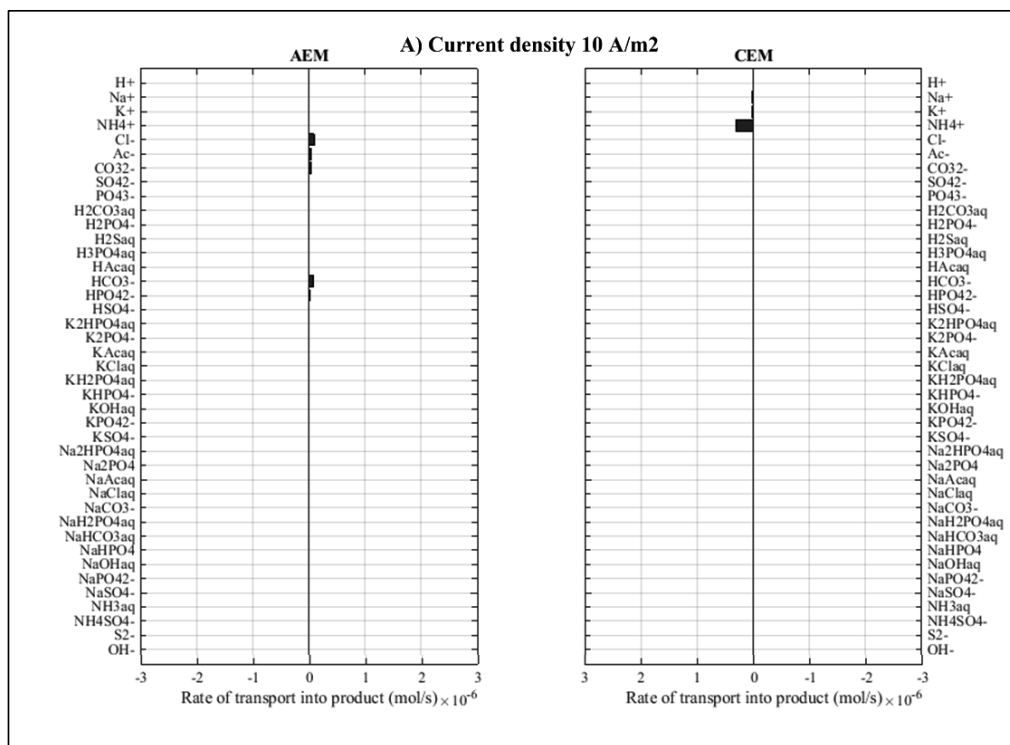


Figure S6.1: Species fluxes at steady state using a current density of 10 A m⁻².

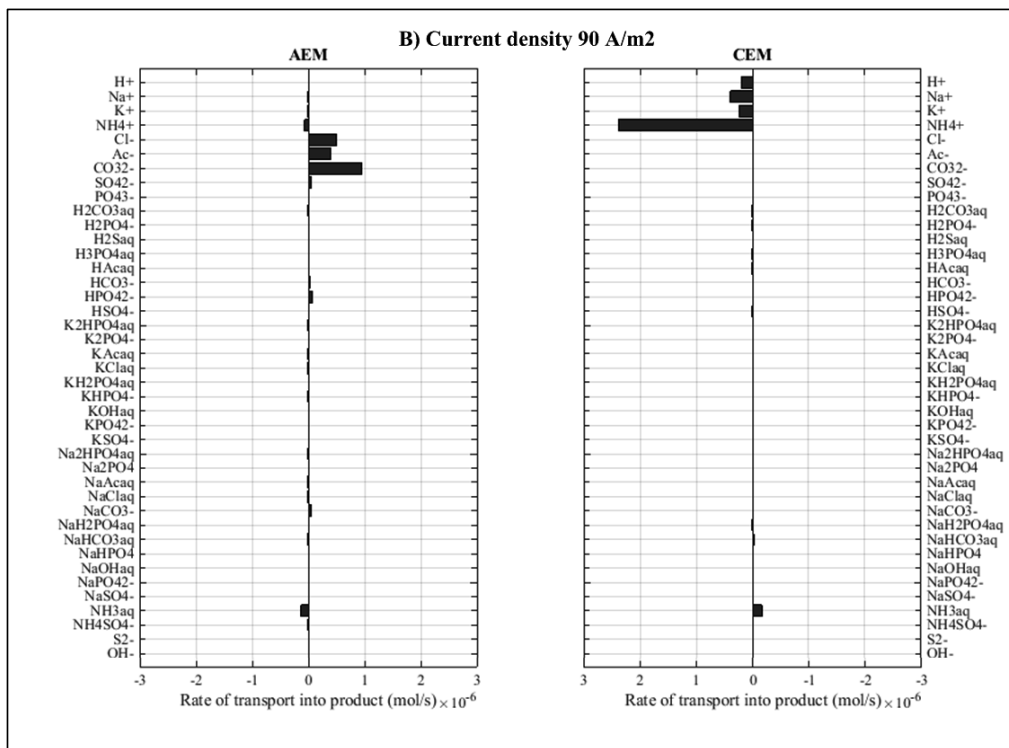


Figure S6.2: Species fluxes at steady state using a current density of 90 A m⁻².

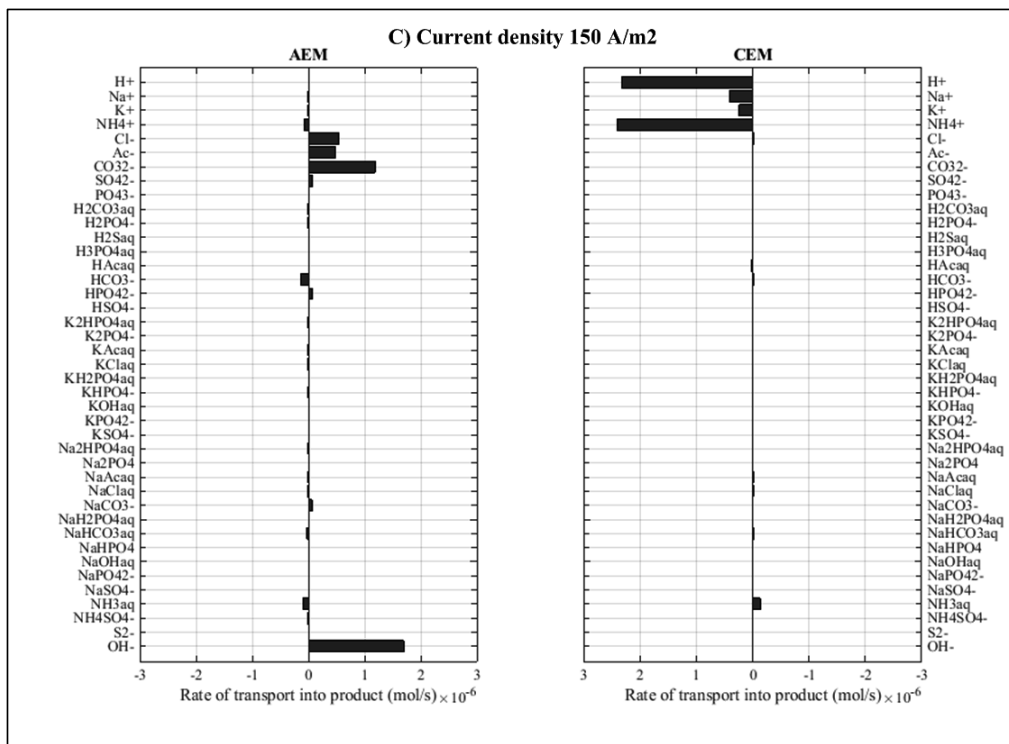


Figure S6.3: Species fluxes at steady state using a current density of 150 A m⁻².

Acetate conversion

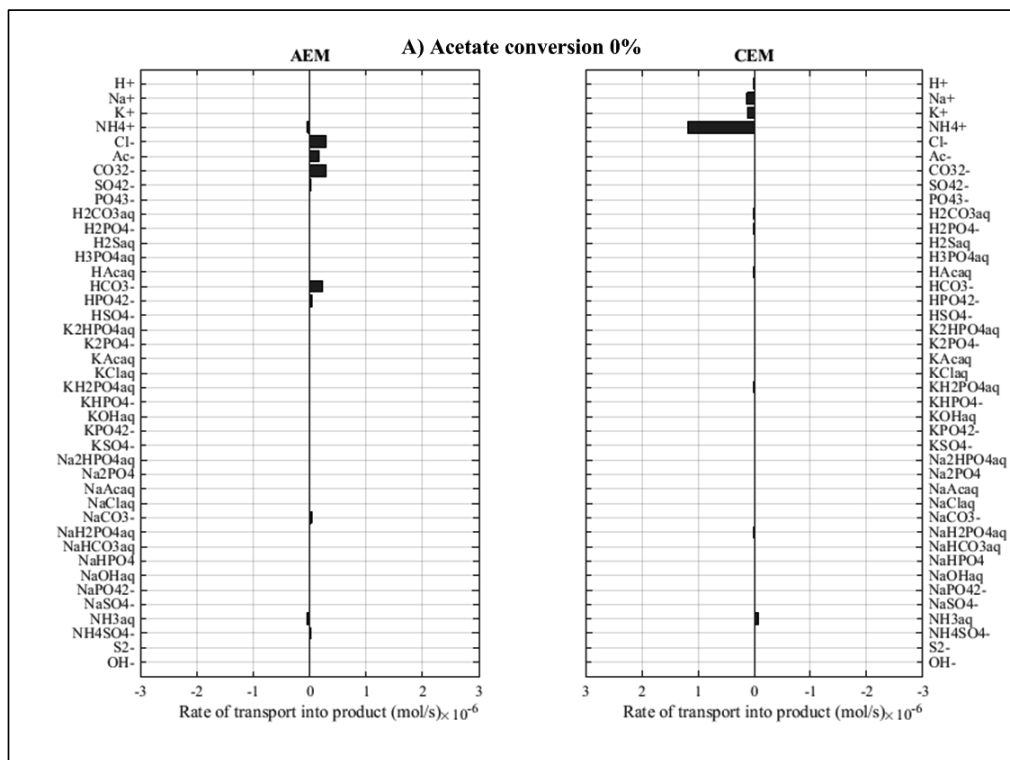


Figure S6.4: Species fluxes at steady state using 0% acetate conversion.

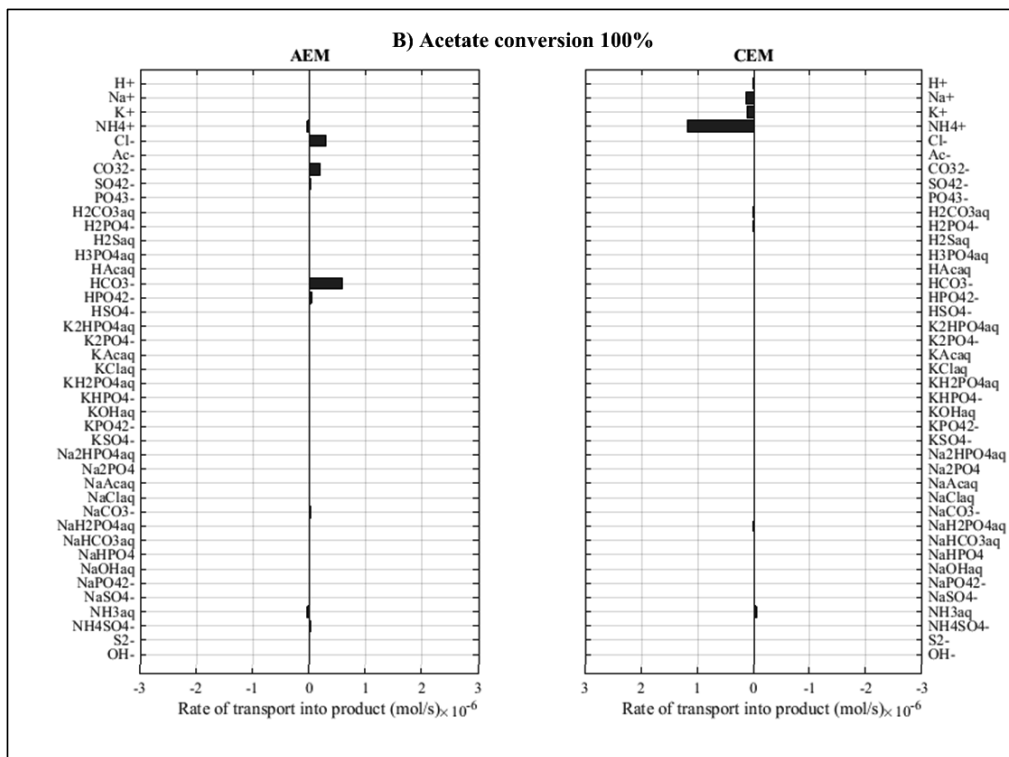


Figure S6.5: Species fluxes at steady state using 100% acetate conversion.

Salt impurity

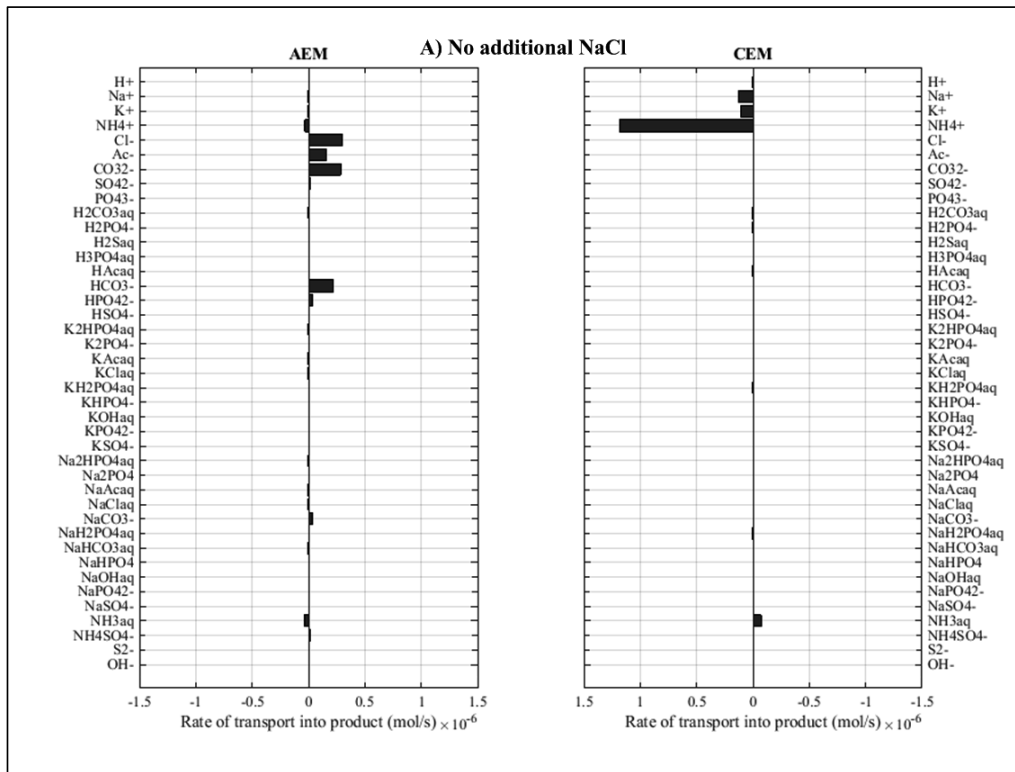


Figure S6.6: Species fluxes at steady state using no additional NaCl.

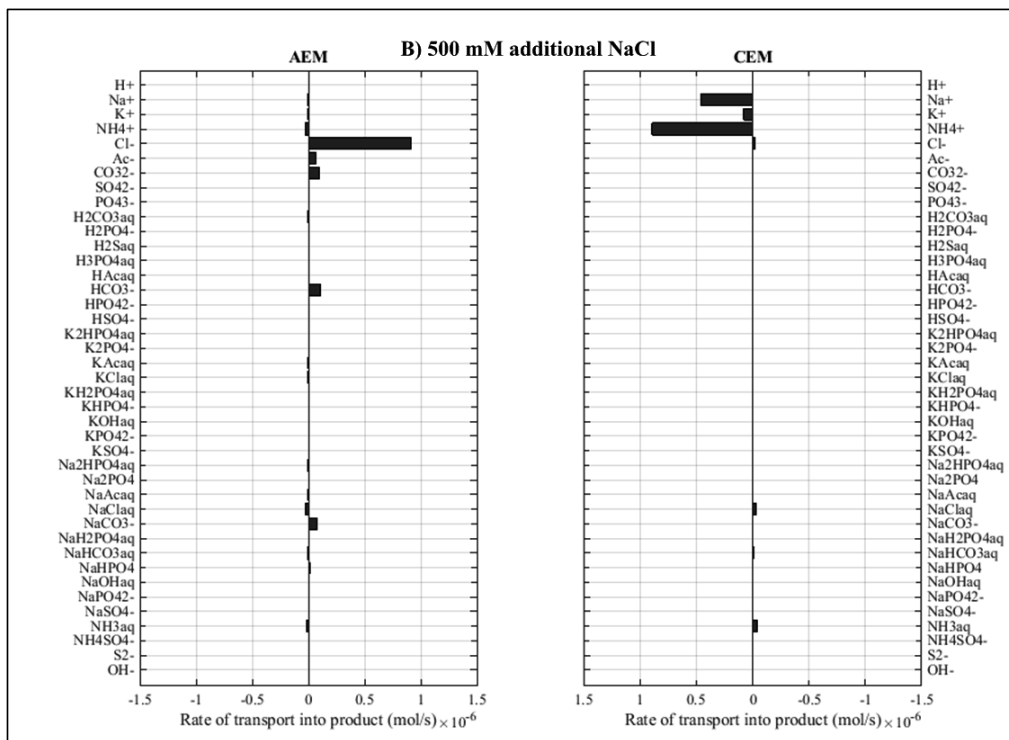


Figure S6.7: Species fluxes at steady state using 500 mM additional NaCl.

Flow rate

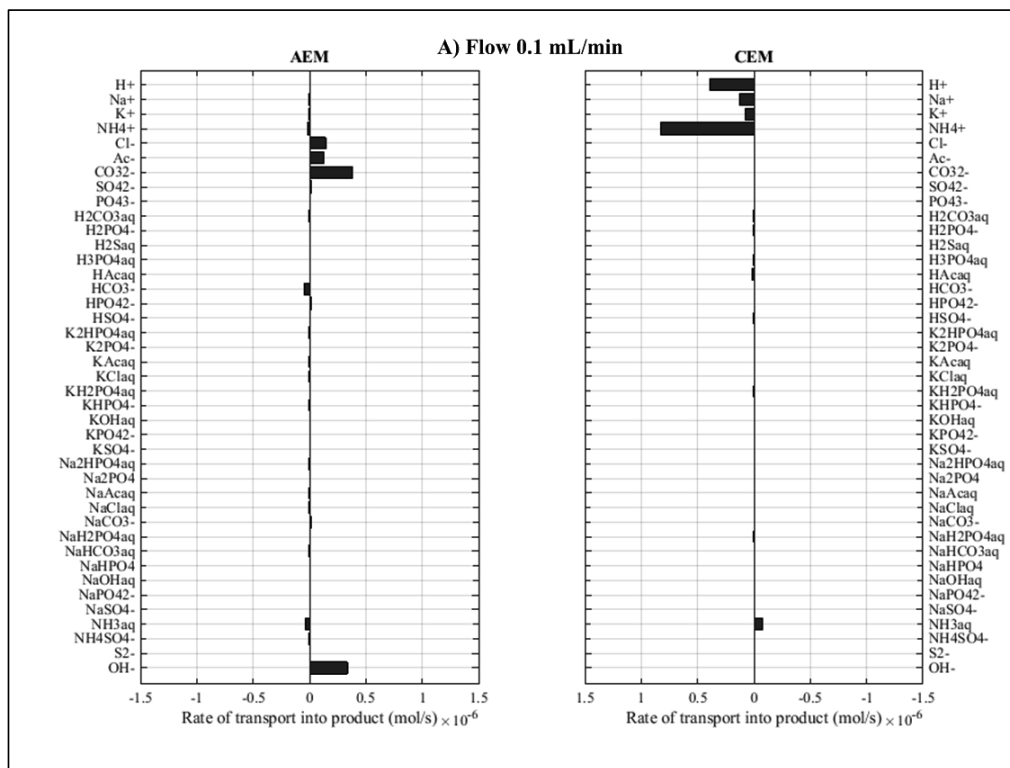


Figure S6.8: Species fluxes at steady state using a flow rate of 0.1 mL min⁻¹.

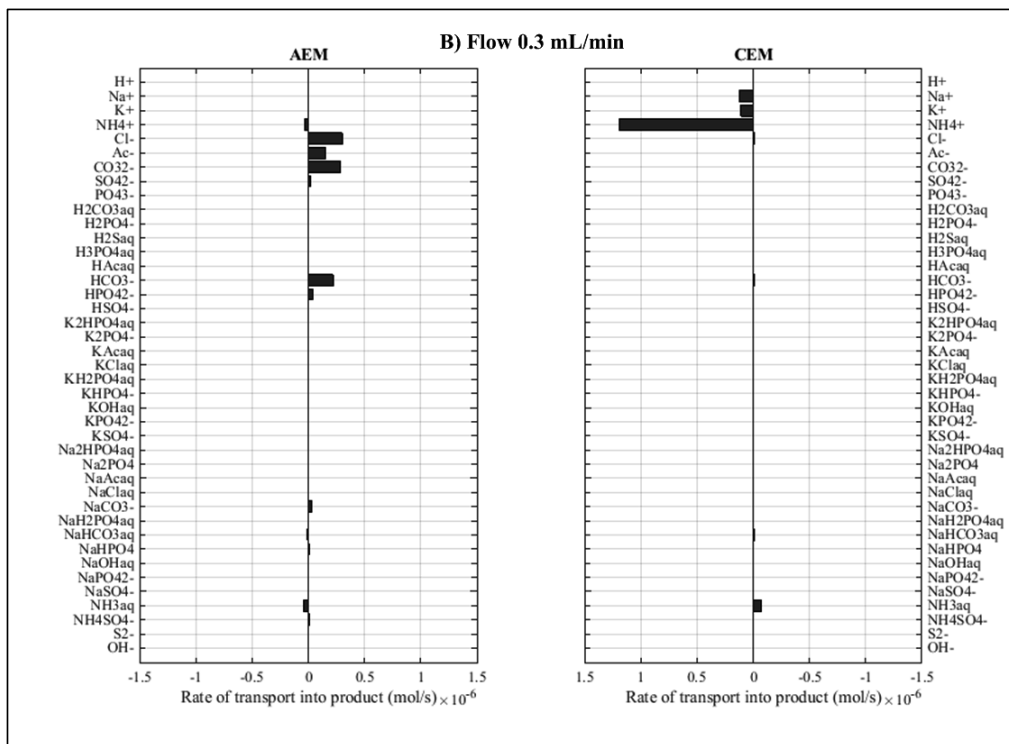


Figure S6.9: Species fluxes at steady state using a flow rate of 0.3 mL min⁻¹.

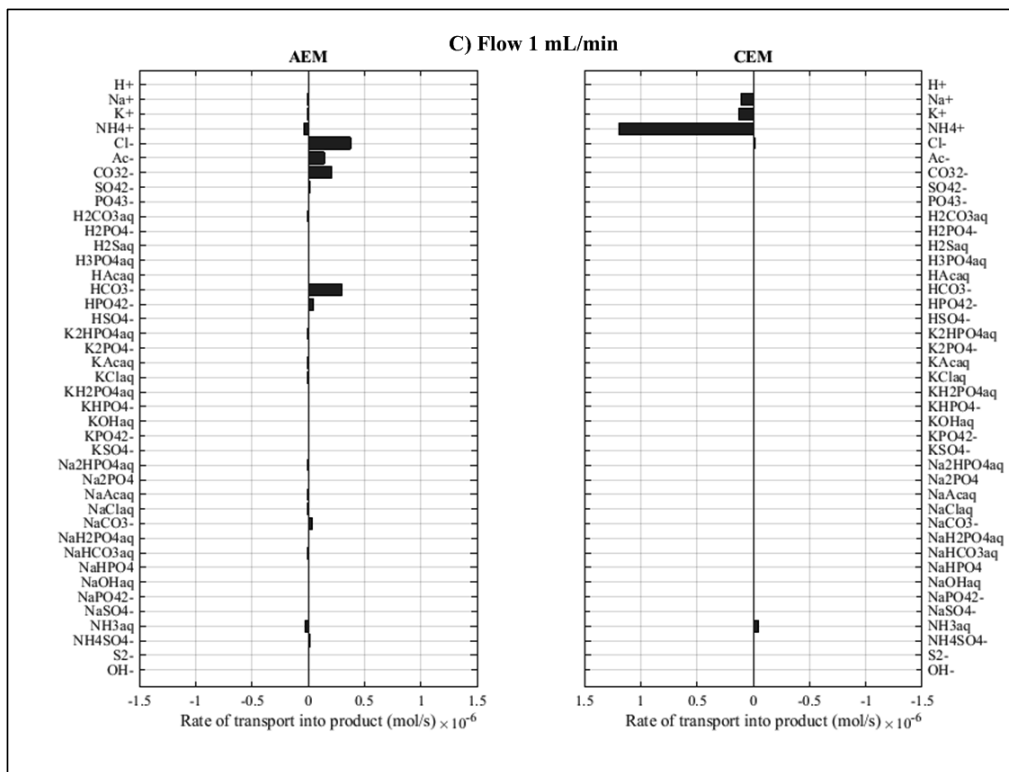


Figure S6.10: Species fluxes at steady state using a flow rate of 1 mL min⁻¹.

Membrane properties

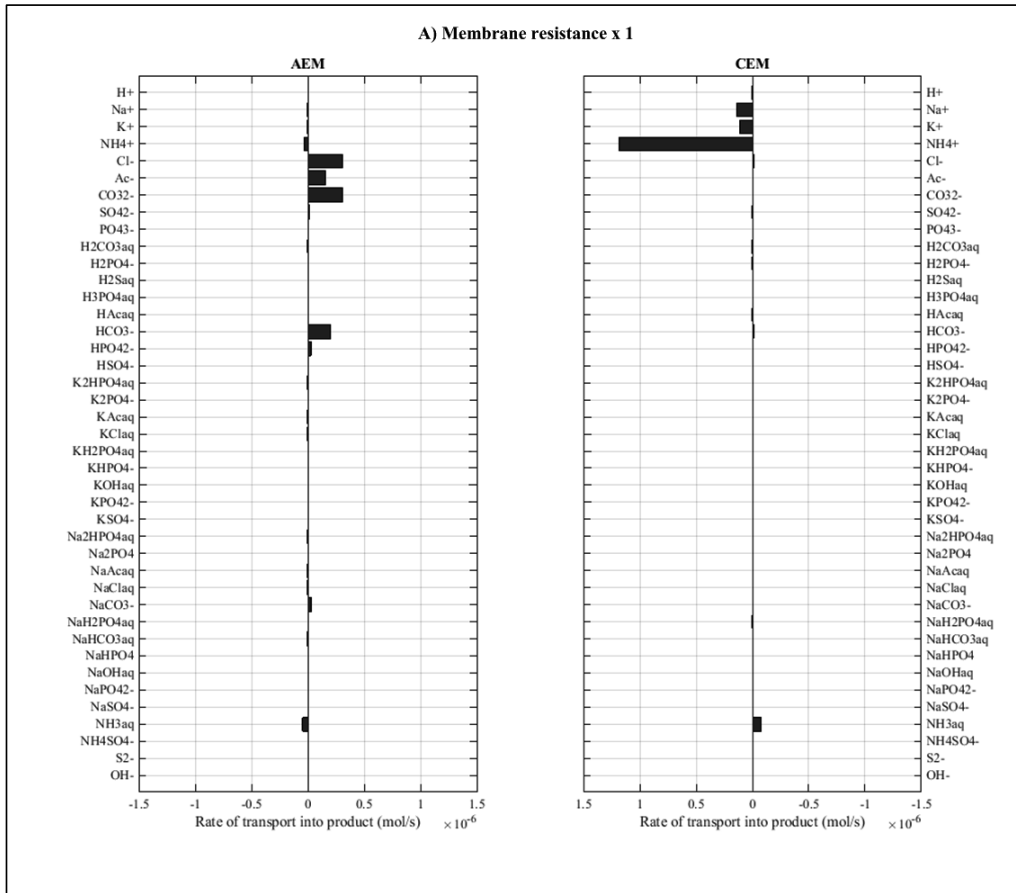


Figure S6.11: Species fluxes at steady state using the original membrane resistance.

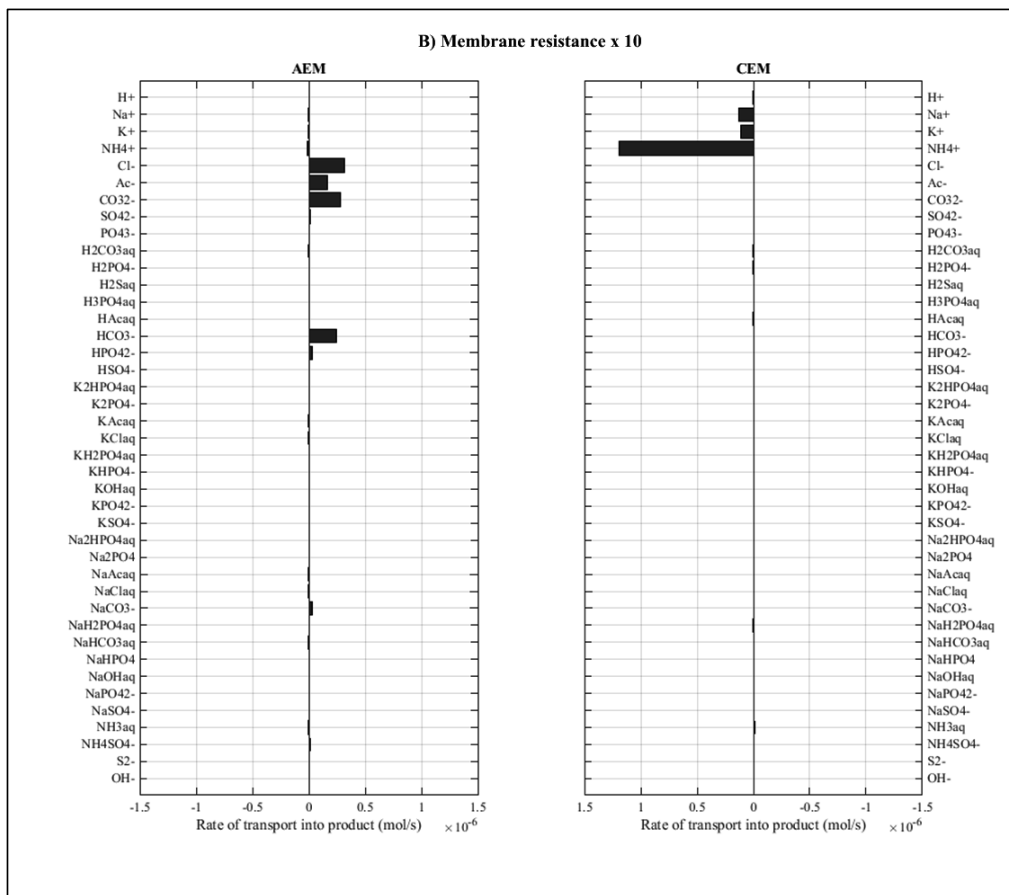


Figure S6.12: Species fluxes at steady state using 10 times the original membrane resistance.

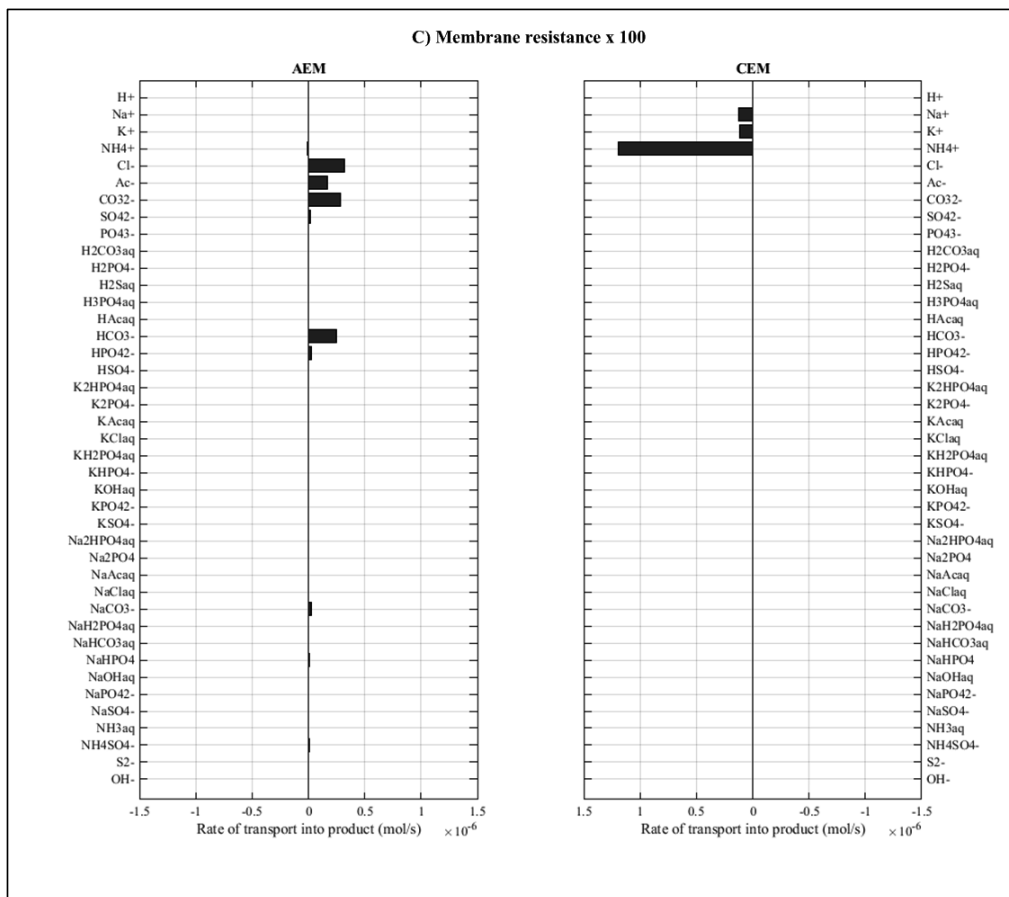


Figure S6.13: Species fluxes at steady state using 100 times the original membrane resistance.

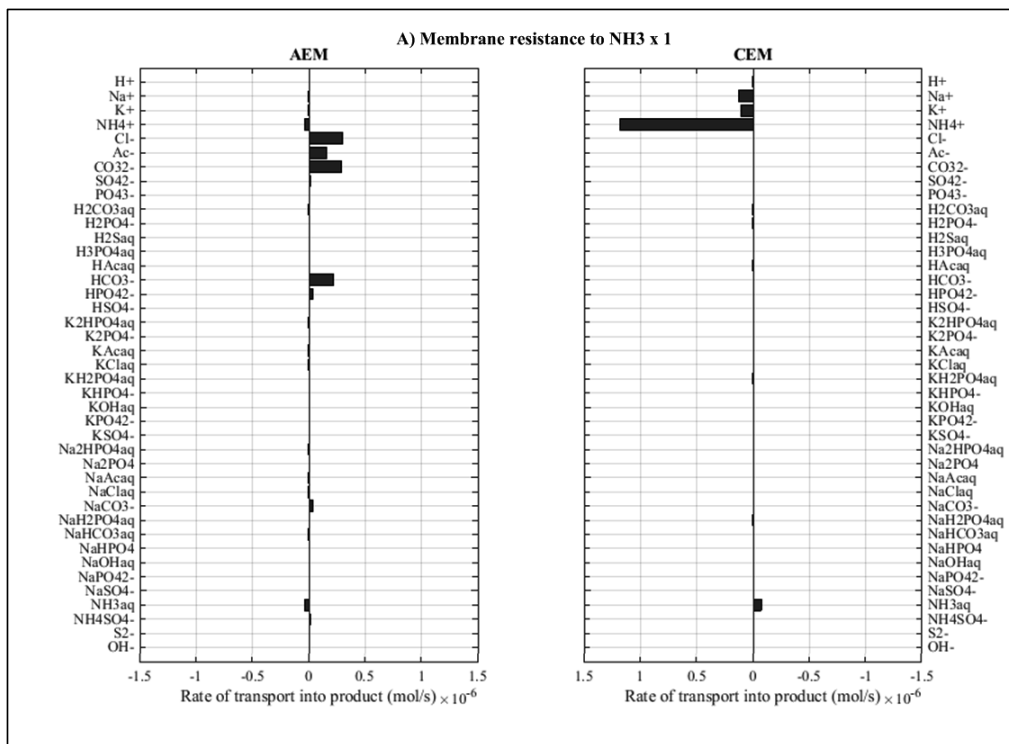


Figure S6.14: Species fluxes at steady state using the original membrane resistance for ammonia.

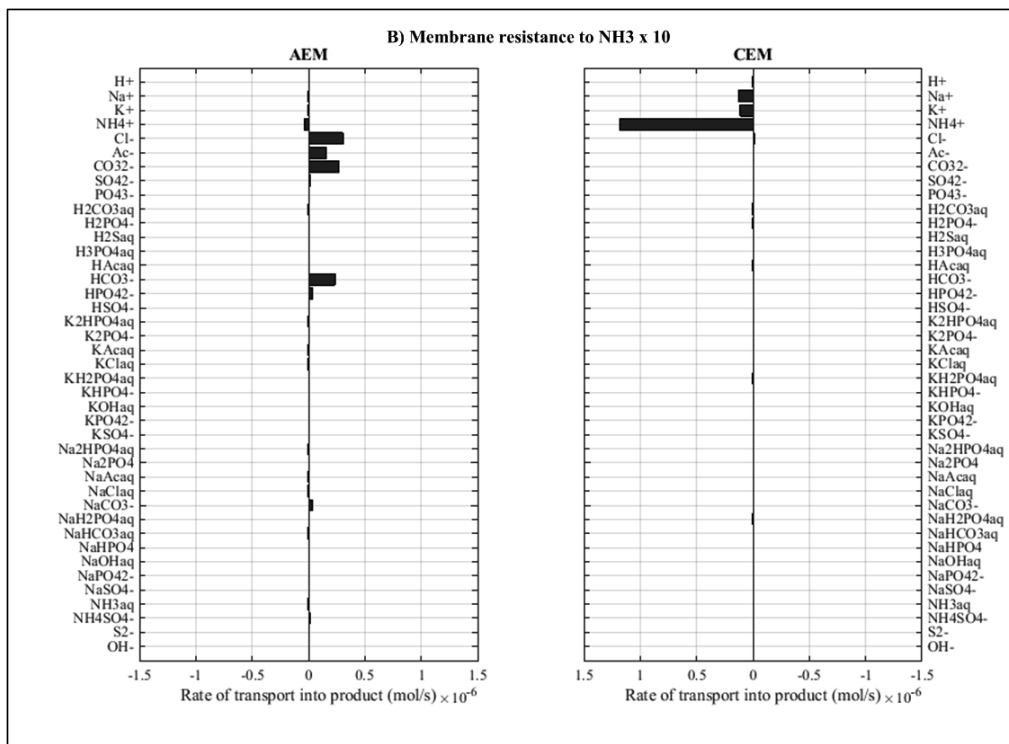


Figure S6.15: Species fluxes at steady state using the 10 times the original membrane resistance for ammonia.

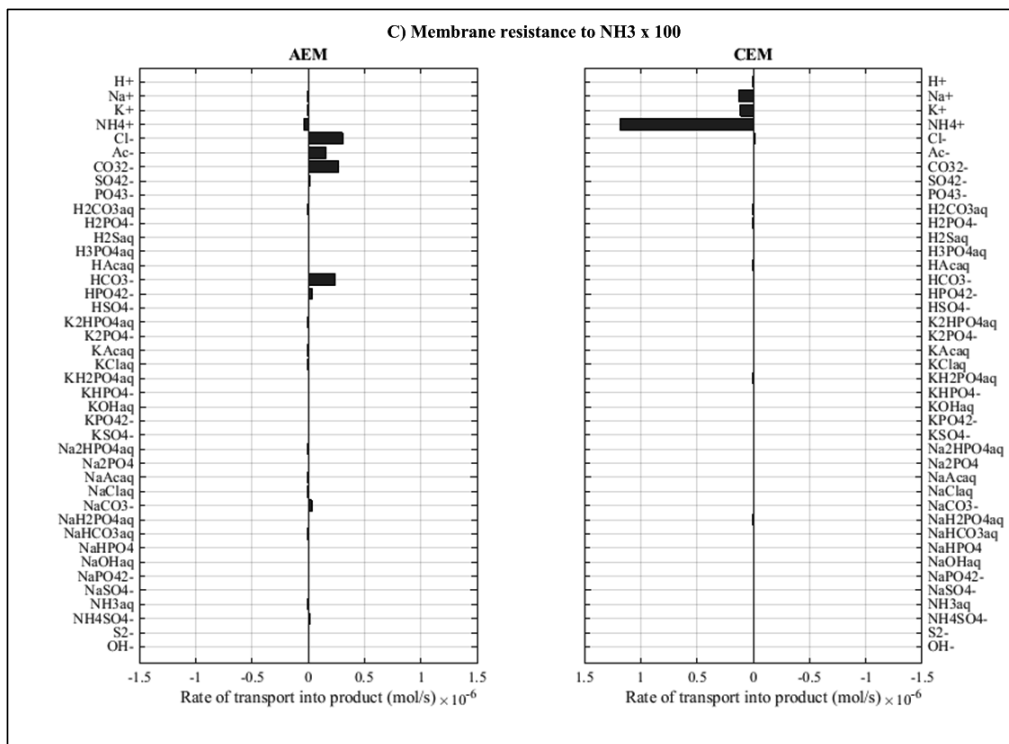


Figure S6.16: Species fluxes at steady state using the 100 times the original membrane resistance for ammonia.

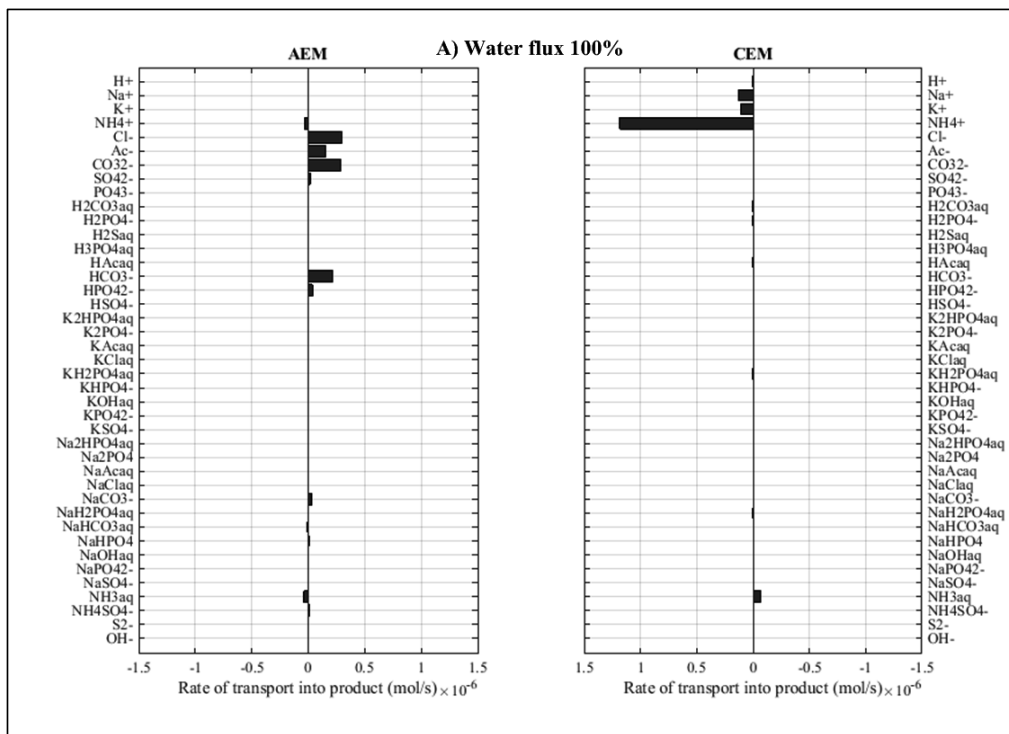


Figure S6.17: Species fluxes at steady state using the original water flux rate.

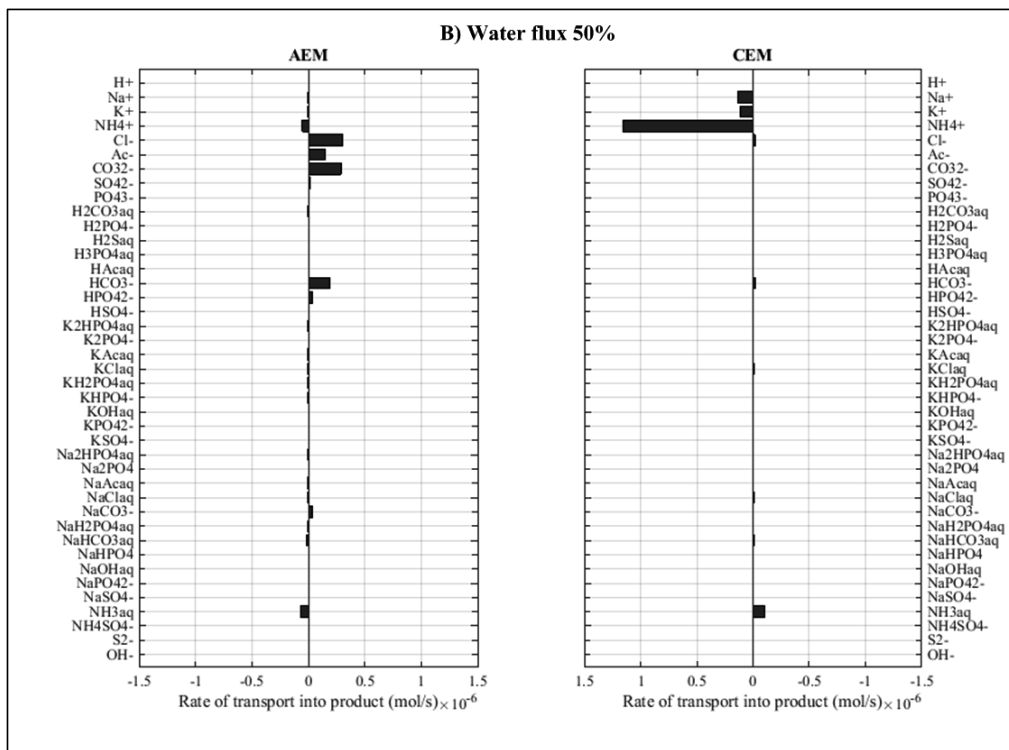


Figure S6.18: Species fluxes at steady state using the 50% of the original water flux rate.

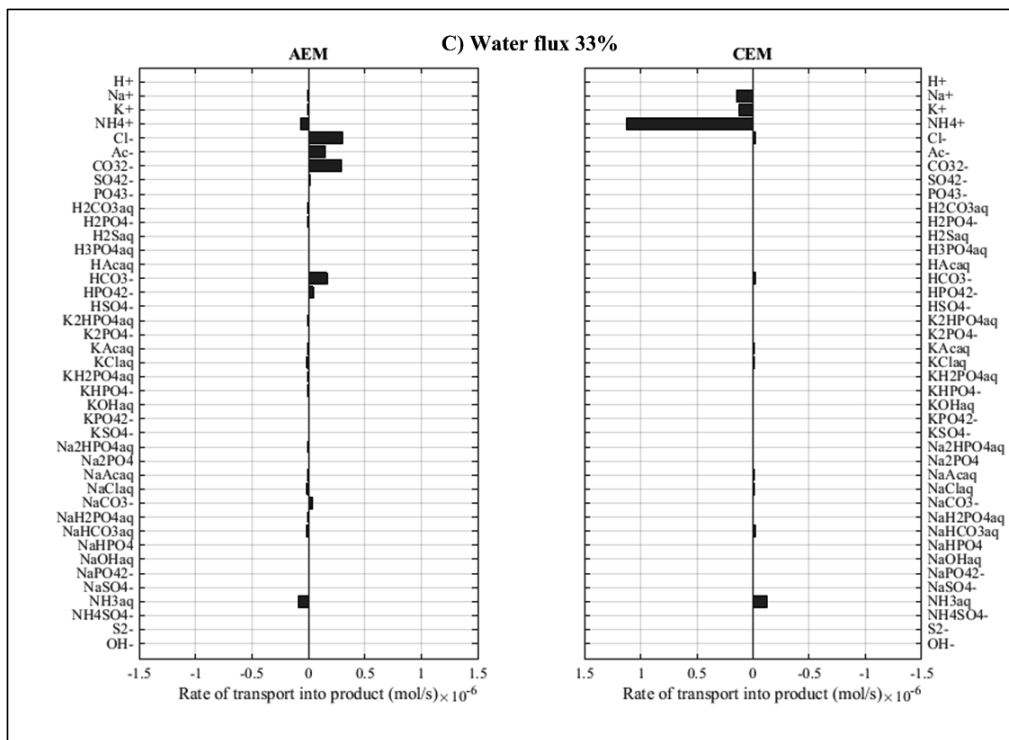


Figure S6.19: Species fluxes at steady state using the 33% of the original water flux rate.

PUBLICATION III

Electrochemical system for selective oxidation of organics over ammonia in urine

Johannes Jermakka, Stefano Freguia, Marika Kokko, Pablo Ledezma

Environmental Science: Water Research & Technology 7 (2021) 942
<https://doi.org/10.1039/D0EW01057J>

Publication reprinted with the permission of the copyright holders.



Cite this: *Environ. Sci.: Water Res. Technol.*, 2021, 7, 942

Electrochemical system for selective oxidation of organics over ammonia in urine†

Johannes Jermakka,[†] Stefano Freguia,^c
Marika Kokko^{‡a} and Pablo Ledezma^{‡b}

Source-separated urine can enable efficient nutrient recycling, but the removal of the organic fraction that is required to ensure a safe nutrient product typically also removes the nitrogen in urine (present as total ammonium nitrogen, TAN). In this study, a reagent-free pH control method was used with a two-chamber electrochemical cell with a boron doped diamond (BDD) anode to oxidize synthetic and real urine at different anodic pH values. Without pH adjustment (pH 8.4), all TAN in urine was oxidized in synthetic urine, but at pH ≤ 3 , 79% \pm 5% of TAN was retained. Simultaneously, $\geq 90\%$ of organic content was removed at all pH values with a pH-independent rate. Two different TAN oxidation regimes with corresponding zero-order (*i.e.* current limited) TAN oxidation rates of -0.02 h^{-1} and -0.002 h^{-1} were identified, separated by a chloride to TAN concentration ratio of approximately 0.2 M/M. The higher TAN oxidation rate is linked to a breakpoint chlorination-type oxidation pathway, whereas the lower rate is linked to a direct oxidation pathway on the BDD surface. In addition to TAN, potassium and phosphorus were conserved at $101\% \pm 6\%$ and $89\% \pm 4\%$, respectively. The proposed technology allows for the selective oxidation of the organic fraction in urine while retaining a high proportion of all other key nutrients for potential reuse as a fertilizer.

Received 1st December 2020,
Accepted 10th March 2021

DOI: 10.1039/d0ew01057j

rsc.li/es-water

Water impact

Urine source-separation offers a technological shift from WWTPs as centralized waste disposal/treatment infrastructure with high energy demand to a series of localized treatments with higher efficiency and concomitant nutrient capture for reuse. This article demonstrates how reagent-free anodic pH-control allows for the advanced oxidation of organics in source-separated urine and conserves nitrogen, potassium and phosphorus, representing a potential pathway for decentralized nutrient recovery and reuse.

1. Introduction

Source-separated human urine contains the majority of main nutrients consumed by adult humans (app. 86–65–76% N–P–K), while comprising less than 1% of produced wastewater.^{1–3} Nitrogen in urine comprises approximately 80% of total nitrogen in municipal wastewater, the removal of which forms a major portion of the total energy consumption of wastewater treatment.^{2,3} Even more energy is used for fixing the same amount of nitrogen from atmospheric N₂ for fertilizer use using the Haber–Bosch-process, which accounts

for 1.4% of global CO₂ emissions.⁴ Technologies treating urine as a feed for nutrient recovery could reduce energy requirements from fixing and removal of nitrogen, redirect forms of used energy to electricity from fossil fuels, reduce nutrient runoff to the environment, reduce mining of phosphorus and potassium and thus form a component of the circular economy of nutrients.

While source-separated urine contains nutrients in ratios suitable for fertilizer use,^{3,5} direct reuse is not favoured in modern societies due to transportation costs, salinity and health and safety issues.^{3,6} Accordingly, the preferred route for urine-derived nutrient reuse is *via* separation and/or extraction, primarily of nitrogen and phosphorus, through a variety of technologies, particularly struvite precipitation^{7–10} and ammonia stripping.^{11,12} However, the sustainability of these approaches has been questioned by their extensive reagent requirement and the involved transport, storage, logistical and energy burdens.³ One potential alternative for nutrient removal/recovery from urine with little or no additional reagents required is electrochemical technology,

^a Faculty of Engineering and Natural Sciences, Tampere University, Finland

^b Advanced Water Management Centre, The University of Queensland, St. Lucia, QLD 4072, Australia

^c Chemical Engineering, The University of Melbourne, Melbourne, VIC 3010, Australia

† Electronic supplementary information (ESI) available. See DOI: 10.1039/d0ew01057j

‡ Permanent address: Tampere University, Faculty of Engineering and Natural Sciences, PO Box 541, 33014 Tampere, Finland. E-mail: johannes.jermakka@tuni.fi

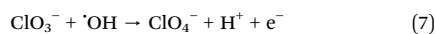
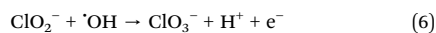
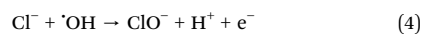
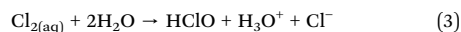
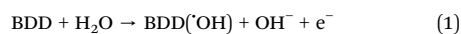


which includes electro dialysis, electro-concentration, microbial electrochemical technologies and combined membrane stripping technologies.^{13–26}

A category of electrochemical technologies called electrochemical advanced oxidation processes (EAOPs) involves water treatment processes using electricity to produce oxidative radicals on electrodes^{27,28} and can be well suited for source-separated urine due to urine's high conductivity.²⁹ EAOPs can be operated without a supply of chemicals or other feeds, allowing for a simplified decentralized implementation, and can be viable even in locations with intermittent power supply from *e.g.* renewable sources.³⁰ Development of small, flexible EAOPs for source-separated urine treatment could allow for a more widespread implementation of decentralized urine collection and nutrient recovery, provided that the latter can be stably preserved. EAOPs have been widely studied for organics oxidation,^{27,28,31} and specifically for the treatment of source-separated urine^{32–35} and latrine water.^{36–41} However, these studies have primarily focused on the complete oxidation of organic matter and TAN into CO₂ and N₂ as a means of localized wastewater treatment for safe release into the environment or for water reuse. The most widely utilized anodic electrode materials for EAOPs are dimensionally stable anodes (DSAs, *e.g.* Ti/IrO₂ and Ti/RuO₂ mixed metal alloys) and boron doped diamond (BDD). DSAs are termed active anodes and form a chemical-type sorption with the formed OH[•]-radical during water electrolysis, while BDD electrodes are termed passive anodes and form a weaker, physical-type sorption with the OH[•]-radical.^{27,28}

In EAOPs, the oxidation pathways for organic materials (TOC, total organic carbon) and ammonium-nitrogen (total ammonium nitrogen, TAN = NH₃ + NH₄⁺) are complex and can differ based on multiple parameters including the electrode material, electrolyte composition, applied potential, mixing and temperature.^{27,42} Three distinct main oxidation pathways are identified: (i) direct oxidation through direct charge transfer on the electrode, (ii) indirect oxidation through reactive oxygen species, most prominently the electrode-bound hydroxide radical (M(OH[•])), and (iii) indirect oxidation through radical species such as oxocarbonates, oxosulfates, oxophosphates and especially chloride radicals (reactive chlorine species, RCS).^{27,28,31,43–45} Electrode oxidation chemistry can be separated into current controlled and mass transport controlled regimes, depending on the applied current density, mixing and concentration, and the chemistry can differ significantly between different regimes.^{27,46}

BDD electrodes favour the formation of weakly adsorbed hydroxyl radicals BDD(OH[•]) (1) that are very strong oxidizing agents ($E^0 = 2.8$ V) and readily scavenged by organic molecules and inorganic anions to form oxidized products or radicals, respectively.^{27,28} In urine, chloride is present at significant concentrations and is readily oxidized by BDD(OH[•]) to form hypochlorite (2) and (3), or react directly and form further oxidized species with the hydroxyl radical (see eqn (4)–(7)).²⁸



While the hydroxyl radical is known to be a primary oxidant for most organic molecules, it is also reported to be a poor oxidant for certain inorganic molecules *e.g.* ammonium and complex organics such as fulvic and humic acids.^{28,34} These separate reaction pathways and oxidation affinities for organic materials and TAN remain a challenge for the practical implementation of EAOPs.³⁴ The relationship and situations where TAN is not oxidized in urine electro-oxidation have not been systematically studied and it remains unclear which parameters control the TOC and TAN oxidation capacity and rates during treatment. A better understanding of specific electro-oxidation pathways and rates under different parameters can allow for a better-informed design of electro-oxidation systems that perform as intended and could also enable selective organics electro-oxidation without TAN oxidation, allowing for selective nitrogen recovery from urine.

In this study, the electro-oxidation of synthetic and real ureolysed source-separated urine was investigated using a BDD anode under varying anodic pH conditions in a two-chamber electrochemical cell. The specific aims were to study the effects of pH on the (i) organics oxidation rate, (ii) TAN oxidation rate, and (iii) chloride oxidation rate and by-product formation. The outcomes provide a novel viewpoint into electro-chemical treatment of source-separated urine and expand the possibilities for selective nutrient recovery with concomitant organics removal.

2. Materials and methods

2.1 Medium composition

A synthetic urine solution representing human source-separated ureolysed urine was designed based on (i) previous investigations at the Swiss Federal Institute of Aquatic Science and Technology (EAWAG),^{47,48} (ii) a literature review of source-separated urine samples,^{5,49–57} (iii) the human urine metabolome,⁵⁸ and (iv) real source-separated urine collected for research at the Advanced Water Management Centre at the University of Queensland, Australia.¹⁸ The four most prevalent organic compounds identified in the human urine metabolome database were included in the recipe: creatinine, hippuric



acid, citric acid and glycine, while the rest of the organic loading was simulated by addition of acetic acid, comprising 15% of total theoretical chemical oxygen demand in the sample. The recipe consisted of (in g L⁻¹): NH₄HCO₃ (22.14), NH₄Cl (0.48), NaCl (2.69), KCl (4.10), NaH₂PO₄ (2.40), Na₂SO₄ (2.41), creatinine C₄H₇N₃O (2.3), hippuric acid C₉H₉NO₃ (0.88), citric acid C₆H₈O₇ (0.88), glycine C₂H₅NO₂ (0.17), ammonium acetate NH₄CH₃CO₂ (2.06) and NH₄OH (25% liquid, 13.8 mL L⁻¹). This formulation simulates urine after ureolysis, which results in complete removal of Mg and Ca through precipitation with phosphate.⁴⁷ This solution was employed as a feed, used as prepared and its composition was monitored through sampling at the start of each experiment. Synthetic urine was chosen to enable consistency when systematically varying the experimental factors.

Furthermore, human source-separated urine was collected from Hiedanranta Kuivaamo-cultural venue in Tampere (Finland), where Digi Toilet Systems Oy operates source-separating dry toilets. Urine was sampled from the male urinals' collection tank, filled during spring and summer 2020. This urine was stored as collected in a closed 1 m³ tank at room temperature until sampling. After sampling, the urine was stored in closed 20 L canisters at +4 °C in the dark until used. The main properties of this real source-separated urine are presented in Table 1. The sampled urine was significantly more dilute and had different TAN/Cl/TOC-ratios than the synthetic urine (Table 1). This can be due to the recreational quality of the collection venue, associated with evening and night-time use and consumption of large amounts of beverages. While not representative of an average 24/7 human urine sample, using this real urine is still beneficial for comparison with the synthetic formulation, as many real source-separation sites comprise similar venues. Due to long term storage, this urine was considered to be fully ureolysed.

Table 1 Measured real and synthetic urine properties. All values in mmol L⁻¹, except pH (unitless) and conductivity (mS cm⁻¹)

Component	Synthetic urine	Real source-separated urine
TAN	522 ± 40	197 ± 3
NO ₃ ⁻	n.d.	n.d.
NO ₂ ⁻	n.d.	n.d.
TOC	286 ± 46	114 ± 17
Cl ⁻	92 ± 5	24.7 ± 0.8
ClO ₃ ⁻	n.d.	n.d.
ClO ₄ ⁻	n.d.	n.d.
K ⁺	70 ± 6	10.4 ± 0.3
Na ⁺	117 ± 8	27.6 ± 1.0
PO ₄ ³⁻	18 ± 2	5.1 ± 0.9
SO ₄ ²⁻	15 ± 2	3.7 ± 0.3
Cl/TAN	0.23 ± 0.02	0.13 ± 0.01
IS	1.23 ± 0.05	0.393 ± 0.009
pH	8.35 ± 0.09	8.5 ± 0.3
Conductivity	37.7 ± 0.8	17.0 ± 0.2

n.d. = not detected. IS = ionic strength.

2.2 Reactor and equipment

Custom reactors were used consisting of acrylic plates forming two parallel compartments of 70 mm × 50 mm × 10 mm each (see Fig. 1), sealed with triple rubber O-rings. Two identical reactor setups were utilized. The anodic compartment was fitted with a Condias Dischem 40 × 40 × 2 mm Nb-BDD electrode,

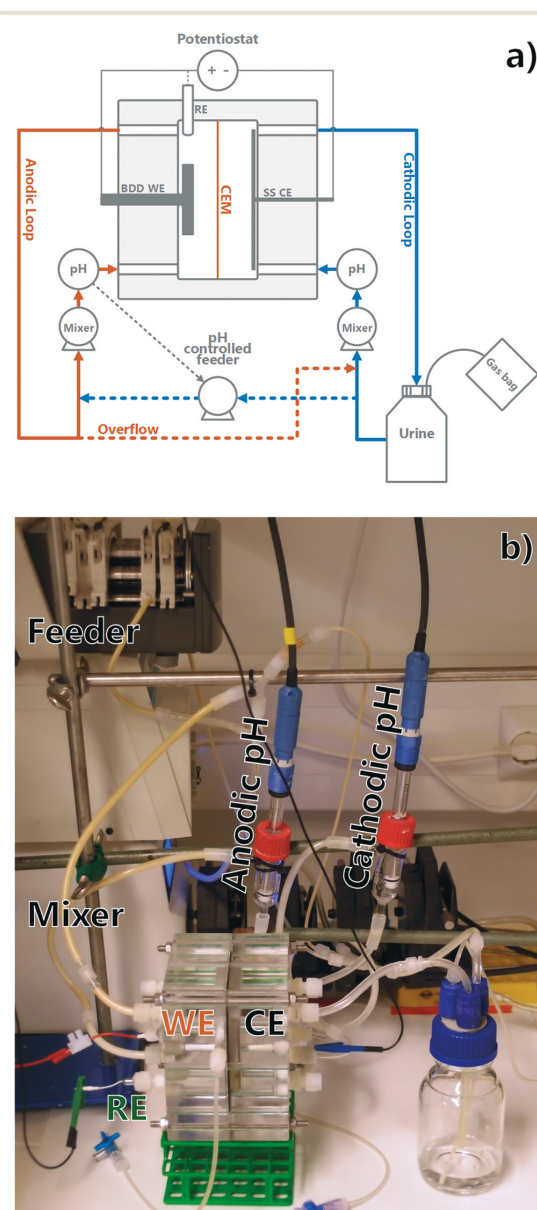


Fig. 1 a) Experiment flowchart (WE = working electrode, CE = counter electrode, RE = reference electrode, BDD = boron doped diamond, SS = stainless steel) and b) picture of the reactor setup.



with a plastic encased copper wire current collector. The current collector was attached using a conductive epoxy (Epo-Tek EJ2189-LV) and silicone sealant. An Ag/AgCl 3 M NaCl reference electrode (BASi, USA) was placed in the anodic chamber to monitor the anodic potential. The cathodic compartment contained a 70 mm × 50 mm stainless steel mesh as a cathode and was separated from the anodic compartment by a cation exchange membrane (CEM) (Membranes International Inc. CMI-7000). The projected surface area of the membrane was 35 cm² and the volume of each chamber was 35 mL, rendering the total reactor working volume as 70 mL. The anodic loop volume containing the anodic reactor chamber and the mixing loop was 57 mL and remained constant throughout all the experiments, whereas the cathodic loop volume was variable due to reactor volume changes (from 150 mL to 89 mL). The anodic and cathodic compartments were connected to online pH meters (Endress+Hauser Liquiline CM448) and both compartments were mixed by circulation pumps, with a chamber mix time of app. 10 seconds (Cole Parmer Masterflex 7523-70). The cathodic loop was circulating from a 150 mL recirculation bottle, the content of which was considered as part of the cathodic loop volume and was added in the beginning of each batch experiment. The anodic loop was fed with a pH-controlled feeding pump (Watson-Marlow 205U) from the cathodic loop and overflowed to the cathodic chamber through gas tight connections. The anodic feeding pump was pH-relay controlled to keep the anodic loop pH constant. A potentiostat (Bio-Logic VMP-3) was used as a power source, recording the voltage applied and electrical energy used. An example of potentiostatic data is included in the ESI† (S7). A constant current of 350 mA, corresponding to a current density of 100 A m⁻² based on the membrane surface area, was applied in all experiments. The anode surface area after current collector connections was estimated at 30 cm², corresponding to an average current density of 117 A m⁻² based on the anode surface area. Finally, the reactors' outlet gas composition was monitored using 100 mL 1 M HCl gas wash bottles or gas bags connected to the recirculation bottle. At the end of an experimental run, a 900 mL sample of gas bag content was transferred onto 1 L glass bottles using a displacement method, washed overnight in 1 M HCl, and analysed in the same way as the gas wash bottle samples. The runs where gas analysis was used and the method used are described in ESI† S1.

2.3 Operation

Batch experiments, referred to as runs in this study, were started with 150 mL of feed in the reactor (anodic loop + cathodic loop). A 1 mL starting sample was taken from the feed outside the reactor. 1 mL samples were taken from the anodic and cathodic compartments twice a day during the run. Runs were continued for 4 or 5 days. After a run, all reactor content was collected, measured by volume by chamber, and sampled for chemical analyses. A control experiment, named "neutral", was performed by connecting the anodic and cathodic loops into a single mixing loop,

forming a continuously stirred-tank reactor. Other experiments are named based on anodic pH level. A total of 19 runs under neutral conditions and for pH values of 5, 3, 2 and 1.5 were undertaken. A detailed list of all runs is presented in ESI† section S1.

2.4 Chemical analyses

Samples were analysed for cations and anions using a Thermo Scientific ICS-1600 ion chromatograph with a Dionex IonPac AS22 column (Cl⁻, ClO₃⁻, ClO₄⁻, NO₂⁻, NO₃⁻, SO₄²⁺, PO₄³⁺) and a Dionex IC-120 with an IonPac CS12A column (Na⁺, NH₄⁺, K⁺, Mg²⁺, Ca²⁺) (Dionex, CA, USA), and total carbon species using a Shimadzu TOC-5000 total organic carbon analyser (Kyoto, Japan). Gas bags were analysed for N₂ content using a Shimadzu GC-2014 GC-TCD with a Supelco Carboxen 1000 60/80 column. For analysis, liquid samples were filtered using 0.45 µm syringe filters into 1.5 ml microcentrifuge tubes, stored after sampling for a maximum of 4 days in a fridge and diluted 50× for TOC analysis and 500× for IC analysis using a two-step dilution method with 15 ml tubes.

2.5 Calculations

Fittings were made using the MatLab R2020a curve fitting tool. Graphs were drawn using Veusz 3.1 distributed under GNU public license. Data analysis was undertaken with Microsoft Excel 2019 Analysis Toolpak. Chemical equilibrium, speciation and precipitation were modelled using Visual MINTEQ 3.1 modelling software (see ESI† S6 for model parameters). Reactor concentrations were calculated from anodic and cathodic loop concentrations by multiplying the value measured by their respective loop volumes and normalizing by the total reactor volume. Due to the reactor configuration, the anodic loop volume remained constant through each run, while the cathodic loop volume was reduced by sampling from both sides and through electrolysis and evaporation (and potential gas leakage). When calculating mass balances, the proportion lost through sampling was accounted for and subtracted from the initial amount. Errors discussed in this article are 95% confidence intervals calculated from standard deviation and sample count using eqn (8), under the assumption that the data were normally distributed.

$$95\% \text{ confidence interval} = 1.96 \cdot \frac{\text{Standard deviation}}{\sqrt{\text{Sample count}}} \quad (8)$$

Results are presented in relation to the initial concentration C/C_0 [mmol L⁻¹/mmol L⁻¹] and initial amount of substance mol/mol₀ [mmol/mmol], simplifying the comparison between different operational parameters. TOC results were fitted with an exponential function, simulating a pseudo 1st-order decay, supplemented with a non-degradable residual TOC fraction as shown in eqn (9). TAN results were fitted with a linear function, simulating a zero-order decay as shown in eqn (10).⁵⁹ Chloride and perchloride concentrations and masses were fitted with



the experimental sigmoidal functions in eqn (11) and (12), which can be used to model combinations of reactions,⁶⁰ enabling the comparison of fits between datasets.

$$\text{TOC}(t) = \text{TOC}_0 e^{-kx} + \text{TOC}_{\text{residual}} \quad (9)$$

$$\text{TAN}(t) = -kt + \text{TAN}_0 \quad (10)$$

$$\text{Cl}(t) = 1 + e^{Ax^{b+C}} \quad (11)$$

$$\text{ClO}_4(t) = A/(B + e^{-Cx}) \quad (12)$$

Rate constants k with 95% confidence interval for both TOC and TAN decay were obtained through the MatLab R2020a curve fitting tool by fitting data into eqn (9) and (10), respectively. No similar rate constant was utilized for the experimental sigmoidal functions (eqn (11) and (12)).

Ionic strength (IS) to compare salinities of samples was approximated using eqn (13).

$$\text{IS} = \frac{1}{2} \sum_{i=1}^n c_i Z_i^2 \quad (13)$$

where c_i is molarity (mol L^{-1}) and Z_i charge for each measured ion (Cl^- , ClO_3^- , ClO_4^- , NO_2^- , NO_3^- , SO_4^{2+} , PO_4^{3+} , Na^+ , NH_4^+ , K^+ , Mg^{2+} , Ca^{2+}). Only measured ions were considered, and no estimation on the effect of organic fraction was made nor corrections for activities.

3. Results and discussion

3.1 Reagent-free pH control

The anodic pH was controlled using a two-chamber cell, where the cathodic eluent is pumped to the anodic chamber loop by a relay pump controlled by the anodic loop pH (see Fig. 1). pH-Graphs can be found in Fig. S1 in the ESI† For all experiments, an anodic pH-equilibration period (approx. 1–2 h) was observed at the beginning of the relay-pump controlled experiments, as the pH in the anodic compartment dropped to the desired value before the relay-controlled circulation pump actuates for the first time. This period can influence the results in the first measuring interval as approx. 30% of the reactor volume is in the anodic loop during this time period and the pH is initially slightly alkaline (pH 8.4) and heavily buffered. After this initial equilibration period, the pH remained stable at the target value, demonstrating the effectiveness of the reagent-free pH control system (see Fig. S1 in the ESI†).

3.2 TAN decay rate is linked to anodic chloride concentration

3.2.1 Measured decay rates at different pH regions. Two separate regimes were observed for TAN decay as different regimes were observed for different anodic pH values (see Fig. 2). The results obtained at anodic pH values of 3, 2 and 1.5 are grouped together (Fig. 2c), as no statistically-significant differences between them were observed in

measured chloride or TAN. At neutral pH, the TAN decay fitted a single zero order decay rate. This implies that TAN removal under these conditions is not limited by TAN mass transfer, but by current density.^{27,46} Mass balance analysis (see later in this section) shows that TAN is oxidized to N_2 , but as we did not measure any specific chemical pathways, we refer to the disappearance of TAN as decay, encompassing destruction through all potential pathways.

At pH 5 (Fig. 2b), TAN decay showed two different linear decay regions, with a regime change at ≈ 24 h. If the initial decay in pH 5 is assumed to continue until 24 h, a similar initial rate of zero-order decay is observed to the neutral-pH runs (Fig. 2a) ($k_{\text{neutral}} = -0.020 \pm 0.002 \text{ h}^{-1}$, $k_{\text{pH=5}}^1 = -0.023 \pm 0.006 \text{ h}^{-1}$), conforming with the same 95% confidence interval. Interestingly, the decay rate observed after the transition in pH 5 is an order of magnitude lower ($k_{\text{pH=5}}^2 = -0.003 \pm 0.002 \text{ h}^{-1}$). This same order of magnitude lower decay rate was also measured in pH values ≤ 3 from the beginning of the experiments ($k_{\text{pH}\leq 3} = -0.002 \pm 0.001 \text{ h}^{-1}$), the rates being similar within a 95% confidence interval.

Clear differences in removal behaviour were also observed for chloride, with different rates of change for the three pH regions: neutral, pH 5 and pH ≤ 3 . In neutral runs (Fig. 2a), the chloride concentration initially remained high ($0.83 \pm 0.04 \text{ Cl/Cl}_0$ at ≈ 24 h), but after a marked drop between 30 and 48 h, it reached $0.02 \pm 0.03 \text{ Cl/Cl}_0$ at ≈ 72 h. In contrast

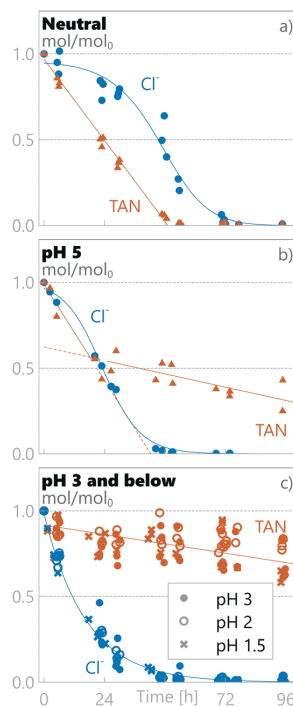
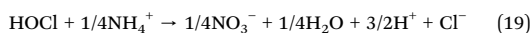
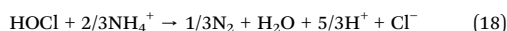
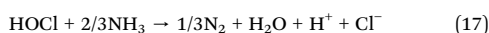
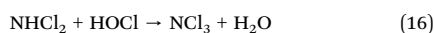
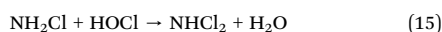
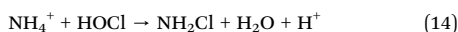


Fig. 2 Measured relative amount of TAN and chloride in synthetic urine in a) neutral pH, b) pH 5 and c) pH 3 and below.

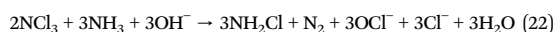
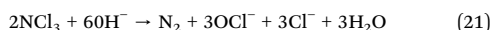


at pH 5, the chloride concentration started dropping immediately at the start of the experiment and reached near-zero values ($0.03 \pm 0.02 \text{ Cl/Cl}_0$) within 48 h. Finally, for the experimental runs at anodic pH values ≤ 3 , the chloride concentration dropped rapidly, reaching $0.03 \pm 0.02 \text{ Cl/Cl}_0$ within the first 48 h. For pH values ≤ 3 , the chloride decay followed pseudo first-order kinetics, implying limitation by mass transfer to the electrode surface and not limitation by current, whereas in higher pH values a first order model did not produce a good fit, and an experimental fit was used (see section 2.5). The chloride decay was more rapid at lower pH: at $\approx 24 \text{ h}$ the Cl/Cl_0 was 0.83 ± 0.04 , 0.51 ± 0.09 and 0.21 ± 0.05 , for neutral, pH 5 and pH ≤ 3 , respectively.

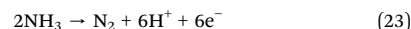
3.2.2 Cl/TAN ratio defines two separate TAN decay regimes. According to the published literature, TAN oxidation on the BDD anode in urine is expected to be linked to the availability of chloride, whereas oxidation of organics can readily proceed through hydroxyl radical oxidation.^{28,34} Breakpoint chlorination is a widely studied chemical phenomenon of organics and TAN oxidation *via* active chlorine ($\text{Cl}_2 + \text{HOCl} + \text{OCl}^-$), a type of reactive chlorine species (RCS), in bulk water near neutral pH,^{61,62} and is often cited as a mechanism that also takes place during electro-oxidation.^{37–39,41,63} Electro-oxidation chemistry can however be dominated by boundary layer phenomena, and a more complicated system of reaction pathways exists, the details of which are yet to be fully elucidated.^{27,28,64} The basis of TAN oxidation *via* RCS is that TAN readily reacts with hypochlorite to form chloramines, including monochloramine, dichloramine and trichloramine, which can further react to form N_2 , oxidize to nitrate or reduce back to ammonium at the cathode. The conventional breakpoint chlorination mechanism's sequential reaction pathways, and equations for overall oxidation are presented in eqn (14)–(19).



Gendel and Lahav (2012)⁶⁴ have argued for an alternative TAN chlorination reaction pathway suggesting direct formation of trichloramine with chlorine as per eqn (20), followed by complex reactions pathways, two sum iterations of which are presented in eqn (21) and (22).



For breakpoint chlorination to proceed, a limiting ratio of RCS to TAN needs to be exceeded for the oxidation to proceed. This value is typically described as a molar ratio near 1.5:1 active chlorine to nitrogen (*i.e.* Cl_2 to $\text{NH}_3\text{-N}$), depending on water characteristics. Below this threshold, active chlorine can be bound as chloramines, and no TAN oxidation *via* breakpoint chlorination mechanisms is observed.⁶⁵ In the absence of chloride, TAN is reported to be oxidized on the electrode surface *via* the direct pathway (see eqn (23)), not through hydroxyl radical oxidation.⁶⁶



While the exact reaction pathways and rates between RCS and TAN on the electrode surface and bulk remain unclear, they are tightly linked to the chloride reaction chemistry at the electrode boundary layer. In our experiments, the rapid TAN decay observed under neutral conditions is expected to proceed through indirect oxidation *via* the hypochlorite radical.^{27,28,64} The observed rapid oxidation under neutral and initial pH 5 conditions in this study is observed to follow zero-order kinetics and is likely limited by RCS production on the electrode (or RCS diffusion from the surface to the bulk). An order of magnitude lower TAN decay is present at pH ≤ 3 and after transition in pH 5, most likely representing the direct oxidation rate (eqn (23)). To understand this difference, more parameters were examined.

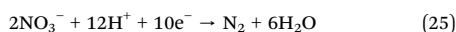
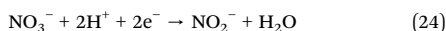
To study the defining parameters for the transition, chloride concentrations (see Fig. 2 and S3 in the ESI†) and chloride to TAN concentration ratios (Cl/TAN) were analysed. The Cl/TAN ratio of the synthetic urine is $0.23 \pm 0.02 \text{ M/M}$, and in neutral runs it rises from this initial value as TAN decays more rapidly than Cl. In pH 5, Cl/TAN remains constant for the first $\approx 24 \text{ h}$ (averaging 0.27 ± 0.02 for the first 24 h), after which it drops sharply to zero. This drop coincides with a clear TAN decay transition. In pH ≤ 3 , Cl/TAN starts dropping instantly, averaging 0.18 ± 0.02 at $\approx 6 \text{ h}$, after which it continues to drop reaching zero by 24 h. Under the same conditions (pH ≤ 3), no rapid TAN decay is observed. While all Cl/TAN values are lower than active chloride to TAN of 3 (or Cl_2/TAN of 1.5, in M/M), commonly described as necessary for breakpoint chlorination, the observation that Cl/TAN is a defining parameter in changing the TAN decay kinetics supports the hypothesis that breakpoint chlorination-type pathways are operational for TAN decay when a high enough Cl/TAN ratio is present. When Cl/TAN is below a threshold, the RCS produced can be absorbed by the chloramines formed from TAN and later reduced back to TAN and chloride.⁶¹ From the results in this study, an experimental threshold Cl/TAN -ratio of $\approx 0.2 \text{ M/M}$ can be approximated for this system. Above this ratio, a higher TAN decay rate of -0.02 h^{-1} is measured, while below this ratio an order-of-magnitude lower TAN decay rate of -0.002 h^{-1} occurs. These observations about different



reaction rates based on the presence of chloride are supported by a previous investigation by Zöllig *et al.*³⁴

3.2.3 TAN mass balances. Depending on the anodic pH, 0.01 ± 0.01 , 0.44 ± 0.15 and 0.79 ± 0.05 of TAN mol/mol₀ were retained as TAN in the system in neutral pH, pH 5 and pH ≤ 3 , respectively (Fig. 5). TAN oxidation pathways and potential stripping were examined through nitrogen mass balance. The nitrogen mass balances in this study were established by measuring TAN from the reactor gas outlet through gas bags or gas washing bottles, as well as measuring TAN, nitrite and nitrate in solution in both chambers of the reactor. N₂ measurements from gas bags confirmed formation of N₂ but were qualitative in nature and were not used for mass balance calculations. TAN oxidation *via* RCS produces nitrogen gas (N₂), or nitrate (NO₃⁻) (eqn (17)–(22)). Nitrate was formed initially at the anode in all runs (average detected maximum in all runs 0.03 ± 0.01 C_{NO₃}/C_{N_{total}}), with lower concentrations detected uniformly at the cathodic compartment. Nitrite was detected almost only at the cathodic compartment (average detected maximum 0.010 ± 0.002 C_{NO₂}/C_{N_{total}}). No NO_x species were measurable by the end of the run, and the nitrate and nitrite concentration patterns suggest that they were lost through nitrate reduction at the cathode, with nitrite as an intermediate reduction product (see ESI† section S4 for details).

TAN was detected in the effluent gas, but regardless of operating parameters, it amounted to $\leq 1\%$ of the initial TAN mass (mol₀), being below the level of error for TAN analyses in the reactor. Nitrogen stripping as NH₃ therefore had no significant role in the TAN balances and conservation in our setup. While the cathodic loop pH was above 9 (reaching 9.5 in pH = 1.5 runs), the cathodic hydrogen generation and mixing was not strong enough to induce significant NH₃ stripping. This is encouraging in the context of nitrogen removal and recovery with EAOPs, as loss of TAN through stripping would require nitrogen re-capture with an acid (*e.g.* H₂SO₄), creating the need for unwanted chemical dosing and added complexity and risk of ammonia gas management. With stripping discarded as a significant N-removal mechanism in all experiments, the most probable reaction pathway for the observed rapid TAN decay was a combination of oxidation reactions with RCS to form N₂ (eqn (14)–(22)) with some oxidation to NO₃⁻ (eqn (19)) with subsequent reduction *via* NO₂⁻ at the cathode to N₂ or TAN (see eqn (24)–(26)).^{64,67–70} The most probable reaction pathway for the observed slow TAN decay is through direct oxidation to form N₂ through adsorption on the BDD surface (see eqn (23)).⁶⁶ The mass balance calculations show that no other statistically significant species for TAN loss from the system were identified than loss as N₂ gas.



3.3 TOC decay rate is pH independent

The oxidation of organic matter was monitored through TOC-measurements (Fig. 3). TOC decay followed pseudo 1st-order kinetics in all experiments, irrespective of the anodic pH level. A residual TOC fraction was observed when the anodic pH was at pH ≤ 5 , indicating that not all TOC could be removed during the timeframe of the experiment (results at pH ≤ 5 were grouped together as they were not statistically significantly different). The resulting TOC concentration decay rates show no statistically-significant difference between all pH regions ($k_{\text{pH=neutral}} = 0.052 \pm 0.010 \text{ h}^{-1}$, $k_{\text{pH}\leq 5} = 0.054 \pm 0.007 \text{ h}^{-1}$), although a difference in the residual TOC concentration was observed between neutral conditions (0.01 ± 0.04 TOC_{residual}/TOC₀) and pH ≤ 5 results (0.06 ± 0.03 TOC_{residual}/TOC₀).

To understand the decay kinetics of TOC, known decay mechanisms are examined: organic molecules in synthetic urine are considered prone to electrochemical oxidation through the complex interplay of both BDD(OH[•])-radicals and indirect oxidation through hypochlorite radicals (or other RCS).^{34,42,71} Zöllig *et al.*³⁴ were able to detect distinct decay rates for chemical oxygen demand (COD) in urine before and after complete oxidation of chloride, showing a higher decay rate in the presence of chloride. In this study, such a distinction in the organics decay rate was not observed. However, it's worth noting that this study was not designed to test the effect of chloride on the TOC decay rate, and all experiments did contain chloride in the beginning of the experiment, a factor which can inhibit detection of change in the decay rate. Regardless of this, the observed pseudo 1st-order decay kinetics match previously-reported observations and support mass-transfer-limited reaction kinetics, considered characteristic of high applied current densities as done in this study.²⁷

The residual TOC at pH ≤ 5 is most likely linked to the presence of RCS. At pH ≤ 5 , chloride is depleted before TOC and none or little RCS is expected to be formed, whereas under neutral conditions TOC is oxidized before chloride is depleted and RCS is expected to be the main chloride oxidation product. RCS is described as a weaker oxidant than BDD(OH[•]) with measured E^0 vs. SHE potentials of 1.36 V for Cl_{2(aq)}, 1.49 V for HClO, and 0.89 V for ClO⁻,⁷² versus 1.65 V for BDD(OH[•]).⁷³

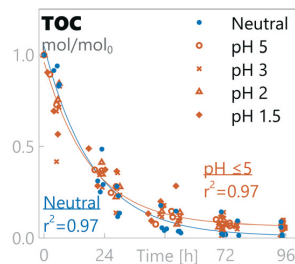


Fig. 3 Relative amount of total organic carbon in synthetic urine at different pH values.



These species have a different reach in the system as BDD(OH[•]) has a very short lifespan of $\approx 10^{-9}$ s (ref. 28) compared to potentially days or weeks for RCS in clean water,⁶¹ and BDD(OH[•]) most likely acts as an oxidant only close to the boundary layer.⁴² BDD(OH[•]) has been reported to react poorly with some substances, including ammonium and some organic acids.²⁸ Our data suggest that TOC contains recalcitrant organic components that remain in the solution when RCS is not available. In synthetic urine, the organic constituents are known, and recalcitrant components are most likely degradation products, but in real urine source components can also form a component of the recalcitrant fraction. Another potentially-linked source of residual TOC can be the formation of recalcitrant chlorinated by-products, as the initial presence of RCS can induce the formation of organochlorinated by-products that can be recalcitrant to oxidation by hydroxyl radicals and other subsequent reactive oxygen species (ROS).^{42,74}

3.4 Chloride by-products

The chloride oxidation was examined through chloride (Cl⁻), chlorate (ClO₃⁻) and perchlorate (ClO₄⁻) concentrations and through a calculated mass balance. This does not account for active chlorine, chloramines, organochlorinated by-products or chlorine lost as Cl₂. The mass balances under different pH conditions are presented in Fig. 4. The results show that, independent of pH values, low levels of chlorate were measured during the runs, corresponding to a middle product in a sequential oxidation from chloride to perchlorate (see eqn (5)–(7)). The average relative maximum chlorate concentration was 0.08 ± 0.03 C_{ClO₃⁻}/C_{Cl_{tot0}} (8% of initial chloride was present as chlorate). For perchlorate measurements, the pH 1.5 data is statistically different from the combined pH 3 & pH 2 dataset and is processed separately. There were clear differences in perchlorate formation between different pH values and final relative perchlorate mass balances of 0.93, 0.67, 0.61 and 0.75 C_{ClO₄⁻}/C_{Cl_{tot0}} were obtained in neutral pH, pH 5, combined pH 3 & pH 2, and pH 1.5, respectively, using eqn (12). These results imply a change in the chloride oxidation pathway as the pH is changed. Less perchlorate is detected at lower pH, which is most likely due to increased Cl₂ gas production but can also be partly due to increased formation of organochlorinated by-products or other chloramines.⁴² While retaining the same total contact times, lower pH corresponds to a lower exchange rate between anodic and cathodic compartments, enabling a faster decrease in chloride, and thus a lower chloride concentration at the anode. This is confirmed by comparing anodic loop samples, which show lower anodic chloride concentration in pH ≤ 3 compared to pH 5 and neutral runs (see Fig. S3†). The final perchloride rises slightly at pH 1.5 compared to pH 3 & 2, with a clearly different form of reaction pathway, which is not visible in the Cl⁻ concentration decay rate. This implies a faster or more direct oxidation pathway at pH 1.5 for chloride, with rate changes in the steps after the initial chloride oxidation.

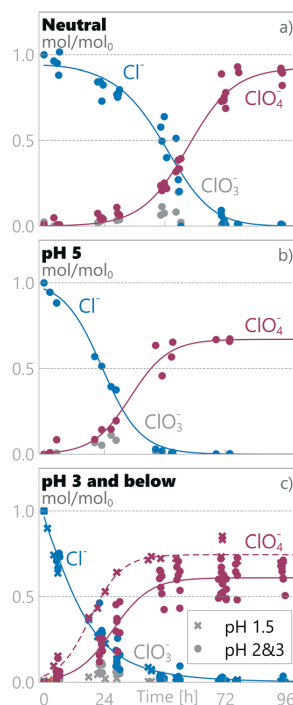


Fig. 4 Relative amount of chloride species in synthetic urine in a) neutral pH, b) pH 5 and c) pH 3 and below.

While the previously presented results on preservation of TAN at acidic pH values are encouraging, it should be noted that chlorate and perchlorate are toxic and persistent substances that are a serious impediment to the implementation of BDD based electro-oxidation technologies in the field,^{75,76} such as the one described in this paper. More research is underway to potentially overcome this challenge using current BDD or DSA materials in novel ways (e.g. combination with electroreduction) or by developing novel electrode materials that allow for safe electro-oxidation in chlorine-rich media.^{43,77–79} There are numerous electrochemical treatment and nutrient recovery technologies tested for source-separated urine (see section 1), each with their own advantages and caveats. Most of these can offer ample opportunities for the development of practical solutions that do not produce toxicity and are able to operate intermittently without addition of reagents. In this development, EAOPs can have a strong role to play as they differ from pure electro-concentration and stripping in their rapid organics oxidation and biological inactivation capabilities.²⁷

3.5 Nutrient balances and potential for recovery

Preservation of the main nutrients in urine during electro-oxidation and removal of organic materials is potentially a benefit for subsequent processing for utilization as a liquid



fertilizer. TAN, phosphate and potassium mass balances for all runs are presented in Fig. 5. TAN retention varied significantly depending on the pH: 0.01 ± 0.01 , 0.44 ± 0.15 and 0.79 ± 0.05 of TAN mol/mol₀ were retained in neutral pH, pH 5 and pH ≤ 3 , respectively. Conservation of K⁺ and PO₄³⁻ was 1.01 ± 0.06 and 0.89 ± 0.04 mol/mol₀ over all pH values, with no statistically significant differences observed between different pH levels. While no loss of K⁺ was detected in the system, a systemic loss of PO₄³⁻ of $11 \pm 4\%$ was detected, most likely due to precipitation. While precipitates were not visually detected, speciation was simulated using Visual MINTEQ 3.1.⁸⁰ According to the model used by MINTEQ, even a small addition of calcium (5–10 mmol L⁻¹) would have induced precipitation of hydroxyapatite (Ca₅(PO₄)₃(OH)) in the cathodic chamber at the pH values it was operated at (8.5–9.5). While calcium was not added to the medium, it was detected in the ≈ 10 mmol L⁻¹ range in the samples, making precipitation a likely source of phosphorus loss. The final concentrations of TAN in neutral pH, pH 5 and pH ≤ 3 were 0.008 ± 0.005 mmol L⁻¹, 0.24 ± 0.09 mmol L⁻¹, and 0.46 ± 0.04 mmol L⁻¹, respectively. The final concentrations of K⁺ and PO₄³⁻ over all pH values were 0.083 ± 0.008 mmol L⁻¹ and 0.021 ± 0.002 mmol L⁻¹, respectively.

Na⁺ and SO₄²⁻ remained in the solution during treatment (average mass balances of 1.07 ± 0.08 and 0.95 ± 0.05 were measured, respectively). Conversely, total inorganic carbon (TIC = CO₂ + HCO₃⁻ + CO₃²⁻) conservation depended on the anodic pH: 0.00 ± 0.00 mol/mol₀ in neutral pH, 0.16 ± 0.06 mol/mol₀ in pH 5, 0.46 ± 0.13 mol/mol₀ in combined pH 2 & 3 and 0.83 ± 0.20 mol/mol₀ in pH 1.5 TIC retention was measured. While TIC is expected to be stripped by low pH, the circulation speed could be a key parameter for the inverse behaviour observed, as lower pH runs have lower volumetric flow of CO_{2(g)} returning to the cathodic loop for redissolution. Chloride was removed completely, replaced by oxidized chlorates and partly removed as chlorine gas (see section 3.4.). These results show that while further work is required for chloride by-product removal, the current method has the capacity to selectively retain the valuable macronutrients N, P, K and S, while removing organic carbon from urine using a reagent-free pH-control system.

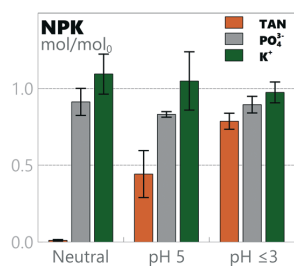


Fig. 5 Nitrogen, phosphorus and potassium (NPK) mass balances for full experiments with synthetic urine at different pH values.

3.6 Real source-separated urine results

The real source-separated human urine collected at a social venue in Tampere, Finland, had different properties to the synthetic urine (see Table 1). The collected urine had only 0.32 $I_{\text{real}}/I_{\text{synthetic}}$, 0.38 $\text{TAN}_{\text{real}}/\text{TAN}_{\text{synthetic}}$ and 0.22 $\text{Cl}_{\text{real}}/\text{Cl}_{\text{synthetic}}$ compared to the synthetic urine used. Using these real urine samples, the TOC was oxidized at all pH levels following a 1st order reaction rate (eqn (9); $k_{\text{urine}} = 0.10 \pm 0.04$ h⁻¹) significantly higher than that measured for synthetic urine ($k_{\text{synthetic}} = 0.05$ h⁻¹) (see Fig. 6). The remaining TOC relative to TOC₀ (0.20 ± 0.04 $\text{TOC}_{\text{residual,urine}}/\text{TOC}_0$) was however higher than in the synthetic urine (0.06 ± 0.03 $\text{TOC}_{\text{residual,pH=5}}/\text{TOC}_0$), but still in a similar absolute measured TOC level (0.020 ± 0.005 mmol L⁻¹ in real urine vs. 0.013 ± 0.009 mmol L⁻¹ in synthetic urine on average). TAN was oxidized following a zero-order constant decay rate of $k_{\text{urine}} = -0.002 \pm 0.001$ h⁻¹, the same as the slow decay rate measured for synthetic urine at pH ≤ 3 within a 95% confidence interval (see section 3.2). As TAN was following a similar decay pattern to that observed for synthetic urine at pH ≤ 3 , so was chloride, following pseudo 1st-order kinetics and rapidly oxidized within the first 24 h for all pH values to form perchlorate (mass balance of 1.07 ± 0.04 $\text{ClO}_4^-/\text{Cl}_0$),

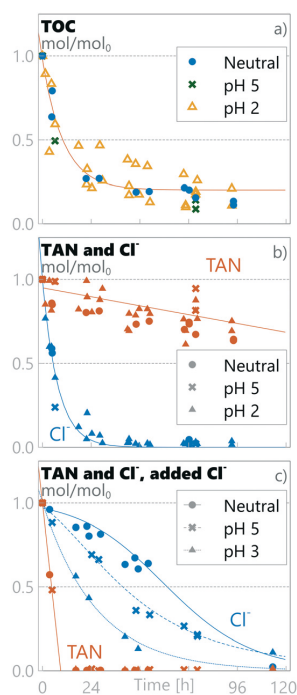


Fig. 6 Relative amount of substances in real urine at different pH values. a) TOC and b) TAN and Cl⁻ in real urine, and c) TAN and Cl⁻ in real urine with surplus chloride. Notice that the initial absolute chloride concentration in real urine with surplus chlorine c) is much higher than in real urine b) (540 vs. 197 mmol L⁻¹).



while similar nitrate and nitrite results were recorded to the synthetic urine (see ESI† section S5).

As discussed in section 3.2, the experiments with synthetic urine indicated that the Cl/TAN ratio has a significant role in TAN oxidation chemistry. When real urine was employed, no rapid TAN oxidation in any pH settings was observed (see Fig. 6b). Real urine had a Cl/TAN-ratio of 0.13 ± 0.01 , lower than experimentally required (≈ 0.2 Cl/TAN) for the rapid oxidation of TAN observed for the synthetic urine. To confirm the effect of the chloride ratio on the complexity of real urine, 150 mL of the collected source-separated urine was supplemented with 28 mL of 3 M KCl, resulting in a chloride concentration of 540 ± 60 mmol L⁻¹, 20× and 5× higher than that in real and synthetic urine samples, respectively, corresponding to seawater salinity and a measured Cl/TAN ratio of 4.1 ± 0.4 . In the presence of this surplus chloride, TAN was rapidly oxidized under all pH conditions following zero-order kinetics with an observed decay rate of $k_{\text{surplusCl}} = -0.11 \pm 0.01$ h⁻¹ (see Fig. 6c), significantly higher than that observed in neutral pH experiments for synthetic urine ($k_{\text{neutral}} = -0.020 \pm 0.002$ h⁻¹). TAN retention in real urine for all pH values was 0.82 ± 0.07 TAN mol/mol₀ (Fig. 6b); when surplus chloride was added, no TAN was retained (Fig. 6c). The P mass balance in real urine was 1.05 ± 0.2 mol/mol₀ over all runs and the K mass balance in runs without KCl addition was 1.9 ± 0.4 mol/mol₀. The reason for the measured K increase is unknown and was not investigated but could be related to nutrient release from organic content. Chloride mass balance did not close in the surplus run, and the ClO_x measured could not account for the chloride lost (see ESI† Fig. S5). The discrepancy could be due to oxidation to chlorine gas, but more likely due to precipitation of a perchlorate salt.⁵⁹

While the pH had no impact on TOC or TAN decay in real urine with surplus chloride, the pH did have a significant effect on the chloride decay rate, with a similar relation to pH as observed for synthetic urine (see section 3.2.1 and eqn (11)). These results suggest that, in our setup, the determining characteristic for TAN preservation was the Cl/TAN ratio, with the anodic pH playing a role in mitigating the removal of chloride to Cl₂ gas and perchlorate, lowering hypochlorite diffusion to the bulk and therefore limiting breakpoint chlorination chemistry for TAN oxidation. In our experiments, the effect of pH was visible only in a specific range of chloride concentrations, where the Cl/TAN-ratio passes through ≈ 0.2 , when a transition from a fast to slow TAN oxidation rate was observed. For synthetic urine, Cl/TAN was at 0.23 ± 0.02 and the anodic pH defines the chloride oxidation pathway and rate, subsequently defining the rate for TAN oxidation. In the real urine, Cl/TAN was naturally lower (0.13 ± 0.01), and no rapid TAN oxidation rate was observed. However, with surplus chloride, Cl/TAN remains above 0.2 (starting at 4.1 ± 0.3) until all TAN is oxidized and no transition was observed regardless of the anodic pH. Based on literature

sources (see section 2.1), source-separated urine Cl/TAN is expected to be in the proximity of ≈ 0.2 , and improper storage can further increase the ratio if TAN is lost. Accordingly, pH control could be essential for selective TAN oxidation in most real urine situations.

3.7 TAN decay and boundary layer chloride chemistry

Based on the measurements done in this study, as well as the published literature, the mechanisms for selective TAN preservation are most probably related to the chloride oxidation pathways at the boundary layer on the electrode surface. In our experiments, the chloride to TAN molar ratio, at a level of ≈ 0.2 , was identified as the defining characteristic for the TAN oxidation rate change. While a more systematic study and detailed measurements are required to confirm a precise limit, a hypothesis for the basis of this limit can be formulated based on the literature.

The electrode surface BDD(OH)⁻-radical readily reacts with chloride to form RCS (eqn (2) and (3)). It can be hypothesised that in neutral pH, there are enough reaction pathways available to scavenge surface BDD(OH)⁻-radicals to a low level, allowing the formed RCS to diffuse off the boundary layer, and further oxidize TAN (and TOC) in the bulk through breakpoint chemistry in regions where the active chloride/TAN ratio is high enough. The dominating RCS in the bulk, hypochlorite, forms chloride after reacting with TAN (it can react also with TOC). This circulation allows for the retention of chloride in the system and continuation of this process until TAN depletion. In low pH however, the rate for further oxidation reactions from RCS to chlorite dominates over RCS diffusion to the bulk electrolyte, causing a rapid drop in chloride concentration, subsequently preventing further TAN oxidation through the breakpoint chlorination mechanism as the hypochlorite concentration does not reach high enough concentrations.^{27,33,81,82} In the absence of chloride, the mechanism for slow TAN decay is most likely ammonia oxidation to N₂ via direct oxidation on the BDD surface, while TOC oxidation proceeds through BDD(OH)⁻-radicals.⁶⁶ These hypotheses are summarized in Fig. 7.

While this study did not focus specifically on chloride chemistry or speciation, it demonstrates that for future research, such emphasis is required if a method for separating TOC and TAN oxidation without perchlorate accumulation is to be realised for the decentralized EAOP treatment of source-separated urine with concomitant nutrient recovery. Based on these results, the key to TAN recovery with selective TOC oxidation relies on controlling the chloride chemistry defining the TAN oxidation regime. It can also require monitoring the composition of the source-separated urine feed, which can be highly variable depending on the source. Also, to make this technology meet regulatory limits, an alternate RCS quenching mechanism or end-pathway will be required to prevent chloride oxidation to perchlorate.



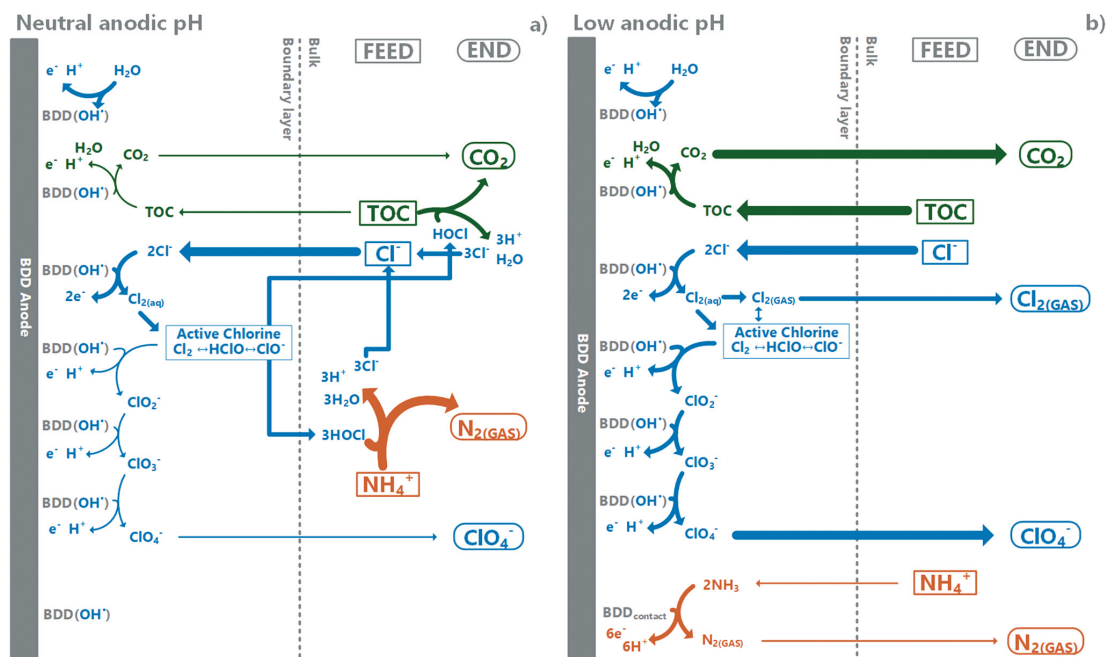


Fig. 7 Hypothesised pathways (simplified) dominating TOC and TAN oxidation under a) neutral and b) low anodic pH-conditions. Boxes indicate feed substances, bubbles end products and arrow widths relative scale of reaction rates. Under neutral conditions, active chlorine diffuses to the bulk and is responsible for most of the TOC and TAN decay measured. At low pH, formed chloride radicals (RCS) have reaction pathways with competitive reaction rates including further oxidation and removal as gaseous chlorine, and diffused active chlorine to the bulk is low and cannot induce breakpoint-chlorination-type TAN decay.

4. Conclusions

- Electrochemical oxidation of urine in low pH allows for the selective oxidation of organics with retainment of all main nutrients N, P and K, enabling subsequent product utilization as a liquid fertilizer through *e.g.* electro-concentration.

- Lowering pH to 3 or below at the anodic chamber using a reagent-free control system stops electrochemical oxidation of TAN in synthetic urine. A retainment of $79 \pm 5\%$ of TAN was measured compared to $1 \pm 1\%$ in neutral pH.

- Over 90% oxidation of organic material TOC was measured in all pH levels. This can enable selective electrochemical oxidation of the urine organics fraction without oxidation of TAN.

- In real urine samples, TAN was retained under all pH levels. When surplus chloride was added, TAN was lost under all conditions. These results confirm the central role of the chloride to ammonium nitrogen ratio as the main parameter defining TAN retainment in the reactor, with a molar ratio of approximately 0.2 Cl/TAN found defining in this system.

- In all experiments, chloride was mainly oxidized to perchlorate, a persistent toxic by-product. To make the proposed technology feasible in the field, an alternate active chlorine quenching mechanism or end-pathway for chlorine still needs to be developed.

Ethical statement

The human urine used was collected from a toilet block in the cultural venue “Hiedanlahti-Kuivaamo” in Tampere, operated by a private company, Digi-Toilet Systems Oy. All experiments were performed in accordance with the guidelines of ‘Responsible Conduct of Research and Procedures for Handling Allegations of Misconduct in Finland’. The human participants were clearly informed of the research use of the collected source-separated urine.

Funding

Johannes Jermakka was supported financially by Maj and Tor Nessling foundation, Walter Ahlström Foundation and The Finnish Cultural Foundation. Pablo Ledezma acknowledges a Development Fellowship from The University of Queensland and the Australian Research Council project LP 150100402 in partnership with Queensland Urban Utilities (QUU) and ABR Process Development.

Author contributions

Johannes Jermakka: conceptualization, methodology, formal analysis, investigation, writing – original draft, visualization, funding acquisition. Marika Kokko: validation, resources,



writing – review & editing, supervision, project administration. Stefano Freguia: conceptualization, methodology, writing – review & editing. Pablo Ledezma: methodology, validation, writing – review & editing, supervision.

Conflicts of interest

None.

References

- 1 E. Friedler, D. Butler and Y. Alfiya, in *Source Separation and Decentralization for Wastewater Management*, ed. T. A. Larsen, K. M. Udert and J. Lienert, IWA Publishing, Oxford, 2013, pp. 241–258.
- 2 D. G. Randall and V. Naidoo, Urine: The liquid gold of wastewater, *J. Environ. Chem. Eng.*, 2018, **6**, 2627–2635.
- 3 P. Ledezma, P. Kuntke, C. J. N. Buisman, J. Keller and S. Freguia, Source-separated urine opens golden opportunities for microbial electrochemical technologies, *Trends Biotechnol.*, 2015, **33**, 214–220.
- 4 M. Capdevila-Cortada, Electrifying the Haber-Bosch, *Nat. Catal.*, 2019, **2**, 1055.
- 5 H. Jönsson, T. A. Stenström, J. Svensson and A. Sundin, Source separated urine-nutrient and heavy metal content, water saving and faecal contamination, *Water Sci. Technol.*, 1997, **35**, 145–152.
- 6 T. A. Larsen, K. M. Udert and J. Lienert, *Source separation and decentralization for wastewater management*, IWA, London, 2013.
- 7 S. Antonini, S. Paris, T. Eichert and J. Clemens, Nitrogen and Phosphorus Recovery from Human Urine by Struvite Precipitation and Air Stripping in Vietnam, *Clean: Soil, Air, Water*, 2011, **39**, 1099–1104.
- 8 B. Etter, E. Tilley, R. Khadka and K. M. Udert, Low-cost struvite production using source-separated urine in Nepal, *Water Res.*, 2011, **45**, 852–862.
- 9 A. Hug and K. M. Udert, Struvite precipitation from urine with electrochemical magnesium dosage, *Water Res.*, 2013, **47**, 289–299.
- 10 J. A. Wilsenach, C. A. Schuurbiens and M. C. van Loosdrecht, Phosphate and potassium recovery from source separated urine through struvite precipitation, *Water Res.*, 2007, **41**, 458–466.
- 11 T. Duong, Z. L. Xie, D. Ng and M. Hoang, Ammonia removal from aqueous solution by membrane distillation, *Water Environ. J.*, 2013, **27**, 425–434.
- 12 A. Zarebska, K. V. Christensen and B. Norddahl, The Application of Membrane Contactors for Ammonia Recovery from Pig Slurry, *Procedia Eng.*, 2012, **44**, 1642–1645.
- 13 M. Ronteltap, M. Maurer and W. Gujer, Struvite precipitation thermodynamics in source-separated urine, *Water Res.*, 2007, **41**, 977–984.
- 14 M. Rodríguez Arredondo, P. Kuntke, A. ter Heijne, H. V. M. Hamelers and C. J. N. Buisman, Load ratio determines the ammonia recovery and energy input of an electrochemical system, *Water Res.*, 2017, **111**, 330–337.
- 15 R. C. Tice and Y. Kim, Energy efficient reconcentration of diluted human urine using ion exchange membranes in bioelectrochemical systems, *Water Res.*, 2014, **64**, 61–72.
- 16 J. Jermakka, E. Thompson Brewster, P. Ledezma and S. Freguia, Electro-concentration for chemical-free nitrogen capture as solid ammonium bicarbonate, *Sep. Purif. Technol.*, 2018, **203**, 48–55.
- 17 P. Ledezma, J. Jermakka, J. Keller and S. Freguia, Recovering Nitrogen as a Solid without Chemical Dosing: Bio-Electroconcentration for Recovery of Nutrients from Urine, *Environ. Sci. Technol. Lett.*, 2017, **4**, 119–124.
- 18 S. Freguia, M. E. Logrieco, J. Monetti, P. Ledezma, B. Viridis and S. Tsujimura, Self-powered bioelectrochemical nutrient recovery for fertilizer generation from human urine, *Sustainability*, 2019, **11**, 1–10.
- 19 P. Kuntke, M. Rodríguez Arredondo, L. Widyakristi, A. Ter Heijne, T. H. J. A. Sleutels, H. V. M. Hamelers and C. J. N. Buisman, Hydrogen Gas Recycling for Energy Efficient Ammonia Recovery in Electrochemical Systems, *Environ. Sci. Technol.*, 2017, **51**, 3110–3116.
- 20 A. K. Luther, J. Desloover, D. E. Fennell and K. Rabaey, Electrochemically driven extraction and recovery of ammonia from human urine, *Water Res.*, 2015, **87**, 367–377.
- 21 J. Desloover, A. Abate Woldeyohannis, W. Verstraete, N. Boon and K. Rabaey, Electrochemical resource recovery from digestate to prevent ammonia toxicity during anaerobic digestion, *Environ. Sci. Technol.*, 2012, **46**, 12209–12216.
- 22 J. Desloover, J. De Vrieze, M. Van De Vijver, J. Mortelmans, R. Rozendal and K. Rabaey, Electrochemical nutrient recovery enables ammonia toxicity control and biogas desulfurization in anaerobic digestion, *Environ. Sci. Technol.*, 2015, **49**, 948–955.
- 23 P. Kuntke, Nutrient and energy recovery from urine, *PhD Thesis*, Wageningen University, 2013.
- 24 M. Rodríguez Arredondo, P. Kuntke, A. W. Jeremiasse, T. H. J. A. Sleutels, C. J. N. Buisman and A. ter Heijne, Bioelectrochemical systems for nitrogen removal and recovery from wastewater, *Environ. Sci.: Water Res. Technol.*, 2015, **1**, 22–33.
- 25 S. Gildemyn, A. K. Luther, S. J. Andersen, J. Desloover and K. Rabaey, Electrochemically and bioelectrochemically induced ammonium recovery, *J. Visualized Exp.*, 2015, **95**, e52405.
- 26 P. Kuntke, P. Zamora, M. Saakes, C. J. N. Buisman and H. V. M. V. Hamelers, Gas-permeable hydrophobic tubular membranes for ammonia recovery in bio-electrochemical systems, *Environ. Sci.: Water Res. Technol.*, 2016, **2**, 261–265.
- 27 C. A. Martínez-Huitle, M. A. Rodrigo, I. Sirés and O. Scialdone, *Chem. Rev.*, 2015, **115**, 13362–13407.
- 28 S. O. Ganiyu and C. A. Martínez-Huitle, *ChemElectroChem*, 2019, **6**, 2379–2392.
- 29 K. Udert, S. Brown-Malker and J. Keller, in *Source Separation and Decentralization for Wastewater Management*, ed. T. A. Larsen, K. M. Udert and J. Lienert, IWA Publishing, Oxford, 2013, pp. 321–336.
- 30 P. Ma, H. Ma, S. Sabatino, A. Galia and O. Scialdone, Electrochemical treatment of real wastewater. Part 1:



- Effluents with low conductivity, *Chem. Eng. J.*, 2018, **336**, 133–140.
- 31 M. Panizza and G. Cerisola, Direct And Mediated Anodic Oxidation of Organic Pollutants, *Chem. Rev.*, 2009, **109**, 6541–6569.
- 32 H. Zöllig, C. Fritzsche, E. Morgenroth, K. M. Udert, H. Zöllig, C. Fritzsche, E. Morgenroth and K. M. Udert, Direct electrochemical oxidation of ammonia on graphite as a treatment option for stored source-separated urine, *Water Res.*, 2015, **69**, 284–294.
- 33 H. Zöllig, A. Remmele, C. Fritzsche, E. Morgenroth and K. M. Udert, Formation of Chlorination Byproducts and Their Emission Pathways in Chlorine Mediated Electro-Oxidation of Urine on Active and Nonactive Type Anodes, *Environ. Sci. Technol.*, 2015, **49**, 11062–11069.
- 34 H. Zöllig, A. Remmele, E. Morgenroth and K. M. Udert, Removal rates and energy demand of the electrochemical oxidation of ammonia and organic substances in real stored urine, *Environ. Sci.: Water Res. Technol.*, 2017, **3**, 480–491.
- 35 K. Cho and M. R. Hoffmann, Urea Degradation by Electrochemically Generated Reactive Chlorine Species: Products and Reaction Pathways, *Environ. Sci. Technol.*, 2014, **48**, 11504–11511.
- 36 J. T. Jasper, O. S. Shafaat and M. R. Hoffmann, Electrochemical Transformation of Trace Organic Contaminants in Latrine Wastewater, *Environ. Sci. Technol.*, 2016, **50**, 10198–10208.
- 37 J. T. Jasper, Y. Yang and M. R. Hoffmann, Toxic Byproduct Formation during Electrochemical Treatment of Latrine Wastewater, *Environ. Sci. Technol.*, 2017, **51**, 7111–7119.
- 38 K. Cho, D. Kwon and M. R. Hoffmann, Electrochemical treatment of human waste coupled with molecular hydrogen production, *RSC Adv.*, 2014, **4**, 4596–4608.
- 39 Y. Yang, L. Lin, L. K. Tse, H. Dong, S. Yu and M. R. Hoffmann, Membrane-separated electrochemical latrine wastewater treatment, *Environ. Sci.: Water Res. Technol.*, 2019, **5**, 51–59.
- 40 X. Huang, Y. Qu, C. A. E. Cid, C. Finke, M. R. Hoffmann, K. Lim and S. C. Jiang, Electrochemical disinfection of toilet wastewater using wastewater electrolysis cell, *Water Res.*, 2016, **92**, 162–172.
- 41 C. M. Chung, S. W. Hong, K. Cho and M. R. Hoffmann, Degradation of organic compounds in wastewater matrix by electrochemically generated reactive chlorine species: Kinetics and selectivity, *Catal. Today*, 2018, **313**, 189–195.
- 42 S. O. Ganiyu and C. A. Martínez-Huitle, Nature, Mechanisms and Reactivity of Electrogenenerated Reactive Species at Thin-Film Boron-Doped Diamond (BDD) Electrodes During Electrochemical Wastewater Treatment, *ChemElectroChem*, 2019, **6**, 2379–2392.
- 43 S. Garcia-Segura, J. D. Ocon and M. N. Chong, *Process Saf. Environ. Prot.*, 2018, **113**, 48–67.
- 44 S. T. McBeath, D. P. Wilkinson and N. J. D. Graham, *Environ. Sci.: Water Res. Technol.*, 2019, **5**, 2090–2107.
- 45 E. Brillas and C. A. Martínez-Huitle, Decontamination of wastewaters containing synthetic organic dyes by electrochemical methods. An updated review, *Appl. Catal., B*, 2015, **166–167**, 603–643.
- 46 C. Comminellis, A. Kapalka, S. Malato, S. A. Parsons, I. Poullos and D. Mantzavinos, Advanced oxidation processes for water treatment: Advances and trends for R&D, *J. Chem. Technol. Biotechnol.*, 2008, **83**, 769–776.
- 47 K. M. Udert, T. A. Larsen, M. Biebow and W. Gujer, Urea hydrolysis and precipitation dynamics in a urine-collecting system, *Water Res.*, 2003, **37**, 2571–2582.
- 48 K. M. Udert, T. A. Larsen and W. Gujer, Fate of major compounds in source-separated urine, *Water Sci. Technol.*, 2006, **54**, 413–420.
- 49 C. Lentner, *Geigy scientific tables*, Basel, Switzerland, 8th edn, 1977.
- 50 S. T. Jaatinen, M. R. T. Palmroth, J. A. Rintala and T. A. Tuhkanen, The effect of urine storage on antiviral and antibiotic compounds in the liquid phase of source-separated urine, *Environ. Technol.*, 2016, **37**, 2189–2198.
- 51 H. Kirchmann and S. Pettersson, Human urine - Chemical composition and fertilizer use efficiency, *Fert. Res.*, 1994, **40**, 149–154.
- 52 P. Kuntke, K. M. Śmiech, H. Bruning, G. Zeeman, M. Saakes, T. H. J. A. Sleutels, H. V. M. Hamelers and C. J. N. Buisman, Ammonium recovery and energy production from urine by a microbial fuel cell, *Water Res.*, 2012, **46**, 2627–2636.
- 53 M. Maurer, W. Pronk and T. A. Larsen, Treatment processes for source-separated urine, *Water Res.*, 2006, **40**, 3151–3166.
- 54 F. Tettenborn, J. Behrendt and R. Otterpohl, *Final report for task 7 of the demonstration project "Sanitation Concepts for Separate Treatment of Urine, Faeces and Greywater" (SCST) Resource recovery and removal of pharmaceutical residues Treatment of separate collected urine*, 2007.
- 55 P. Zamora, T. Georgieva, I. Salcedo, N. Elzinga, P. Kuntke and C. J. N. Buisman, Long-term operation of a pilot-scale reactor for phosphorus recovery as struvite from source-separated urine, *J. Chem. Technol. Biotechnol.*, 2017, **92**, 1035–1045.
- 56 K. M. Udert, M. Wachter and M. Wächter, Complete nutrient recovery from source-separated urine by nitrification and distillation, *Water Res.*, 2012, **46**, 453–464.
- 57 B. Etter, A. Hug and K. M. Udert, Total Nutrient Recovery from Urine - Operation of a Pilot-Scale Nitrification Reactor, *WEF/IWA Int. Conf. Nutr. Remov. Recover*, 2013, pp. 1–4.
- 58 S. Bouatra, F. Aziat, R. Mandal, A. C. Guo, M. R. Wilson, C. Knox, T. C. Bjorndahl, R. Krishnamurthy, F. Saleem, P. Liu, Z. T. Dame, J. Poelzer, J. Huynh, F. S. Yallou, N. Psychogios, E. Dong, R. Bogumil, C. Roehring and D. S. Wishart, The Human Urine Metabolome, *PLoS One*, 2013, **8**(9), e73076.
- 59 S. Zumdahl and D. DeCoste, *Chemical Principles*, 2012.
- 60 N. Kyurkchiev and S. Markov, Sigmoidal Functions: Some Computational and Modelling Aspects, *Biomath Commun.*, 2014, **1**(2), DOI: 10.11145/j.bmc.2015.03.081.
- 61 S. J. Randtke, in *White's Handbook of Chlorination and Alternative Disinfectants*, John Wiley and Sons, 5th edn, 2010, pp. 68–173.



- 62 E. A. Kobylinski and A. Bhandari, in *White's Handbook of Chlorination and Alternative Disinfectants*, John Wiley and Sons, 5th edn, 2010, pp. 326–362.
- 63 A. Romano, A. M. Urriaga and I. Ortiz, Optimized energy consumption in electrochemical-based regeneration of RAS water, *Sep. Purif. Technol.*, 2020, **240**, 116638.
- 64 Y. Gendel and O. Lahav, Revealing the mechanism of indirect ammonia electrooxidation, *Electrochim. Acta*, 2012, **63**, 209–219.
- 65 H. Shorney-Darby and L. L. Harms, in *White's Handbook of Chlorination and Alternative Disinfectants*, John Wiley and Sons, 5th edn, 2010, pp. 230–325.
- 66 N. L. Michels, A. Kapalka, A. A. Abd-El-Latif, H. Baltruschat and C. Cominellis, Enhanced ammonia oxidation on BDD induced by inhibition of oxygen evolution reaction, *Electrochem. Commun.*, 2010, **12**, 1199–1202.
- 67 M. J. Martin De Vidales, M. Millán, C. Sáez, P. Cañizares and M. A. Rodrigo, What happens to inorganic nitrogen species during conductive diamond electrochemical oxidation of real wastewater?, *Electrochem. Commun.*, 2016, **67**, 65–68.
- 68 S. Garcia-Segura, E. Mostafa and H. Baltruschat, Electrogeneration of inorganic chloramines on boron-doped diamond anodes during electrochemical oxidation of ammonium chloride, urea and synthetic urine matrix, *Water Res.*, 2019, **160**, 107–117.
- 69 Y. J. Shih, Y. H. Huang and C. P. Huang, Oxidation of ammonia in dilute aqueous solutions over graphite-supported α - and β -lead dioxide electrodes ($\text{PbO}_2\text{/G}$), *Electrochim. Acta*, 2017, **257**, 444–454.
- 70 Y. Zeng, C. Priest, G. Wang and G. Wu, Restoring the Nitrogen Cycle by Electrochemical Reduction of Nitrate: Progress and Prospects, *Small Methods*, 2020, **4**, 2000672.
- 71 J. Boudreau, D. Bejan and N. J. Bunce, Competition between electrochemical advanced oxidation and electrochemical hypochlorination of acetaminophen at boron-doped diamond and ruthenium dioxide based anodes, *Can. J. Chem.*, 2010, **88**, 418–425.
- 72 C. A. Martínez-Huitle and E. Brillas, Decontamination of wastewaters containing synthetic organic dyes by electrochemical methods: A general review, *Appl. Catal., B*, 2009, **87**, 105–145.
- 73 E. Brillas, I. Sirés and M. A. Oturan, Electro-fenton process and related electrochemical technologies based on fenton's reaction chemistry, *Chem. Rev.*, 2009, **109**, 6570–6631.
- 74 B. P. Chaplin, G. Schrader and J. Farrell, Electrochemical destruction of N-Nitrosodimethylamine in reverse osmosis concentrates using boron-doped diamond film electrodes, *Environ. Sci. Technol.*, 2010, **44**, 4264–4269.
- 75 J. Radjenovic and D. L. Sedlak, Challenges and Opportunities for Electrochemical Processes as Next-Generation Technologies for the Treatment of Contaminated Water, *Environ. Sci. Technol.*, 2015, **49**, 11292–11302.
- 76 S. Garcia-Segura, J. Keller, E. Brillas and J. Radjenovic, Removal of organic contaminants from secondary effluent by anodic oxidation with a boron-doped diamond anode as tertiary treatment, *J. Hazard. Mater.*, 2015, **283**, 551–557.
- 77 M. Herraiz-Carboné, S. Cotillas, E. Lacasa, Á. Moratalla, P. Cañizares, M. A. Rodrigo and C. Sáez, Improving the biodegradability of hospital urines polluted with chloramphenicol by the application of electrochemical oxidation, *Sci. Total Environ.*, 2020, **725**, 138430.
- 78 S. Cotillas, E. Lacasa, M. Herraiz, C. Sáez, P. Cañizares and M. A. Rodrigo, The Role of the Anode Material in Selective Penicillin G Oxidation in Urine, *ChemElectroChem*, 2019, **6**, 1376–1384.
- 79 G. O. S. Santos, K. I. B. Eguiluz, G. R. Salazar-Banda, C. Sáez and M. A. Rodrigo, Understanding the electrolytic generation of sulfate and chlorine oxidative species with different boron-doped diamond anodes, *J. Electroanal. Chem.*, 2020, **857**, 113756.
- 80 J. P. Gustafsson, *Visual MINTEQ 3.1 user guide*, Dep. L. Water Resour. Eng. R. Inst. Technol., Stockholm, Sweden, 2014, pp. 1–73.
- 81 L. R. Czarnetzki and L. J. J. Janssen, Formation of hypochlorite, chlorate and oxygen during NaCl electrolysis from alkaline solutions at an $\text{RuO}_2/\text{TiO}_2$ anode, *J. Appl. Electrochem.*, 1992, **22**, 315–324.
- 82 C. D. N. Brito, D. M. De Araújo, C. A. Martínez-Huitle and M. A. Rodrigo, Understanding active chlorine species production using boron doped diamond films with lower and higher sp³/sp² ratio, *Electrochem. Commun.*, 2015, **55**, 34–38.



1 Electrochemical system for selective 2 oxidation of organics over ammonia in 3 urine

4 Johannes Jermakka^{1,3}, Stefano Freguia², Marika Kokko¹ and Pablo Ledezma³

5 ¹Faculty of Engineering and Natural Sciences, Tampere University, Finland. Permanent address:
6 Tampere University, Faculty of Engineering and Natural Sciences, PO Box 541, 33101 Tampere,
7 Finland.

8 ²Chemical Engineering, The University of Melbourne, Melbourne, VIC 3010, Australia

9 ³Advanced Water Management Centre, The University of Queensland, St. Lucia, QLD 4072, Australia

10 **Declarations of interest:** none

11 Supplementary information

12 S1. List of runs

13 Runs were named in order of execution and are listed in Table 1. Runs irrelevant to the research
14 question of this article, as well as runs that failed due to leakages or other technical problems are not
15 included in this list. 30 runs were included in this study.

16 Table S1 Runs

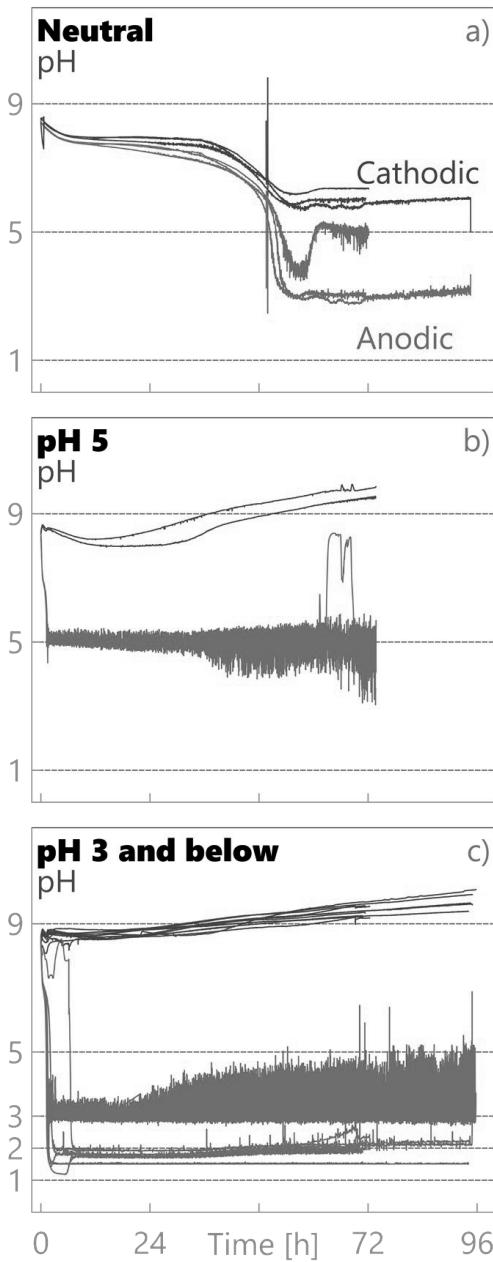
Run	Feed	pH	Duration, h	Gas TAN Analysis
B15	Simulated	Neutral	72	No gas capture
B17	Simulated	5	95	Gas Wash Bottle
B20	Simulated	Neutral	72	Gas Wash Bottle
B22	Simulated	Neutral	95	Gas Wash Bottle
B23	Simulated	5	74	Gas Wash Bottle
B25	Simulated	3	96	Gas Wash Bottle
B27	Simulated	3	95	Gas Bag
B28	Simulated	2	95	Gas Bag
B29	Simulated	3	72	Gas Bag
B30	Simulated	2	72	Gas Bag
B31	Simulated	1.5	94	Gas Bag
B32	Simulated	Neutral	94	Gas Bag
B33	Simulated	1.5	71	No gas capture
B34	Simulated	2	71	No gas capture
B41	Simulated	3	71	No gas capture
B42	Simulated	2	71	No gas capture
B43	Simulated	3	95	Gas Bag

B44	Simulated	2	95	Gas Bag
B47	Simulated	1.5	43	Gas Bag
B36	Real Urine	Neutral	94	Gas Bag
B38	Real Urine	Neutral	72	No gas capture
B40	Real Urine	2	93	Gas Bag
B45	Real Urine	5	76	No gas capture
B46	Real Urine	2	76	No gas capture
B48	Real Urine	2	43	Gas Bag
B49	Real Urine	2	71	No gas capture
B55	Real Urine + KCl	3	113	No gas capture
B56	Real Urine + KCl	Neutral	113	No gas capture
B57	Real Urine + KCl	5	76	No gas capture
B58	Real Urine + KCl	Neutral	52	No gas capture

17

18 S2. Measured pH in anodic and cathodic compartments

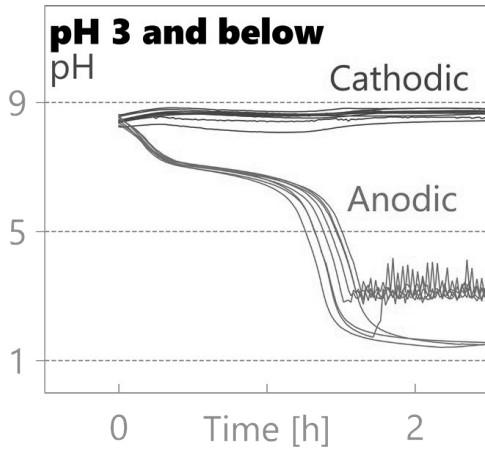
19 pH in anodic and cathodic compartments in all runs are presented overlaid in Figure S1. The pH in the
20 neutral runs (Figure S1a) remained similar in anodic and cathodic compartments until 48h, after which
21 a separation in anodic and cathodic pH's was detected, indicating a loss of buffering capacity. The
22 explanations for the observed overall drop in reactor pH were not identified. Anodic pH
23 measurements in runs at pH 5 and pH 3 are noisy as these pH's are in a rapidly changing region. The
24 anodic pH rise in b) at ~60h is due to a temporary pump failure. Anodic pH rise in c) at 0-12h is due to
25 pH probe bypass error.



26

27 Figure S1 pH in the anodic and cathodic compartment during experiments with simulated urine in a) neutral runs, b) in pH 5
 28 and c) in pH's 3, 2 and 1.5.

29 The initial pH drop is presented in more detail in Figure S2. A buffering effect in the anodic loop is
 30 clearly visible at pH 6.5-7 for the first 75min after which a rapid drop to pH 2 is observed. In pH 3 runs,
 31 this drop is cut by pH relay regulated pump.

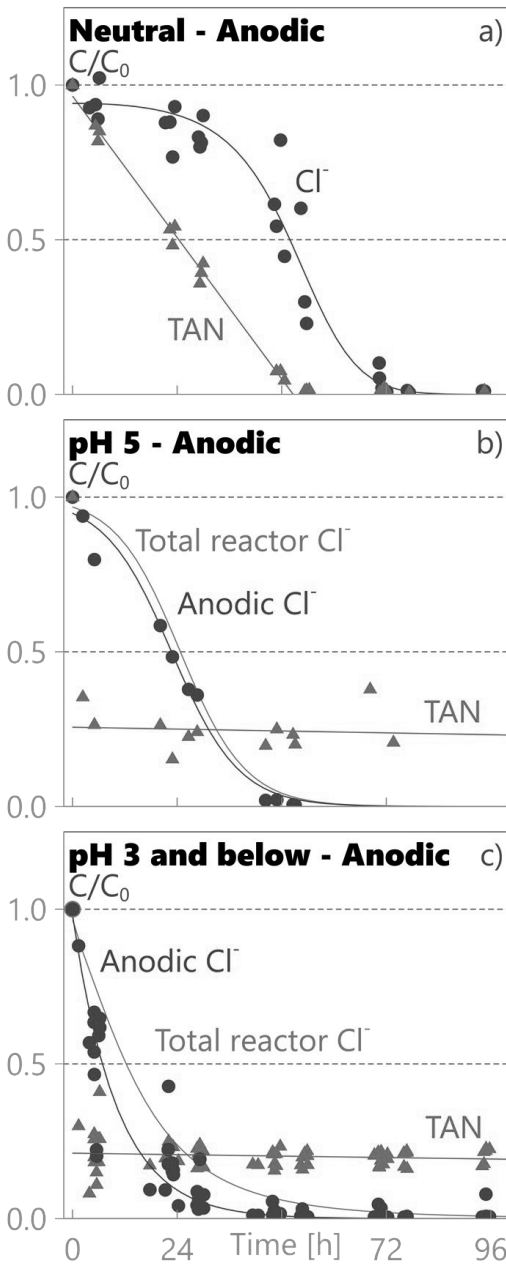


32

33 Figure S2 pH in the anodic and cathodic compartment during experiments with simulated urine in pH
 34 3 and below during the first 2h.

35 S3. Anodic compartment TAN and chloride concentrations

36 Anodic compartment TAN and chloride concentration are presented in Figure S3. In neutral pH (Figure
 37 S3a), the concentrations are identical to full reactor concentrations, as the system is fully mixed. In pH
 38 5 and $\text{pH} \leq 3$, TAN concentration rapidly drops to a relative concentration level between 0.2-0.25 C/C_0
 39 and remains stable. Chloride concentration is presented in parallel with the average full reactor
 40 concentration and a more rapid drop in chloride concentration is visible in $\text{pH} \leq 3$ compared at the
 41 anode compared to full reactor results (see Figure S3c).



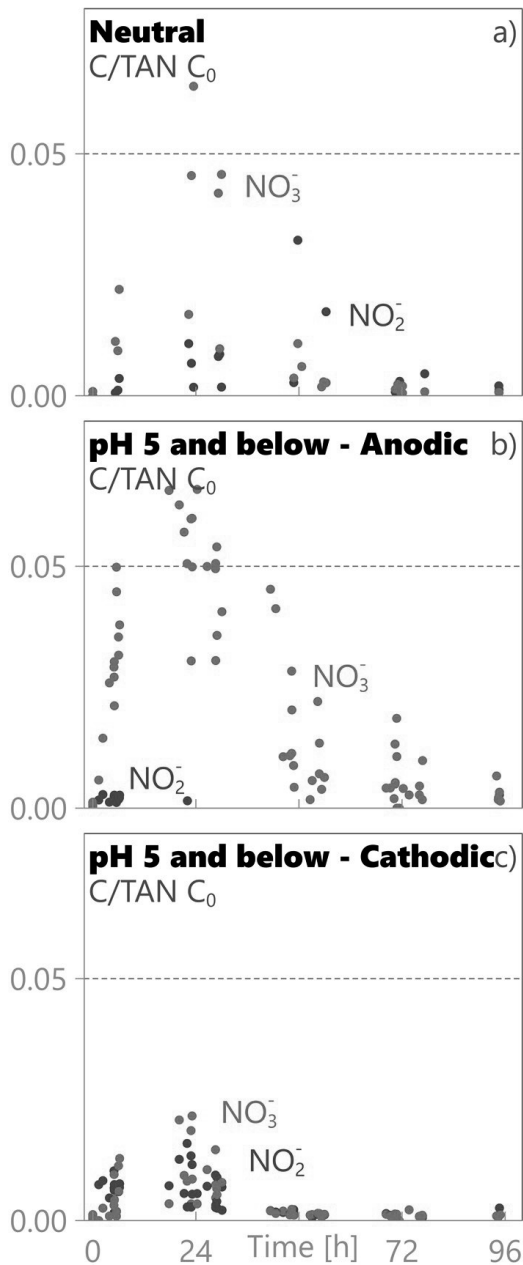
42

43 Figure S3 TAN and chloride concentrations in the anodic compartment and the chloride trend in the whole reactor in a)
 44 neutral pH, b) pH 5 and c) pH 3 and below.

45 S4. NO_x by-products

46 Measured nitrate and nitrite concentrations are presented in Figure S4, presented as fractions to
 47 initial TAN (C/C_0). In neutral pH (Figure S4a), both nitrate and nitrite are detected in the system and

48 both species are removed within the timeframe of the experiment. In experiments with $\text{pH} \leq 5$,
49 formation of nitrate is visible in the anodic chamber (Figure S4b) during the first 24h, after which
50 nitrate is removed. Nitrite is detected almost entirely in the cathodic compartment, during first 36h
51 when nitrate concentration is the highest.

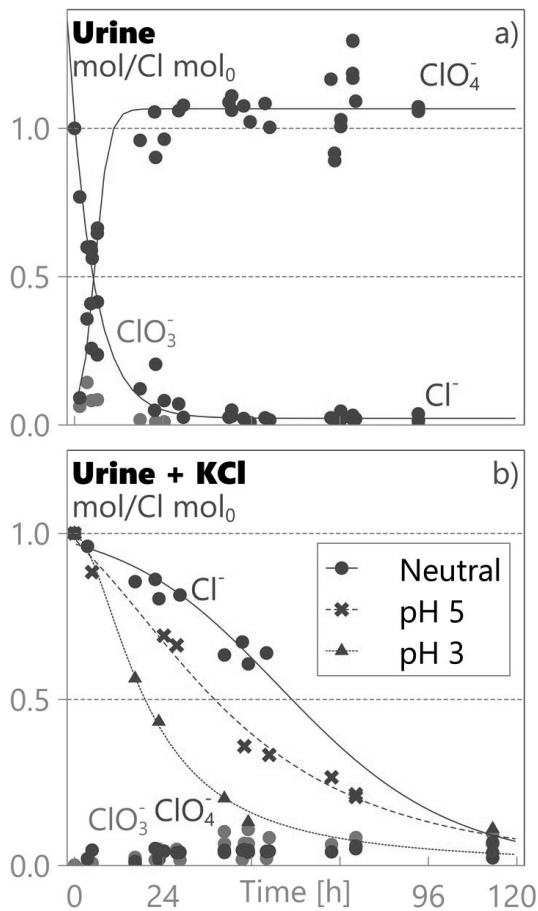


52

53 Figure S4 Relative nitrate and nitrite concentrations in simulated urine relative to initial TAN (C/C_0) in a) neutral pH in the
54 whole reactor, and in the b) anodic compartment of runs with $\text{pH} \leq 5$ and c) cathodic compartment of runs with $\text{pH} \leq 5$.

55 S5. Real urine measurements

56 Chlorine mass balance in real urine is presented in Figure S5. In real urine (Figure S5a), chloride is
57 converted to perchlorate within the first 24h. Chlorate is detected as an intermediate product. When
58 surplus chloride is added as potassium chloride (Figure S5b), only a small fraction of lost chloride is
59 detected as perchlorate. This is at least partly due to precipitation as potassium perchlorate which
60 was collected and analysed on the membrane at the cathodic chamber in these runs. Rate of chloride
61 removal at neutral pH, pH 5 and pH 3 was clearly different in these three regions, indicating a change
62 in chloride oxidation pathway on the anode.

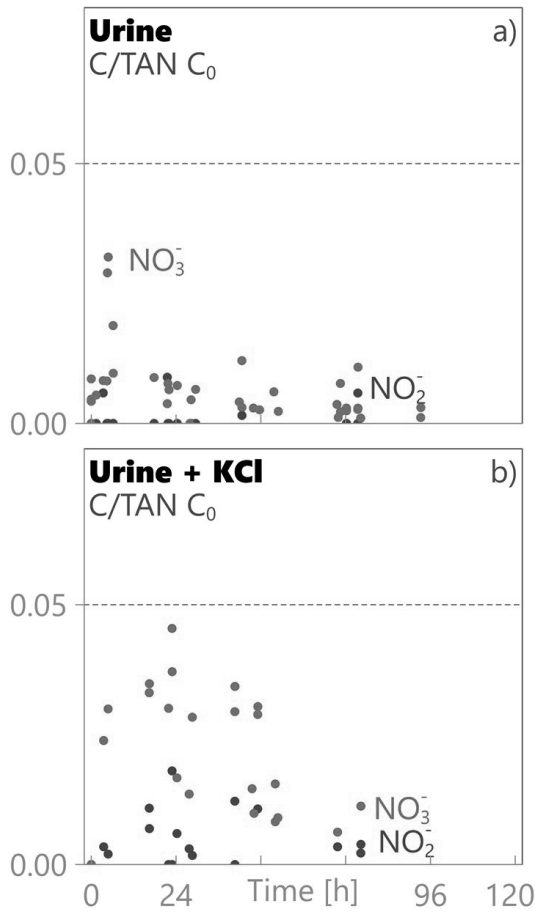


63

64 Figure S5 Relative amounts of chloride, chlorate and perchlorate compared to initial reactor amount of chloride in a) real
65 urine and b) chloride supplemented urine.

66 Nitrate and nitrite concentrations are presented in Figure S6. Only small amounts of nitrate and
67 negligible amounts of nitrite were detected in real urine, corresponding to the observation that very

68 little nitrogen was oxidized. In surplus chloride, higher nitrate and nitrite were detected, similar to
69 levels observed in synthetic urine.



70

71 Figure S6 Relative nitrate and nitrite concentrations relative to initial TAN (C/C₀) in a) real urine and b) chloride
72 supplemented urine.

73

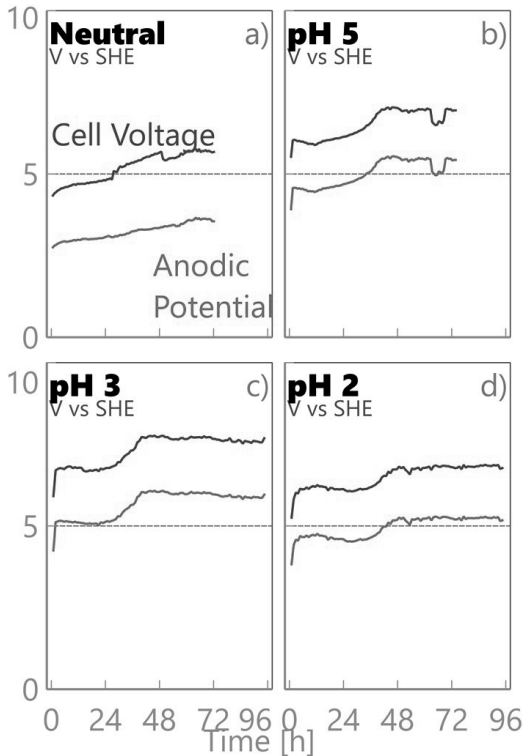
74 S6. Minteq parameters

75 Table S2 Utilized Minteq parameters.

Parameter	Value
Alkalinity is specified in this problem	Yes
Option of alkalinity calculation	Normal
Terminate if charge imbalance exceeds 30 %?	No
Choose the number of iterations:	2000
Method for activity correction	Davies, b=0.3
Oversaturated solids	Are not allowed to precipitate
Minimum concentration of species	1E-300
Minimum value of saturation index for solids	-500
Maximum value of saturation index for solids	500
Model parameter set	HFO (Dzombak & Morel)
Interface model	2-pK DLM
Specific surface area m ² /g	600
Site density, no1	2.25581
Site density no2	0.05639

76

77 S7. Examples of measured potentiostatic data



78

79 Figure S7 Example of recorded cell voltage and anodic potentials in different pH values.

PUBLICATION IV

**Electro-concentration of urine designed for separation of sodium from
nitrogen**

Johannes Jermakka, Emma Thompson Brewster, Stefano Freguia, Pablo Ledezma,
Marika Kokko

Separation and Purification Technology 276 (2021) 119275

Publication reprinted with the permission of the copyright holders.



Electro-concentration of urine designed for separation of sodium from nitrogen

Johannes Jermakka^{a,d,*}, Emma Thompson Brewster^b, Stefano Freguia^c, Pablo Ledezma^d, Marika Kokko^a

^a Faculty of Engineering and Natural Sciences, Tampere University, Finland. Permanent address: Tampere University, Faculty of Engineering and Natural Sciences, PO Box 541, 33101 Tampere, Finland

^b Faculty of Environment, Science and Engineering, Southern Cross University, Lismore, Australia

^c Department of Chemical Engineering, The University of Melbourne, Parkville, Australia

^d Advanced Water Management Centre, The University of Queensland, Brisbane, Australia

ARTICLE INFO

Keywords:

Source-separated urine
Electro-concentration
Nutrient recovery
Salinity control

ABSTRACT

Source-separated urine is a natural liquid fertilizer used by humanity for millennia. Urine use in modern nutrient recycling can be hindered by high relative salinity, non-optimal macro-nutrient ratio, presence of pathogens, and organic micropollutants. In this study, an electrochemical system was used to oxidize and concentrate synthetic urine into a product concentrate and a waste concentrate, also releasing a treated low nutrient load effluent. The system comprised two electrochemical reactors with separate concentration chambers and two circulation loops. Each circulation loop was comprised of two electrodes of opposite polarity, one from each of the two reactors. The pH levels in each loop were controlled electrochemically without chemical addition, allowing for selective ammonium (total ammonium nitrogen, TAN) and sodium (Na) separation into the product concentrate and the waste concentrate, respectively. In addition to pH, which was controlled by the relative current of the two reactors, the concentrate characteristics were controlled by the absolute potentials applied, affecting the oxidation reactions present. The double reactor system was able to divert a waste concentrate with a relative volume of 4% vs. the feed. The waste concentrate contained 14% of the influent Na but only 1% of the influent TAN, effectively removing sodium while removing very little TAN. This demonstrates a proof of concept for Na/TAN ion separation using electrochemical pH control. Compared to a single reactor control, between 12 and 17% reduction in Na/TAN ratio was achieved in the product concentrate with a specific energy consumption of 11–22 kWh kgN⁻¹. A total TAN recovery of 56–76% into the product concentrate was demonstrated. A wide range of tailoring parameters could be used for optimizing the redox chemistry and product characteristics. This novel technology shows promise for optimization for fertilizer production from source-separated urine.

1. Introduction

Overproduction and overuse of fertilisers are recognised to be exceeding sustainable planetary boundaries, and recovery and reuse of nutrients from waste streams is becoming increasingly investigated as a possible solution [1,2]. Promoting a circular economy through the recovery and reuse of nutrients in fertiliser products is a key goal of sustainable city design [3,4]. The paradigm of source separated urine is a possible path forward [5]. The urine fraction of municipal wastewater volume is approximately 1%, but it contains 80% of N and 50% of P discharged by humans [6,7]. Separation of urine from the rest of the

municipal wastewaters could allow for more efficient nutrient recovery as well as minimised transport and downstream separation costs. Decentralised systems are particularly suited to source separation, as they ease treatment efficiency and save energy [2,8]. Many studies already illustrate strong potential for nutrient recovery from source-separated urine [9–13].

Urine contains both macro- and micro-nutrients which can benefit soil health and plant growth. Nitrogen (largely present as urea, then ammonium), phosphorus (largely present as phosphate) and potassium are the key macronutrients, while calcium, magnesium, sulfur, and trace metals are important micronutrients [9]. Salinization is the

* Corresponding author.

E-mail address: johannes.jermakka@tuni.fi (J. Jermakka).

<https://doi.org/10.1016/j.seppur.2021.119275>

Received 17 March 2021; Received in revised form 21 June 2021; Accepted 6 July 2021

Available online 10 July 2021

1383-5866/© 2021 The Authors. Published by Elsevier B.V. This is an open access article under the CC BY license (<http://creativecommons.org/licenses/by/4.0/>).

accumulation of water-soluble salts in the soil [14]. Urine contains sodium and other salts, which contribute to salinization. Anthropogenic soil salinization is a global issue across the agricultural sector and is an important consideration when researching next-generation fertilizers [15–17]. After repeated application of urine or urine concentrates, the soil's electrical conductivity, sodicity and salinity are commonly shown to increase, which reduces soil health [10,18]. The concentration of soluble salts in urine varies by diet, water consumption and climate, and there is also considerable variability in tolerance between different crop types [14]. This makes it difficult to define a general criterion for salt application. However, conventional fertilisers are also a leading contributor to anthropogenic soil salinization [14].

When scaling up the use of urine as a fertiliser, several logistical and technological issues emerge. Liquid transport and handling costs require processing to minimise the volume by concentrating and/or separating the nutrients from the liquid and non-nutrient components. Freguia et al. [9] and Alemayehu et al. [10] outline that existing technology options fall into the categories of struvite precipitation, ammonia stripping, evaporation/distillation, absorption/adsorption, fertigation, as well as membrane distillation and membrane filtration. However, each of these options is associated with at least one of the following challenges: high energy consumption, chemical additions required, and/or decrease in soil health after repeated application due to increased salinity.

Yet another option is electro-concentration where a current is applied between two electrodes accompanied with charged ions migrating across ion exchange membranes located in parallel to the electrodes. Ledezma et al. [19] and Jermakka et al. [20] demonstrated a chemical free approach to nutrient recovery from source-separated urine using a two-membrane electro-concentration system. In these previous studies, ammonium migrated across the cation exchange membrane (CEM) from the anolyte to a middle chamber, forming a product concentrate. Other cations such as sodium and potassium also enter the product through the CEM. The final composition of the product reflects the feed composition entering the reactor, with a similar proportion of e.g. ammonium and sodium (albeit more concentrated) in the final product [20,21]. Relative ion transfer can be affected by differences in ionic mobility or membrane permselectivity (e.g. PO_4^{3-} vs. SO_4^{2-}) [22]. Ion movement is affected by solution pH due to competition by H^+ and OH^- at non-neutral conditions, and speciation differences. For example, ammonium-ammonia equilibrium has a pKa of 9.25 at 25 °C [23]. Ammonia is uncharged at high pH values and therefore should not migrate across the CEM due to electromotive force, while sodium and other cations will remain charged and available for migration. This behaviour is exploited for the first time in this study towards the electrochemical separation of sodium from ammonium in source-separated urine.

In this study, selective product formation was evaluated using a two reactor electro-concentration process, that allows reagent-free pH adjustment and ion separation into a product concentrate and a waste concentrate. The effects of pH values and ammonia-ammonium speciation on product characteristics were determined with the aim to demonstrate the production of a lower-sodium nutrient product from synthetic source-separated urine. In addition, the influence of process parameters, such as whole cell voltages and anode potentials, on product characteristics and energy requirements were studied. This work demonstrates the effects of different applied currents to the two reactors on sodium separation, nutrient retainment, energy consumption and by-product formation.

2. Materials and methods

2.1. Medium composition

A synthetic urine solution representing ureolysed urine was utilized as described in previously published work [24] (for details, see

Supplementary information S7). The recipe simulates urine after complete removal of Mg^{2+} and Ca^{2+} through precipitation with phosphate during ureolysis (Table 1). The feed was prepared as required and feed composition was monitored through sampling at the start of each batch experiment. Synthetic urine was chosen to enable consistency when systematically varying the experimental factors.

2.2. Reactor set-up and equipment

Custom reactors were used consisting of acrylic plates forming three parallel compartments of 70 mm × 50 mm × 10 mm each (Fig. 1). The anodic compartment of each reactor was fitted with Condiacs Diachem 40 × 40 × 2 mm Nb-BDD electrode, with a steel nut and rod current collector attached using a conductive epoxy (Epo-Tek EJ2189-LV) and protected from liquid contact with silicon cover. An Ag/AgCl 3 M NaCl reference electrode (BASi, USA) was placed in the anodic chamber to monitor the anodic potential. The cathodic compartment contained a 70 mm × 50 mm stainless-steel mesh as a cathode with a stainless-steel wire current collector. The concentrate compartment was located between the anodic and cathodic compartments, separated from the anodic compartment by a CEM (Membrane International Inc. CMI-7000), and from the cathodic compartment by an Anion Exchange Membrane (AEM) (Membrane International Inc. AMI-7001). The concentration chamber was filled with 6 mm diameter glass beads for volume reduction. The projected surface area of each membrane was 35 cm², the volume of the anodic and cathodic chambers was 35 mL each, and the volume of the concentration chambers was measured as 20 ± 0.6 mL each.

The reactor set-up (Fig. 1), was operated in a continuous feed mode. It consisted of two identical reactors as described above, fluidically connected in series forming two rapid mixing loops, mixed with circulation pumps (Cole Parmer Masterflex 7523–70) and monitored for pH using online pH meters (Endress + Hauser Liquiline CM448, Orbisint CPS11D sensor). The left mixing loop (anodic loop) links the anodic chamber of the main reactor (product reactor) and the cathodic chamber of the supplementary reactor (waste reactor). The right mixing loop (cathodic loop) links inversely. Anodic and cathodic loops were fed with peristaltic pumps (Ismatec ISM834C Reglo Digital) each at a constant flowrate of 39 ± 2 mL h⁻¹, resulting in loop HRTs of 2.5 h. The effluents of these loops were combined to one mixed reactor loop stream, from where excess liquid overflowed into an effluent bottle. Formed gases in the reactor (O_2 , H_2 , Cl_2 , CO_2) exited the reactor freely from then mixed reactor loop stream. Fresh urine was mixed with the rest of the mixed reactor loop stream, after which it was recycled back to the reactor. Fresh synthetic urine was fed with a peristaltic pump (Watson-Marlow 205U) at a constant flowrate (13.8 ± 0.5 mL h⁻¹) resulting in a hydraulic retention time (HRT) of 12.8 – 15.9 h for the synthetic urine in the reactor system (Table 2). In an alternate flow-pattern experiment (cathodic feed, C-F), feed was directed only to the cathodic loop, which overflowed to the anodic loop and then to the effluent (loop HRT was set to 3.8 h). The flowgraph of the reactor setups is shown in supplementary information S6. Two identical parallel reactor setups were utilized in the study. A potentiostat (Bio-Logic VMP-3) was used as a power source in

Table 1
Measured synthetic urine properties. All values in mmol L⁻¹.

Component	Synthetic Urine
TAN	470 ± 35
TIC	248 ± 1
TOC	187 ± 11
Cl ⁻	164 ± 7
K ⁺	70 ± 3
Na ⁺	113 ± 4
PO ₄ ³⁻	29 ± 1
SO ₄ ²⁻	19 ± 1

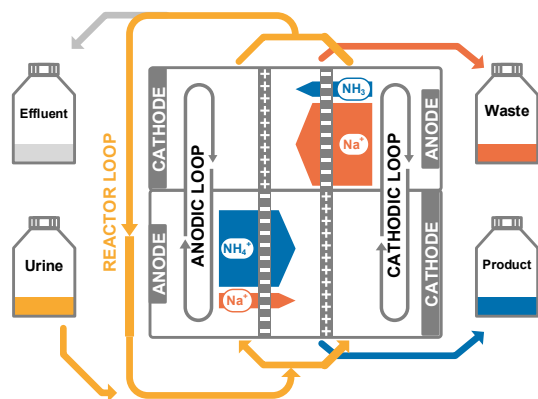


Fig. 1. Experiment flowchart with product (bottom) and waste (top) reactors. — = Cation Exchange Membrane, +++ = Anion Exchange Membrane. Arrows with ions represent the relative ionic efficiencies of sodium and TAN in the Trickle-experiment.

galvanostatic mode, recording the current applied to the cell, the electrical energy used, the cell voltage and the working potential of the anodes in each reactor.

2.3. Operation

Reactors were started with synthetic urine in all compartments, including in the middle chamber. A constant current was set for product and waste reactors and flow rates in all pumps were kept constant (Table 2). Samples of 1 mL were taken daily from anodic and cathodic loops (from the product reactor) and product and waste concentration chambers. When the anodic and cathodic loop pH and reactor potentials had stabilized (95% of measurement results showed below 5% variation to the average), a 24–72 h mass balance measurement was initiated with empty effluent, product, and waste bottles. Product and waste bottle contents are concentrates but are referred to as simply product and waste for brevity in this article. At the end of a mass balance measurement, the volume of urine, product, waste, and effluent bottles were measured, and their contents were sampled for analysis. Four or five

consecutive mass balance measurements were performed for each run, with means with 95% confidence intervals were calculated for concentrations. Loop feed pump speed was measured periodically between runs, and urine feed pump speed was monitored at each time point through urine volume measurements.

All experiments used a fixed synthetic urine feed rate of 13.8 ± 0.5 mL h⁻¹. The maximum current densities in the product and waste reactors were limited by a maximum cell voltage of 10 V (limited by the potentiostat). Increasing current densities resulted in increasing resistance caused by ion depletion during the runs, limiting the magnitude of current densities that could be applied. In the first experiment, there was no current applied to the waste reactor and a high current density of 100 A m⁻² was applied to the product reactor, creating a strong pH-split between the anodic and cathodic loops (Table 2). The control current density was selected experimentally to achieve a minimum of 75% reduction in ionic content for a fixed system retention time. This experiment acted as a control representing a three-chamber electro-concentration reactor for source-separated urine (Control; CTRL). Second, to study the initial effect of including the waste reactor, the waste reactor was turned on with an arbitrary very low current density (2.9 A m⁻²) to have a minimal impact on the loop pH's, but to illustrate the ionic composition harvested into the waste (Trickle; TRKL). The third experiment aimed at maximizing the volume of waste, while maintaining the cathodic loop pH above 10 as at pH 10 TAN is still mostly in NH₃-form and non-responsive to the electro-motive force responsible for the electro-concentration to the waste (Maximum Volume; MAX). Suitable current densities in this and the following experiments were determined by manually adjusting both product and waste current densities, while simultaneously monitoring cathodic loop pH and product reactor cell voltage (limited to ≤ 10 V).

The fourth experiment aimed to study the effect of lower cathodic pH for TAN separation (close to pK_a of TAN, 9.25). For this experiment the waste reactor current was increased, and product reactor current was decreased (Narrow Gap; NRW). The fifth experiment was to study the effect of lower anodic potential in the product reactor, so the currents of the product and waste reactors were lowered, while keeping the cathodic pH above 10 (Low Potential; LOW). Finally, the effect of an alternate feeding strategy was studied in the sixth experiment, where feed was directed only to the cathode instead of both anode and cathode (see supplementary information S6 for detailed description). Again, cathodic pH was kept close to 10 (Cathodic Feed; C-F).

Table 2

Electrochemical data, pH's and retention times measured in this study. Errors represent 95% confidence intervals. Potentials are given against standard hydrogen electrode (SHE). P = product reactor, W = waste reactor. Detailed pH and potentiostatic data for all experiments are presented in the supplementary information chapter S1 and S2.

Run	1	2	3	4	5	6
Name	Control	Trickle	Maximum Volume	Narrow Gap	Low Potential	Cathodic Feed
Abbr.	CTRL	TRKL	MAX	NRW	LOW	C-F
Product Current [A m ⁻²]	100	100	57.1	42.9	48.6	85.7
Waste Current [A m ⁻²]	0	2.9	11.4	22.9	7.1	11.4
Product Anode potential, [V vs SHE] ¹	3.9 (3.5–4.0)	4.2 (3.8–4.4)	5.3 (4.8–5.4)	3.4 (3.1–3.4)	3.4 (3.2–3.4)	4.2 (3.9–4.2)
Product Cell voltage,	7.4 (7.0–7.6)	8.3 (7.8–8.5)	9.1 (8.2–9.4)	5.7 (5.3–5.7)	5.9 (5.6–5.9)	8.0 (7.6–8.0)
Waste Anode potential, [V vs SHE] ¹		1.8 (1.5–1.9)	2.2 (2.0–2.2)	2.9 (2.5–3.0)	2.4 (2.1–2.5)	3.3 (2.3–3.5)
Waste Cell voltage, [V] ¹		2.3 (1.8–2.4)	3.8 (3.6–3.8)	5.1 (4.6–5.3)	4.0 (3.5–4.1)	5.1 (4.2–5.3)
Anodic loop pH	1.8 ± 0.02	2.0 ± 0.05	3.5 ± 0.05	6.7 ± 0.20	6.3 ± 0.3	7.9 ± 0.3
Cathodic loop pH	12.0 ± 0.03	11.8 ± 0.10	10.1 ± 0.05	9.2 ± 0.03	10.2 ± 0.06	9.8 ± 0.15
Reactor HRT [h]	15.1 ± 0.2	15.9 ± 0.3	14.5 ± 0.3	12.8 ± 0.9	15.6 ± 1.0	15.2 ± 0.2
Loop HRT's [h]	2.5 ± 0.2	2.5 ± 0.2	2.5 ± 0.2	2.5 ± 0.2	2.5 ± 0.2	3.8
Specific Energy Consumption [kWh kgN ⁻¹]	21.0 ± 1.8	21.6 ± 1.1	18.0 ± 0.4	13.1 ± 0.4	11.3 ± 1.3	21.7 ± 1.0
TAN to product [mg]	76 ± 4	70 ± 2	62 ± 1	56 ± 4	68 ± 3	76 ± 4
TAN recovery [kgN m ⁻³ d ⁻¹]	7.4 ± 0.3	7.8 ± 0.1	7.4 ± 0.2	6.3 ± 0.4	6.4 ± 0.6	7.2 ± 0.5

¹ Measurement variation given as average (min_{95%}–max_{95%}) from the measurement series. This is done to give a range of noise, but to omit peak disturbance measurements that have a negligible effect on mass balances.

2.4. Sample analysis

Samples were tested for conductivity and pH using a Mettler Toledo SevenMulti Conductivity meter with an Inlab 752 probe, and a WTW 330i pH meter with a Hamilton SlimTrode probe, respectively. Samples were analysed for cations, anions and total carbon species using Ion Chromatography Thermo Scientific ICS-1600 with a Dionex IonPac AS22 Column (Cl, ClO₃, ClO₄, NO₂, NO₃, SO₄²⁻, PO₄³⁻), Dionex IC-120 with a IonPac CS12A column (Na⁺, NH₄⁺, K⁺, Mg²⁺, Ca²⁺) (Dionex, CA, USA), and Total Organic Carbon Analyser TOC-V_{CPH} (Shimadzu, Japan), respectively. For analysis, samples were filtered using a 0.45 µm syringe filters into 1.5 mL microcentrifuge tubes, stored after sampling for a maximum of 4 days in a fridge and diluted 100x for TOC analysis and 2000x for IC analysis using a two-step dilution using glass tubes.

2.5. Calculations

Graphs were drawn using Veusz 3.1 and Origin 2019b. Data analysis was done using Microsoft Excel. Errors discussed in this article represent 95% confidence intervals calculated from standard deviation and sample count using Eq. (1). They assume data is normally distributed. Four or five mass balances were measured for each setting, but depending on the parameter, some measurements did not succeed, and actual count of measurements varied between 2 and 5 for each parameter.

$$95\% \text{ confidence interval} = 1.96 \cdot \frac{\text{Standard deviation}}{\sqrt{\text{Sample count}}} \quad (1)$$

The ion efficiency for ammonium transfer was calculated using Eq. (2).

$$\text{Ionefficiency} = \frac{n_{\text{NH}_4} \times Z_{\text{NH}_4}}{Q/F} \quad (2)$$

where n_{NH_4} is the amount of ammonium transferred (mol), Z_{NH_4} is charge of ammonium (+1), Q is the charge passed through the potentiostat (Coulomb, C) and F the Faraday constant (96485.33C mol⁻¹). For the ion efficiency calculations for sodium and potassium, n_{NH_4} and Z_{NH_4} are replaced accordingly. For specific energy consumption, kWh/kgN is used as a unit, referring to kWh per kg of NH₄-N.

3. Results and discussion

3.1. TAN and Na can be separated using a double reactor configuration

The product sodicity (Fig. 2a) and the contribution of ammonium,

sodium and potassium to the charge transport over CEM in the product reactor and the waste reactor (Fig. 2c) were determined. The missing ion efficiency (current leakage) visible in Fig. 2c consists mainly of H₃O⁺ ions and, to a smaller degree, of cation leakage from the concentrate through AEM. In the TRKL (TRICKLE) experiment, a small auxiliary current was passed through the waste reactor, and while only 4% of total feed volume was diverted to the waste, the product sodicity (Na/TAN) decreased by 11% (see Fig. 2a). The relatively large sodicity decrease was due to the good waste reactor performance as the cathodic loop pH was highly alkaline (pH 11.8), preventing H₃O⁺-ion and TAN movement to the waste. Consequently, the waste reactor ion efficiency was measured at 100% for TAN, Na and K (see Fig. 2c) and collected waste contained 14 ± 1% of Na mass while only 1 ± 1% of TAN mass.

In the NRW (Narrow Gap) experiment, the applied current densities resulted in a cathodic loop pH close to 9 (pH 9.2) which was not sufficient for efficient TAN/Na separation (see Fig. 2a), and similar waste and product sodium compositions were observed in this experiment (see Supplementary FigS4). In the MAX (Maximum Volume) and the LOW (Low Current) experiments, the applied product and waste reactor currents resulted in a cathodic loop pH close to 10 (10.1 ± 0.1 and 10.2 ± 0.1 measured, respectively). The product sodicity (Na/TAN) was reduced by 14 and 12% for MAX and LOW, respectively, compared to CTRL. Product reactor ion efficiency improved significantly as the anodic loop pH increased from being highly acidic (≤2) in CTRL and TRKL to more neutral in MAX, NRW and LOW (>3.5). The TAN ion efficiency over product reactor CEM was only 34–36% for CTRL and TRKL, but 60–68% for MAX, NRW and LOW. The change is presumably due to reduced current leakage by H₃O⁺ [21].

In the C-F (Cathodic Feed) experiment, the reactor loop circulated sequentially through the cathodic loop and the anodic loop, unlike in the five previous experiments. The pH thus first rose in the cathodic loop close to pH 10 (9.8 ± 0.15) and then dropped back to neutral (pH 7.9 ± 0.3) in the anodic loop, but with diminished buffer capacity. The product sodicity (Na/TAN) was reduced by 17% compared to CTRL. Product ion efficiency over CEM was similar to CTRL (TAN ion efficiency at 39 ± 3%), implying a large current leak. This could be due to a local pH drop on the anodic chamber caused by low buffer capacity, and undetected by the online loop pH meter (measured anodic loop pH of 7.9), but this hypothesis was unconfirmed.

Soil salinity and soil sodicity can limit urine use as a fertilizer due to high salt content [10,14]. This study shows that it is possible to separate ammonium and other cations using membrane electro-concentration with reagent-free pH control via the use of double electro-chemical reactors. These proof-of-concept results demonstrate a 4 – 17% salinity

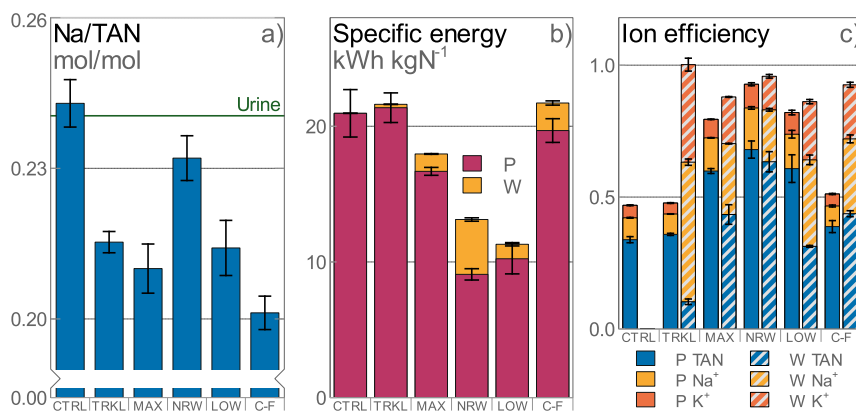


Fig. 2. a) Product sodicity indicated by Na/TAN concentration ratio, b) specific energy consumption in product reactor (P) and waste reactor (W) against TAN captured in the product, and c) contribution of ammonium cation NH₄⁺ (TAN), sodium cation Na⁺ (Na) and potassium cation K⁺ (K) to the charge transport over CEM in product reactor and waste reactor, in respect to the currents passing over their respective reactors.

reduction due to high pH at the cathodic loop rendering TAN non-mobile for electro-concentration into a waste concentrate. This selective removal of non-TAN cations into the waste leaves a higher relative TAN concentration in the reactor to be recovered as a concentrated product. In this study, the largest impact for the sodicity removal was due to the cathodic pH, which is the key parameter allowing for Na/TAN separation. To the authors' knowledge, this is the first investigation that addresses urine-derived fertiliser sodicity reduction through electro-chemical methods.

3.2. Energy consumption depends on the extent of ion removal

The TAN mass balance is presented in Fig. 3a and specific energy consumption in Fig. 2b and Table 2. Using two reactors can lower the specific energy consumption for nitrogen capture (11 kWh kgN⁻¹ in LOW) compared to one reactor set-up (CTRL; 21 kWh kgN⁻¹) as the fraction of energy utilized by the waste reactor is small (<10% of total energy in all experiments, except 31% in NRW), while TAN capture into product remains consistently high, > 56% in all the experiments. The aim of this study was not to minimize energy consumption, but for the first time to demonstrate and to maximize TAN recovery while removing unwanted Na⁺. Thus, current densities and cell potentials utilized are high, which increases energy consumption significantly. However, the experiments already show that decreasing energy consumption is possible. In MAX and LOW, the cathodic loop pH was set to 10 with product reactor current densities of 57.1 and 42.9 A m⁻², respectively. While MAX and LOW resulted in similar levels of TAN recovery into the product from the feed (62 ± 1 and 68 ± 3% mass, respectively), LOW uses only 60% of the specific energy compared to MAX (18.0 ± 0.4 and 11.3 ± 1.3 kWh kgN⁻¹, respectively). Growing energy consumption corresponds to the extent of ion removal from the effluent. Comparison of specific energy consumption for TAN capture and remaining fraction of TAN in the effluent gives 11.3 kWh kgN⁻¹ and 20% for LOW, 18.0 kWh kgN⁻¹ and 12% for MAX, and 21.7 kWh kgN⁻¹ and 9% for C-F, respectively (see Fig. 2b and Fig. 3a).

3.3. TAN losses are linked to chloride oxidation chemistry

TAN and chloride mass balances (Fig. 3) show a fraction of feed TAN and chloride undetected in product, waste or effluent marked as loss. TAN and chloride losses show synchronized behaviour between experiments (Fig. 3), which can be linked to changes in chloride oxidation pathways. TAN oxidation chemistry on BDD in chloride containing media is complex and is affected by electrode potential and electrolyte pH, and the exact reaction mechanisms for urine remain unclear [24–27]. As a simplification, previous literature and results indicate that

at sufficiently high chloride to TAN concentration ratio, an intermediate oxidation product, hypochlorite (HOCl/OCl⁻), can accumulate in the bulk and react with TAN to form chloramines and produce the oxidation reaction known as “breakpoint chlorination”, which can rapidly oxidize TAN into N₂ and reduce hypochlorite back into chloride. A limiting Cl/TAN ratio has traditionally been cited around 1.25 – 1.75Cl/TAN mol/mol [28], but our results illustrate a possibly lower limiting ratio for urine using BDD at ~ 0.2Cl/TAN mol/mol [24]. If Cl/TAN ratio is not high enough, breakpoint chlorination-type rapid oxidation is not observed. In low anodic pH (<pH 3), chloride oxidation can favour pathways that produces high amounts of chlorate and perchlorate, reducing the Cl/TAN ratio and thus, TAN oxidation [24].

The reactor system in the current study has two BDD anodes at different pH values both connected to circulation loops with stainless-steel cathodes that can potentially immediately reduce the produced hypochlorite and chloramine species [29–31], affecting the extent of breakpoint chlorination in each loop. The observed TAN loss is assumed to be mostly N₂ gas, as nitrate and nitrite both had negligible concentrations. Additionally, nitrate and nitrite concentrations in all measured samples were below the EU drinking water standard 50 mg NO₃ L⁻¹ and 0.5 mg NO₂ L⁻¹, see supplementary information S3. TAN losses through ammonia stripping was also previously shown to be negligible in this reactor type and setting. While high pH cathodic conditions are suitable for ammonium volatilization, the closed reactor configuration without external gas flow hinders volatilization. [24]

Cl losses involve reactions forming product species such as chloramines, chlorinated organics, and hypochlorite, but these species are not expected to concentrate to a significant degree and concentrations of these species are expected to remain low relative to initial urine chloride concentration [28], and it is thus assumed that chloride loss in the system comprises mostly chlorate, perchlorate and chlorine gas formation [25,26]. Hypochlorite speciation (HOCl/OCl⁻, pKa 7.5) can also affect the oxidation chemistry.

The largest chloride and TAN losses were observed in TRKL and MAX (15–17% TAN, 68 – 74% Cl), which were approximately double the losses of the control reactor CTRL (6% TAN, 36% Cl) (see Fig. 3). The increase in chloride and TAN losses is assumed to be due to indirect oxidation of TAN in the cathodic loop. This can be due to oxidation pathway differences in the anodic and cathodic loops. The TAN breakpoint oxidation pathway at the anodic loop is expected to be suppressed by the low pH at the product reactor anode, directing chloride oxidation towards chlorate and perchlorate formation and not to hypochlorite release from the anode, required for breakpoint chlorination [24]. On the cathodic loop, the pH is alkaline, and no such suppression of hypochlorite concentration is expected. This is supported by the lower chlorate and perchlorate formation (10% and 5% of initial chloride) in

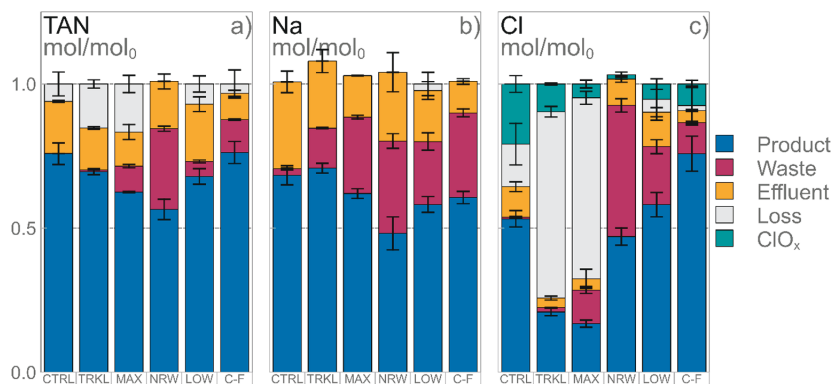


Fig. 3. a) Total ammonium nitrogen (TAN), b) Na and c) Cl mass balances, respectively. Units are mol of species in relation to moles in the feed. Loss indicates a fraction of feed mass not measured in product, waste or effluent. ClO_x = chlorate (ClO₃) + perchlorate (ClO₄).

TRKL and MAX compared to CTRL (21%).

In the last three experiments, NRW, LOW and C-F, TAN losses ($\leq 11\%$) and chloride losses ($\leq 10\%$) were smaller. In NRW, no measurable TAN or chloride loss was detected. One hypothesis for no measured loss would be the absence of TAN or Cl oxidation pathways, but this is highly unlikely as both anodic potentials (3.4 and 2.9 V vs. SHE for product and waste reactor, respectively) are above the anode potential suitable for hypochlorite formation, expected to proceed at 1.4 – 1.6 V vs. SHE on BDD [32]. A more likely hypothesis is that chloride oxidation to hypochlorite and subsequently to chloramines are likely occurring in all experiments, but these species can be immediately reduced back to chloride and TAN at the stainless-steel cathodes in the same loop. If a similar hypochlorite/chloramine reduction rate is induced at the cathode, this can counter the hypochlorite/chloramine production at the cathode before reaching concentrations required for breakpoint chlorination to proceed in either loop [24,33–39]. Understanding the TAN loss mechanisms can further improve salinity removal without TAN removal in the future.

Fig. 4 illustrates the measured chloride and TAN losses plotted against the difference in measured product and waste reactor anode potentials ($P_{\text{anode P}} - P_{\text{anode W}}$), used as a compound measure for oxidation – reduction potential for the reactor system, in each experiment. A more precise method would be to compare the anodic and cathodic potentials present in each loop separately, but as cathodic potentials were not measured, comparison of reactor anodic potentials directly can be justified, as they are proportional to the cathodic potentials on the opposite side of the cell [33,34]. Fig. 4 shows a correlation (with R^2 of 0.92 and 0.93 for chloride and TAN, respectively) between measured product and waste reactor potentials ($P_{\text{anode P}} - P_{\text{anode W}}$), and measured TAN and chloride losses, supporting the hypothesis of simultaneous anodic oxidation and cathodic reduction present in both loops.

The result showing low or no production of chlorates or perchlorates with high potential on a BDD in the presence of chloride containing media is a significant finding as chlorinated by-products can be inhibitory for the application of advanced oxidation processes [40]. By utilizing a separate cathode next to the active anode, it can be possible to independently control the reduction rate and potential from the oxidation rate and potential, allowing the inhibition of formation of chlorates and perchlorates. Relatively-high concentrations of chlorate or perchlorate were formed in multiple experiments (see Supplementary information S5), which are toxic and persistent substances and related to anodic oxidation on selected electrode materials (including BDD) in the presence of chloride [40]. The technology described in this article is not electrode-specific and Na/TAN separation using the same method can be

envisioned without the production of chlorate or perchlorate by using other dimensionally-stable electrodes with lower overpotentials.

3.4. Organic and inorganic carbon exit the system through different mechanisms

A reduction of 33–45% TOC was observed in all the experiments (see Fig. 5) as the TOC was oxidized into carbon dioxide and removed as gas. 67–83% of the remaining TOC concentrated in the product, except in NRW, where only 46% of remaining carbon was recovered in the product. The steady oxidation rate of TOC, which is not significantly changed with function to anodic potential, chloride concentration, or pH, implies a separate set of oxidation pathways compared to chloride and TAN oxidation. Further analysis on these pathways can be found in previous work [24]. TOC is also transferred into the waste proportional to the current density ratio of the waste and product reactors. However, due to preferential movement of other charge carriers, TOC starts concentrating only when some initial buffer capacity is depleted, indicating that the existing TOC has low relative ionic conductivity [20,21,41–43]. The presence of chlorate and perchlorate infers a possibility for the presence of chlorinated organic by-products that can be persistent and harmful [40], and different electrode materials and lower anodic potentials should be considered to avoid formation of these by-products.

The fate of inorganic carbon (IC) is controlled by pH: Whenever the anodic loop pH is below the pK_a of $\text{CO}_2/\text{HCO}_3^-$ (pH 6.4 at 25 °C), then IC is volatilized as CO_2 (27–35% reduction measured for CTRL, TRKL, MAX and LOW) and can leave the system as a gas through the reactor loop. For NRW and C-F, IC loss is only $12 \pm 5\%$ and $5 \pm 5\%$ with anodic pH of 6.8 and 7.8, respectively. The pH also controls the electrochemical movement of IC and when the anodic pH was low (pH < 4) and IC was predominantly uncharged (H_2CO_3), it did not concentrate into the waste (0–2% mass in waste product). In NRW and C-F, the anodic pH was > 6.8, and a significant part of IC mass concentrated into the waste from the anodic loop side as it existed as predominantly charged species, (HCO_3^- and CO_3^{2-}). This resulted in IC comprising $21 \pm 2\%$ and $15 \pm 1\%$ of the mass in the waste for NRW and C-F, respectively.

3.5. Product characteristics

The product in this study had an average NPK concentration of 2.4–1.8–2.0 (see Table 3). Consumer chemical liquid fertilizers, such as lawn fertilizers or houseplant fertilizers have varied NPK concentrations ranging from products with high equal NPK concentrations (20–20–20) to a wide array of products with a variety of lower NPK concentrations.

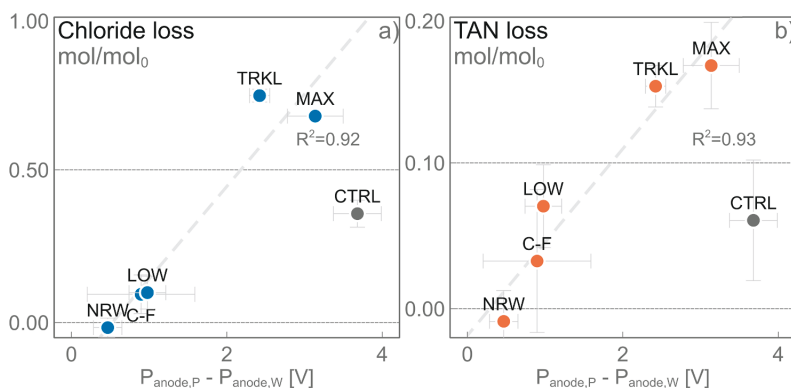


Fig. 4. a) Cl and b) TAN losses plotted against the difference of product and waste reactor anode potentials, an indicator of the oxidation potential for chloride compounds in the reactor. CTRL is not part of the fitting data, but it is included in the graph for comparison.

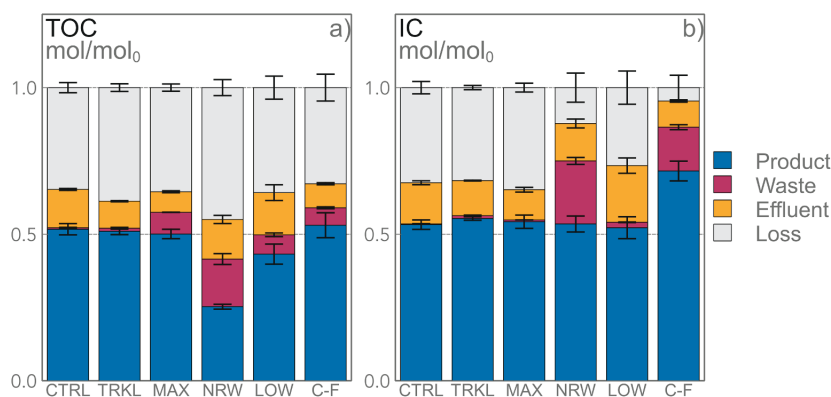


Fig. 5. Total organic carbon (TOC) and inorganic carbon (IC) mass balances in the different runs.

Organic liquid fertilizers refer to soil amendment products derived from natural sources (animal by-products, rock powder, seaweed), typical examples including e.g. 5–2–2 NPK fish emulsion or 2–3–1 NPK seaweed emulsion [44]. The world's first commercial urine fertilizer Aurin, based on nitrification and concentration through distillation, has 4.2–0.4–1.8 NPK [45]. The product concentrate obtained in this study is close in NPK concentration to a typical organic liquid fertilizer composition currently on sale for household consumption. The product concentrate also has high concentration of sulfate, another main nutrient, and concentrate product from real urine is expected to contain also other nutrients such as iron, boron, copper, and zinc as well as residual amounts of magnesium and calcium. Salinity can be an issue in long term use for a urine nutrient [14], and even partial reduction of sodicity as achieved in this proof-of-concept study, can allow increased use. Furthermore, the effect and mitigation of ClO_x needs to be considered separately to account for potential toxicity concerns (see [supplementary information S5](#) for ClO_x concentrations) or novel removal technologies [46].

The technology meets EU wastewater treatment criteria for organic reduction and nitrogen reduction and can be considered a partial treatment technology (depending on local legislation and implementation), as well as a nutrient recovery technology. Even partial separate treatment of urine can bring significant environmental benefits for waste water treatment reduced sewer corrosion [47], and reduced wastewater treatment energy consumption and greenhouse gas emissions [48].

Table 3

Averages of measured concentrations in the feed, product and waste concentrates, and effluent. Values in mmol L^{-1} , if not stated otherwise.

Parameter	Urine	Product	Waste ¹	Effluent
TAN	470 ± 40	1700 ± 200	420 ± 370	97 ± 18
PO_4	29 ± 1	72 ± 7	41 ± 22	14 ± 2
K	70 ± 3	210 ± 30	300 ± 40	15 ± 5
SO_4	19 ± 1	55 ± 5	76 ± 40	5 ± 1.3
Na	110 ± 10	370 ± 40	430 ± 60	31 ± 9
Cl	250 ± 10	290 ± 50	210 ± 170	12 ± 3
TOC	190 ± 20	450 ± 70	150 ± 110	28 ± 5
IC	250 ± 10	760 ± 120	240 ± 300	43 ± 9
NPK ²	0.7–0.7–0.7	2.4–1.8–2	0.6–1–2.8	0.1–0.4–0.1

¹ The waste values are an average from TRKL, LOW and C-F experiments as they produced a waste product with similar NPK composition – for results for MAX and NRW, see supplementary information S2.

² NPK are N, P and K values used in fertilizer labelling (in most countries). They refer to percentage by weight of elemental N, P_2O_5 and K_2O in the product. If the product contains some other form of P or K than P_2O_5 or K_2O , the value is given as the amount of P_2O_5 or K_2O needed for the equivalent amount. This unit is used for reader for easy comparison with consumer products and industrial data.

3.6. Parameter optimization

This study was purposely limited in framing: the hydraulic retention times and reactor configuration were kept constant to allow comparison between experiments. Fixed hydraulic retention times limited the selected electric currents: the aim was to reduce at least 75% of feed ionic content either through electro-oxidation or electro-concentration. The ionic conductivity was lowered by 74–88% during the experiments (CTRL and LOW had the lowest ion removal of 74 and 75%, respectively, and MAX and C-F the highest ion removal of 85 and 88%, respectively). Similar ion removal with lower currents can be achieved by extending reactor hydraulic retention times. Longer loop retention times allow further pH separation, while longer reactor retention times allow additional ion removal. This concept can be simplistically illustrated by comparing the results between MAX and LOW experiments. In MAX and LOW the waste and product reactor current density ratio is of similar magnitude (W/P 0.2 and 0.15 for MAX and LOW, respectively), while the product reactor anodic potentials are at a different level (5.3 and 3.4 V vs. SHE for MAX and LOW, respectively). When comparing results between the two runs, the product Na/TAN aligns (Na/TAN $21.0 \pm 0.5\%$ for MAX and $21.4 \pm 0.6\%$ for LOW), total power use for LOW is 46% lower (1.12 W in MAX and 0.61 W in LOW) and specific power use for TAN capture in LOW is 37% lower (18.0 kWh/kgN in MAX and 11.3 kWh/kgN in LOW). In addition, TAN and Cl losses were significantly lower in LOW compared to MAX (7 vs. 17% for TAN and 10 vs. 68% for Cl in LOW and MAX, respectively).

These experiments provide a proof-of-concept to show that Na/TAN separation can be achieved using reagent-free pH-controlled electro-concentration. It identified the cathodic loop pH as the most important parameter for Na/TAN separation to succeed, and points out the loop and reactor retention times and anodic potentials as key parameters for energy use optimization, TAN loss minimization, harmful by-production mitigation and TAN capture maximization. The idea of pH selective electro-concentration has potential applications outside the field of urine and wastewater treatment.

4. Conclusions

- Electro-concentration of synthetic source-separated urine in a novel reagent-free double reactor set-up enables reduction of sodicity of up to 17% with up to 76% TAN recovery.
- Electrochemical pH control allows for ion-specific Na and TAN separation due to NH_3 inertness to electromotive force. 17% lower sodicity (Na/TAN) in the product was achieved at specific energy consumption of 22 kWh kgN^{-1} and 12% lower sodicity at 11 kWh

kgN⁻¹, compared to a single reactor control with 21 kWh kgN⁻¹ without sodicity reduction.

- The redox chemistry on BDD anode and stainless-steel cathode electrodes resulted in a wide distribution of nitrogen and chloride reaction chemistry and product species, enabling diverse opportunity for product tailoring and optimization.
- To further improve the process performance and lower the specific energy consumption, lower anodic potentials should be favoured. Further, to reduce by-product formation, alternative electrode materials should be tested.

Funding

Johannes Jermakka was supported financially by The Finnish Cultural Foundation and the Emil Aaltonen Foundation. Pablo Ledezma acknowledges an ECR Development Fellowship from The University of Queensland.

CRedit authorship contribution statement

Johannes Jermakka: Conceptualization, Investigation, Methodology, Formal analysis, Writing – original draft, Visualization, Funding acquisition. **Emma Thompson Brewster:** Investigation, Writing – original draft. **Stefano Freguia:** Conceptualization, Methodology, Writing – review & editing. **Pablo Ledezma:** Methodology, Writing – review & editing, Validation. **Marika Kokko:** Validation, Writing – review & editing, Resources, Supervision, Project administration.

Declaration of Competing Interest

The authors declare that they have no known competing financial interests or personal relationships that could have appeared to influence the work reported in this paper.

Appendix A. Supplementary material

Supplementary data to this article can be found online at <https://doi.org/10.1016/j.seppur.2021.119275>.

References

- [1] J. Rockström, W. Steffen, K. Noone, Å. Persson, F.S. Chapin, E. Lambin, T. M. Lenton, M. Scheffer, C. Folke, H.J. Schellnhuber, B. Nykvist, C.A. de Wit, T. Hughes, S. van der Leeuw, H. Rodhe, S. Sörlin, P.K. Snyder, R. Costanza, U. Svedin, M. Falkenmark, L. Karlberg, R.W. Corell, V.J. Fabry, J. Hansen, B. Walker, D. Liverman, K. Richardson, P. Crutzen, J. Foley, Planetary boundaries: Exploring the safe operating space for humanity, *Ecol. Soc.* 14 (2009), <https://doi.org/10.1038/461472a>.
- [2] T.A. Larsen, K.M. Udert, J. Lienert, Source separation and decentralization for wastewater management, IWA, London, 2013.
- [3] A.G. Capodaglio, P. Ghilardi, J. Boguniewicz-Zablocka, New paradigms in urban water management for conservation and sustainability, *Water Pract. Technol.* 11 (2016) 176–186, <https://doi.org/10.2166/wpt.2016.022>.
- [4] S. Daneshgar, A. Buttafava, A. Callegari, A.G. Capodaglio, Economic and energetic assessment of different phosphorus recovery options from aerobic sludge, *J. Clean. Prod.* 223 (2019) 729–738, <https://doi.org/10.1016/j.jclepro.2019.03.195>.
- [5] T.A. Larsen, A.C. Alder, R.L.L. Eggen, M. Maurer, J. Lienert, Source separation: Will we see a paradigm shift in wastewater handling? *Environ. Sci. Technol.* 43 (2009) 6121–6125, <https://doi.org/10.1021/es803001r>.
- [6] M. Johansson, H. Jönsson, C. Höglund, A. Richert Stintzing, L. Rodhe, Final Report for Source-Separated Human Urine: A Future Source of Fertilizer for Agriculture in the Stockholm Region, Stockholm Vatten, Stockholmshem & HSB National Federation, Stockholm, Sweden, 2001.
- [7] E. Friedler, D. Butler, Y. Alfia, Wastewater composition, in: T.A. Larsen, K. M. Udert, J. Lienert (Eds.), *Source Sep.* IWA Publishing, Oxford, Decentralization Wastewater Manag., 2013, pp. 241–258.
- [8] A.G. Capodaglio, A. Callegari, D. Ceconet, D. Molognoni, Sustainability of decentralized wastewater treatment technologies, *Water Pract. Technol.* 12 (2017) 463–477, <https://doi.org/10.2166/wpt.2017.055>.
- [9] S. Freguia, M.E. Logrieco, J. Monetti, P. Ledezma, B. Virdis, S. Tsujimura, Self-powered bioelectrochemical nutrient recovery for fertilizer generation from human urine, *Sustain.* 11 (2019) 1–10, <https://doi.org/10.3390/su11195490>.
- [10] Y.A. Alemayehu, S.L. Asfaw, T.A. Terfie, Nutrient recovery options from human urine: A choice for large scale application, *Sustain. Prod. Consum.* 24 (2020) 219–231, <https://doi.org/10.1016/j.spc.2020.06.016>.
- [11] K.M. Udert, M. Wächter, M. Wächter, Complete nutrient recovery from source-separated urine by nitrification and distillation, *Water Res.* 46 (2012) 453–464, <https://doi.org/10.1016/j.watres.2011.11.020>.
- [12] J.A. Wilsenach, C.A. Schuurbers, M.C. van Loosdrecht, Phosphate and potassium recovery from source separated urine through struvite precipitation, *Water Res.* 41 (2007) 458–466, <https://doi.org/10.1016/j.watres.2006.10.014>.
- [13] S.K.L.L. Ishii, T.H. Boyer, Life cycle comparison of centralized wastewater treatment and urine source separation with struvite precipitation: Focus on urine nutrient management, *Water Res.* 79 (2015) 88–103, <https://doi.org/10.1016/j.watres.2015.04.010>.
- [14] A. Richert, R. Gensch, H. Jönsson, T.-A. Stenström, L. Dagerskog, Practical Guidance on the Use of Urine in Crop Production, 2010.
- [15] R. Mukhopadhyay, B. Sarkar, H.S. Jat, P.C. Sharma, N.S. Bolan, Soil salinity under climate change: Challenges for sustainable agriculture and food security, *J. Environ. Manage.* 280 (2021), 111736, <https://doi.org/10.1016/j.jenvman.2020.111736>.
- [16] A. Litalien, B. Zeeb, Curing the earth: A review of anthropogenic soil salinization and plant-based strategies for sustainable mitigation, *Sci. Total Environ.* 698 (2020), 134235, <https://doi.org/10.1016/j.scitotenv.2019.134235>.
- [17] I.N. Daliakopoulos, I.K. Tsanis, A. Koutroulis, N.N. Kourgiyalas, A.E. Varouchakis, G. P. Karatzas, C.J. Ritsema, The threat of soil salinity: A European scale review, *Sci. Total Environ.* 573 (2016) 727–739, <https://doi.org/10.1016/j.scitotenv.2016.08.177>.
- [18] M.Y. Boh, J. Sauerborn, Effect of NaCl-Induced Salinity and Human Urine Fertilization on Substrate Chemical Properties, *Open J. Soil Sci.* 04 (2014) 16–25, <https://doi.org/10.4236/ojss.2014.41003>.
- [19] P. Ledezma, J. Jermakka, J. Keller, S. Freguia, Recovering Nitrogen as a Solid without Chemical Dosing: Bio-Electroconcentration for Recovery of Nutrients from Urine, *Environ. Sci. Technol. Lett.* 4 (2017) acs.estlett.7b00024, <https://doi.org/10.1021/acs.estlett.7b00024>.
- [20] J. Jermakka, E. Thompson Brewster, P. Ledezma, S. Freguia, Electro-concentration for chemical-free nitrogen capture as solid ammonium bicarbonate, *Sep. Purif. Technol.* 203 (2018) 48–55, <https://doi.org/10.1016/j.seppur.2018.04.023>.
- [21] E. Thompson Brewster, J. Jermakka, S. Freguia, D.J.D.J. Batstone, Modelling recovery of ammonium from urine by electro-concentration in a 3-chamber cell, *Water Res.* 124 (2017), <https://doi.org/10.1016/j.watres.2017.07.043>.
- [22] M. Yasukawa, T. Suzuki, M. Higa, Salinity gradient processes: Thermodynamics, applications, and future prospects, *Elsevier B.V.*, 2018, <https://doi.org/10.1016/B978-0-444-63961-5.00001-8>.
- [23] W. Stumm, J.J. Morgan, Aquatic chemistry: chemical equilibria and rates in natural waters, *Choice Rev., Online.* 33 (1996) 33–6312, <https://doi.org/10.5860/choice.33-6312>.
- [24] J. Jermakka, S. Freguia, M. Kokko, P. Ledezma, Electrochemical system for selective oxidation of organics over ammonia in urine, *Environ. Sci. Water Res. Technol.* 7 (2021) 942–955, <https://doi.org/10.1039/d0ew01057j>.
- [25] C.A. Martínez-Huitile, M.A. Rodrigo, I. Sirés, O. Scialdone, Single and Coupled Electrochemical Processes and Reactors for the Abatement of Organic Water Pollutants: A Critical Review, *Chem. Rev.* 115 (2015) 13362–13407, <https://doi.org/10.1021/acs.chemrev.5b00361>.
- [26] S.O. Ganiyu, C.A. Martínez-Huitile, C.A. Martínez-Huitile, Nature, Mechanisms and Reactivity of Electrogenerated Reactive Species at Thin-Film Boron-Doped Diamond (BDD) Electrodes During Electrochemical Wastewater Treatment, Wiley-VCH Verlag (2019), <https://doi.org/10.1002/celc.201900159>.
- [27] H. Zöllig, A. Remmele, E. Morgenroth, K.M. Udert, Removal rates and energy demand of the electrochemical oxidation of ammonia and organic substances in real stored urine, *Environ. Sci. Water Res. Technol.* 3 (2017) 480–491, <https://doi.org/10.1039/c7ew00014f>.
- [28] C.T. Jafvert, R.L. Valentine, Reaction scheme for the chlorination of ammoniacal water, *Environ. Sci. & Technol.* 26 (2002) 577–586, <https://doi.org/10.1021/es00027a022>.
- [29] M. Rudolf, I. Rousar, J. Krysa, Cathodic reduction of hypochlorite during reduction of dilute sodium chloride solution, *J. Appl. Electrochem.* 25 (1995) 155–165, <https://doi.org/10.1007/BF00248173>.
- [30] D.V. Girenko, A.B. Velichenko, Selection of the Optimal Cathode Material to Synthesize Medical Sodium Hypochlorite Solutions in a Membraneless Electrolyzer, *Surf. Eng. Appl. Electrochem.* 54 (2018) 88–95, <https://doi.org/10.3103/S1068375518010052>.
- [31] S.Y. Basha, V. V. Goncharuk, R.D. Chebotareva, V.N. Belyakov, V.M. Linkov, Production of sodium hypochlorite in an electrolyser equipped with a ceramic membrane, in: *Desalination, Elsevier Science Publishers B.V.*, 1999, pp. 77–82, [https://doi.org/10.1016/S0011-9164\(99\)00156-3](https://doi.org/10.1016/S0011-9164(99)00156-3).
- [32] Y. Einaga, Diamond electrodes for electrochemical analysis, *J. Appl. Electrochem.* 40 (2010) 1807–1816, <https://doi.org/10.1007/s10800-010-0112-z>.
- [33] S.J. Randtke, Chemistry of Aqueous Chlorine, White's Handb, Chlorination Altern. Disinfect. Fifth Ed. 2 (2010) 68–173, <https://doi.org/10.1002/9780470561331.ch2>.
- [34] E.A. Kobylinski, A. Bhandari, Chlorination of Wastewater, White's Handb, Chlorination Altern. Disinfect. Fifth Ed. (2010) 326–362, <https://doi.org/10.1002/9780470561331.ch5>.
- [35] A. Romano, A.M. Urriaga, I. Ortiz, Optimized energy consumption in electrochemical-based regeneration of RAS water, *Sep. Purif. Technol.* 240 (2020), 116638, <https://doi.org/10.1016/j.seppur.2020.116638>.

- [36] J.T. Jasper, Y. Yang, M.R. Hoffmann, Toxic Byproduct Formation during Electrochemical Treatment of Latrine Wastewater, *Environ. Sci. Technol.* 51 (2017) 7111–7119, <https://doi.org/10.1021/acs.est.7b01002>.
- [37] K. Cho, D. Kwon, M.R. Hoffmann, Electrochemical treatment of human waste coupled with molecular hydrogen production, *RSC Adv.* 4 (2014) 4596–4608, <https://doi.org/10.1039/c3ra46699j>.
- [38] Y. Yang, L. Lin, L.K. Tse, H. Dong, S. Yu, M.R. Hoffmann, Membrane-separated electrochemical latrine wastewater treatment, *Environ. Sci. Water Res. Technol.* 5 (2019) 51–59, <https://doi.org/10.1039/c8ew00698a>.
- [39] S. Garcia-Segura, J.D. Ocon, M.N. Chong, Electrochemical oxidation remediation of real wastewater effluents — A review, *Process Saf. Environ. Prot.* 113 (2018) 48–67, <https://doi.org/10.1016/j.psep.2017.09.014>.
- [40] J. Radjenovic, D.L. Sedlak, Challenges and Opportunities for Electrochemical Processes as Next-Generation Technologies for the Treatment of Contaminated Water, *Environ. Sci. Technol.* 49 (2015) 11292–11302, <https://doi.org/10.1021/acs.est.5b02414>.
- [41] A.J. Faulkner, L.R. Bard, *Electrochemical Methods: Fundamentals and Applications*, 2nd Edition, 2008. <https://www.wiley.com/en-ir/Electrochemical+Methods:+Fundamentals+and+Applications,+2nd+Edition-p-9780471043720> (accessed February 16, 2021).
- [42] S. Zumdahl DeCoste, *Chem. Principles* (2012).
- [43] W.M. Haynes, *CRC Handbook of Chemistry and Physics*. 92nd Edition, Greece, 2012.
- [44] A. Card, D. Whiting, C. Wilson, J. Reeder, D. Goldhaimer, *Organic Fertilizers* (2015).
- [45] B. Etter, K.M. Udert, *VUNA Handbook on Urine Treatment* (2016) 22, <https://doi.org/10.13140/RG.2.2.29444.53122>.
- [46] C. Ren, P. Yang, J. Sun, E.Y. Bi, J. Gao, J. Palmer, M. Zhu, Y. Wu, J. Liu, A Bioinspired Molybdenum Catalyst for Aqueous Perchlorate Reduction, *J. Am. Chem. Soc.* 143 (2021) 7891–7896, <https://doi.org/10.1021/jacs.1c00595>.
- [47] S. Freguia, K. Sharma, O. Benichou, M. Mulliss, H.K. Shon, Sustainable engineering of sewers and sewage treatment plants for scenarios with urine diversion, *J. Hazard. Mater.* 415 (2021), 125609, <https://doi.org/10.1016/j.jhazmat.2021.125609>.
- [48] U. Badeti, N.K. Pathak, F. Volpin, U. Dorji, S. Freguia, H.K. Shon, S. Phuntsho, Impact of source-separation of urine on effluent quality, energy consumption and greenhouse gas emissions of a decentralized wastewater treatment plant, *Process Saf. Environ. Prot.* 150 (2021) 298–304, <https://doi.org/10.1016/j.psep.2021.04.022>.

Electro-concentration of urine designed for separation of sodium from nitrogen

Authors: Johannes Jermakka^{1,4}, Emma Thompson Brewster², Stefano Freguia³, Pablo Ledezma⁴, Marika Kokko¹

¹Corresponding author. Email: johannes.jermakka@tuni.fi. Faculty of Engineering and Natural Sciences, Tampere University, Finland. Permanent address: Tampere University, Faculty of Engineering and Natural Sciences, PO Box 541, 33101 Tampere, Finland.

²Faculty of Environment, Science and Engineering, Southern Cross University, Lismore, Australia

³Department of Chemical Engineering, The University of Melbourne, Parkville, Australia

⁴Advanced Water Management Centre, The University of Queensland, Brisbane, Australia

Declarations of interest: none

Supplementary information

S1. Stability of runs

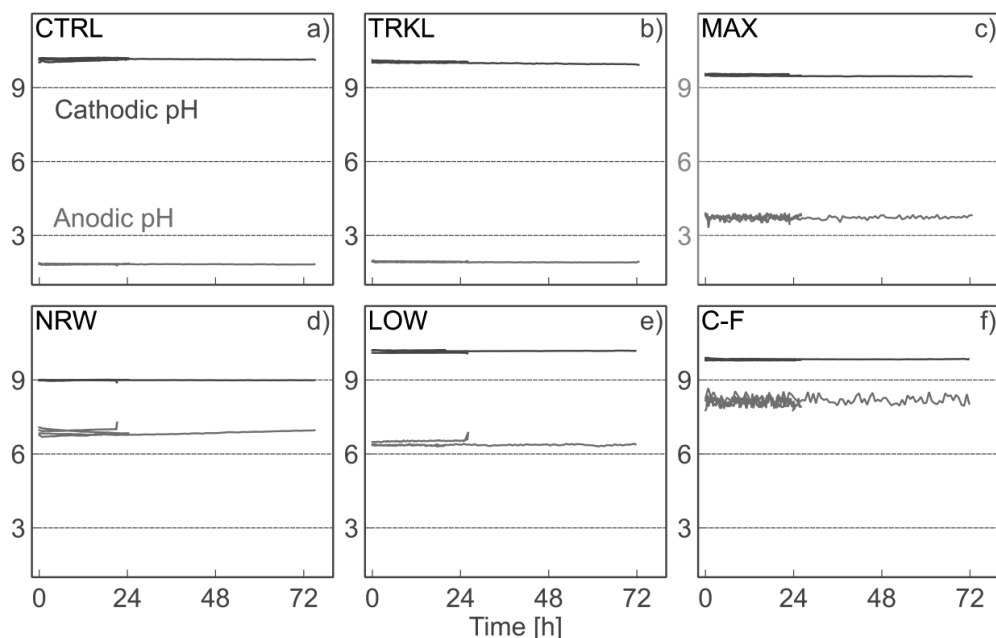


Figure S1 Reactor loop pH for different experiments as measured by the Endress+Hauser online meter. These measurements were used for stability tracking, sample was measured separately. For some runs, the cathodic pH measurements for the online pH probe and the sample pH probe do not match due to calibration problems in the online-probe, and sample pH measurements are used in results analysis.

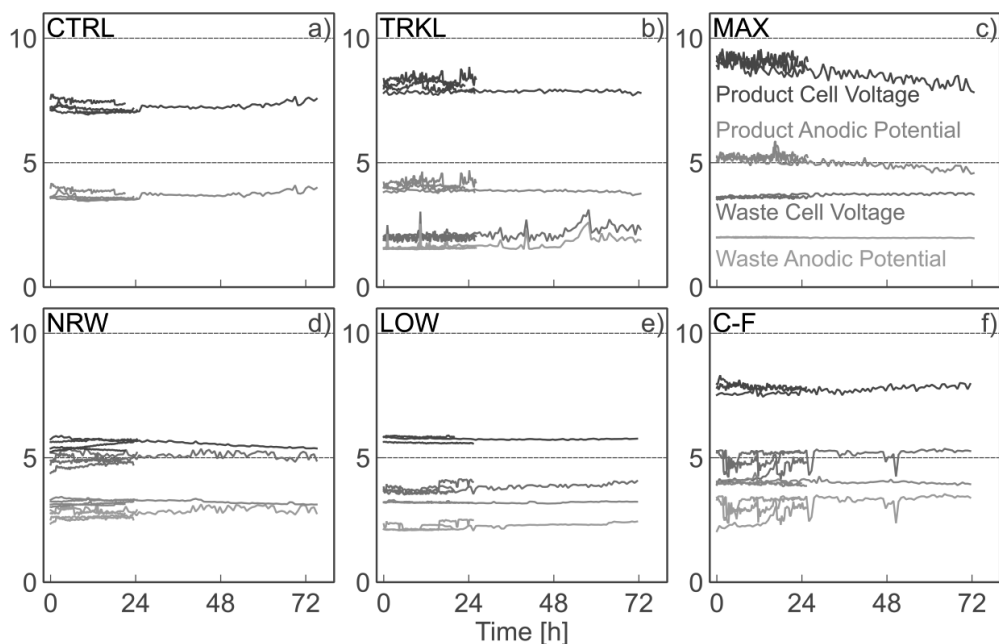


Figure S2 Product reactor and waste reactor cell voltages and anodic potentials (vs. SHE).

Table S1 Sample pH's from different chambers in the reactor system. Errors represent 95% confidence intervals.

Run	1	2	3	4	5	6
Name	Control	Trickle	Maximum Volume	Narrow Gap	Low Potential	Cathodic Feed
Abbr.	CTRL	TRKL	MAX	NRW	LOW	C-F
Urine Feed	8.5 ± 0.1	8.5 ± 0.1	8.5 ± 0.1	8.5 ± 0.1	8.5 ± 0.1	8.5 ± 0.1
Anodic pH	1.76 ± 0.02	1.94 ± 0.05	3.51 ± 0.05	6.74 ± 0.2	6.25 ± 0.25	7.88 ± 0.3
Cathodic pH	12.04 ± 0.03	11.79 ± 0.14	10.09 ± 0.04	9.21 ± 0.03	10.18 ± 0.06	9.79 ± 0.15
Product pH	8.96 ± 0.01	8.96 ± 0.01	9.19 ± 0.01	8.81 ± 0.07	8.93 ± 0.06	8.07 ± 0.04
Waste pH	9.15 ± 0.28	9.14 ± 0.08	7.32 ± 0.36	8.23 ± 0.06	8.55 ± 0.05	8.63 ± 0.02
Effluent pH	8.88 ± 0.05	8.92 ± 0.01	8.11 ± 0.01	7.92 ± 0.09	8.09 ± 0.36	7.86 ± 0.07

S2. Mass balances and concentrations for measured species

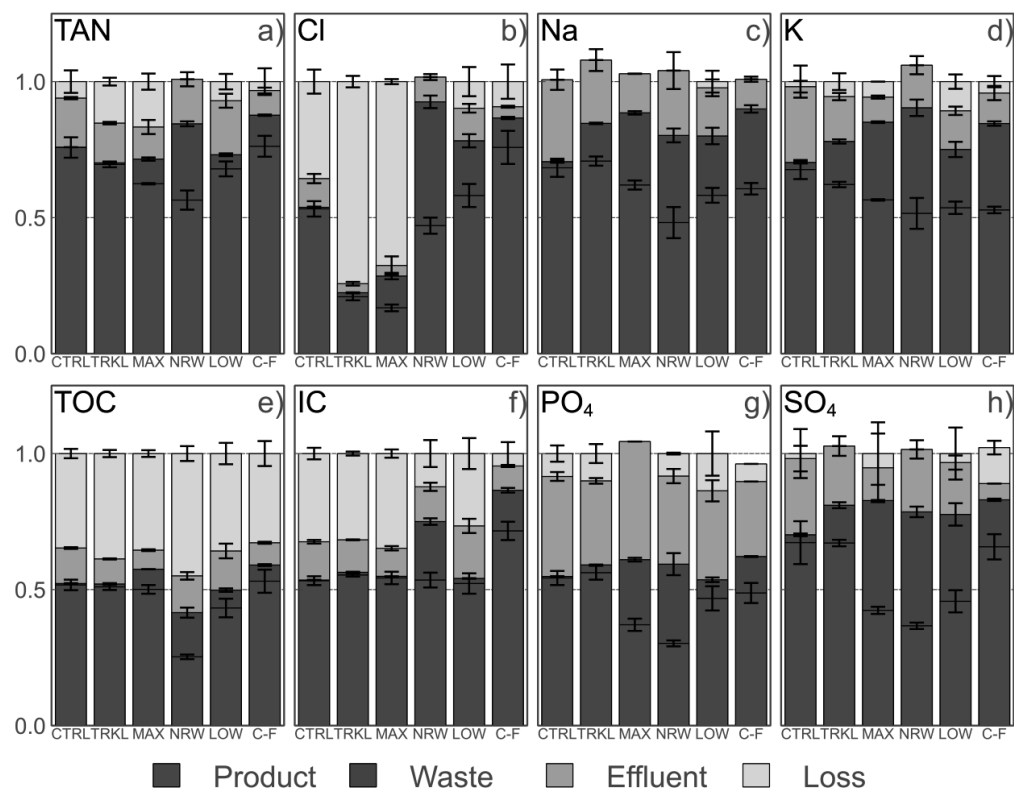


Figure S3 Mass balances for measured species. Units are mol/mol₀, representing fractions of moles from the feed measured in the product, waste and effluent. Fraction that was not measured was measured as lost – the amounts within the reactor staid stable during the experiments.

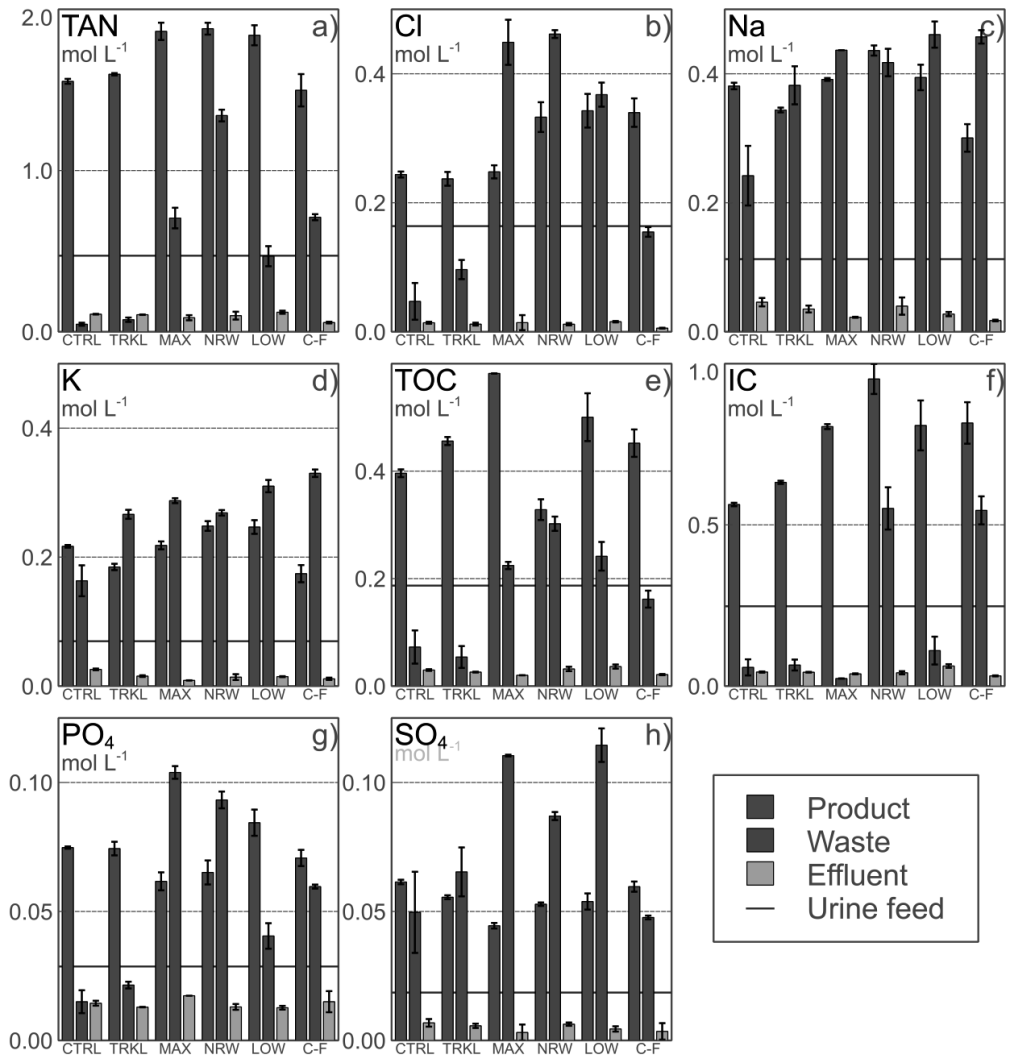


Figure S4 Concentrations for measured species, in mol L⁻¹.

Table S2 Averages of measured concentrations for all experiments in the feed, product and waste concentrates, effluent as well as anodic and cathodic loops in the reactor system. Values in mmol L⁻¹, except conductivity in mS cm⁻¹. Measurements with errors or that were not measured marked with 'na'.

Parameter	Product	Waste	Effluent	Anodic loop	Cathodic loop
Control experiment, CTRL					
TAN	2180 ± 30	70 ± 20	150 ± 10	60 ± 10	290 ± 10
PO ₄	1900 ± 20	380 ± 120	370 ± 30	na	na
K	2040 ± 20	1540 ± 230	240 ± 20	120 ± 10	570 ± 30
SO ₄	70 ± 10	20 ± 10	10 ± 10	na	na
Na	880 ± 20	560 ± 110	110 ± 20	60 ± 30	200 ± 40
Cl	110 ± 10	110 ± 20	110 ± 10	170 ± 10	70 ± 40
TOC	1550 ± 20	50 ± 10	110 ± 10	na	na
IC	30 ± 10	20 ± 10	na	na	na
Cond, mS cm ⁻¹	98.7 ± 0.3	29.0 ± 5.6	10.75 ± 0.2	11.5 ± 0.1	8.3 ± 0.2
Trickle experiment, TRKL					
TAN	2240 ± 10	100 ± 20	150 ± 10	60 ± 10	290 ± 20
PO ₄	1890 ± 70	540 ± 40	330 ± 10	410 ± 50	Na
K	1740 ± 50	2510 ± 70	150 ± 20	110 ± 10	370 ± 60
SO ₄	70 ± 10	20 ± 10	10 ± 10	20 ± 10	Na
Na	790 ± 10	880 ± 70	110 ± 60	na	Na
Cl	100 ± 20	110 ± 10	120 ± 10	200 ± 0	50 ± 30
TOC	1600 ± 10	70 ± 20	110 ± 10	10 ± 10	0 ± 10
IC	30 ± 10	60 ± 20	na	10 ± 10	na
Cond, mS cm ⁻¹	128.8 ± 30	64.3 ± 13	12.0 ± 2.9	12.5 ± 3.1	7.7 ± 1.8
Maximum volume experiment, MAX					
TAN	2610 ± 80	990 ± 90	120 ± 30	50 ± 20	210 ± 80
PO ₄	1570 ± 90	2640 ± 70	na	240 ± 40	na
K	2060 ± 60	2710 ± 40	80 ± 10	80 ± 30	110 ± 60
SO ₄	60 ± 10	100 ± 10	na	na	na
Na	900 ± 10	1000 ± 10	50 ± 10	40 ± 10	70 ± 30
Cl	100 ± 50	80 ± 30	100 ± 20	200 ± 0	220 ± 10
TOC	1860 ± 60	710 ± 70	90 ± 20	0 ± 10	na
IC	na	10 ± 10	na	na	na
Cond, mS cm ⁻¹	124.5 ± 44	119 ± 44	7.4 ± 3	2.8 ± 1.4	4.7 ± 2.0
Narrow Gap experiment, NRW					
TAN	2630 ± 60	1880 ± 60	140 ± 40	90 ± 30	130 ± 30
PO ₄	1650 ± 120	2370 ± 90	330 ± 30	na	na
K	2340 ± 80	2530 ± 50	130 ± 50	90 ± 30	90 ± 20
SO ₄	70 ± 10	90 ± 10	10 ± 10	na	na
Na	1000 ± 20	960 ± 50	90 ± 40	70 ± 20	70 ± 30
Cl	80 ± 10	90 ± 30	100 ± 30	170 ± 10	300 ± 20
TOC	1880 ± 40	1340 ± 40	100 ± 30	na	na
IC	na	na	na	na	na
Cond, mS cm ⁻¹	113.6 ± 2.7	112.9 ± 0.5	7.4 ± 0.5	5.3 ± 1.0	6.5 ± 0.6
Low Potential experiment, LOW					
TAN	2580 ± 90	660 ± 90	170 ± 20	100 ± 20	260 ± 50

PO ₄	2140 ± 130	1030 ± 130	320 ± 20	400 ± 40	na
K	2320 ± 100	2920 ± 90	140 ± 10	150 ± 40	210 ± 50
SO ₄	80 ± 10	40 ± 10	10 ± 10	0 ± 10	0 ± 10
Na	910 ± 50	1060 ± 50	60 ± 10	60 ± 20	90 ± 20
Cl	70 ± 10	60 ± 50	90 ± 10	190 ± 10	240 ± 30
TOC	1840 ± 70	470 ± 70	120 ± 10	10 ± 10	0 ± 10
IC	na	10 ± 10	na	na	na
Cond, mS cm ⁻¹	110.4 ± 4.4	80.5 ± 3.0	10.0 ± 0.6	7.5 ± 0.9	5.7 ± 0.4
<hr/>					
Cathodic Feed experiment, C-F					
TAN	2100 ± 150	1000 ± 30	80 ± 10	80 ± 10	220 ± 40
PO ₄	1800 ± 80	1510 ± 20	na	270 ± 20	290 ± 70
K	1640 ± 130	3110 ± 60	110 ± 20	110 ± 30	210 ± 80
SO ₄	70 ± 10	60 ± 10	20 ± 10	10 ± 10	0 ± 10
Na	690 ± 50	1050 ± 30	40 ± 10	40 ± 10	90 ± 30
Cl	80 ± 10	80 ± 10	110 ± 10	180 ± 10	160 ± 20
TOC	1500 ± 110	710 ± 20	60 ± 10	0 ± 10	10 ± 10
IC	10 ± 10	30 ± 10	na	na	na
Cond, mS cm ⁻¹	110.6 ± 1.9	80.5 ± 0.9	5.0 ± 0.2	6.2 ± 1.7	8.5 ± 2.7

S3. Na and K mass balance comparison

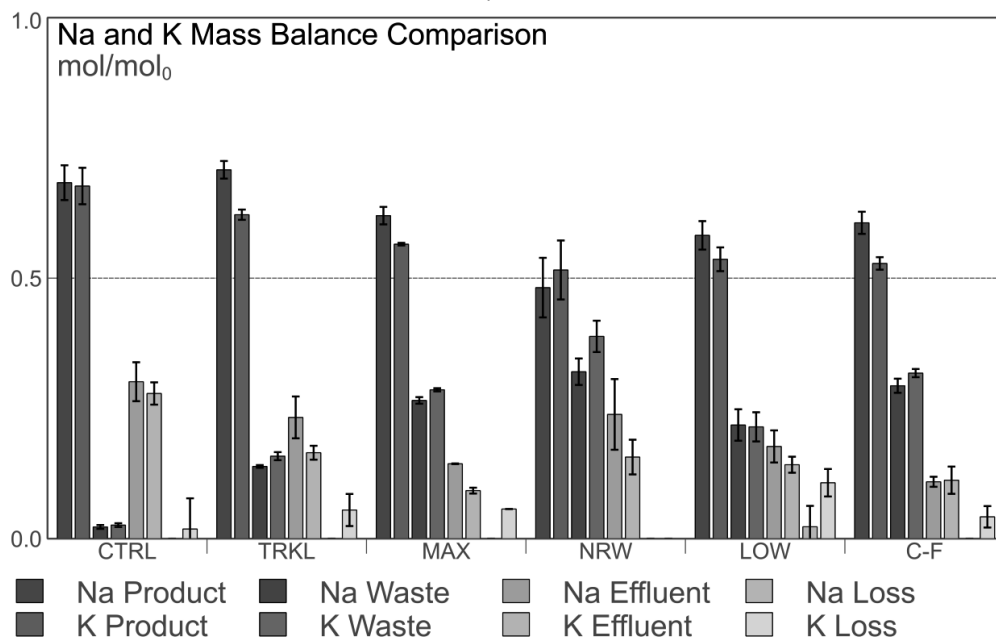


Figure S5 Sodium and potassium mass balances in the different runs.

S4. Nitrate and nitrite measurements

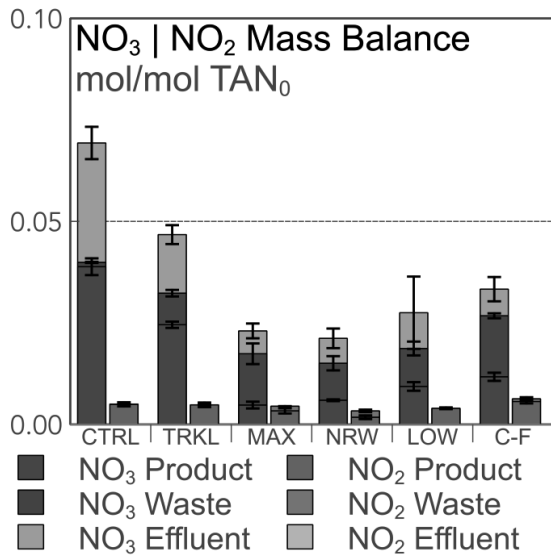


Figure S6 Nitrate and nitrite mass balances in the different runs, mol relative to mol TAN in feed.

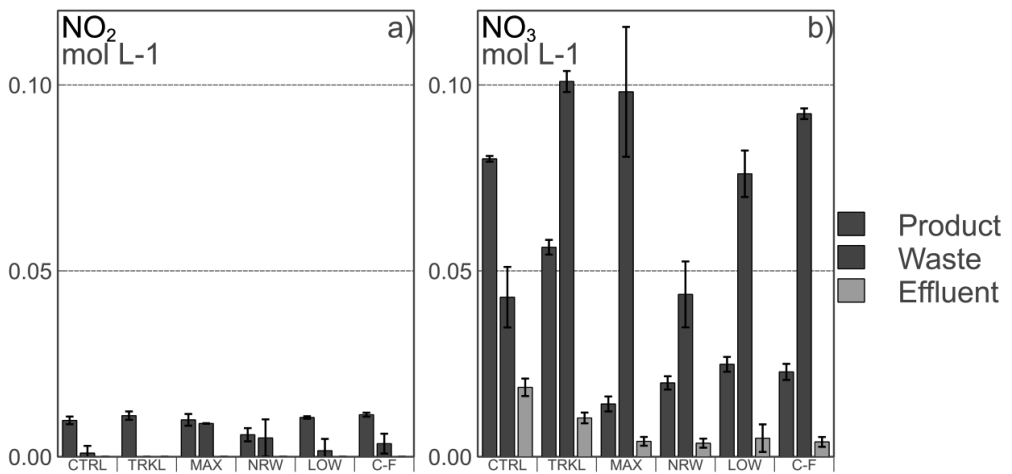


Figure S7 Nitrate and nitrite concentrations in the different runs.

S5. Chlorate and perchlorate measurements

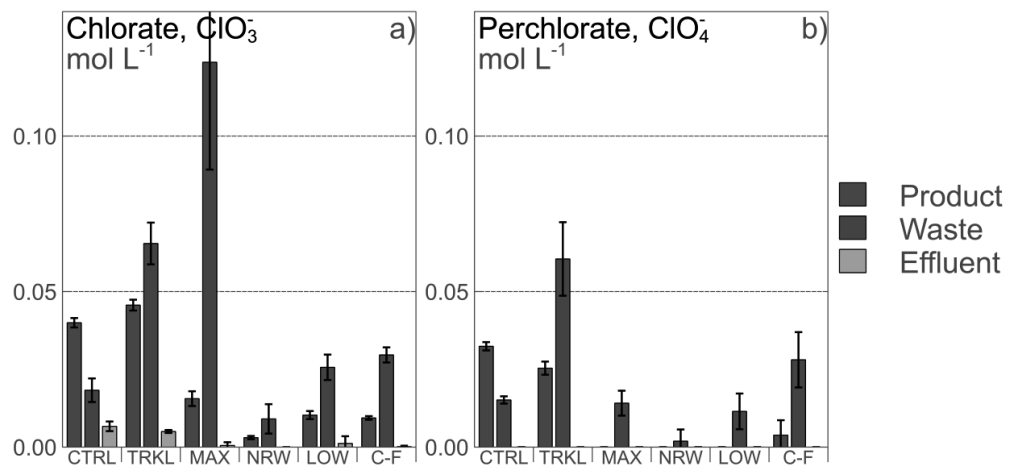


Figure S8 Chlorate and perchlorate concentrations in the different runs.

S6. Feeding flowgraphs

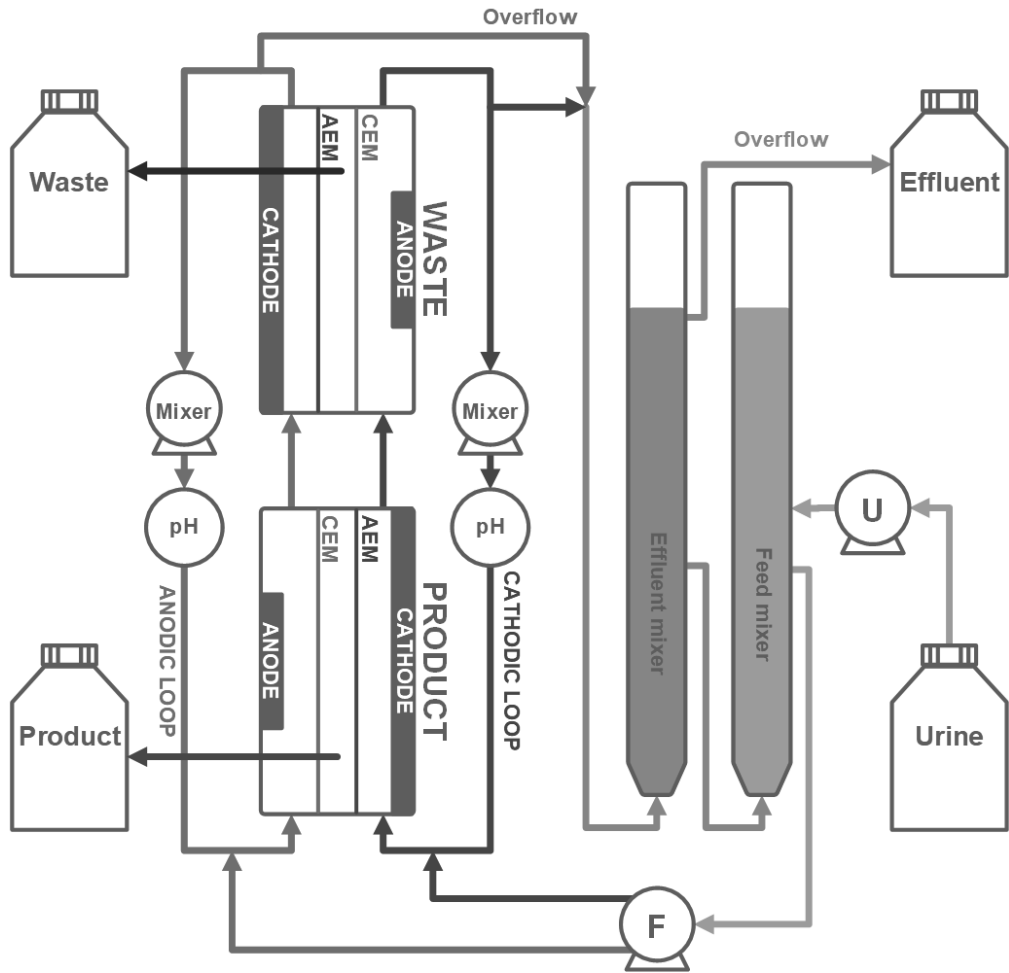


Figure S9 Feeding flowgraph for the double reactor.

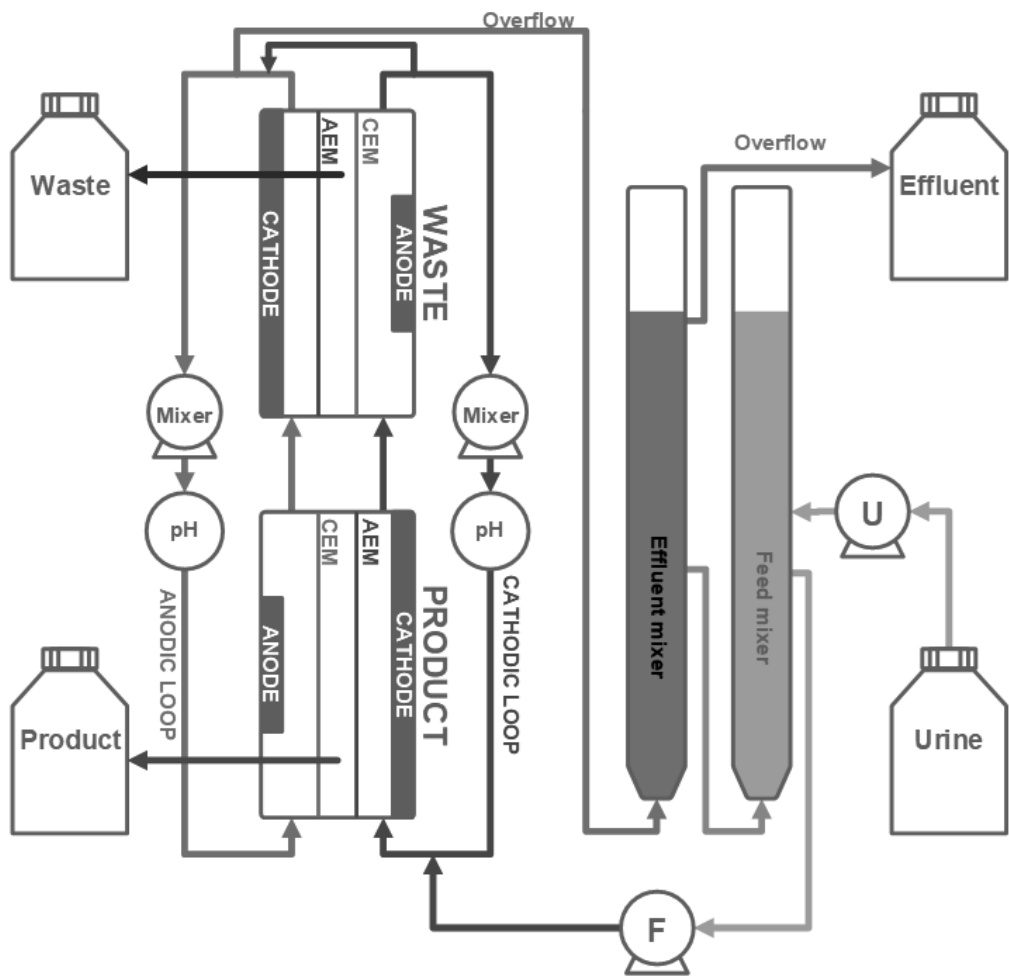


Figure S10 Feeding flowgraph for Cathodic Feed (C-F) experiment.

S7. Synthetic urine recipe

A synthetic urine solution representing human source-separated ureolysed urine was designed based on (i) previous investigations at the Swiss Federal Institute of Aquatic Science and Technology (EAWAG) (ii) literature review of source-separated urine samples (iii) The Human Urine Metabolome and (iv) real source-separated urine collected for research at the Advanced Water Management Centre at The University of Queensland, Australia. The four most prevalent organic compounds identified in the human urine metabolome database were included in the recipe: Creatinine, Hippuric Acid, Citric Acid and Glycine, while the rest of organic loading was simulated by addition of Acetic Acid, comprising 15% of total Theoretical Chemical Oxygen Demand in the sample. The recipe consisted of (in g L⁻¹): NH₄HCO₃ (22.14), NH₄Cl (0.48), NaCl (2.69), KCl (4.10), NaH₂PO₄ (2.40), Na₂SO₄ (2.41), Creatinine C₄H₇N₃O (2.3), Hippuric Acid C₉H₉NO₃ (0.88), Citric Acid C₆H₈O₇ (0.88), Glycine C₂H₅NO₂ (0.17), Ammonium Acetate NH₄CH₃CO₂ (2.06) and Ammonium Hydroxide NH₄OH (25 % liquid, 13.8mL L⁻¹). This formulation simulates urine after ureolysis, which results in complete removal of Mg and Ca through precipitation with phosphate. This solution was employed as feed, used as prepared and its composition was monitored through sampling at the start of each experiment. Synthetic urine was chosen to enable consistency when systematically varying the experimental factors.

